Isern, A.R., Anselmetti, F.S., Blum, P., et al., 2002
Proceedings of the Ocean Drilling Program, Initial Reports Volume 194

7. Sites 1196 and 1199[1]

Shipboard Scientific Party[2]

INTRODUCTION

Sites 1196 and 1199 were both drilled into the top of the southern carbonate platform on the Marion Plateau. Site 1196 (proposed Site CS-06A) was drilled in 304 m of water, 20 km east of the Great Barrier Reef margin (Fig. **F1**). The site is positioned at the intersection of regional seismic line MAR07 (SP 2808) (Fig. **F2**) and local grid line MAR70 (SP 178). Two holes were drilled (Hole 1196A: 0–672.2 meters below seafloor [mbsf]; and Hole 1196B: 0–265.3 mbsf) through a 663-m sequence of carbonate platform sediments overlying a phosphate-rich substrate. One hole was drilled at Site 1199 (proposed Site CS-16A; 0–419.5 mbsf). This site is located in 315.7 m of water ~5 km northeast of Site 1196 (Fig. **F1**). The site is positioned on regional seismic line MAR20 (SP 2690).

Sites 1196 and 1199 provide information on the initiation and facies development of the Southern Marion Platform (SMP), the nature of unconformities separating each platform phase, and the age and nature of the section equivalent to the northern platform drilled at Site 1193 (Fig. **F7,** p. 67, in the "Leg Summary" chapter). Postcruise analysis of recovered samples will enable the study of fluid flow processes within the carbonate platform as interpreted from the pore waters from adjacent slope sites (Sites 1197 and 1198).

Scattering of seismic energy within the well-indurated southern carbonate platform makes it difficult to determine seismically the stratigraphy and nature of sediment deposition underneath the platform cap. Despite this, analysis of regional seismic data suggested that Sites 1196 and 1199 should penetrate a thick sequence of late Miocene–Pliocene carbonate platform sediments representing the deposition of the youngest phase of carbonate platform growth observed on the Marion Plateau. The base of this sequence was predicted to overlie basinal sediments shed from the northern platform drilled at Site 1193. Drilling at

F1. Bathymetry map, p. 44.

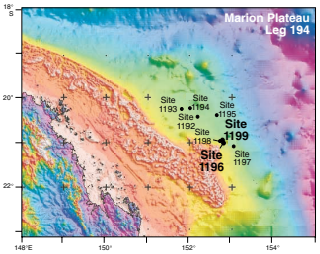

F2. Seismic line MAR13, p. 45.

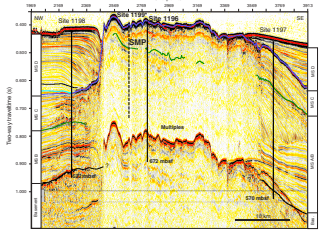

[1]Examples of how to reference the whole or part of this volume.
[2]Shipboard Scientific Party addresses.

Ms 194IR-107

Sites 1196 and 1199 only partially confirmed this interpretation. Although not conclusive, evidence from these sites suggests that only the upper 130 to 150 m of the platform facies could have accreted during the late Miocene, overturning the working hypothesis that this platform was completely of late Miocene to early Pliocene age. This discovery also necessitates a lower-amplitude sea level change for this time interval than was originally predicted.

OPERATIONS

Sites 1196 (proposed Site CS-06A) and 1199 (proposed Site CS-16A) are within the Great Barrier Reef Marine Park. All operations adhered to the guidelines established by the Great Barrier Reef Marine Park Authority. A beacon was dropped on Site 1196 coordinates at 0139 hr on 30 January 2001. A strong eastward current moved the beacon ~150 m from the original launching position, so the vessel was offset 140 m to the east to compensate for the displacement of the beacon. The corrected precision depth recorder indicated a water depth of 308.4 m.

Site 1196

Hole 1196A

Hole 1196A was spudded with the rotary core barrel (RCB) system at 0410 hr on 30 January (Table T2, p. 87, in the "Leg Summary" chapter; Tables T1, T2). Penetration into the hard carbonate cap of the carbonate platform by 9.6 m required 3.8 hr. At 85.8 mbsf, the drill string became stuck during the connection of a joint of pipe. The drill string could not be pulled up without stalling the top drive, although circulation and rotation were maintained. The string was freed after 5.5 hr of slowly working the drill string back up the hole and pulling with up to 220 kilopounds (kips). The bit was reamed back to the bottom of the hole and coring resumed nearly 10 hr after the hole problems began. To reduce the risk of the pipe becoming stuck, the hole was flushed with mud sweeps following the retrieval of each core and additional wiper trips were made at 285 and 429 mbsf. The pipe became stuck and was freed again after a connection was made with the bit at 499 mbsf. Coring was terminated at 672.2 mbsf, well below the original target depth of 570 mbsf. Acoustic basement was not penetrated; attempting to do so might have compromised the potential for downhole logging. A total of 86.37 m of core was recovered (12.9% average recovery).

The wireline triple combination (triple combo) tool string was made up with the Lamont-Doherty Earth Observatory (LDEO) natural gamma spectrometry tool (NGT) on top and the LDEO temperature tool at the bottom of the string for the first run. The NGT experienced electrical problems when lowered in the pipe. The tool string was brought back on deck, and the NGT was removed. The shortened string was deployed but could not pass a tight spot at ~520 mbsf. The hole was logged up from that depth. The hole diameter was >17 in for long distances, likely a result of the wiper trips and frequent mud sweeps performed to maintain the hole. The temperature tool was recovered with loosened connections, and the brass bottom nosepiece (~4 in long) was missing. Its loss was attributed to significant vibration of the drill pipe due to a strong southwesterly current.

T1. Coring summaries, p. 119.

T2. Expanded coring summaries, p. 121.

For the second wireline run, the Formation MicroScanner (FMS) sonic velocity tool string was deployed. The tools encountered an obstacle in the pipe at ~135 meters below rig floor (mbrf), which could have been the missing piece of the temperature tool. After pumping was not successful in moving the obstruction, the tools were recovered. The top drive was picked up, and a core barrel was lowered to force the obstacle down the hole. This effort was successful, and the FMS/Sonic combination was deployed after setting back the top drive. The tight spot at 524 mbsf encountered on the first run prevented the tool from further penetration. Logging was initiated at that depth. Two FMS/Sonic passes were logged.

The third run was a check shot survey with the well seismic tool (WST) with 13 stations successfully shot between 94.4 and 523.5 mbsf. Logging operations ended at 0700 hr on 4 February.

Hole 1196B

A new RCB bit was affixed to the bottom-hole assembly (BHA), and the vessel was offset 20 m east of Hole 1196A. The plan for Hole 1196B was to rotary core through the top of the carbonate platform to a depth of 110 mbsf, recover the RCB BHA and deploy the advanced diamond core barrel (ADCB), reenter Hole 1196B, and core to ~360 mbsf. The 110-m pilot hole was required for lateral support of the ADCB drilling assembly, which is composed of slick-profile 6-in drill collars and is not as robust as the RCB assembly. Deploying a free-fall funnel (FFF) at this point would have facilitated reentry with the ADCB. However, this would have required reaming a 4-m deep, large-diameter (14 in) pilot hole to accommodate the casing of the FFF in the hard seafloor formation (first pipe trip); reentering bare rock with the RCB to drop the FFF (second pipe trip); and deploying the ADCB (third pipe trip). Instead, attempting a bare-rock reentry directly with the ADCB into the RCB pilot hole (one pipe trip only) seemed a wiser use of time at minimal risk.

The bit tagged the seafloor at 304.2 m water depth, and Hole 1196B was spudded with the RCB at 0410 hr on 30 January. The drilling results were similar in drilling time and recovery to the first hole. Following the recovery of Core 194-1196B-6R, the vessel was forced to wait on weather, as the heave was routinely exceeding the shallow-water guideline threshold of 2 m. The bit was pulled back to 19.4 mbsf, and coring was suspended for 11.25 hr. The peak value of heave was 3 m. Coring then resumed and advanced to the target depth of 110 mbsf. Average recovery for that interval was 10%.

Once the bit was on deck, the weather was still unfavorable for shallow water operations and deemed too rough for ADCB coring. It was decided to move on to the next site (Site 1197) and return when the environmental conditions promised better success for ADCB reentry and coring. The vessel departed Site 1196 at 0415 hr on 6 February. The beacon remained on the seafloor.

Return to Hole 1196B

After initial operations at Site 1197 (see **"Operations,"** p. 1, in the "Site 1197" chapter) and completion of Site 1198 (see **"Operations,"** p. 1, in the "Site 1198" chapter), the weather had abated and coring with the ADCB in Hole 1196B appeared feasible. ADCB coring was attempted in anticipation of achieving better recovery than that achieved with the RCB. The 8-nautical mile (nmi) trip from Site 1198 to Hole

1196B was accomplished in 40 min, and the beacon signal was reacquired at 0545 hr on 11 February.

Before reentering Hole 1196B with the ADCB after leaving it open for 5 days, the hole was reentered with the RCB and washed ahead to 110 mbsf to ensure a clean and stable hole for the ADCB reentry. It took <50 min to position the ship so that the RCB system could be reentered into the hole, which was clearly visible from the television transmission. The hole was reentered at 0950 hr on 11 February with the active heave compensator (AHC) in operation. About 1 m of soft sediment fill was cleaned from the hole above 110 mbsf.

The drill string was recovered, and the ADCB drilling assembly was deployed. A strong current made it difficult to position the bit directly over the borehole. At 2130 hr on 11 February, after 1.75 hr of maneuvering, Hole 1196B was reentered with the ADCB with the AHC in operation (Fig. F3). ADCB coring advanced from 110 to 265.3 mbsf (Cores 13Z–51Z). Unlike the standard coring systems, the ADCB does not have a float shoe to prevent the cuttings and loose material in the annulus from backing up into the BHA during the wireline retrieval and running in of core barrels. Therefore, mud was spotted at the bit after each core was cut and before withdrawing the core barrel via the wireline.

F3. Bare-rock reentry of Hole 1196B with an ADCB bit without the aid of a free-fall funnel, p. 46.

Because of diminishing returns and the interest in conserving time for use at an additional site at the end of the leg, coring was terminated before reaching the target depth of 360 mbsf. Total recovery from the 155.3 m interval cored was 17.92 m, or an average of 11.5%. The RCB recovery for a comparable interval (17 cores from 105.0 to 268.4 mbsf) from Hole 1196A was 10.4%. The ADCB recovery in the interval from 110 to 128.1 mbsf was 7.5 m, or 41.4%. This recovery was considerably better than the RCB results for a corresponding interval (26.8%) in Hole 1196A. Beyond this depth, the recovery of the ADCB was comparable with the RCB results. The heave while coring in Hole 1196B rarely exceeded 1 m.

Although this system is still in the development stage, the ADCB acquired 35 hr of continuous operation without hardware problems, broken parts, improper seating of the core barrel, or downtime of any kind. Slip and basket core catchers were both used with moderate success despite the limited recovery in this difficult hole. The operation of the ADCB with the liners worked better than expected. The handling and core extrusion problems experienced during the first deployment of the ADCB on Leg 193 were not encountered during Leg 194. The PDC bit on loan from the Japanese Drilling Company worked quite well, with the overall rate of penetration exceeding initial estimates.

Although the 6-in drill collars were an unusual size for our operation and required drill collar slips and dog collars, the drill crew worked efficiently and managed to have all of the drilling equipment secured only 6 hr after coring was terminated. The beacon was successfully recovered, and the drilling equipment was secured by 1700 hr on 13 February as the vessel began the short return transit to Site 1197.

Site 1199

After a revisit of Site 1197 (13–17 February), the vessel proceeded to Site 1199 (proposed Site CS-16A). This transit was accomplished with extended thrusters, using the dynamic positioning system, which took 5.9 hr. The beacon was launched at 0705 hr on 18 February while the drill string was being deployed to 313 m. Operations were suspended

for 3.5 hr to wait for the maximum heave to abate from the measured 2.5 m to <2 m.

Hole 1199A

Hole 1199A was spudded with the RCB at 1235 hr on 18 February (Table T2, p. 87, in the "Leg Summary" chapter; Tables T1, T2). Rotary coring advanced to a final depth of 419.5 mbsf by 0845 hr on 21 February. A maintenance wiper trip was made from 187 to 71 mbsf, and ~4 m of soft fill was found. The recovery from the top 159.8 m of the hole was 83.6 m (52.3%) and was cored with a slow average rate of penetration (ROP) at 4.7 m/hr. Part of the reason for the extended coring time in the top of the platform was that not more that 5 kips of bit weight could be applied without putting the BHA in compression. As the hole deepened, bit weight was gradually added and the ROP increased. Below 159.8 mbsf, the recovery dropped off dramatically and the ROP increased substantially. The average recovery from 159.8 to 419.5 mbsf was 3.3%. The total recovery for the hole was 92.16 m, or 22.0%.

A wiper trip was completed, the bit was released, the hole was displaced with 125 barrels of sepiolite mud, and the end of pipe was placed at the depth of 85.7 mbsf in preparation for logging. The triple combo tool string reached a depth of 418 mbsf, which was about 2 m above total depth (TD) of the hole, and a successful log was completed. The FMS/Sonic tool suite was subsequently lowered in the hole but would not move past an obstruction at 118 mbsf, presumably because of a possible karst cave. After 1 hr of countless attempts, the tool was recovered. The drill pipe was lowered to ~210 mbsf in order to widen the narrow hole, and the FMS/Sonic tool suite was lowered once more in the hole. It still was not possible to clear the interval at 118 mbsf. Logging was initiated above this horizon, and we measured a hole deviation of 7.5°, which is likely the cause of repeated failures to reenter the hole. Two sections were added to the tool suite in a final and fruitless attempt at reaching the bottom of the hole. Logging operations were terminated at 1000 hr on 19 February.

The drill string was recovered and the beacon was retrieved. The BHA was disassembled, and the vessel was secured for the extended sea voyage to Guam. The vessel left the location at 1415 hr on 22 February.

LITHOSTRATIGRAPHY AND SEDIMENTOLOGY

Site 1196

Sediments recovered at Site 1196 consist of well-lithified, shallow-water carbonates (limestone and dolostone), which make up a significant carbonate edifice (SMP) that overlies a phosphatic-rich siliciclastic substrate. The surface of this carbonate platform is overlain by a variably thick veneer of hemipelagic sediments as seen on seafloor photographs taken during the precruise site survey (Fig. F6, p. 66, in the "Leg Summary" chapter). In some places, the platform surface outcrops at the seafloor. The carbonate sediment succession was divided into four major units on the basis of carbonate mineralogy and the nature of constitutive particles (Fig. F4; Table T3). Unit I (Hole 1196A: 0.0–182.2 mbsf; Hole 1196B: 0.0–184.9 mbsf) is mainly composed of dolomitic floatstone and rudstone. Unit II (Hole 1194A: 182.2–345.8 mbsf; Hole 1196B: 184.9 mbsf–bottom of hole) consists of nondolomitized skeletal

F4. Lithologic summary, Site 1196, p. 47.

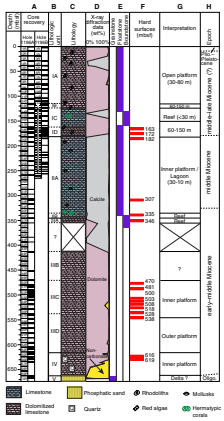

T3. Lithologic units recovered at Site 1196, p. 130.

floatstone/grainstone characterized by the occurrence of shallow-water fauna. Within Subunit IIA, calcareous nannofossils indicate an age of 15.2 to 13.3 Ma (see "Biostratigraphy and Paleoenvironments," p. 16). Unit III (345.8–617.1 mbsf) is typically composed of variously colored, coarse crystalline dolostone. Unit IV (617.1–662.6 mbsf) also consists of dolostone, but in addition it contains a significant amount of siliciclastic particles. The underlying siliciclastic substrate, Unit V, is composed of dark sandstone, claystone, and phosphatic sands of late Oligocene age (see "Biostratigraphy and Paleoenvironments," p. 16).

Lithologic Units

Unit I (Hole 1196A: 0.0–182.2 mbsf; Hole 1196B: 0.0–184.9 mbsf; Late[?] to Middle[?] Miocene)

In Hole 1196A, the top of Unit I corresponds to a highly corrugated, iron-stained surface (Fig. F5), which was likely shaped by both subaerial (karstic dissolution) and submarine (bioerosion and currents) processes. This surface is partially overlain by a 1-cm-thick bed of skeletal wackestone that yielded a planktonic foraminiferal assemblage with a maximum age of 3.2 Ma (Fig. F6) (see "Biostratigraphy and Paleoenvironments," p. 16). Because this wackestone layer is so thin, it was not recorded as a separate lithologic unit. In Hole 1196B, the top of Unit I is capped by a 2-cm-thick stromatolitic crust (Figs. F7, F8). Unit I was divided into four subunits based on biotic assemblage. Subunits IA, IB, and ID are mostly dolomitic in composition, whereas Subunit IC is predominantly calcitic.

Subunit IA (Hole 1196A: 0.0–117.2 mbsf; Hole 1196B: 0.0–122.9 mbsf)

This subunit consists of dolomitic floatstone/rudstone characterized by the occurrence of centimeter-sized rhodoliths and coral fragments in a moderately sorted grainstone matrix (Fig. F9). This matrix contains larger benthic foraminifers, red algae, mollusks, and rare bryozoan fragments. Examination of one thin section from the uppermost part of Subunit IA, just below its corrugated upper surface, further revealed the occurrence of *Halimeda* debris (Fig. F10). Color varies downcore from pale yellow to pale brown. Both intergranular and moldic porosity occur. In the uppermost part of Subunit IA, pores are filled by a complex succession of cements and internal sediments, including early isopachous fibrous rims, vadose silt, blocky spar fringes, and micrite (Fig. F10). Dolomitization is not pervasive (calcitic horizons are preserved), and skeletal components are still identifiable. A single piece of skeletal wackestone with planktonic foraminifers, possibly an artifact related to drilling, was found between 20 and 30 cm in Section 194-1196A-1R-1. The base of Subunit IA is marked by the rapid disappearance of centimeter-sized rhodoliths at the bottom of Cores 194-1196A-13R and 194-1196B-16Z.

Subunit IB (Hole 1196A: 117.2–125.9 mbsf; Hole 1196B: 122.9–130.5 mbsf)

This thin unit consists of light brown, well-lithified, dolomitized skeletal floatstone with a recrystallized grainstone matrix (Fig. F11). The coarse (>2 mm) fraction amounts to ~30% of the rock volume and predominantly includes elongated fragments of branching coralline algae and centimeter-sized mollusk shells. Numerous molds of flat, larger benthic foraminifers also occur. Faint, low-angle cross-bedding is visible in some intervals (Fig. F11). Dolomitization is more pervasive than in Subunit IA, but rock texture is still visible. The lower parts of Subunits

F5. Close-up photograph of uppermost part of Core 194-1196A-1R, p. 48.

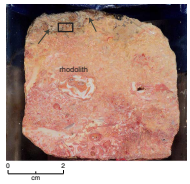

F6. Photomicrograph of corrugated upper surface of the platform carbonates, p. 49.

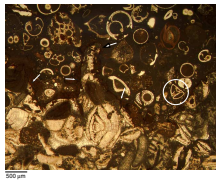

F7. Close-up photograph of stromatolitic crust, p. 50.

F8. Photomicrograph of stromatolitic crust, p. 51

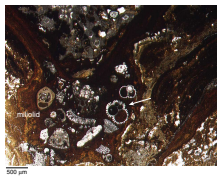

F9. Close-up photograph of macrofacies of dolomitic floatstone/rudstone, p. 52.

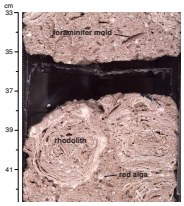

IA and IB correspond to marked peaks in natural gamma ray (NGR) intensity, with increasing amplitude downcore (see "Core Physical Properties," p. 27, and "Downhole Measurements," p. 32). The boundary between Subunits IB and IC is sharp and occurs near the base of Core 194-1196A-14R and within Core 194-1196B-20Z.

Subunit IC (Hole 1196A: 125.9–162.8 mbsf; Hole 1196B: 130.5–145.0 mbsf)

This poorly recovered, moderately lithified unit is characterized by light gray to white skeletal rudstone, floatstone, and boundstone rich in centimeter-sized hermatypic coral debris, mollusk shell fragments, and rhodoliths (Fig. F12). Coralline algae and bryozoan clasts, broken echinoid spines, and larger benthic foraminifers occur also in the finer-grained matrix. Both intergranular and moldic porosities are frequent throughout this interval, which, unlike overlying units, is essentially composed of calcium carbonate. In Hole 1196B, this reefal facies alternates with dolomitic floatstone containing molds of larger benthic foraminifers, coral, and bivalve fragments. The upper part of Subunit IC (Core 194-1196A-15R) correlates with low NGR values (see "Core Physical Properties," p. 27, and "Downhole Measurements," p. 32). The boundary between Subunits IC and ID corresponds to a thin micritic crust near the top of Core 194-1196A-18R that was not recovered in Hole 1196B. The difference in thickness of this subunit in Hole 1196A and 1196B (14.5 vs. 36.9 m) exceeds the depth errors resulting from coring. This difference implies that Subunit IC is laterally variable in thickness.

Subunit ID (Hole 1196A: 162.8–182.2 mbsf; Hole 1196B: 145.0–184.9 mbsf)

The top of Subunit ID corresponds to marked peaks in resistivity and velocity in the downhole logs (see "Downhole Measurements," p. 32). Subunit ID is mostly composed of pale brown to brown dolomitic floatstone with a grainstone matrix. Main constituents include whitish, elongated fragments of branching coralline algae; small (<1 cm) rhodoliths; mollusk shells; rare bryozoan detritus; larger benthic foraminifers, which essentially occur as molds; and minor coral debris. The occurrence of rhodoliths and rare coral fragments is the main difference between this facies and that observed in Subunit IB. Overall sorting is poor in this subunit. A crude lamination generated by an abrupt change in grain size can be observed in some intervals (Fig. F13). Within this subunit, the grainstone matrix is pervasively dolomitized and with moldic porosity. Below the micritic crust forming the boundary with Subunit IC, the uppermost 15 cm of Subunit ID (Hole 1196A) is characterized by a dense, mottled dolomicrite with rare molds and no texture preserved. In the bottom of Core 194-1196A-18R, an interval of rhodalgal boundstone and rudstone was observed. The top of Core 194-1196A-19R contains a dense, brown, iron-stained, 1-cm-thick layer that may represent an exposure surface. The boundary between Units I and II occurs within Sample 194-1196A-20R-1, 27 cm, and at the top of Core 194-1196B-33Z. It corresponds to a sharp color and facies change in Unit I and to a thin dolomitic crust in Unit II (Fig. F14).

Unit II (Hole 1196A: 182.2–345.8 mbsf; Hole 1196B: 184.9 mbsf–Bottom of Hole; Early[?] to Middle Miocene)

In Hole 1196A, the top of Unit II consists of a dense, dark brown dolomitic floatstone/rudstone interval (194-1196A-20R-1, 27–40 cm) (Fig. F14) containing abundant molds of branching coral and rare fragments of branching coralline algae. Pervasive dolomitization has removed

F10. Photomicrograph showing microfacies of grainstone matrix, p. 53.

F11. Close-up photograph of macrofacies of dolomitic floatstone, p. 54.

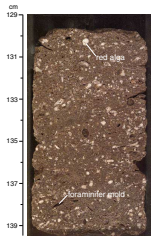

F12. Close-up photograph of coral boundstone/rudstone, p. 55.

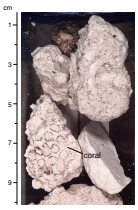

F13. Close-up photograph of dolomitic floatstone, p. 56.

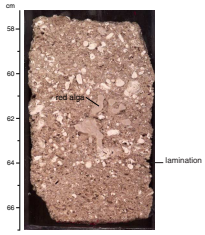

F14. Close-up photograph of Unit I/II boundary, p. 57.

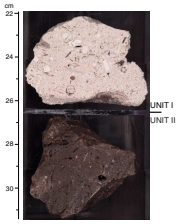

much of the fine-grained matrix texture. Unit II was deposited in a shallow-water depositional setting (see "Biostratigraphy and Paleoenvironments," p. 16). This unit has been divided into two subunits on the basis of textural and biotic changes.

Subunit IIA (Hole 1196A: 182.2–335.9 mbsf; Hole 1196B: 184.9 mbsf–Bottom of Hole)

This subunit consists of light gray to pale brown, well-lithified, poorly sorted, skeletal floatstone with a silt-sized grainstone matrix (Fig. F15). Predominant constituents are porcellaneous larger benthic foraminifers (alveolinids and soritids) and centimeter-sized, disarticulated but unbroken mollusk shells. Coral, bryozoan, and rare *Halimeda* debris were also observed. The fine grainstone matrix mostly contains abraded coralline-algae clasts and small benthic foraminifers (miliolids) in a sparry calcite cement (Fig. F16). Thread-like dark patches up to 1 cm long are interpreted as preserved seagrass roots. Organic matter and clays also occur in this subunit (See "Geochemistry," p. 24). Bioturbation is visible in some intervals. Within this subunit, moldic porosity is common and fenestral porosity is observed in Section 194-1196A-22R-1. Well-sorted, coarser grainstone intervals, about 0.2–0.4 m thick, occur near 230 mbsf (Cores 194-1196A-25R and 194-1196B-45Z) and at 317 mbsf (Core 194-1196A-34R). Rare nannofossils yielded an early to middle Miocene age (13.6–18.2 Ma) (316.0 mbsf [Core 194-1196A-34R] and 218.0 mbsf [Core 194-1196B-40Z]). Benthic foraminiferal data further constrain the age of Subunit IIA to between 15.2 and 13.3 Ma (see "Biostratigraphy and Paleoenvironments," p. 16). The lower part of Subunit IIA is characterized by thin horizons with dark brown, dense micrite mottles. One of these horizons (Section 194-1196A-33R-1, 42–88 cm; 307.4 mbsf) corresponds to exceptionally high values in NGR, resistivity, and sonic velocity in the downhole logging record (see "Downhole Measurements," p. 32). The facies change between Subunit IIA and IIB occurs between Cores 194-1196A-35R and 36R; the boundary itself was not recovered.

Subunit IIB (335.9–345.8 mbsf)

This thin subunit is represented by a pale beige to white, well-lithified, poorly sorted skeletal rudstone/boundstone. The very coarse (>1 cm) fraction includes colonial hermatypic corals, red algae, and mollusk (gastropod and bivalve) fragments. The matrix of Subunit IIB is dominated by micrite. *Lithophaga* borings are common, as is moldic porosity. A possible oolitic grainstone occurs at the top of Core 194-1196A-36R. The boundary with underlying Unit III occurs at Sample 194-1196A-37R-1, 30 cm (345.8 mbsf) (Fig. F17), and is characterized by a marked change in rock composition from pure calcite to mixed calcite and dolomite mineralogy (Fig. F4). This boundary corresponds to the downhole transition in NGR values, which decrease from a maximum at 306.0 mbsf near the base of Unit II to minimum values at the top of Unit III (see "Downhole Measurements," p. 32).

Unit III (345.8–617.1 mbsf; Early to Middle[?] Miocene)

This ~270-m-thick unit consists of coarse crystalline dolostone. Depositional textures have, for the most part, been erased by pervasive dolomitization, and only the ghosts or molds of original rock constituents can be observed. Four subunits have been determined on the basis of color; trace minerals; the presence or absence of molds; and, in one case, the identification of primary rock components.

F15. Close-up photograph of skeletal floatstone, p. 58.

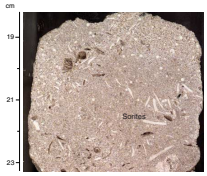

F16. Photomicrograph of skeletal floatstone, p. 59.

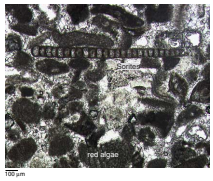

F17. Close-up photograph of Unit II/III boundary, p. 60.

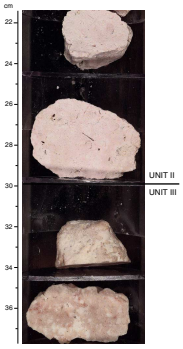

Subunit IIIA (345.8–355.3 mbsf)

This subunit consists of a mottled, pinkish white to light brown, recrystallized, dolomitic rudstone with a grainstone matrix (Fig. F17). Ghosts of rhodoliths, branching and massive corals, and dissolved mollusk fragments were identified.

Poorly Recovered Interval (355.3–412.7 mbsf)

Only 0.22 m of sediment was recovered from this ~60 m interval. These sediments consist of cream-white dolomitic floatstone, including centimeter-sized rhodoliths and coralline algae fragments in a grainstone matrix. Because of their similarity to the facies of Subunit IA, these rocks were first interpreted to have fallen down the hole. However, there are also similarities to lithologic intervals recovered from Subunit IIB, between 285 and 410 mbsf, at Site 1199.

Subunit IIIB (412.7–470.4 mbsf)

This core interval is characterized by a brilliant white, sucrosic dolostone ("snowstone") (Fig. F18). Rare relicts of centimeter-sized rhodoliths and branching coralline algae are preserved along with scattered, millimeter-sized, lenticular molds of larger benthic foraminifers. Dolomite content is close to 100% (Fig. F4), except in the upper part of Core 194-1196A-44R where a weak reaction to HCl occurs. This subunit is visually homogenous despite the presence of several peaks in sonic velocity between 450 and 460 mbsf (see **"Downhole Measurements,"** p. 32) that likely correspond to unrecovered horizons of different lithologic composition. The lower boundary of Subunit IIIB corresponds to a reddish interval at the top of Core 194-1196A-50R.

F18. Close-up photograph of macrofacies of the sucrosic dolostone, p. 61.

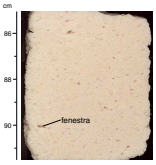

Subunit IIIC (470.4–537.7 mbsf)

This subunit is characterized by a mottled, recrystallized, well-lithified dolostone showing various colors from white to pinkish to brown. Ghosts of rhodoliths, mollusk shells, and coralline algal fragments are visible in hand specimens. Fragments of echinoid spines and plates surrounded by a rim of syntaxial cement can be seen in thin section (Fig. F19). A small algal or coral buildup is present near the bottom of Core 194-1196A-53R. Intercrystalline, shelter, moldic, and possibly fenestral porosities were observed (Fig. F20). Moldic porosity results from the dissolution of larger benthic foraminifers. Dolomitization is pervasive in this subunit and euhedral dolomite rhombs up to 200 µm in size were observed in thin section (Fig. F19). The lower portion of Subunit IIIC contains several millimeter- to centimeter-thick, dense, brown or red-colored layers (Fig. F20) interpreted as exposure surfaces. The occurrence of several veins filled by dark-red, fine-grained dolostone (e.g., interval 194-1196A-51R-1, 128–147 cm) suggests that this interval is fractured. This interpretation is corroborated by FMS data (see **"Downhole Measurements,"** p. 32). The base of this subunit has been placed immediately above a 6-cm-thick, dense dolomicrite zone at the top of Core 194-1196A-57R.

F19. Photomicrograph showing microfacies of variegated dolostone, p. 62.

F20. Close-up photograph of possible exposure surface in variegated dolostone, p. 63.

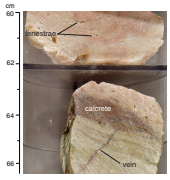

Subunit IIID (537.7–617.1 mbsf)

The lowermost portion of Unit III is characterized by very pale brown to olive-brown, well-lithified dolostone with abundant centimeter-sized molds resulting from the dissolution of benthic foraminifers (Fig. F21). Some molds are horizontally aligned, and there is an overall fining-upward trend, suggesting that the original sediment was laminated and graded. Other important constituents, most of which are barely visible,

F21. Close-up photograph of macrofacies from Subunit IIID, p. 64.

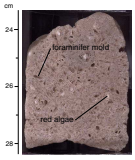

include rhodoliths, coralline algae, and mollusk fragments. Original rock texture has been lost. Two decimeter-thick intervals of light gray, dolomitic, skeletal packstone/grainstone with abundant larger benthic foraminifers occur in Samples 194-1196A-63R-1, 62 and 134 cm. The boundary between Units III and IV, corresponds to a 5-cm-thick, dense dolomicrite crust found in Core 194-1196A-65R.

Unit IV (617.1–662.6 mbsf; Early[?] to Middle Miocene)

This lowermost lithologic unit includes various dolostone facies, all of which contain siliciclastic material, such as quartz and lithoclasts. Glauconite is also present in certain intervals. These facies occur in meter-scale sequences separated by iron-stained zones interpreted as exposure surfaces. The following lithologies were distinguished on the basis of color, sedimentary structure, and noncarbonate mineral content:

1. Grayish dolomitic grainstone, common echinoid spines, common molds of larger benthic foraminifers, and glauconite present;
2. Light red dolomitic rudstone, large rhodoliths common, and glauconite and quartz present (Fig. F22);
3. Laminated brown dolostone, centimeter-thick layers of sand-sized skeletal particles (echinoids?), quartz and lithoclasts present, and well-preserved cross lamination;
4. Greenish white dolostone with common glauconite and quartz (Fig. F22); and
5. Yellowish laminated dolostone with ~30% quartz, phosphate grains, and bivalve shells.

Unit IV preserves a strong remanent magnetization, possibly linked to the occurrence of magnetite (see "Paleomagnetism," p. 22). The lower limit of this unit occurs at the base of Core 194-1196A-68R. No material was recovered from Core 194-1196A-69R.

F22. Close-up photograph of facies variability in Unit IV, p. 65.

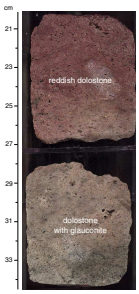

Unit V (Hole 1196A: 662.6 mbsf–Bottom of Hole [672.2 mbsf]; Late Oligocene)

Core 194-1196A-70R contains dark rocks (Fig. F23) of late Oligocene age (see "Biostratigraphy and Paleoenvironments," p. 16), which form the substrate for the carbonate platform described above. These rocks were described at macroscopic scale as sandstone and claystone. However, examination of two thin sections indicates the presence of phosphatic sands.

F23. Close-up photograph of macrofacies of Oligocene rocks, p. 66.

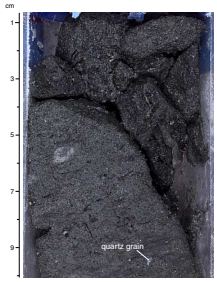

Discussion

Paleoenvironmental Reconstruction

Paleodepositional environments, essentially determined from petrographic and sedimentological data, are proposed for each lithologic unit at Site 1196. Additional paleoenvironmental interpretation based on microfossil assemblages can be found in "Biostratigraphy and Paleoenvironments," p. 16.

Unit I

Rhodolith-bearing dolomitic floatstones, similar to those occurring in Subunit IA, were recovered from Leg 133, Sites 816 and 826, on the northern margin of the Marion Plateau (Shipboard Scientific Party, 1991). The coralline algae species and associations found in these rocks suggest that they accumulated in a neritic, storm-influenced, open-plat-

form environment, at a water depth estimated between 30 and 80 m (Martín et al., 1993). This depth estimate is corroborated by the study of larger foraminiferal assemblages (Chaproniere and Betzler, 1993), which further indicate normal-salinity waters. Finer grain size, occurrence of delicate fragments of branching red algae, and the lack of centimeter-sized rhodoliths in Subunits IB and ID suggest a lower-energy, possibly deeper (up to 100 m) depositional setting for these lithologies. By contrast, the floatstone/boundstone facies rich in centimeter-sized hermatypic coral debris typical of Subunit IC probably corresponds to an in situ, shallow (< 30 m) reefal buildup.

Unit II

The occurrence of seagrass (roots and rare blades) and the larger foraminiferal assemblage (see **"Biostratigraphy and Paleoenvironments,"** p. 16) shows that the nondolomitized skeletal floatstone characterizing Subunit IIA was deposited in a shallow-water (10 to 30 m) setting. This shallow-water setting is further suggested by the occurrence of fenestrae (Core 194-1196A-22R); a well-sorted grainstone interpreted as former shoal, or even coastal sand (Cores 194-1196A-25R and 34R); and micritic crusts and mottled zones reminiscent of pedogenic calcrete profiles (Cores 194-1196A-33R and 35R) (see Tucker and Wright, 1990). The presence of rare coccoliths in this succession (Cores 194-1196A-34R and 40Z) does not contradict this interpretation, as coccoliths may be distributed from the open ocean to inshore lagoonal settings and even estuaries (Haq, 1978). The energy level during deposition of Subunit IIA was relatively high, possibly because of current action, as indicated by the lack of mud in the silt-sized floatstone matrix (Fig. **F16**). The skeletal rudstone/boundstone at the base of Unit II (Subunit IIB) likely corresponds to a shallow (patch) reef facies.

Unit III and IV

Pervasive dolomitization precludes accurate reconstruction of the paleodepositional setting of the lowermost two carbonate units encountered at Site 1196. For each subunit, however, the following scenarios can be suggested:

- Subunit IIIA: Based on the occurrence of poorly preserved branch- and dome-shaped corals, this subunit can be interpreted as a (dolomitized) reefal buildup.
- Subunit IIIB: The homogeneous texture and the presence of rare fenestrae within this sucrosic dolostone suggests it may be derived from carbonate mud deposited in a tidal-flat setting.
- Subunit IIIC: The variegated dolostones of Subunit IIIC contain ghosts of centimeter-sized rhodoliths and numerous echinoid fragments, indicating deposition on a platform in normal salinity waters. If the dense, reddish layers observed in the lower part of this unit are indeed exposure surfaces (Fig. **F18**), water depth must have been equal to or less than the amplitude of high-frequency sea level changes at that time.
- Subunit IIID: Although it is more pervasively dolomitized, Subunit IIID is lithologically similar to Subunits IB and ID, and could thus have been deposited in a moderate energy open-platform setting. The two intervals of skeletal limestone with abundant larger benthic foraminifers (Core 194-1196A-63R) are interpreted as storm beds.

Unit IV: Because of the presence of sand-sized siliciclastic grains, this unit is interpreted to be an inner-platform sediment. A water depth close to the amplitude of high frequency sea level fluctuations would account for the facies variability.

Sea Level History

Determining the magnitude and timing of eustatic sea level variations during the Miocene, particularly during the middle Miocene (Zones N12–N14), was one of the prime objectives of Leg 194. As such, the following points can be made regarding sea level variations over the platform at Site 1196:

1. During this time period, platform subsidence kept pace with long-term (second order) sea level change as all recovered units reflect a broadly similar depositional setting with water depth between 10 and 100 m.
2. Of prime importance will be the paleoenvironmental classification of the numerous indurated surfaces observed near the top of Unit IV, and the bottom parts of Subunits IIIC, IIA, and ID (Fig. F4). If subaerial, these surfaces could be interpreted as third-order sequence boundaries and would further indicate that water depth on the platform was close to the amplitude of the middle Miocene high-frequency sea level changes during the corresponding time intervals. If submarine, they would correspond to condensed horizons and suggest that this area was submerged during most of its history.
3. A possible lithologic record of the major middle Miocene (Zones N12–N14) drop in sea level could be the transition between Subunits ID and IC, when water depths rapidly diminished from ~100 to < 30 m.

Site 1199

Site 1199 is located 5 km to the east of Site 1196, slightly more proximal to the platform edge. The sedimentary succession was subdivided into three major units on the basis of carbonate mineralogy and nature of constituent particles (Fig. F24; Table T4). Unit I (0.0–159.8 mbsf) is characterized by dolomitic floatstone, rudstone, and a thin reefal interval. Unit II (159.8–410.0 mbsf) consists of nondolomitized skeletal floatstone/grainstone with shallow-water fauna. Unit III (410.0 mbsf–bottom of hole) was recovered in the core catcher of the last core and is represented by 15 cm of sucrosic dolostone. These units were further subdivided into subunits as described in the following sections.

F24. Lithologic summary, Site 1199, p. 67.

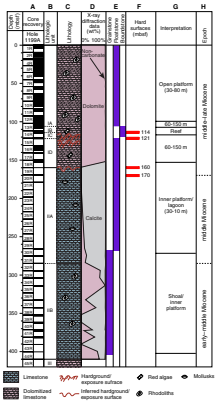

T4. Site 1199 lithologic units and tentative correlation with units defined at Site 1196, p. 131.

Lithologic Units

Unit I (0.0–159.8 mbsf; Middle[?] to Late[?] Miocene)

Subunit IA (0.0–106.6 mbsf). This subunit is identical to the one found at the same level at Site 1196. It consists of whitish to pale brown dolomitic floatstone/rudstone, characterized by the occurrence of centimeter-sized rhodoliths and coral fragments in a moderately sorted grainstone matrix. This matrix contains small benthic foraminifers, coralline algae, mollusk shells, and rare bryozoan fragments. Whole echinoids are preserved locally, and bioturbation is common in these intervals (Cores 194-1199A-12R and 13R). The top 50 cm of Subunit IA includes a reddish horizon with pronounced moldic porosity, grading to a dense,

nonporous whitish zone, and then to unaltered rock. This succession could represent a pedogenic profile. Increased recovery at Site 1199, as compared to Site 1196, provided the following new information:

1. Internal sediment within some geopetal structures consists of skeletal wackestone with planktonic foraminifers (Fig. F25). The latter might provide new biostratigraphic constraints on the age of Subunit IA .
2. Two facies, which probably reflect distinctive hydrodynamic energy conditions, can be distinguished: (a) floatstone with large (>5 cm) rhodoliths in an abundant grainstone matrix, and (b) rudstone with smaller rhodoliths (<2 cm). These facies occur in decimeter-thick alternating intervals. Crude coarse-tail grading can be locally observed in these rudstones (Fig. F26).
3. Subunit IA locally includes zones several tens of centimeters thick, where the rock is denser and shows a pink color.
4. Lastly, this unit is characterized by strong NRM intensity with respect to underlying Subunit IB.

The transition between Subunits IA and IB occurs at 106.6 mbsf in Core 194-1199A-13R and is marked by the sharp disappearance of centimeter-sized rhodoliths.

Subunit IB (106.6–114.1 mbsf). This thin subunit consists of very pale brown, well-lithified, dolomitized skeletal floatstone with a recrystallized grainstone matrix (Fig. F27). The coarse (>2 mm) fraction predominantly includes elongated fragments of branching coralline algae and centimeter-sized mollusk shells. Numerous molds of flat, larger benthic foraminifers also occur. This lithology is very similar to that observed at Site 1196, between 117.2 and 125.9 mbsf (Hole 1196A), and 122.9 and 130.5 mbsf (Hole 1196B). As in Hole 1196A, the base of Subunit IB corresponds to a marked peak in NGR intensity (see **"Core Physical Properties,"** p. 27, and **"Downhole Measurements,"** p. 32). The boundary between Subunits IB and IC is sharp and occurs at 114.1 mbsf within Core 194-1199A-14R (Fig. F27).

Subunit IC (114.1–121.9 mbsf). This subunit is characterized by beige to pink rudstone/boundstone (Fig. F27) that contains centimeter-sized hermatypic coral debris, branching coralline algae fragments, and larger benthic foraminifers. Except for rare molds, this lithology is massive and, unlike the corresponding interval at Site 1196, pervasively dolomitized. In addition, this subunit is locally leached and infiltrated by reddish silt (Fig. F28). The boundary between Subunits IC and ID occurs at 121.9 mbsf in Core 194-1199A-15R (Fig. F29).

Subunit ID (121.9–159.8 mbsf). The top of this subunit corresponds to a 3-cm-thick red layer rich in silt-sized quartz grains (Fig. F29). Below this layer, Subunit ID is mostly composed of whitish to brown dolomitic floatstone with a grainstone matrix. Primary constituents include elongated fragments of branching coralline algae, small (<1 cm) rhodoliths, mollusk shells, rare bryozoan detritus, larger benthic foraminifers that essentially occur as molds, and rare coral debris. The grainstone matrix is pervasively dolomitized with moldic porosity. Dense, dark brown dolomicrite zones, with rare molds but no texture preserved, are found in the lower part of the unit. This lithology is identical to that of Subunit ID at Site 1196, which occurs between 162.8 and 182.2 mbsf in Hole 1196A, and 145.0 and 184.9 mbsf in Hole 1196B. The boundary

F25. Close-up photograph of geopetal structure, p. 68.

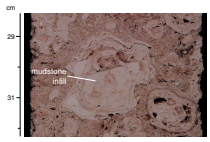

F26. Close-up photograph of interval of coarse-tail grading of rhodoliths, p. 69.

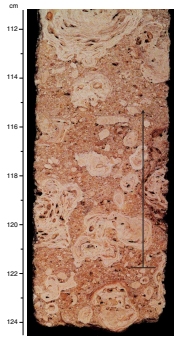

F27. Close-up photograph of Subunit IB/IC boundary, p. 70.

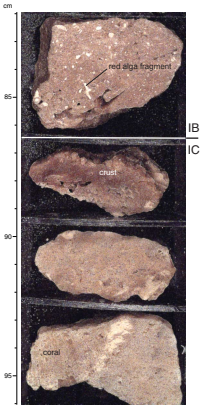

F28. Close-up photograph of vuggy porosity and infiltrated reddish silt within dolomitic skeletal rudstone, p. 71.

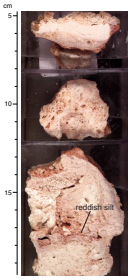

between Subunit ID and Unit II occurs between Cores 194-1199A-18R and 19R; it was not recovered.

Unit II (159.8–410.0 mbsf; Early[?] to Middle Miocene)

The lack of exposure or hardground horizons at the top of Core 194-1199A-19R suggests that the uppermost portion of Unit II has not been recovered. The dolomitic coral framestone occurring at this level in Hole 1196A was not found at this site. The uppermost interval of Unit II corresponds to low values in resistivity, density, and NGR intensity in the downhole physical property record (see **"Downhole Measurements,"** p. 32). Unit II can be partitioned into two subunits (IIA and IIB).

Subunit IIA (159.8–285.0 mbsf). This unit consists of pale brown to beige, well-lithified, slightly dolomitized skeletal floatstone with a silt-sized grainstone matrix (Fig. **F30**). Millimeter-sized constituents include larger benthic foraminifers (alveolinids), thin mollusk shells, which commonly appear as molds, and rare coral fragments. The fine grainstone matrix possibly contains red-algae clasts. Subunit IIA is also characterized by thin horizons with dark brown, dense micrite mottles and dark centimeter-thick crusts. It corresponds to an interval of relatively high NGR values in the downhole logging record (see **"Downhole Measurements,"** p. 32). Contrary to its lateral equivalent at Site 1196, Subunit IIA is slightly dolomitized and more lithified. The boundary between Subunits IIA and IIB occurs at 285.0 mbsf in Core 194-1199-32R.

Subunit IIB (285.0–410.0 mbsf). This highly porous, friable limestone unit is characterized by two facies that form meter-scale alternations. The first facies is a white to pale yellow, well-sorted, skeletal grainstone (Fig. **F31**). Grains have been leached and bioclast identification is difficult. Small benthic foraminifers, echinoid spine fragments, coralline algae and possibly *Halimeda* detritus have been recognized. Rare, meter-thick, more lithified, dolomitized intervals occur within this lithology. The second facies is slightly darker and includes centimeter-sized rhodoliths. In Hole 1196A, rare pieces of similar petrographic composition have been recovered from Cores 194-1196A-41R and 42R. Because of their rarity, small size, and similarity with shallower units at that site, they were assumed to have fallen down the hole. Hole 1196A further includes, at this level, a partly dolomitic coral rudstone facies that was recovered at Site 1199.

Unit III (410.0–419.5 mbsf [Bottom of Hole]; Early to Middle[?] Miocene)

The core catcher of the last core retrieved from Hole 1199A contains 5 cm of brilliant white, sucrosic dolostone similar to that found in Hole 1196A. Thus, it is concluded that this interval formed as an independent unit, although we can not totally exclude that it represents a dolomitized interval within Subunit IIB.

Discussion

Paleoenvironmental Reconstruction

Paleodepositional environments, as outlined below, have been determined from petrographic and sedimentological data and are proposed for each lithologic unit from Site 1199.

F29. Close-up photograph of Subunit IC/ID boundary, p. 72.

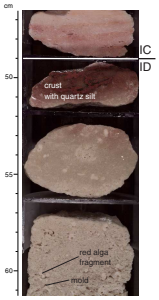

F30. Close-up photograph of Subunit IIA lithology, p. 73.

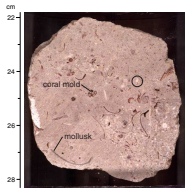

F31. Close-up photograph of Subunit IIB lithology, p. 74.

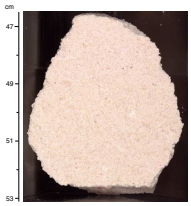

Unit I

The rhodolith-bearing dolomitic floatstone found in Subunit IA suggests deposition on an open-platform at water depths estimated to be between 30 and 100 m (middle neritic; see **"Biostratigraphy and Paleoenvironments,"** p. 16). The occurrence of wackestone with planktonic foraminifers in intraparticle voids reinforces the validity of these depth estimates. Varying hydrodynamic energy, likely related to storm action, is supported by the presence of distinctive facies (floatstone with large rhodoliths and rudstone with small rhodoliths) and crude coarse-tail grading in some sediment intervals. Further study is required to determine whether the dense pink-colored zones correspond to exposure horizons or, more likely, to submarine hardgrounds. As discussed for Site 1196, the dolomitic floatstones rich in coralline algae fragments characterizing Subunit IB were also deposited in an open-platform setting, possibly at slightly deeper water depths. The dolomitic coral-rich rudstone of Subunit IC represents a shallow reefal facies. These rocks overlie, and are overlain by, reddish crusts interpreted as exposure surfaces. Widespread vuggy porosity and the presence of internal sediment consisting of reddish silt further support this interpretation. Downhole logging data (see **"Downhole Measurements,"** p. 32), as well as these diagenetic features suggest that Subunit IC has been pervasively karstified. As with Subunit IB, Subunit ID was deposited in a low-energy open-platform setting.

Unit II

The slightly dolomitic floatstone, rich in porcellaneous benthic foraminifers (alveolinids), mollusk shells, and rare coral fragments characterizing Subunit IIA, was probably deposited in an inner-platform setting at shallow-water (<30 m) depths. In contrast to its lateral equivalent at Site 1196, no evidence of seagrass roots or blades was found in Subunit IIA to support this paleoenvironmental interpretation. Shallow-water deposition is supported by the presence of several horizons with centimeter-thick brown crusts, interpreted as calcretes, and brown mottles possibly corresponding to rhizoliths. The well-washed, whitish, skeletal grainstone found in Subunit IIB could represent high-energy shoal deposits laid down in relatively shallow water. By contrast, the alternating rhodolith-rich, skeletal floatstone could represent a slightly deeper depositional setting analogous to that of Subunit IA.

Unit III

Limited recovery and pervasive dolomitization prevent accurate reconstruction of the paleodepositional setting of this sucrosic dolostone.

Sea Level History

The stratigraphic succession recovered at Hole 1199A consists of diverse carbonate facies that reflect variations in accommodation space during the middle, and possibly the late Miocene. A progressive shallowing-up trend is recorded from the high-energy shoal facies of Subunit IIB to the lower-energy, shallow inner-platform or lagoonal sediments typical of Subunit IIA. The presence of several potential exposure horizons in this interval suggests that water depth may have been comparable to the amplitude of middle Miocene high-frequency sea level changes. In contrast to Site 1196, no exposure surface was recovered from the top of Unit II. A rapid sea level fall must have occurred after deposition of Subunit ID, as shown by the direct superposition of an ex-

posure surface on this open-platform facies. Marked reddening and the presence of quartz silt of possible eolian origin further indicate an important hiatus at this level, which could correspond to the middle/upper Miocene boundary. Accommodation space was limited during deposition of the Subunit IC reefal unit, which is karstified and framed by exposure surfaces. Following a transgression and a deepening-upward trend during most of Subunit IB deposition, conditions became shallower again throughout Subunit IA, leading to subaerial exposure and pedogenesis at the end of this last phase of carbonate platform growth.

BIOSTRATIGRAPHY AND PALEOENVIRONMENTS

Site 1196

Hole 1196A is composed of 662.6 m of Miocene limestone and dolomite underlain by upper Oligocene siliciclastics. Calcareous nannofossils found near the middle of the carbonate platform sequence indicate an age of 13.6–18.2 Ma. Nannofossils were also found in claystone directly below the carbonate platform sequence beginning at Core 194-1196A-70R), providing an estimated age of 24.2–24.6 Ma. The latter sample was also examined for planktonic foraminifers, but only rare, non–age diagnostic taxa were found. Core catcher samples of lithified reef facies were not processed for nannofossils or planktonic foraminifers, as representative samples proved to be barren of these microfossils. A thin section of Sample 194-1196A-1R-1, 1–4 cm, contained age-diagnostic planktonic foraminifers of the *Globorotalia tosaensis–truncatulinoides* lineage and provided a maximum age of 3.2 Ma.

Microscopic analysis of biogenic constituents including benthic foraminifers provided data for biostratigraphic analysis and paleoenvironmental interpretation. Distinctive benthic foraminifers in Samples 194-1196A-25R-1, 78 cm, through 35R-1, 38 cm, and 194-1196B-33Z-1, 79–81 cm, through 51Z-1, 0–5 cm, indicate an age of 13.3–15.2 Ma. Core catcher samples were the primary basis for analysis, supplemented by thin sections and direct core observations. Table **T5** summarizes those observations.

T5. Summary of biostratigraphic and paleoenvironmental interpretations, Site 1196, p. 132.

Calcareous Nannofossils

Hole 1196A

Although the first two core catcher samples were processed for nannofossils examination, no specimens were found. The remaining core catcher samples are lithified reef facies and were not processed for nannofossils. However, Sample 194-1196A-34R-1, 40–44 cm, from a thin siltstone bed near the middle of the carbonate platform (see **"Lithostratigraphy and Sedimentology,"** p. 5) contains the following taxa: *Coccolithus pelagicus, Reticulofenestra haqii, Reticulofenestra producta, Sphenolithus abies,* and *Sphenolithus heteromorphus*. The presence of the last species constrains the age of the sample to 13.6–18.2 Ma. Another sample from the last core immediately below the carbonate platform (Sample 194-1196A-70R-1, 133 cm) contains common well-preserved nannofossils including *Zyghrablithus bijugatus, Reticulofenestra bisecta,* and *Cyclicargolithus floridanus*. This assemblage, coupled with the absence of *Sphenolithus ciperoensis,* suggests an age of 24.2–24.6 Ma.

Hole 1196B

Samples 194-1196B-20Z-CC, 32Z-CC, 45Z-CC, and 47Z-CC are barren of calcareous nannofossils. Sample 194-1196B-40Z-1, 2 cm, contains rare nannofossils including *S. heteromorphus,* which constrains the age to 13.6–18.2 Ma. Samples 194-1196B-40Z-1, 18 cm, and 49Z-CC also contain rare nannofossils, which reflect impoverished assemblages of middle to early Miocene age.

Benthic Foraminifers

Hole 1196A

Benthic foraminifers characteristic of shallow carbonate platform environments are abundant throughout most of the sequence sampled in Hole 1196A (Table **T5**). Rhodoliths and red algal fragments are the major constituents of the limestones and dolomites, found in Samples 194-1196A-1R-1, 112–114 cm (1.12 mbsf), through 65R-5, 30–33 cm (621 mbsf).

In lithologic Unit I (see **"Lithostratigraphy and Sedimentology,"** p. 5), benthic foraminifers belonging to the common tropical genus *Amphistegina* are abundant in most rhodolith-dominated facies. In this facies, benthic foraminifers are sufficiently well preserved to be identified in hand specimen or by surficial examination using a stereomicroscope (e.g., Samples 194-1196A-1R-1, 112–114 cm [1.12 mbsf], through 10R-1, 132–134 cm [87.12 mbsf]; Table **T5**). Thin sections are required to determine the taxa of larger benthic foraminifers that accompany *Amphistegina*. For example, Sample 194-1196A-1R-1, 1–4 cm, confirmed not only the presence of very robust, often broken and rounded *Amphistegina* but also exceptionally robust *Operculina complanata* and a small piece of a specimen of *Lepidocyclina* sp.

In Samples 194-1196A-9R-2, 73–75 cm (78.25 mbsf), through 16R-1, 74–76 (144.24 mbsf), and 18R-3, 118–121 (166.85 mbsf), through 19R-3, 60–62 cm (175.8 mbsf), the larger benthic foraminifers were primarily seen as molds of varying morphologies (Table **T5**).

The benthic foraminiferal assemblage in Samples 194-1196A-20R-1, 111–113 cm (183.01 mbsf), through 35R-1, 38–40 cm (326.68 mbsf) (lithologic Subunit IIA; see **"Lithostratigraphy and Sedimentology,"** p. 5) is characterized by abundant porcellaneous foraminifers of the order Miliolina. Of key importance is the occurrence of *Flosculinella botangensis* (Fig. **F32**), which is believed to be restricted to Zones N9–N10 (13.3–15.2 Ma) in northern Australia (Chaponiere, 1984). These alveolinids occur with large soritid foraminifers including an unknown species with characteristics of the genus *Cyclorbiculina* (Fig. **F33**), as well as very abundant members of the family Miliolidae. In Samples 194-1196A-39R-1, 0–2 cm (364.7 mbsf), through 42R-1, 14–16 cm (393.64 mbsf), which are part of lithologic Subunit IIIA (see **"Lithostratigraphy and Sedimentology,"** p. 5), small rhodoliths occur in a grainstone that contains abundant *Lepidocyclina* and *Amphistegina*.

Samples 194-1196A-44R-1, 107–109 cm (413.75 mbsf), through 65R-5, 30–33 cm (620.95 mbsf), which make up lithologic Unit III and the top of Unit IV (see **"Lithostratigraphy and Sedimentology,"** p. 5), are heavily dolomitized, and generally larger foraminifers are only preserved as molds. In Samples 194-1196A-44R-1, 107–109 cm (413.75 mbsf), though 51R-4, 56–58 cm (484.93 mbsf), Sample 194-1196A-53R-4, 122–124 cm (504.92 mbsf), and Samples 194-1196A-62R-1, 42–47 cm (586.22 mbsf), through 63R-2, 46–48 cm (597.45 mbsf), abundant

F32. Photomicrograph of transverse section of *Flosculinella botangensis* specimen, p. 75.

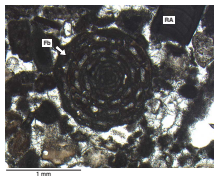

F33. Photomicrograph of vertical section of a Soritidae specimen, p. 76.

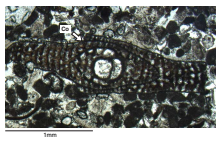

molds indicate that large, flat benthic foraminifers were an important constituent of the original sediment. In Samples 194-1196A-57R-3, 30–32 cm (540.93 mbsf), through 61R-2, 46–48 cm (578.13 mbsf), molds indicative of robust larger benthic foraminifers are abundant. In Samples 194-1196A-64R-3, 145–150 cm (609.5 mbsf), and 65R-5, 30–33 cm (620.95 mbsf), the molds are smaller and indicative of abundant *Amphistegina* in the original sediment. Samples 194-1196A-52R-6, 46–48 cm (497.60 mbsf), and 54R-1, 127–129 cm (510.17 mbsf), through 56R-2, 47–49 cm (529.75 mbsf), appear to have a fine grainstone fabric with red algal and soritid debris, which may originally have been similar to Subunit IIA.

Lithologic Unit IV includes various facies of siliciclastic-rich dolostone (see **"Lithostratigraphy and Sedimentology,"** p. 5). Two samples from this unit, Samples 194-1196A-66R-4, 106–108 cm (629.78 mbsf), and 67R-2, 90–93 cm (635.98 mbsf), contain fragments of bryozoans and red algae with abundant larger foraminifers, particularly *Operculina complanata*. Lithologic Unit V was dominantly siliciclastic and phosphatic; marine nannofossils were recovered from Sample 194-1196A-70R-1, 133 cm.

Hole 1196B

Benthic foraminifers characteristic of shallow carbonate platform environments are abundant throughout the sequence sampled in Hole 1196B (Table **T5**), which was wholly within lithologic Units I and II (see **"Lithostratigraphy and Sedimentology,"** p. 5). Rhodoliths, red algal crusts, and fragments are the major constituent of algal-dominated facies found in Samples 194-1196B-1R-3, 37–40 cm (3.29 mbsf), through 32Z-1, 27–29 cm (180.47 mbsf). As in Hole 1196A, benthic foraminifers belonging to the common tropical genus *Amphistegina* are major constituents of the grainstone and packstone matrices of the rhodolith-dominated facies that are sufficiently well preserved to identify the foraminifers in hand specimen or by surficial examination using a stereomicroscope. Thin sections are required to determine the range of taxa of larger benthic foraminifers.

The benthic foraminiferal assemblage in Samples 194-1196B-33Z-1, 79–81 cm (185.69 mbsf), through 51Z-1, 0–5 cm (260.6 mbsf) (lithologic Subunit IIA; see **"Lithostratigraphy and Sedimentology,"** p. 5), contains abundant porcellaneous foraminifers of the order Miliolina. *F. botangensis* (Fig. **F32**) is again abundant in samples from this subunit. In addition, *Astrotrillina howchini,* which has commonly been found in association with *F. botangensis* by Chaproniere (1981, 1984), was also recorded in Sample 194-1196B-49Z-1, 30–37 cm (251.5 mbsf).

Interpretation

Biostratigraphic evidence provided in Table **T5** indicates a late Oligocene to possible late Miocene age range for the sequence sampled at Site 1196. The occurrence in lithologic Subunit IIA of the alveolinid, *F. botangensis,* whose age range is Zones N9–N10 (N12?), combined with data provided by nannofossils for Sample 194-1196A-34R-1, 40–44 cm (317.0 mbsf), and 194-1196B-40Z-1, 2 cm (217.8 mbsf), indicates a middle Miocene age between 13.3 and 15.2 Ma for that subunit.

Interpreting paleowater depths and depositional environments is somewhat problematic, given the poor core recovery (~13%; see **"Operations,"** p. 2). Rhodoliths and red algae, which are the dominant constituents of most of the rocks in this sequence, can dominate carbonate facies from intertidal to depths of 150 m (Tsuji, 1993).

Likewise, the larger benthic foraminifers can occur over this range. *Amphistegina, Operculina, Cycloclypeus,* and *Lepidocyclina* are genera whose assemblages and test morphologies tend to reflect ambient light levels and water motion. Robust morphologies are most common in shallow, high light, high energy environments, often <10 m and generally <30 m water depth. For example, the robust, frequently broken *Amphistegina* specimens seen in the thin section from Sample 194-1196A-1R-1, 1–4 cm, may indicate beach sand, particularly when considered along with the cementation history that suggests subaerial exposure (see **"Lithostratigraphy and Sedimentology,"** p. 5). Flatter morphologies are typical of deeper, quieter, lower-light conditions below 60 m. Very flat morphologies and the predominance of very large *Cycloclypeus* spp. are typically found at depths between 100 and 150 m. No biofacies indicative of these extremes were seen in the sequence.

Shape trends in the larger foraminiferal tests and molds, combined with information on the presence and types of coralline algae, coral, and other lithologic details (see **"Lithostratigraphy and Sedimentology,"** p. 5) were used to interpret paleowater depths as shown in Table **T5** and are summarized below. Thin section analyses will undoubtedly refine or revise these interpretations.

Unit V is partly siliciclastic and of unknown water depths. Unit IV is mixed siliciclastics and bioclastic carbonates. In modern reef and open-shelf environments, *Operculina* are most commonly found at middle neritic depths (30–100 m) (Hohenegger, 1999). However, they can live in shallower environments where limited siliciclastic input diminishes water transparency (e.g., Hallock, 1984). The abundance of relatively robust *Operculina* in the middle of this interval, which contains not only significant siliciclastics but also exposure surfaces, likely indicates an inner-neritic water-depth range of <30 m.

Highly dolomitized intervals of Unit III are difficult to interpret because red algal crusts and fragments are often the only identifiable constituent. A possible exposure surface at the base of Subunit IIID, overlain by dolomites with *Amphistegina*-type molds then flat *Lepidocyclina*- and *Operculina*-type molds, may indicate a deepening upward from inner to middle neritic depths (Table **T5**). This interval is followed by more robust molds, indicating shallowing into Subunit IIIC. Several possible exposure surfaces have been observed within Subunit IIIC (see **"Lithostratigraphy and Sedimentology,"** p. 5). The upward return to fabrics with flat *Lepidocyclina*- and *Operculina*-type molds suggests another deepening to middle neritic depths in the upper part of Subunit IIIB and in Subunit IIIA. The larger foraminiferal molds again become more robust in Subunit IIB, indicating shallowing to possible exposure surfaces near the base of Subunit IIA.

The soritid and miliolid foraminifers abundant in Subunit IIA commonly occur in association with seagrass. Thus, the abundance of these foraminifers, combined with frequent occurrences of trace fossils that probably derive from seagrass blades and roots, indicate that much of Subunit IIA was deposited in water depths of <10 m, certainly no deeper than 30 m. The grainstone fabric of these sediments, as noted in sample thin sections 194-1196A-33R-1, 19–23 cm, and 33R-1, 121–125 cm, indicate sufficient water motion to remove mud-sized particles despite the sediment baffling potential of the seagrass. This fabric indicates a shallow, open-platform setting, perhaps similar to Seranilla Bank on the Nicaraguan Rise in the western Caribbean (Triffleman et al., 1992), rather than a sheltered lagoonal setting.

Interestingly, the 143-m-thick Subunit IIA provides the strongest evidence for a prolonged episode of very shallow water. It is also the best age-constrained interval at 13–15 Ma, which is also approximately the time of the highest sea level stand during the middle Miocene (Haq et al., 1987). Open-platform sedimentation rates can be estimated in the range of 20–50 cm/k.y. (e.g., Hallock, 1981). Thus, 143 m of sediment could represent ~0.3–0.7 m.y. of accumulation. It may be more problematic explaining the availability of 143 m of accommodation space through this interval, as sea level rise was likely <100 m within the third-order cycle 2.4 (Haq et al., 1987), and subsidence rates are estimated to be an order of magnitude lower (see the Leg 194 Scientific Prospectus).

Possible exposure surfaces are interpreted at the top of Subunit IIA and in Subunit ID (see **"Lithostratigraphy and Sedimentology,"** p. 5). Subunit IC appears to represent a reef interval characterized by coral/algal boundstones. The grainstones of Subunit IB are quite similar to those in Subunit ID and could possibly represent carbonate sands shed from a reef. The history of the late middle Miocene sea level fall may be contained within the Subunits ID–IB interval. Subunit IA likely represents a deepening upward to middle neritic depths in an open-platform setting. This was followed by a final shallowing trend to possible beach sands at the top, just below a hiatal surface, which is discussed in more detail in **"Lithostratigraphy and Sedimentology,"** p. 5.

The age of Unit I is uncertain. The occurrence of *Lepidocyclina* spp. near the top of lithologic Unit I (i.e., a fragment in Sample 194-1196A-1R-1, 1–4 cm [0.01 mbsf] and a whole specimen in Core 194-1196A-6R-1, 76 cm [48.26 mbsf]) suggests a middle Miocene age (Zone N12) for the shallow-water carbonates at the platform top (Chaproniere 1981, 1984; Chaproniere and Betzler, 1993). However, recent studies from the Queensland Plateau indicate that the range of *Lepidocyclina* extends into the late Miocene (Betzler, 1997). Very recent data from Papua New Guinea also indicate that *Lepidocyclina* may extend into the late Miocene to at least Zone N16 (8.4 Ma) (Allan et al., 2000). Results from offshelf sites from Leg 194 could provide clarification of the upper age range of *Lepidocyclina* in this region.

Site 1199

Hole 1199A consists of 410.1 m of Miocene limestones and dolomites, as indicated by the assemblages of larger benthic foraminifers. Core catcher samples of lithified reef facies were not processed for nannofossils or planktonic foraminifers, as representative samples proved to be barren of these microfossils. Distinctive benthic foraminifers in several samples between Sample 194-1199A-20R-1, 93 cm (170.3 mbsf), and 30R-1, 39 cm (265.9 mbsf), indicate an age of 13.3–15.2 Ma for this interval. Core catcher samples were the primary basis for analysis, supplemented by direct core observations. Table T6 summarizes these observations.

T6. Summary of biostratigraphic and paleoenvironmental interpretations, Site 1199, p. 135.

Benthic Foraminifers

Hole 1199A

Benthic foraminifers characteristic of shallow carbonate platform environments are abundant throughout most of the sequence in Hole 1199A (Table T6). Red algae (as rhodoliths) and larger benthic foraminifers are the major constituents of both limestones and dolomites that

are found in Samples 194-1199A-1R-4, 21–23 cm (4.52 mbsf), through 45R-1, 16–18 cm (410.1 mbsf) (see "Lithostratigraphy and Sedimentology," p. 5).

In lithologic Subunit IA (see "Lithostratigraphy and Sedimentology," p. 5), benthic foraminifers belonging to the common tropical genus *Amphistegina* are abundant as at Site 1196. Large individual specimens of *Lepidocyclina* were seen in Samples 194-1199A-6R-3, 50 cm (39.2 mbsf), and 7R-2, 20 cm (46.7 mbsf), confirming a Miocene age. The assemblages of larger benthic foraminifers in Unit I indicate euphotic depths of <100 m.

The benthic foraminiferal assemblages between Samples 194-1199A-20R-1, 93–95 cm (170.3 mbsf), and 30R-1, 39–41 cm (265.9 mbsf) Subunit IIA; see "Lithostratigraphy and Sedimentology," p. 5), are more variable than comparable intervals at Site 1196. Nevertheless, porcellaneous foraminifers of the order Miliolina are again important sediment constituents in this interval. The sporadic occurrence of *F. botangensis* (Table T6) is of key significance, as it is believed to be restricted to Zones N9–N10 (13.3–15.2 Ma) in northern Australia (Chaproniere, 1984). Soritids are much less prominent in this interval than at the comparable depths at Site 1196 (see Table T5).

Samples 194-1199A-35R-1, 130–132 cm (315 mbsf), through 45R-1, 16–18 cm (410.1 mbsf), which are part of lithologic Subunit IIB (see "Lithostratigraphy and Sedimentology," p. 5), represent a larger benthic foraminiferal and red algal-dominated grainstone to floatstone facies that was not seen at Site 1196. The assemblage of larger benthic foraminifers, characterized by the overwhelming dominance of *Lepidocyclina* in Subunit IIB, differs from that in Subunit IA, which is more diverse and tends to be dominated by *Amphistegina*.

Interpretation

Biostratigraphic evidence provided by the larger benthic foraminifers indicates a Miocene age for the sequence sampled at Site 1199. The occurrence in lithologic Subunit IIA of the alveolinid *F. botangensis,* whose range is Zones N9–N10 (Chaproniere, 1981, 1984), indicates a middle Miocene age for this subunit. As at Site 1196, the occurrence of *Lepidocyclina* in Unit I suggests a middle to late Miocene age (i.e., Chaproniere, 1981, 1984; Chaproniere and Betzler, 1993; Betzler, 1997).

The red algae and larger benthic foraminifers found in Unit I can dominate carbonate facies from intertidal to depths of 150 m (Hallock, 1984; Tsuji, 1993). Shape trends in the larger foraminiferal tests and molds, combined with information on the presence and types of coralline algae, coral, and other lithologic details (see "Lithostratigraphy and Sedimentology," p. 5), suggest paleowater depths as <100 m (Table T6).

Paleodepth estimates for lithologic Subunit IIA are not as straightforward as at comparable platform depths at Site 1196. At Site 1199, soritids were much less common, and no organic trace fossils were observed that would indicate a seagrass environment. Sediments at Site 1199 were subject to poor recovery and were relatively more variable. Combined with the 22-m elevation difference in the unit top between sites (182 mbsf at Site 1196 and 160 mbsf at Site 1199) (see "Lithostratigraphy and Sedimentology," p. 5), this facies variability on the scale of kilometers suggests some relief on the platform top. Paleowater depths are conservatively interpreted as shallower than 30 m throughout this interval.

Lithologic Subunit IIB is dominated by larger foraminifer-rich grainstone and floatstone with varying proportions of red algae. The abundance, robustness, and sorting of the *Lepidocyclina* indicate a range of paleowater depths between intertidal and <100 m.

PALEOMAGNETISM

Site 1196

The natural remanent magnetization (NRM) of archive core sections of RCB cores from Site 1196 was measured at 5-cm intervals, where practical, using the pass-through cryogenic magnetometer. Many sections were not measured in their entirety because they contained fragments that had possibly rotated within the core barrel. In Hole 1196B, an additional measurement difficulty was that the diameter of the recovered ADCB cores was too large to fit in the magnetometer. To measure these cores intact, intervals <6 cm in length were rotated so that they would fit into the magnetometer. The downhole +z-component then became the +y-component of the instrument. This reorientation has been noted in the ODP database. Unfortunately, this precluded the use of the most favorable longer intervals from measurement. NRM was measured throughout using a 5-mT and 30-mT alternating-field (AF) demagnetization.

In addition, discrete samples were collected from Hole 1196A. These were used to aid the interpretation of the long-core record of magnetization by providing additional measurements of polarity and basic magnetic characterization.

Results

Long-Core Measurements and Magnetostratigraphy

The principal difficulty at Site 1196 was poor recovery. The sediments were, for the most part, reasonably magnetized with average NRM intensities of 10^{-3} A/m, and the magnetization showed well-defined trends on AF demagnetization (Fig. **F34**). The characteristic remanent magnetization (ChRM) appeared after 30-mT demagnetization. The inclination and the total intensity are presented for Hole 1196A in Figure **F35.** The poor recovery precludes detailed magnetostratigraphic interpretation, although intervals of reversed polarity predominate toward the top of the recovered section. The magnetization intensity increases markedly in some of the red-stained lithologies and in the dark material at the bottom of the hole.

Data from 1196B were collected on RCB cores to a depth of 104 mbsf and below, for an interval of ~100 m on cores drilled with the ADCB. Because the sampled ADCB cores were measured in an unorthodox configuration, only the y-component is plotted and, in this coordinate system, a positive y is equivalent to a reversed polarity. The results are shown in Figure **F36** with the inclination from Hole 1196A for the uppermost 200 mbsf. Despite some intervals in which there are conflicting results between Holes 1196A and 1196B, the data from Hole 1196B are consistent with the interpretation of a predominantly reversed polarity in this interval.

F34. Zijderveld plot for long-core interval, p. 77.

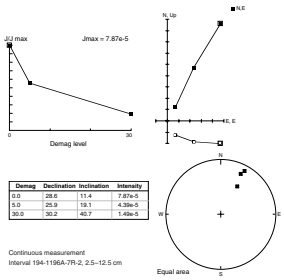

Demag	Declination	Inclination	Intensity
0.0	28.6	11.4	7.87e-5
5.0	25.9	19.1	4.39e-5
30.0	30.2	40.7	1.49e-5

F35. Long-core measurements of intensity and inclinations, p. 78.

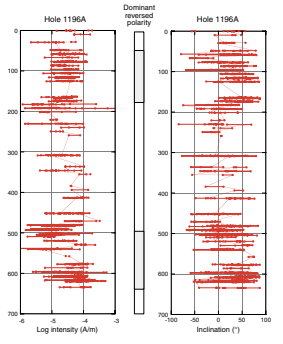

F36. Long-core measurements for Holes 1196A and 1196B, p. 79.

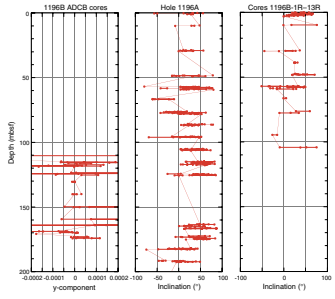

Discrete Samples

A relatively large number of discrete samples were studied at this site in an attempt to correlate magnetic properties with the range of lithologies encountered and to investigate the possible expression of diagenesis in magnetic properties and magnetization. Standard rock magnetism analysis was carried out on discrete samples (see "Paleomagnetism," p. 15, in the "Explanatory Notes" chapter), and samples with sufficiently strong intensity of magnetization were subjected to principal component analysis. Of the few samples magnetized strongly enough to permit analysis of NRM, most were very stable against AF demagnetization. An extreme example of one of the red-stained intervals is shown in Figure F37.

The downhole variation of NRM, anhysteretic remanent magnetization (ARM), and isothermal remanent magnetization (IRM) reveals that in the uppermost 200 mbsf the sediments generally have a relatively low magnetic content and are weakly magnetized (Fig. F38). The ratio of IRM acquired in a 100-mT field to IRM is close to one in almost all of the samples measured, indicating magnetite as the dominant phase. The notable exception is the interval between 610 and 626 mbsf, where the red-stained lithologies predominate and where intensity values are extreme (Fig. F39). The ratio of IRM after 40-mT demagnetization to the initial IRM exhibits overall values near to one-tenth, with the only exception again in the interval between 610 and 626 mbsf where values reach one. This pattern is consistent with the dominance of magnetite in most of the section, and hematite as the dominant magnetic phase between 610 and 626 mbsf.

Beneath the red cemented sequence, Sample 194-1196A-70R-3, 94–96 cm, comes from the dark siliciclastic unit at the base of the recovered section and appears to be an excellent paleomagnetic recorder, as indicated by its AF demagnetization behavior. The acquisition of IRM suggests that magnetite is the dominant magnetic phase present.

Site 1199

Results

Long-Core Measurements and Magnetostratigraphy

Because of good recovery at Site 1199, it was possible to produce a limited magnetic stratigraphy. The average magnetization of Site 1199 sediments is ~$10^{-3.5}$ A/m. Intensities vary between $10^{-4.5}$ and $10^{-2.5}$ A/m. These variations tend to occur across polarity transitions; however, a remarkable upcore intensity increase of two orders of magnitude occurs at about 103 mbsf (Fig. F40B). This level coincides with the change from Subunit IA to Subunit IB (see "Lithostratigraphy and Sedimentology," p. 5). It also coincides with a polarity transition from reversed to normal. The sediments showed a well-defined and stable magnetization trend on AF demagnetization (Fig. F41). As a result, we obtained what appears to be a ChRM with a slight normal overprint isolated between 20- and 30-mT demagnetization steps.

Measured inclination and total intensity after 30-mT demagnetization are presented for Site 1199A in Figure F40. Because data were collected on RCB cores, the data sets are shifted toward normal polarities as seen at Site 1196. Intervals with highly negative inclination were considered normal, whereas intervals with gentle-negative to positive inclination were considered reversed polarity. Poor core recoveries

F37. Zijderveld plot for Sample 194-1196A-65R-3, 94–96 cm, p. 80.

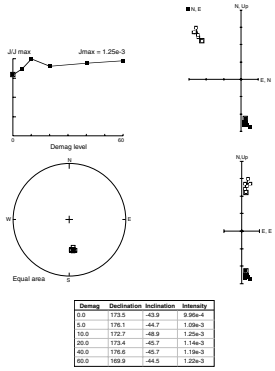

Demag	Declination	Inclination	Intensity
0.0	173.5	-43.9	9.96e-4
5.0	176.1	-44.7	1.09e-3
10.0	172.7	-48.9	1.25e-3
20.0	173.4	-45.7	1.14e-3
40.0	176.6	-45.7	1.19e-3
60.0	169.9	-44.5	1.22e-3

F38. Variation of intensity of NRM, ARM, and IRM, p. 81.

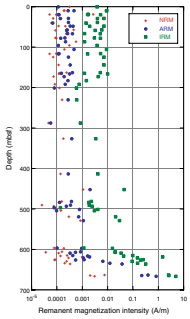

F39. Variation of rock magnetism parameters, p. 82.

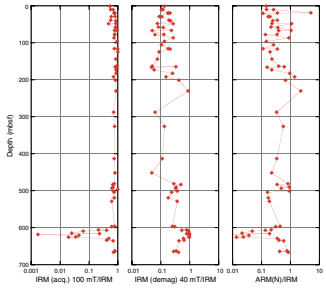

F40. Long-core measurements, p. 83.

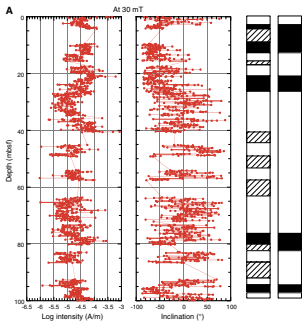

make interpretation difficult for a few intervals, as shown by hatched rectangles in F40. For all these cases, observed polarity continues across nonrecovery intervals.

Data from Site 1196, where intensive rock magnetic studies were performed, indicate that for the top 150 mbsf, the dominant magnetic mineral carrying remanence is magnetite. Some rock magnetic analyses performed at this site showed magnetic behavior similar to that of Hole 1196A. The magnetite is characterized by small values of *R* (point of intersection of IRM acquisition and IRM demagnetization), indicating the interacting nature of the magnetite, which suggests a diagenetic history perhaps related to zones of dolomitization (see "Lithostratigraphy and Sedimentology," p. 5). No effect of this history on the direction of magnetization has been observed. Instead, preliminary results suggest that the dolomitization has no impact on the preservation of the original ChRM.

F41. Example of an orthogonal vector component diagram, p. 85.

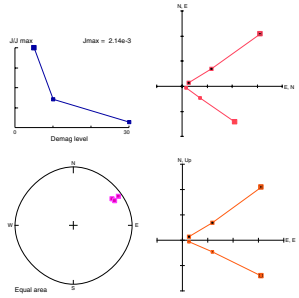

AGE MODEL

The age model for the carbonate platform sequence sampled at Site 1196 (672 mbsf; Oligocene to Pleistocene) and Site 1199 (420 mbsf; Miocene to Pleistocene) is poorly defined (Table T7; Fig. F42) (see "Biostratigraphy and Paleoenvironments," p. 16). At Site 1196, one planktonic foraminifer datum at the very top of the sequence and one nannoplankton datum at the very bottom of the sequence define the total age range of the sequence. In addition, the age range of *Sphenolithus heteromorphus* in two samples and the age range of the larger benthic foraminifer *Flosculinella botangensis,* observed between 183 and 327 mbsf, constrain the middle part of the section to the middle Miocene. This important observation rejects the original working hypothesis for Site 1196, which presumed that the middle Miocene was represented here by distal slope deposits and not a carbonate platform. At Site 1199, *Flosculinella* was observed in a depth interval similar to that at Site 1196.

A magnetostratigraphy could not be established at Sites 1196 and 1199 because of poor core recovery (see "Paleomagnetism," p. 22).

Sedimentation rates are not presented because of the poor biostratigraphic resolution. Age picks for lithologic and seismic unit boundaries are presented in Figure F42 and Table T8; uncertainty in the age picks is in the range of a few million years.

T7. Age-depth control points, p. 137.

F42. Age-depth model and sedimentation rates, p. 86.

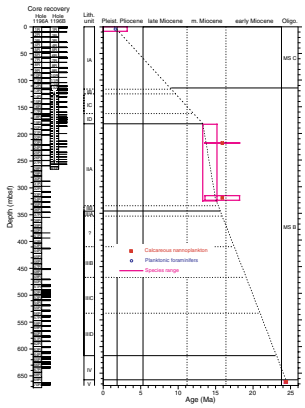

T8. Age picks, p. 138.

GEOCHEMISTRY

Site 1196

Volatile Hydrocarbons

Concentrations of volatile hydrocarbon gases were not measured at Site 1196 because of the generally porous nature of the strata.

Interstitial Water Chemistry

Poor core recovery and the dolomitized and highly indurated lithologies encountered during drilling at Site 1196 prevented pore water sampling.

X-Ray Diffraction Carbonate Mineralogy

Ninety-three sediment samples were analyzed for carbonate mineralogy from Site 1196 (Fig. **F43;** Table **T9**). Carbonate mineralogy in the recovered lithologies varies greatly from pure dolostones to pure limestones. Lithologic Unit IA, the upper 180 m of section, is predominantly dolomite with two relatively thin limestone units between 30 and 50 mbsf and 65 and 75 mbsf. In contrast, lithologic Unit II, from 180 to 350 mbsf, is a nearly pure limestone unit. Lithologic Subunit IIIA is also primarily calcite (Fig. **F43;** Table **T9**). Only one sample over the depth interval from 350 to 400 mbsf was found to contain significant dolomite (>40 wt%). Lithologic Subunits IIIB, IIIC, and IIID and Unit IV are all heavily to completely dolomitized. Only at the base in the lowermost sample is calcite again present.

F43. Carbonate mineralogy, p. 87.

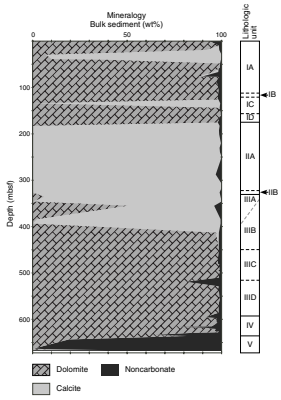

Sedimentary Geochemistry

Results

Calcium carbonate ($CaCO_3$) contents at Site 1196 range from ~0.5 to 108 wt%. Measurements are calibrated for calcite; thus, the presence of dolomite can generate values >100 wt%. Total organic carbon (TOC) content is mostly near zero at Site 1196 except between ~185 and 260 mbsf (up to >0.3 wt%) and from ~640 mbsf to total depth (up to >0.8 wt%). These relative TOC enrichments coincide with reduced carbonate contents, particularly in the lower horizon. Note that TOC content values from Rock-Eval pyrolysis and carbon-nitrogen-sulfur analyses provide similar profiles but with different values (Fig. **F44;** Tables **T10, T11**).

T9. Calcite, dolomite, and noncarbonate minerals, p. 139.

Hydrogen index (HI) values at Site 1196 range from 0 to 300 mg HC/g TOC (Fig. **F44;** Table **T11**), but the low TOC content of some intervals limits the reliability of these values. We performed duplicate and triplicate analyses on low TOC samples with a resulting error of <10%. Oxygen index (OI) values vary from 0 to 65,200 mg CO_2/g TOC (Table **T11**). The high OI values are attributed to the thermal degradation of carbonate minerals during pyrolysis and are not considered in this interpretation. T_{max} values range from 311° to 439°C (Table **T11**), although the most reliable values cluster between 400° and 420°C.

F44. Carbon, HI, and sulfur results, p. 88.

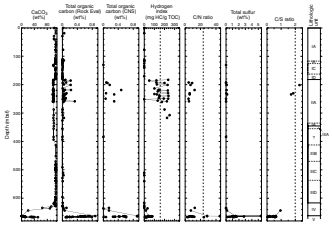

Total sulfur (S) content in Site 1196 sediments ranges from 0.0 to ~5.38 wt% (Fig. **F44;** Table **T10**), and its distribution is similar to that of TOC. C/N and C/S ratios (Fig. **F44;** Table **T10**) are compatible with interpretations of a marine-dominated environment of formation, although C/N ratios indicative of terrigenous organic matter input were observed in the basal lithologic unit.

T10. Carbon, nitrogen, sulfur, and hydrogen concentrations, p. 140.

T11. Rock-Eval pyrolysis results, p. 143.

Discussion

Variations in the generally high $CaCO_3$ content of sediments at Site 1196 mostly reflect variations in carbonate mineralogy (i.e., calcite or dolomite) and the ratio of biogenic carbonate to terrigenous sedimentation through time. Little to no organic matter was detected in Unit I. However, slightly higher TOC (up to >0.3 wt%) was measured between ~180 and 260 mbsf associated with an interval containing seagrass (see **"Biostratigraphy and Paleoenvironments,"** p. 16). This organic matter is associated with slightly reduced $CaCO_3$ contents, which may have resulted from dilution by detritus associated with the elevated TOC. On the other hand, the lack of organic matter in the overlying and under-

lying dolostone intervals may be a function of organic matter destruction during dolomitization.

The slightly elevated HI (average = ~171) and low C/N ratios through this interval are compatible with a marine origin for the organic matter, although the HI values are close to the boundary region between marine (Type II) and terrestrial (Type III) organic matter. Brackish and marine coastal plants and grasses are known to have a carbon isotope chemistry intermediate between more open marine plants and land plants (Hunt, 1996), which may explain the HI values in the boundary region between Types II and III organic matter. Of further interest are the two C/S values within this "seagrass" interval, which approach and fall within the slightly brackish water field (Fig. **F44**).

$CaCO_3$ content (>105 wt%) indicative of dolostones was measured from ~413 to 628 mbsf, an interval that coincides with lithologic Subunits IIIB–IIID and the upper half of Unit IV (see **"Lithostratigraphy and Sedimentology,"** p. 5). With this interval, TOC content is effectively zero (see **"Biostratigraphy and Paleoenvironments,"** p. 16). From 628 mbsf, $CaCO_3$ content displays a gradual decrease to a depth of ~640 mbsf (roughly lithologic Unit IV), with some variation. $CaCO_3$ content variations exist within a section containing meter-scale cycles of dolostone with quartz overlain by dolostone with glauconite, rudstone, and iron-stained crusts (see **"Lithostratigraphy and Sedimentology,"** p. 5).

Below the interval of $CaCO_3$ variations, $CaCO_3$ content drops to near zero at ~663 mbsf and then gradually increases to ~40 wt%, corresponding to the quartz sandstones and claystones of lithologic Unit V. TOC content in Unit V is as high as 0.9 wt% and covaries with carbonate content. Hydrogen index values and C/N ratios are indicative of terrigenous organic matter input to the seafloor during this time, and C/S values suggest the deposition occurred in seawater. The highest S (5.38%) value thus far during Leg 194 was measured in this interval.

Site 1199

Volatile Hydrocarbons

Concentrations of volatile hydrocarbon gases were not measured at Site 1199 because of the generally porous nature of the strata.

Interstitial Water Chemistry

The dolomitized and highly indurated lithologies encountered during drilling on Site 1199 prevented pore water sampling.

X-Ray Diffraction Carbonate Mineralogy

Forty-six sediment samples were analyzed for carbonate mineralogy from Site 1199 (Fig. **F45;** Table **T10**). In lithologic Unit I from 0 to 152.2 mbsf, the only carbonate mineral present is dolomite. At the transition from lithologic Unit I to Unit II, the carbonate mineralogy changes to 100 wt% calcite. Dolomite remains low, between 0 and 20 wt%, through lithologic Unit IIA, although poor core recovery caused the samples to be widely spaced. For example, only three samples cover the interval from 169 to 265 mbsf. In lithologic Unit II, the mineralogy varies greatly. In general, dolomite is the most common mineral in the upper half of Subunit IIB, whereas calcite is dominant in the lower half.

F45. Carbonate and noncarbonate fraction, p. 89.

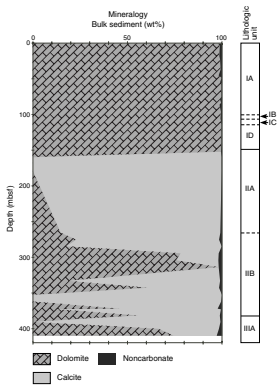

Sedimentary Geochemistry

Results

Calcium carbonate ($CaCO_3$) content at Site 1199 ranges from ~93 to 110 wt% (Fig. F46; Table T12). Measurements are calibrated for calcite; thus, the presence of dolomite can generate values >100 wt% (Fig. F46; Table T13).

F46. Carbonate content, p. 90.

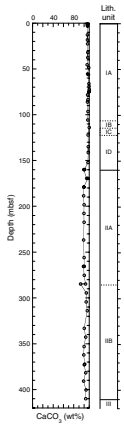

T12. Inorganic carbon, p. 145.

T13. X-ray diffraction mineralogy, p. 146.

CORE PHYSICAL PROPERTIES

Site 1196

Evaluation of core physical properties at Site 1196 included nondestructive measurements of bulk magnetic susceptibility and natural gamma radiation primarily on split cores using the multisensor track (MST). A small number of full cores were also processed through the MST, although low recovery at Site 1196 limited its use. Additionally, the large diameter of cores recovered with the ADCB (Cores 194-1196B-13Z through 51Z) was too large for MST analysis. *P*-wave velocity (x-, y-, and z-direction), bulk density, grain density, and porosity were determined from ~9.5-cm³ cubic samples. Thermal conductivity was measured on lithified core samples.

Density and Porosity

Overall, bulk density ranges between 1.9 and 2.75 g/cm³ and generally increases downhole to ~500 mbsf (Fig. F47). From 500 to 672 mbsf, bulk density values slightly increase to 2.2 g/cm³. Bulk density shows higher scatter throughout the entire interval, and no apparent relation exists between density and the lithologic units. The phosphatic-rich sands of lithologic Unit V at the bottom of Hole 1196A (see "Lithostratigraphy and Sedimentology," p. 5) have an average bulk density of 2.2 g/cm³.

Grain density values average 2.80 g/cm³ and range between 2.55 and 2.95 g/cm³ (Fig. F47). The downhole variations in grain density are consistent with dolomite abundance (see "Geochemistry," p. 24) because dolomite has a higher grain density (2.866 g/cm³) than calcite (2.710 g/cm³). Apart from the intervals 480–520 mbsf and 610–630 mbsf and a few outliers, grain density values exceed 2.80 g/cm³ only in dolomite-rich intervals (Fig. F48). This indicates that in these platform carbonates, grain density can be used as a proxy for dolomite content.

The porosity profile mirrors the bulk density profile. Data are extremely scattered and range from 2% to 51%, reflecting the dominant role of local cementation and dissolution in the carbonate rocks (Fig. F47). The highest porosity values are found in dolomite-rich intervals with abundant moldic porosity mainly caused by dissolution of benthic foraminifers (lithologic Units I, III, and IV) (see "Lithostratigraphy and Sedimentology," p. 5). Lithologic Unit I is dominated by both intergranular and moldic porosity, and porosity ranges from 10% to 51%. Lower porosity values (2%–23%) occur at the base of lithologic Subunit IIA, which corresponds to a higher natural gamma radiation and higher velocity values (see below). Lithologic Unit III has millimeter-sized lenticular molds (lithologic Subunit IIIB) and centimeter-sized molds that are aligned (lithologic Subunit IIID) (see "Lithostratigraphy and Sedimentology," p. 5), and porosity varies between 3% and 38%. The over-

F47. Bulk density, grain density, and porosity, p. 91.

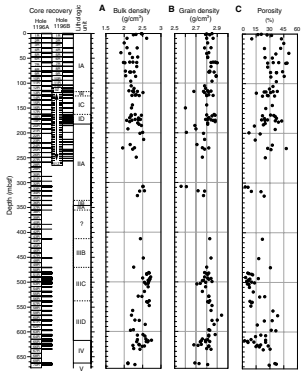

F48. Grain density and dolomite content, p. 92.

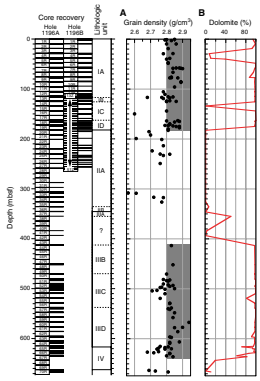

all porosity profile shows no clear downhole trend, indicating that porosity is mainly controlled by dissolution and dolomitization rather than compaction. Porosity values of lithologic Unit V average 32%.

Compressional Wave Velocity

Compressional wave velocity (x-, y-, and z-direction) for Site 1196 was measured with the PWS3 contact probe system on ~9.5-cm³ samples. Velocity values vary between 2300 and 6600 m/s (Fig. F49). On average, PWS3 velocity is ~1700 m/s higher than velocities derived from sonic logging data and interval velocities from check shot data (see further discussion in "Downhole Measurements," p. 32). In lithologic Units I and II, the average velocity is 4600 m/s, which is ~700 m/s lower than in lithologic Units III and IV, indicating a downhole velocity increase. Velocity in lithologic Unit V is low, with an average of 2200 m/s. Anisotropy is significant and ranges from –9% to 14% (Fig. F49). Most of the anisotropy values (71%) are positive, meaning that the velocity in the z-direction is lower than average velocity in the x- and y-directions (see "Core Physical Properties," p. 21, in the "Explanatory Notes" chapter). This is a common feature in well-bedded sediments, characterized by horizontally aligned grains and pores.

A crossplot of velocity vs. porosity for Site 1196 shows a general inverse relationship (Fig. F50). The measured velocities can be compared with the time-average equation of Wyllie et al. (1956). The abundance of moldic porosity in the platform carbonates can be correlated with the large number of porosity-velocity pairs that have positive deviations from the time-average equation because the pores are integrated in a rigid framework (see "Core Physical Properties," p. 24, in the "Site 1193" chapter). The phosphatic- and quartz-rich sands of lithologic Unit V deviate negatively from the time-average equation because the velocity of quartz is lower than the velocity of carbonate minerals (Fig. F50).

Thermal Conductivity

Thermal conductivity values at Site 1196 show a downhole increasing trend consistent with bulk density and porosity trends (Fig. F51). Values range from ~0.8 to ~3.5 W/(m·K). A direct inverse relationship should exist between porosity and thermal conductivity (see "Core Physical Properties," p. 21, in the "Explanatory Notes" chapter). The majority of the measured thermal conductivity values lies roughly on the theoretical limestone curve, giving confidence to the measured thermal conductivity (Fig. F52). Three outliers with thermal conductivity values >3.3 W/(m·K) are phosphatic-rich sands from lithologic Unit IV (see "Lithostratigraphy and Sedimentology," p. 5).

Magnetic Susceptibility and Natural Gamma Ray

The quality of the magnetic susceptibility (MS) and NGR data at Site 1196 is degraded in RCB sections where the core is disturbed and/or undersized with respect to the inner diameter of the liner (Fig. F53). Generally, these cores are not run through the MST. However, at Site 1196, MST data were used as an aid in the logging interpretation to identify the exact core horizon of peaks detected in hostile environment gamma ray sonde (HNGS) logging data (see "Downhole Measurements," p. 32). Because of the change in sample volume, NGR and MS units and

F49. *P*-wave velocity and anisotropy of *P*-wave velocity, Site 1196, p. 93.

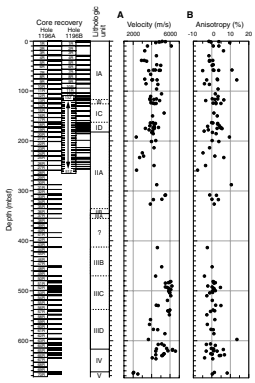

F50. Crossplot of velocity vs. porosity, Site 1196, p. 94.

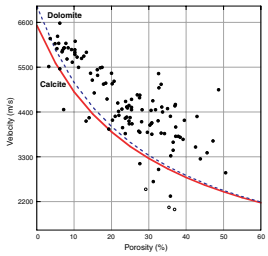

F51. Thermal conductivity, Site 1196, p. 95.

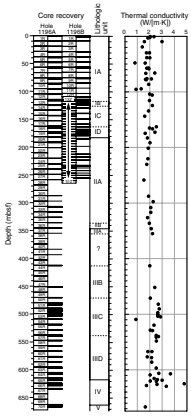

F52. Crossplot of thermal conductivity vs. porosity, Site 1196, p. 96.

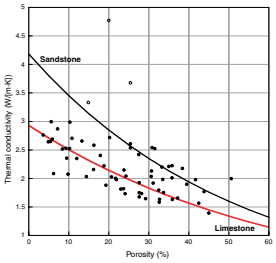

amplitudes measured from half cores require some thought. Figure F54 compares NGR and MS measured from both full and half cores. Surprisingly, there is no statistical difference between the full-core and half-core NGR values. This is in contrast to the MS full-core and half-core values, which show a constant offset. The change in sign is unlikely to be real and reflects the inapplicability of the MST calibrations relative to processing half cores. Consequently, no corrections were applied to the NGR amplitudes. This was also the case for the MS data, as these units are not in SI format.

MS ranges from –8 to 5 × 10^{-6} SI (Fig. F53). A purely diamagnetic interval from 20 to 105 mbsf correlates with most of lithologic Subunit IA, meaning that the carbonates are clean and free from magnetic minerals and bacteria (see "Lithostratigraphy and Sedimentology," p. 5). For the remainder of the site, data are too scarce for correlations because of low core recovery.

NGR values range from 0 to 65 counts per second (cps) (Fig. F53), with local maxima at 117 to 126 mbsf and 307 to 318 mbsf. However, NGR data just above and below these intervals are missing, and therefore a comparison with HNGS data was important. Over the first 70 mbsf, logging was performed through the drill pipe, which attenuated the true HNGS reading. The Schlumberger log interpretation chart GR-3 (Schlumberger, 1998) describes the procedure for correcting the amplitude of NGR data measured throughout the drill pipe. A parameter, *t,* is calculated that represents the sum of density-thickness products for the pipe, any cement sheath, and the borehole fluid (Schlumberger, 1998). Because of the pipe thickness and the lack of casing cement, the Schlumberger equation for *t* can be simplified to give

$$t = 2.54\ \rho_{csg}\ (OD_{csg} - ID_{csg})/2,$$

where ρ_{csg} is the pipe density (7.83 g/cm³), OD_{csg} is the outer diameter of the pipe (8.25 in), and ID_{csg} is the inner diameter of the pipe (4.125 in). For Sites 1196 and 1199, the *t* parameter is 41 g/cm². Using the relationship between the *t* factor and the NGR attenuation correction factor as a function of the logging tool diameter (3.375 in), the correction factor is ~7. Consequently, HNGS values from 0 to 70 mbsf were multiplied by 7 (Fig. F53). Comparison of the NGR with the corrected HNGS data shows that the maximum NGR values often follow the trend in the HNGS log. Downhole increasing trends are visible between 0 and 126 mbsf (~10 to ~60 cps) and between 126 and 318 mbsf (~10 to ~65 cps). NGR maxima at 117–126 mbsf and 307–318 mbsf match peaks in the downhole logging data and correspond to the bottom of lithologic Subunit IB and the bottom of lithologic Subunit IIA (see "Lithostratigraphy and Sedimentology," p. 5). The HNGS peak at 126.5 mbsf logging depth could be placed at Core 194-1196A-14R (124.3–126.0 mbsf). The two NGR maxima could be related to either a hardground or an exposure surface, as the rocks are well-lithified and have high velocity and low porosity.

Site 1199

Introduction

Evaluation of core physical properties at Site 1199 included nondestructive measurements of bulk MS and natural gamma radiation on whole cores using the MST. Low recovery at Site 1199 limited the use of the MST. *P*-wave velocity (x-, y-, and z-direction), bulk density, grain

F53. Magnetic susceptibility and natural gamma radiation, Site 1196, p. 97.

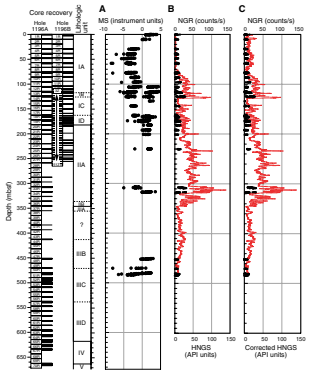

F54. Comparison of NGR and MS measurements, p. 98.

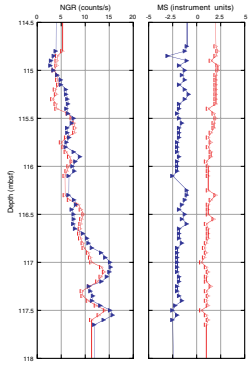

density, and porosity were determined from ~9.5-cm³ cubic samples. Thermal conductivity was measured on lithified core samples.

Density and Porosity

At Site 1199, gamma ray attenuation (GRA) bulk density ranges between 1.3 and 2.4 g/cm³ and moisture and density (MAD) bulk density ranges between 1.4 and 2.7 g/cm³ (Fig. F55). On average, MAD density values are 0.3 g/cm³ higher than the maximum GRA density values. This difference is the result of intracore spaces and undersized cores. MAD density is 2.2 g/cm³ at the top of the hole and increases to 2.7 g/cm³ between 90 and 110 mbsf, which coincides with the bottom 17 m of lithologic Subunit IA and its boundary with lithologic Subunit IB (see "Lithostratigraphy and Sedimentology" p. 5). From 110 to 170 mbsf, MAD density decreases to 2.2 g/cm³. Below 170 mbsf, bulk density shows high scatter, and no apparent relation exists between density and the lithologic units.

Grain density values average 2.79 g/cm³, range between 2.70 and 2.85 g/cm³, and do not show any clear downhole trends (Fig. F55). Average grain density is consistent with dolomite abundance (see "Geochemistry," p. 24) because dolomite has a higher grain density (2.87 g/cm³) than calcite (2.71 g/cm³).

Porosity values range from 3%–48%. The porosity profile with depth mirrors the bulk density profile. Porosity starts at ~30% at the top of the hole, decreases to 3% between 90 and 110 mbsf, and increases back to 20% at 170 mbsf. Lithologic Unit I is dominated by both intergranular and moldic porosity, and values range from 2% to 33%. Below 170 mbsf, porosity values are scattered between 14% and 48%. (Fig. F55). The highest porosity values are found at the top of lithologic Unit I, which has pronounced moldic porosity (see "Lithostratigraphy and Sedimentology," p. 5). The lowest porosity values (2%–12%) exist at the boundary between lithologic Subunits IA and IB (see "Lithostratigraphy and Sedimentology," p. 5) and correspond to high bulk density values (2.7 g/cm³), local maxima in natural gamma radiation and magnetic susceptibility, and high velocity values (5500 m/s). The overall porosity profile shows no clear downhole trend, suggesting that porosity is mainly controlled by dissolution and dolomitization and not by compaction.

F55. GRA and MAD bulk density, grain density, and porosity, p. 99.

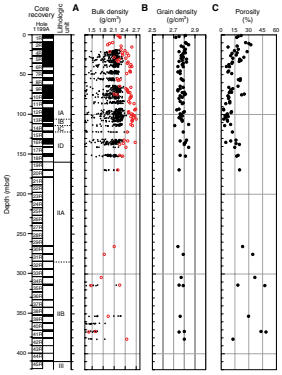

Compressional Wave Velocity

Compressional wave velocity (x-, y-, and z-direction) for Site 1199 was measured with the PWS3 contact probe system on ~9.5-cm³ samples. Velocity mirrors the porosity and bulk density profiles and varies between 3000 and 5500 m/s (Fig. F56). Velocity starts at 4000 m/s at the top of the hole, increases to 5500 m/s between 100 and 110 mbsf, and decreases to 3950 m/s at 170 mbsf. Anisotropy of velocity ranges from –5% to 11% (Fig. F56). Most of the anisotropy values (81%) are positive, meaning that the velocity in the z-direction is lower than average velocity in the x- and y-directions (see "Core Physical Properties," p. 21, in the "Explanatory Notes" chapter). This is a common feature in well-bedded sediments, characterized by horizontally aligned grains and pores. In Site 1199 sediments, the positive anisotropy is most likely caused by aligned moldic porosity, as no apparent bedding is visible as a result of intense dolomitization. However, Hole 1199A was drilled with

F56. *P*-wave velocity and anisotropy of *P*-wave velocity, Site 1199, p. 100.

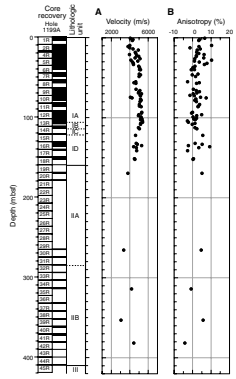

an inclination of ~7° (see "Operations," p. 2), which may have some effect on the anisotropy.

A crossplot of velocity vs. porosity for Site 1199 shows a general inverse relationship (Fig. F57). The measured velocities can be compared with the time-average equation (Wyllie et al., 1956). The abundance of moldic porosity in the platform carbonates may explain the large number of porosity-velocity pairs that have positive deviations from the time-average equation because the pores are integrated in a rigid framework (see "Core Physical Properties," p. 24, in the "Site 1193" chapter). Porosity-velocity pairs from the boundary region between lithologic Subunits IA and IB (90–110 mbsf) have the lowest porosity and the highest velocity values and plot below the time-average equation.

F57. Crossplot of velocity vs. porosity, Site 1199, p. 101.

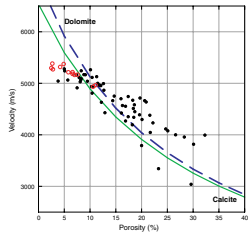

Thermal Conductivity

Thermal conductivity values at Site 1199 increase downhole (Fig. F58). Values range from ~2.0 to ~3.2 W/(m·K). From 265 to 382 mbsf, thermal conductivity ranges from 1.5 to 2.2 W/(m·K). A direct inverse relationship should exist between porosity and thermal conductivity (see "Core Physical Properties," p. 21, in the "Explanatory Notes" chapter). The majority of the measured thermal conductivity values lie around the theoretical limestone curve, giving confidence to the measured thermal conductivity (Fig. F59) (Keen and Beaumont, 1990).

F58. Thermal conductivity, Site 1199, p. 102.

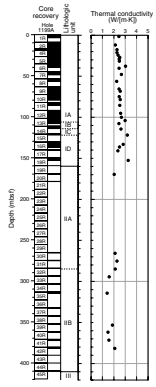

Magnetic Susceptibility and Natural Gamma Ray

The quality of the MS and NGR data at Site 1199 is degraded because the RCB cores are disturbed and/or, in most parts, are undersized with respect to the inner diameter of the liner (Fig. F60).

From 0 to 141 mbsf, MS ranges from –2 to 20 × 10^{-6} SI and shows no obvious trend with depth (Fig. F60). Most of the values are below 5 × 10^{-6} SI. Two small spikes of 8 × 10^{-6} SI exist at 101 and 123 mbsf, and a spike of 22 × 10^{-6} SI exists at 141 mbsf. Below 141 mbsf, data are too scarce for correlations because of low core recovery.

Natural gamma radiation values range from 0 to 138 cps, with apparent local maxima at ~39 mbsf, from 95 to 114 mbsf, from 132 to 137 mbsf, and at ~170 mbsf (Fig. F60). Over the first 70 mbsf, downhole logging was performed through the drill pipe, which attenuated the HNGS reading (see "Downhole Measurements," p. 32). A density-correction factor of 7 was applied to the HNGS data for that interval to correct for the pipe effect (see "Core Physical Properties," p. 27) (Schlumberger, 1998). A comparison of the NGR data and the corrected HNGS data shows a good correlation. Maximum NGR values often follow the trend in the HNGS log (Fig. F60). Downhole increasing trends are visible between 0 and 40 mbsf (~10 to ~24 cps) and between 40 and 114 mbsf (~10 to ~83 cps). A single NGR spike is visible at 170 mbsf and is part of an interval with high natural gamma radiation in the HNGS data from 160 to 180 mbsf. Downhole logging data show that most of the natural gamma radiation originates from uranium (see "Downhole Measurements" p. 32). NGR maxima at 114.06 and 169.65 mbsf can be correlated with the cores and correspond to intervals just above interpreted exposure surfaces (see "Lithostratigraphy and Sedimentology," p. 5). This may reflect increased uranium accumulation during initial flooding, which decreases as flooding continues.

F59. Crossplot of thermal conductivity vs. porosity, Site 1199, p. 103.

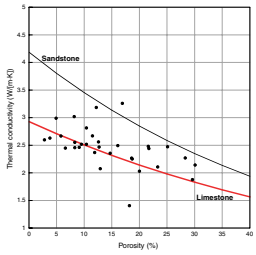

F60. Magnetic susceptibility and natural gamma radiation, Site 1199, p. 104.

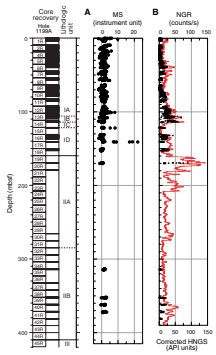

DOWNHOLE MEASUREMENTS

Site 1196

Logging Operations

Logging operations began on 3 February 2001 at 1030 hr (Table T14). Strong currents and waves caused significant vibration of the drill pipe. The triple combination tool string with the LDEO multisensor gamma ray tool (MGT) at the top and the LDEO temperature tool at the bottom experienced an electrical malfunction when it was lowered in the pipe. Therefore, the entire tool string was brought back on the rig floor, and the MGT was removed. At 1215 hr, the shortened tool string was lowered to a tight spot at ~520 mbsf, which is 152.2 m above TD (672.2 mbsf). Because the tool experienced overpull, logging started only at 510 mbsf. During the run, vibration loosened several joints and unscrewed the end piece (~4 in long) of the temperature tool.

For the second run, the FMS/Sonic combination was lowered. Unexpectedly, the tool encountered an obstacle in the pipe at ~135 mbrf that might have been the lost piece of the temperature tool. Pumping did not free the pipe, and the tools were pulled back on deck. A core barrel was lowered to punch the obstacle into the hole. This attempt was successful; the FMS/Sonic combination was lowered again into the hole to 838 mbrf (524 mbsf), and logging started. To check the repeatability and to improve data recovery in the enlarged intervals of the hole, the FMS/Sonic pass was repeated.

The third run involved the check shot survey with the WST with a 300-in³ air gun as a source in 7 m water depth next to the stern of the ship and 49 m horizontal distance away from the drill string. Traveltime was successfully measured at 13 stations between 408.4 and 837.5 mbrf (94.4 and 523.5 mbsf) (Table T15). The end of logging operations was 4 February 2001 at 0530 hr.

Data Quality

The combination of a wide hole and a hard formation impacted the data quality (Fig. F61). The hole was more than 17 in for long intervals so that the hostile environment lithodensity logging tool, accelerator porosity sonde detectors, and FMS pads did not always come in contact with the borehole wall. In particular, in the interval between 446 and 472.5 mbsf, neutron porosity values reach a maximum of 100 porosity units (pu) and density values are ~1 g/cm³, indicating that the tools measured only borehole fluid. Nevertheless, at least one of the FMS pads usually had contact during both passes so that features like fractures or sediment textures could be recorded. The second pass of the FMS showed good repeatability of the images, thus improving confidence in the reliability of the FMS data set.

The velocity log was noisy because of acoustic reverberation in the high-velocity formation. After the LDEO Borehole Research Group processed for cycle skipping, the data quality improved significantly. Log velocities are generally lower than those from discrete core measurements (see Fig. F62). The WST produced clear first arrivals for the time-depth conversion (Table T15).

T14. Logging operations, Hole 1196A, p. 147.

T15. Time-depth correlation, p. 148.

F61. Summary of geophysical logs, Site 1196, p. 105.

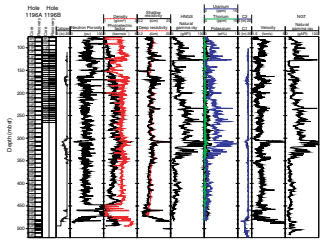

F62. Time-depth curves, p. 106.

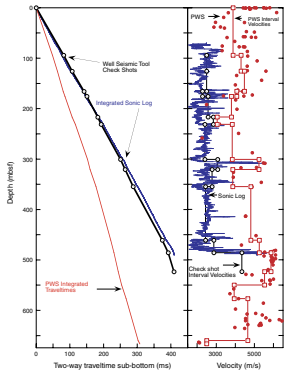

Logging Results

The most useful geological information was collected by the natural gamma ray and resistivity tools (Fig. F61). Additionally, FMS images reveal the bedding character that was difficult to discern in low-recovery intervals. They are particularly helpful for identifying unit boundaries, mainly because these boundaries are related to hardgrounds or firmgrounds where the hole was less enlarged. Based on the logs and the FMS images, four log units, which appear to accurately record the development of multiple platform phases at this site, can be distinguished. Within these log units, subunits are recognized that may be related to internal phases of individual platform growth or facies changes during a growth phase (Fig. F63).

Log Unit 1 (76–128.4 mbsf)

Logging Unit 1 extends from the top of the measured interval to 128.4 mbsf, where uranium and resistivity values dramatically drop (Fig. F63). To this depth, uranium and resistivity values increase gradually with several peaks, increasing variability downhole. The boundary bed (128.4 to 125 mbsf) causes a high peak in total spectral gamma ray (HSGR), with an increase of the uranium content to 10 ppm, which is also accompanied by resistivity and velocity peaks. The FMS image of the 2.5-m-thick boundary bed shows a sharp lower boundary (Fig. F64A).

Logging Unit 1 correlates with the dolomitic floatstone of lithologic Subunit IB and the dolomitic floatstone/rudstone of lithologic Subunit IA (see "Lithostratigraphy and Sedimentology," p. 5). Based on the FMS image and the high peaks in HSGR and resistivity, the lower boundary of Subunit IB is sharp and reminiscent of a flooding surface. The variability in the log signatures, particularly in several resistivity peaks within logging Unit 1, is probably the result of hard cemented layers below exposure surfaces.

Logging Unit 2 (128.4–163 mbsf)

Both the upper and lower boundary of logging Unit 2 are marked by an abrupt shift in resistivity and velocity values. At the upper boundary, HSGR also decreases dramatically downhole, whereas only a slight shift downhole to higher values occurs at the lower boundary. Internally, the unit shows uniform low resistivity values and generally low HSGR values, with few peaks (Fig. F63).

The boundary between lithologic Subunits IB and IC is correlated with the log change separating logging Units 1 and 2. The log unit itself coincides with lithologic Subunit IC, which is a reefal facies composed of skeletal rudstone/boundstone alternating with dolomitic floatstone (see "Lithostratigraphy and Sedimentology," p. 5).

Logging Unit 3 (163–345.5 mbsf)

The upper boundary of logging Unit 3 is placed at 163 mbsf, where both resistivity and velocity rapidly increase downhole and HSGR values start to fluctuate around a higher median (Figs. F61, F63). The unit can be subdivided into three intervals based on the variation in the uranium log. The top interval (163–213 mbsf) is characterized by high-frequency, high-amplitude resistivity fluctuations that decrease in amplitude and frequency within the interval. The velocity log displays a similar pattern of high variability (Fig. F63). The uranium content fluctuates moderately around a near-linear trend, with a basal 6.5-m-thick package of reduced uranium values of about 2 ppm. Some very conduc-

F63. Interpretation of geophysical logging data, p. 107.

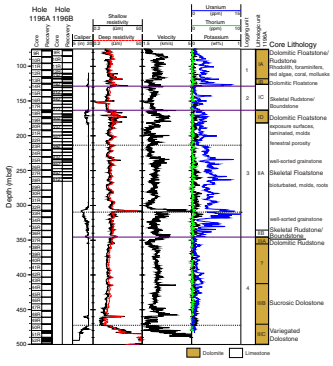

F64. FMS images, 121–130.2 and 160–166.2 mbsf, p. 108.

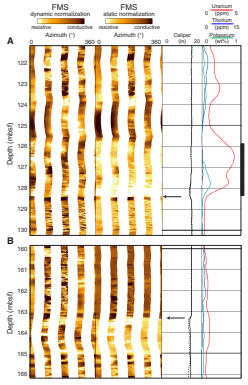

tive layers, seen in the FMS log, with low HSGR and velocity streaks between 163 and 175 mbsf might be dissolution features in this portion of the platform.

The boundary to the underlying logging interval at 213 mbsf is marked by a downhole increase in the HSGR (~20 gAPI), increased resistivity, and a drop in velocity (Fig. F63). The lower boundary at 309.5 mbsf is placed at the base of a distinct peak in resistivity (~20 Ωm) and velocity (~5 km/s) and very low neutron porosities (~10 pu). The FMS log images this peak as a bed with a sharp lower boundary and with characteristics similar to the overlying sediments, whereas the sediments below have an overall finer character caused either by reduced porosity or component size (Fig. F65). Above this basal layer, the uranium is generally high (>3 ppm). Peaks in the uranium log repeatedly correspond to increased resistivity values. Distinct peaks in the two logs occur at about 235 mbsf, which might be related to a major event of exposure and subsequent flooding.

The lowermost interval (309.3–345.5 mbsf) is characterized by uranium contents that steadily increase uphole from 4 to 15 ppm. The major uranium peaks in this interval are positively correlated with small resistivity and velocity peaks.

Logging Unit 3 is correlated with lithologic Subunits ID, IIA, and IIB. The top of lithologic Subunit ID coincides with the upper boundary, and the base of lithologic Subunit IIB coincides with the lower boundary of logging Unit 3. However, the three above-described logging intervals of logging Unit 3 do not coincide with the three lithologic subunits. Lithologic Subunit IIB is the base of the entire unit (Fig. F63). Lithologic Subunit ID is only part of the top interval of the logging unit. Nevertheless, the dolomitic floatstone of lithologic Subunit ID corresponds to the high resistivity and velocity values at the top of logging Unit 3. High peaks are interpreted to mark several exposure events toward the end of this platform growth phase. Moldic porosity observed in the cores supports the interpretation of exposure. In addition, this top part shows pervasive dolomitization that partly explains the high velocity and resistivity values in this log interval. The low resistivity and HSGR at the base of this top logging interval might be the record of a recovered grainstone with fenestral porosity indicative of a beach(?) deposit (see **"Lithostratigraphy and Sedimentology,"** p. 5).

The logging interval of logging Unit 3 with increased uranium content correlates to the middle part of the skeletal floatstone with grainstone matrix of lithologic Subunit IIA that is interpreted to represent open lagoonal platform facies (see **"Lithostratigraphy and Sedimentology,"** p. 5). A likely reason for the increased accumulation of uranium in this lagoonal facies might be the more anoxic environment and an increased organic carbon content.

The trend of increasing HSGR values of the lowermost logging interval of logging Unit 3 (309.3–345.5 mbsf) indicates changing facies, potentially a regressive trend. Sedimentologically, no trend is discernable, possibly because of low recovery. Cores from this interval record a thin-bedded unit with mottled mudstones, grainstones, and exposure horizons probably deposited in very shallow water (see **"Lithostratigraphy and Sedimentology,"** p. 5).

Logging Unit 4 (345.5–524 mbsf)

The upper boundary to logging Unit 4 is placed at 345.5 mbsf, where both HSGR and velocity decrease markedly. Logging Unit 4 shows, on average, the lowest gamma ray values for the logged interval. Based on

F65. FMS image, 303.5–311 mbsf, p. 109.

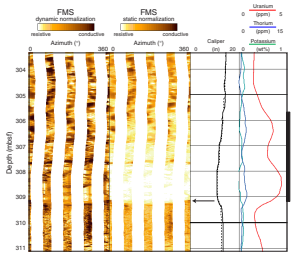

variations in the resistivity, velocity, and density logs, a subdivision can be made at 472.5 mbsf. From 345.5 to 472.5 mbsf, the hole is enlarged to a diameter of more than 17 in, which is the maximum opening of the caliper (Fig. F61). It is narrower only at ~460 mbsf, where a peak in resistivity indicates a densely cemented bed or hardground that was not recovered in core. Despite low resistivity values above this horizon, velocity log values are high. Above 446 mbsf, the HSGR increases slightly and the resistivity log shows only few excursions to higher values.

From 472.5 mbsf to the bottom of the logged interval at 524 mbsf, the downhole increasing high density (2.6 g/cm³), resistivity (100 Ωm) and velocity values (5 km/s) indicate a hard formation. This change is corroborated by the narrower borehole diameter starting at this depth, resulting in clear and complete FMS images (Fig. F65). In the images, a highly fractured interval is recognized, in which fractures have an average dip orientation of 160°/60° (Fig. F66).

Logging Unit 4 corresponds to lithologic Subunits IIIA to IIIC. Overall the logs do not show much variation, and a discrimination of lithologic Subunit IIIA (dolomitic rudstone) from Subunit IIIB (sucrosic dolomite) is not possible in the logs. The top of lithologic Subunit IIIC consists of well-lithified dolostones and is characterized by high velocity and resistivity values (Fig. F63).

F66. FMS image of a fractured interval, p. 110.

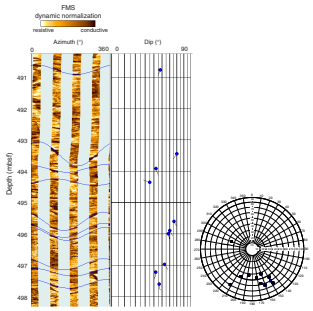

Discussion

The main objective at Site 1196 was to determine the initiation and facies development of the SMP. Lithology and ages of the recovered rocks clearly indicate that the SMP grew in several phases (see "Lithostratigraphy and Sedimentology," p. 5, and "Biostratigraphy and Paleoenvironments," p. 16). Consequently, cores at Site 1196 penetrated an edifice of multiple amalgamated platforms, which were established on a glauconite-rich substrate (see "Lithostratigraphy and Sedimentology," p. 5). The log facies record the evolution in these multiple platforms. Logging Unit 4 provides the rather uniform log signature of a pervasively dolomitized platform. The high-resistivity portion below 472.5 mbsf might be part of the oldest platform phase, which is early Miocene in age. Logging Unit 3, with its three log intervals, is interpreted to be the middle Miocene growth phase as indicated by biostratigraphic data (see "Age Model," p. 24). The facies of this middle Miocene SMP starts with a reef that is overlain by high-energy platform margin sediments (lithologic Subunit IIB and the bottom of Subunit IIA; see "Lithostratigraphy and Sedimentology," p. 5). Increasing HSGR and velocity values from 345.5 to 309.5 mbsf are the log expressions of this regressive trend. Subsequent flooding of the platform establishes a thick lagoonal to open shelf facies (lithologic Subunit IIA), which is overlain by shallower (beach) facies and packages with exposure surfaces (lithologic Subunit IIB). The increased resistivity and velocity values are the physical expression of this sedimentologic facies succession (Fig. F63). The interpreted dissolution features in the FMS images at 170.2–173 mbsf and 174.5–174.7 mbsf indicate karstification at the top of this middle Miocene platform.

Because the middle/late Miocene boundary is biostratigraphically not constrained, the base of the late Miocene SMP, the youngest platform growth phase, is at the base of either lithologic Subunit IC or IB. If the boundary is at the base of lithologic Subunit IC, the late Miocene platform would start at 163 mbsf at the base of logging Unit 2, with low resistivity, velocity, and HSGR in a reefal facies. The karst features and

the related variable thickness of lithologic Subunit ID below 168 mbsf, as recognized in Holes 1196A and 1196B, give evidence of long-term exposure on top of the dolomitized interval of lithologic Subunit ID (see "Lithostratigraphy and Sedimentology," p. 5). A slight trend of increasing HSGR values in the first 20 m is reminiscent of the regressive trend at the bottom of the middle Miocene platform between 345.5 and 309.5 mbsf. Peaks in HSGR, resistivity, and velocity mark a flooding surface at 128.4 mbsf, above the reef, and the establishment of a floatstone unit that is similar in the log expression of the lagoonal facies of the middle Miocene platform. This flooding surface at the base of logging Unit 1 could alternatively be the base of the late Miocene platform. Such an interpretation is supported by seismic stratigraphy data (see "Seismic Stratigraphy," p. 40) and the occurrence of a major exposure horizon at the equivalent interval at Site 1199.

Time-Depth Conversion

A check shot survey was performed using the single-channel WST and a 300-in³ air gun. The tool was lowered to a maximum depth of 523.5 mbsf in Hole 1196A, and the traveltime was measured at 12 stations (Table **T15**). The resulting traveltime-depth curve is displayed in Figure **F62.** This time-depth relationship is similar to estimates obtained by integrating the sonic log but is vastly different when the velocities of the discrete samples measured with the *P*-wave sensor (PWS) are used. The values from discrete samples are generally much higher; in many cases, the difference is over 2 km/s (Fig. **F62**). Although such differences can be caused by shipboard sampling bias (hard vs. soft), pressure differences (burial vs. surface), or dispersion (ultrasonic vs. seismic frequency), the observed large difference might be mainly explained by the sampling bias produced as a result of the selective recovery of the hard portions of the formation. In addition, FMS images document fractures at certain intervals of the platform, which also slow down the formation velocity. Nevertheless, the offset of the downhole and lab velocity values is unusually large when compared to other data sets, in which PWS data often are very close to the velocities determined in the WST experiment (Eberli, Swart, Malone et al., 1997). At Site 1194, for example, the PWS velocities were generally lower than the log data (see "Downhole Measurements," p. 22, in the "Site 1194" chapter). The significance of the large difference at this site becomes evident when the time-depth conversion of both data sets is compared: 300 ms (two-way traveltime [TWT]) would translate into 345 mbsf using the integrated sonic log, 365 mbsf using the check shot interval velocities, and 655 mbsf using the integrated traveltimes of the PWS data. Because the reliability of the shipboard velocity data is generally difficult to estimate, a WST experiment is critical for a precise time-depth conversion.

Site 1199

Logging Operations

Logging operations started at 1700 hr on 21 February 2001 with rigging up the wireline. At 1830 hr the triple combo tool string was deployed in Hole 1199A. Two narrow spots were encountered at 118 mbsf and 204 mbsf, but were passed after few attempts. The tool string was lowered to a depth of 418 mbsf, which was 1.5 m above the TD of 419.5 mbsf of Hole 1199A. A first logging run started from this depth uphole.

For the second run, the FMS/Sonic tools were lowered into the hole (Table T16) but could not pass a tight spot at 129.2 mbsf, and the tools were pulled back onto the rig floor. The drill pipe was advanced to ~210 mbsf to widen the narrow hole. The tools were lowered again in the hole but could not pass beneath 129.2 mbsf. Hence, logging started above this horizon. The tool measured a hole deviation of 7.5°, which is probably the cause of repeated failure to pass the critical spot, most likely a cave at 129.2 mbsf. In a last attempt to reach the bottom of the hole, two sections with bowsprings were added to the lower part of the tool string. This attempt also failed, and logging operations terminated at 1000 hr.

T16. Logging operations, Hole 1199A, p. 149.

Log Quality

Caliper readings of the first run showed a nearly constant hole diameter of 11 in for most of the measured sections (Fig. F67). In three intervals, the caliper opened to its maximum range, indicating a hole larger than 17 in. Two of these intervals between 118–129.2 mbsf and 155–162 mbsf, respectively, are most likely karst caves, as bit drops were reported during coring. The third interval (185–210 mbsf) is an enlarged borehole. The otherwise good hole conditions resulted in very good log quality for the first run. The second short logging run covers part of the top of the first cave, resulting in poor-quality FMS and velocity data. However, the transition from the karstified reef into lithologic Subunit IB, which could be the base of the late Miocene growth phase of the SMP, is well imaged.

F67. Composite logs, Hole 1199A, p. 111.

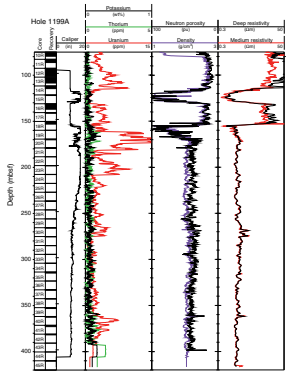

Log Results

The logging data in Hole 1199A provide important information on the lithology and architecture of the middle to late Miocene SMP edifice, especially in the lower part of the hole where core recovery was low. Site 1199 is only 5 km east-northeast of Site 1196, on the SMP, but significant differences between this site and Site 1196 can be identified, despite similarities in the log responses for individual units. A similar subdivision into three logging units is recognized, although thickness variations in logging Units 2 and 3 provide evidence for significant lateral facies heterogeneities and a complicated architecture of the entire platform edifice. As at Site 1196, the dominant contribution to the HSGR signal in Hole 1199A is caused by high uranium concentrations.

F68. Interpretation of geophysical logging data, Hole 1199A, p. 112.

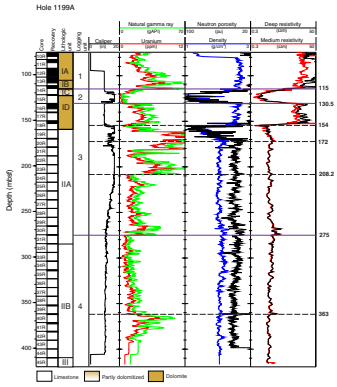

Logging Unit 1 (75–115 mbsf)

Logging Unit 1 consists of an interval with high resistivity and HSGR values (Fig. F68). A peak of high resistivity marks the boundary to the next logging unit. The FMS image shows a sharp boundary and overall little open pore space (Fig. F69). The first peak of resistivity and HSGR at 115 mbsf correlates to the base of the overlying dolomitic floatstone of lithologic Subunit IB. The highly dolomitized rocks show the lowest porosity and density measured on Leg 194.

F69. FMS image, 103.5–120 mbsf, Site 1199, p. 113.

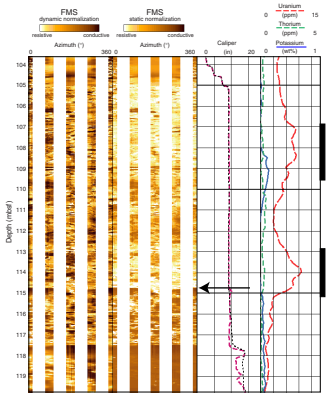

Logging Unit 2 (115–130.5 mbsf)

Readings of 100 pu porosity and density around 1 g/cm³ in logging Unit 2 indicate the presence of a water-filled karst cave of ~10 m thickness. This zone corresponds to the reefal interval of lithologic Subunit IC that is capped by an exposure horizon (see **"Lithostratigraphy and Sedimentology,"** p. 5). Bit drops were reported while cutting in Core

194-1199A-14R, supporting the interpretation that major karst caves occur in this interval. The low recovery of Core 194-1199A-15R and the log responses imply a greater thickness for lithologic Subunit IC.

Logging Unit 3 (130.5–275 mbsf)

Logging Unit 3 corresponds to lithologic Subunits ID and IIA, likely representing the middle Miocene platform growth phase. Based on changes in uranium concentration, density, porosity, and resistivity, four intervals can be distinguished (Fig. F68). The top interval of logging Unit 3 (130.5–154 mbsf) is characterized by high resistivity (~20 Ωm) and density (~2.6 g/cm^3) and low neutron porosity (15 pu). Below 154 mbsf, resistivity and density decrease drastically, which again is interpreted as a karst cave. This section extends down to 172 mbsf, with slowly decreasing neutron porosity from 100 pu down to 50 pu. The HSGR does not correlate with the other logs. It increases dramatically at 161 mbsf and stays generally high, with large variations (20–140 gAPI) down to 208.2 mbsf, where it shows a sharp drop to low values around 20 gAPI. In the lowermost interval, the HSGR shows variations but with lower amplitudes (15–40 gAPI).

The top interval of logging Unit 3 corresponds to floatstone (lithologic Subunit ID), which is pervasively dolomitized and densely cemented. The karst cave below, indicated by 100% porosity, separates the top 24.5 m from a 200-m-thick section of skeletal floatstone and grainstone (lithologic Subunit IIA), which builds a major part of the platform succession.

Logging Unit 4 (275–418 mbsf)

Logging Unit 4 displays low variability and a near linear trend of slightly decreasing resistivity and density and increasing porosity and HSGR (Fig. F68). Based on the HSGR, two intervals can be subdivided. Between 275 and 363 mbsf, the HSGR values are on average low (~15 gAPI) with small variations. The boundary to the lower interval is placed at 363 mbsf at the top of a downhole decreasing trend in the HSGR log. Furthermore, this boundary is also characterized by a small peak in density, porosity, and resistivity, indicating the development of a hardground. Logging Unit 4 corresponds to lithologic Subunit IIB that is composed of skeletal grainstone and floatstone. Because of low core recovery, a detailed core-log correlation is somewhat tenuous.

Correlation of Site 1196 and 1199

Lithologic correlation of Sites 1196 and 1199, both drilled into the SMP, is difficult because of low recovery. Only logging data provide a continuous record of the multiple platform growth phases. In both holes, four logging units were distinguished that are related to the Miocene platform growth phases. Preliminary shipboard analysis shows a good correlation in logging Units 1 and 2 to a depth of 163 and 115 mbsf, respectively (Figs. F70, F71). Below these depths, the correlation is more interpretative. Two scenarios of correlating log responses between Sites 1196 and 1199 are presented below. The favorite one is discussed in detail, whereas the second possibility is only briefly addressed. The most useful logs for the correlation are the resistivity and uranium logs.

In both Holes 1196A and 1199A, logging Units 1 and 2 show a similar log response pattern (Fig. F70). Logging Unit 2 shows low uranium values and is abruptly overlain by a succession in logging Unit 1, dis-

F70. Cross-correlation of log responses, p. 114.

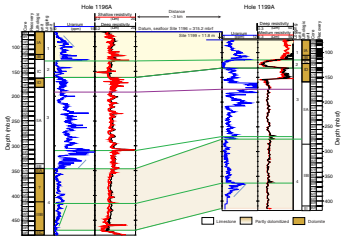

F71. Alternative correlation of log responses, p. 115.

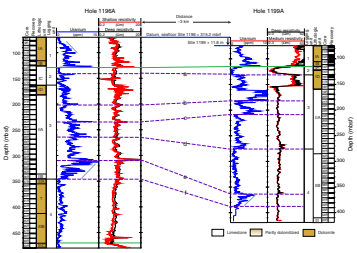

playing at its base very high uranium values that decrease upward. The correlation of logging Unit 3 is more complicated. At both sites, the top of logging Unit 3 is a high resistivity interval, corresponding to a dolomitic floatstone (lithologic Subunit ID). The range of porosity, density, and resistivity data is similar in this unit at both sites, but the uranium signature differs. For example, extremely high and strongly fluctuating uranium values (up to 15 ppm) in the top 50 m of Hole 1199A are not present in Hole 1196A. Consequently, the resistivity is used for correlation. In both holes, resistivity in the top of logging Unit 3 shows high-frequency, high-amplitude variations that decrease and, at 172 mbsf, change into a low-frequency resistivity signal that fluctuates downhole around a near-linear median. This change is taken as a correlation horizon (purple line in Fig. **F70**). Toward the bottom of logging Unit 3, resistivity shows two peaks. The lower of these peaks is the log unit boundary and is used as another correlation horizon. The strata in between the peaks has a high uranium content but varies in thickness between the two sites by nearly 30 m. If this correlation between the two holes is correct, then logging Unit 3, which records the strata from the middle Miocene growth phase, is 39.5 m thinner at Site 1199 than it is at Site 1196. Karstification with its base at 172 mbsf at Site 1199 seems not to follow this difference, as it is found at the same depth at Site 1196 (Fig. **F70**).

In logging Unit 4, resistivity shows a slightly decreasing downhole trend with few peaks in both holes, whereas uranium differs. At Site 1199, uranium has increasing values and variability from 386.2 to 363 mbsf, above which an abrupt decrease to lower values and variability occurs. This log character is similar, although with lower values, to the corresponding interval in Hole 1196A between 410 and 346 mbsf. Thus the top of the uranium increase at 363 mbsf, in connection with a resistivity peak, is used as a correlation horizon. This correlation makes lithologic Unit III (dolomitized rudstone) in Hole 1196A equivalent to lithologic Subunit IIB (skeletal grainstone and floatstone) in Hole 1199A. Recovery of lithologic Subunit IIIA (Hole 1196A) is, however, minimal, which might produce a biased recovery of dolomitized rocks (see **"Lithostratigraphy and Sedimentology,"** p. 5). Assuming that the correlation is correct, a thickness variation of ~50 m of equivalent facies can be postulated in the two holes (Fig. **F70**).

The second possibility of correlating log signatures based on the uranium would result in variable thickness of correlated packages and no general dip from one site to the other (Fig. **F71**). The most consistent correlative surface for both interpretations is the boundary between logging Units 1 and 2. Below this surface, four major correlation surfaces (*a, d, e,* and *f*) can be traced. Two additional surfaces (*b* and *c*) are distinguished but considered to be of minor prominence. Surface *a* marks the lower boundary of an interval with low uranium values. The sharp downhole increase in uranium with a following interval of higher uranium concentrations down to surface *d* at Site 1199 is related to a similar interval with elevated uranium concentrations at Site 1196 between surfaces *a* and *d* (Fig. **F71**). Surfaces *e* and *f* mark the upper and lower boundaries of an interval with a log signature that is very characteristic of increasing uranium concentrations. This pattern can be recognized in both holes and triggered the correlation based on uranium.

The resulting correlation scheme would be more consistent with the lithologic correlation, as it relates most of lithologic Subunit IIB in Hole 1199A to lithologic Subunits IIA and IIB in Hole 1196A. However, the scheme would correlate different log units in the two holes, which were

determined independently. In addition, the role of uranium as a primary facies indicator is not unambiguous, as it can be remobilized with migrating fluids. Furthermore, this correlation would create up to 70 m of topography on the shallow-water platform over a distance of only ~3 km, which is unlikely, considering the overall shallow-water facies retrieved in the cores.

SEISMIC STRATIGRAPHY

Sites 1196 and 1199 penetrated the SMP. The drowned and current-swept top of this platform edifice forms the modern seafloor. Site 1196 is positioned in a water depth of 304 m at the intersection of regional seismic lines MAR07 and MAR70 at shotpoints 2808 and 178, respectively (Fig. **F8,** p. 68, in the "Leg 194 Summary" chapter). Site 1199 is positioned in 316 m of water on line MAR20 at shotpoint 1341. Figures **F72** and **F2** display line MAR20 with the margin-parallel projected location of Site 1999. The two sites can be correlated along lines MAR70 and MAR20 as shown in Figure **F73.**

The main goal at these sites was to drill a complete section of the SMP into underlying basement in order to investigate the platform growth history, which can be linked to the slope and plateau record of other Leg 194 sites. Site 1996 penetrated to a depth of 672.2 through a thick platform section into a thin siliciclastic unit, but did not reach basement. Site 1999 is located ~3 km from Site 1996 and penetrated a 419.5-m-thick succession of platform sediments.

The irregular, scoured hard top of the platform (Fig. **F72**) yields a very high impedance contrast with the water column that scatters most of the acoustic energy from the seismic source. Consequently, only very limited subsurface information is available from underneath the platform. Two sites drilled on the upcurrent and downcurrent flanks of this platform (Sites 1198 and 1197, respectively) provide the seismic sequence stratigraphic framework that may be correlated with the platform subsurface.

Time-Depth Conversion

Downhole seismic measurements at Site 1196 were performed at 12 check shot stations between 94 and 523 mbsf, which provided an accurate time-depth correlation that is used to calibrate the integrated downhole velocity curve (see **"Downhole Measurements,"** p. 32). Velocity information was provided by the downhole sonic log data and, in the upper ~80 mbsf, where the pipe in the hole prevented downhole measurements, by *P*-wave velocity measurements on cores (see **"Core Physical Properties,"** p. 27). The resulting traveltime-to-depth correlation is shown in Figure **F11,** p. 73, in the "Leg 194 Summary" chapter. No check shot or sonic log is available for Site 1199, and the Site 1196 velocity-depth trend was used instead.

The velocity data, together with downhole density data, was used to calculate a seismic impedance curve for generation of a synthetic seismogram (Fig. **F74**). A normal polarity, zero-phase wavelet of 80-ms length was statistically extracted from the seismic data of line MAR20 and used for convolution of the downhole impedance curve and calculation of the synthetic seismogram.

F72. Multichannel line MAR07, Site 1196, p. 116.

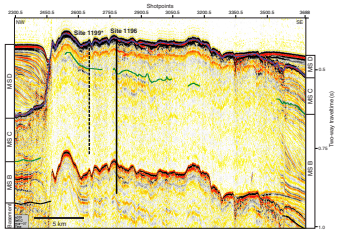

F73. Multichannel line MAR70 connected with seismic line MAR20, p. 117.

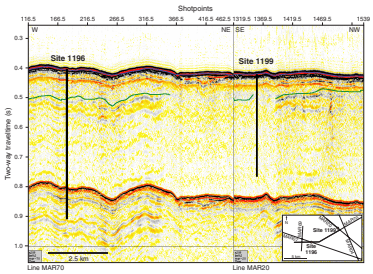

F74. Synthetic seismogram plotted on line MAR07, p. 118.

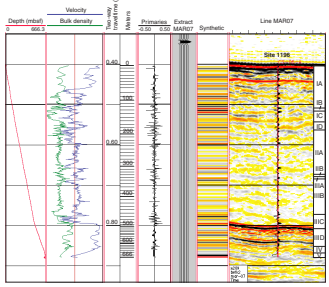

Seismic Facies and Geometries

The top of the SMP platform is characterized by a high-amplitude reflection that scatters and attenuates almost all seismic energy. The seismic facies is, consequently, almost transparent. In most areas, however, one broad low-frequency reflection can be traced at ~100 ms TWT below the platform top. This reflection does not mimic the seafloor morphology. Its topography is highly irregular and thus suggestive of a karstic surface (Fig. F72). It also forms an elevated rim at the upcurrent platform margin that is neither a multiple nor a velocity effect of the overlying platform top. The reflection overall dips to the southeast beyond the downcurrent slope of the platform and appears to correlate with the seismic Megasequence B/C boundary (Site 1197) (Fig. F2). The intraplatform reflection could thus be the platform equivalent of B/C and separate the middle Miocene growth phase of the SMP from the late Miocene growth phase.

Correlation with Cores

Sites 1196 and 1199 sediments consist mostly of shallow-water carbonates, which overlie a thin siliciclastic unit representing the flooding of the basement during the latest Oligocene and the earliest Miocene. Large parts of the section are dolomitized (see "Lithostratigraphy and Sedimentology," p. 5). For the upper part (0-~170 mbsf) of the lithocolumn, both sites seem to have very similar sedimentary records, whereas differences increase deeper in the platform. Of prime interest for seismic stratigraphy is the origin of the low-frequency intraplatform reflection at ~100 ms TWT. Using the time-depth curve from the check shots, 100 ms is the equivalent of ~110 mbsf. In both cores, this depth coincides with a zone, displaying numerous indications of subaerial exposure (caliche crusts, vadose silt, and very indurated cemented lithology). In addition, drilling operations revealed several holes that also are indicative of an extensive karst system and just below that depth. In both holes, a depth of 110–130 mbsf matches the transition between lithologic Subunits IA through ID. Subunits IA and IB are rhodolithic dolostones that overlie a reefal interval (Subunit IC), which is only partly dolomitized and overlies another dolomitic floatstone unit. Evidence of exposure occurs above and below Subunit IC. The position of the intraplatform reflection at approximately the same depth was confirmed by the synthetic seismogram, which also shows a high amplitude at ~120 mbsf (Fig. F74). Consequently, the low-frequency reflection can likely be correlated with those exposure indications between 110 and 130 mbsf. However, as a result of the broad reflection character, the seismic pick of the boundary is not very accurate. In addition, it is biostratigraphically not proven whether this platform horizon truly separates the middle Miocene SMP from an overlying late Miocene growth phase. Alternatively, the middle to late Miocene boundary could be located slightly deeper at 163 mbsf, as discussed in "Downhole Measurements," p. 32.

REFERENCES

Allan, T.L., Trotter, J.A., Whitford, D.J., and Korsch, M.J., 2000. Strontium isotope stratigraphy and the Oligocene-Miocene T-letter "stages" in Papua New Guinea. *In* Buchanan, P.G., Grainge, A.M., and Thornton, R.C.N. (Eds.), *Proc. Fourth Petrol. Conv:* Port Moresby, 155–168.

Betzler, C., 1997. Ecological control on geometries of carbonate platforms: Miocene/Pliocene shallow-water microfaunas and carbonate biofacies from the Queensland Plateau (NE Australia). *Facies,* 37:147–166.

Chaproniere, G.C.H., 1981. Australasian mid-Tertiary larger foraminiferal associations and their bearing on the East Indian Letter Classification. *BMR J. Aust. Geol. Geophys.,* 6:145–151.

Chaproniere, G.C.H., 1984. The Neogene larger foraminiferal sequence in the Australian and New Zealand regions, and its relevance to the East Indian Letter Stage classification. *Palaeogeogr., Palaeoclimatol., Palaeoecol.,* 46:25–35.

Chaproniere, G.C.H., and Betzler, C., 1993. Larger foraminiferal biostratigraphy of Sites 815, 816, and 826, Leg 133, northeastern Australia. *In* McKenzie, J.A., Davies, P.J., Palmer-Julson, A., et al., *Proc. ODP, Sci. Results,* 133: College Station, TX (Ocean Drilling Program), 39–49.

Dunham, R.J., 1962. Classification of carbonate rocks according to depositional texture. *In* Ham, W.E. (Ed.), *Classification of Carbonate Rocks*. AAPG Mem., 108–121.

Eberli, G.P., Swart, P.K., Malone, M.J., et al., 1997. *Proc. ODP, Init. Repts.,* 166: College Station, TX (Ocean Drilling Program).

Hallock, P., 1981. Production of carbonate sediments by selected foraminifera on two Pacific coral reefs. *J. Sediment. Petrol.,* 51:467–474.

Hallock, P., 1984. Distribution of larger foraminiferal assemblages on two Pacific coral reefs. *J. Foraminiferal Res.,* 14:250–261.

Haq, B.U., 1978. Calcareous nannoplankton. *In* Haq, B.U., and Boersma, A. (Eds.), *Introduction to Marine Micropaleontology:* New York (Elsevier), 79–107.

Haq, B.U., Hardenbol, J., and Vail, P.R., 1987. Chronology of fluctuating sea levels since the Triassic. *Science,* 235:1156–1167.

Hohenegger, J., 1999. Larger foraminifera—microscopical greenhouses indicating shallow-water tropical and subtropical environments in the present and past. *Occasional Papers*. Kagoshima Univ. Res. Central Pacific Islands, 32:19–45.

Hunt, J.M., 1996. *Petroleum Geochemistry and Geology* (2nd ed.): New York (W.H. Freeman and Co.).

Keen, C., and Beaumont, C., 1990. Geodynamics of rifted continental margins. *In* Keen, M.J., and Williams, G.L. (Eds.), *Geology of the Continental Margin of Eastern Canada*. Geol. Soc. Am., 1:391–472.

Martín, J.M., Braga, J.C., Konishi, K., and Pigram, C.J., 1993. A model for the development of rhodoliths on platforms influenced by storms: middle Miocene carbonates of the Marion Plateau (northeastern Australia). *In* McKenzie, J.A., Davies, P.J., Palmer-Julson, A., et al., *Proc. ODP, Sci. Results,* 133: College Station, TX (Ocean Drilling Program), 455–460.

Schlumberger, 1998. *Log Interpretation Charts:* Houston (Schlumberger).

Shipboard Scientific Party, 1991. Principal results and summary. *In* Davies, P.J., McKenzie, J.A., Palmer-Julson, A., et al., *Proc. ODP, Init. Repts.,* 133 (Pt. 1): College Station, TX (Ocean Drilling Program), 59–72.

Triffleman, N.J., Hallock, P., Hine, A.C., and Peebles, M., 1992. Morphology, sediments, and depositional environments of a small, partially drowned carbonate platform: Serranilla Bank, Nicaraguan Rise, Southwest Caribbean Sea. *J. Sediment. Petrol.,* 62:591–606.

Tsuji, Y., 1993. Tide influenced high energy environments and rhodolith-associated carbonate deposition on the outer shelf and slope off the Miyako Islands, southern Ryukyu Island arc, Japan. *Mar. Geol.,* 113:255–271.

Tucker, M.E., and Wright, P.V., 1990. *Carbonate Sedimentology:* Oxford (Blackwell Sci. Publ.).

Wyllie, M.R.J., Gregory, A.R., and Gardner, L.W., 1956. Elastic wave velocities in heterogeneous and porous media. *Geophysics,* 21:41–70.

Figure F1. Bathymetry map showing locations of Leg 194 sites. Sites 1196 and 1199 are shown in bold.

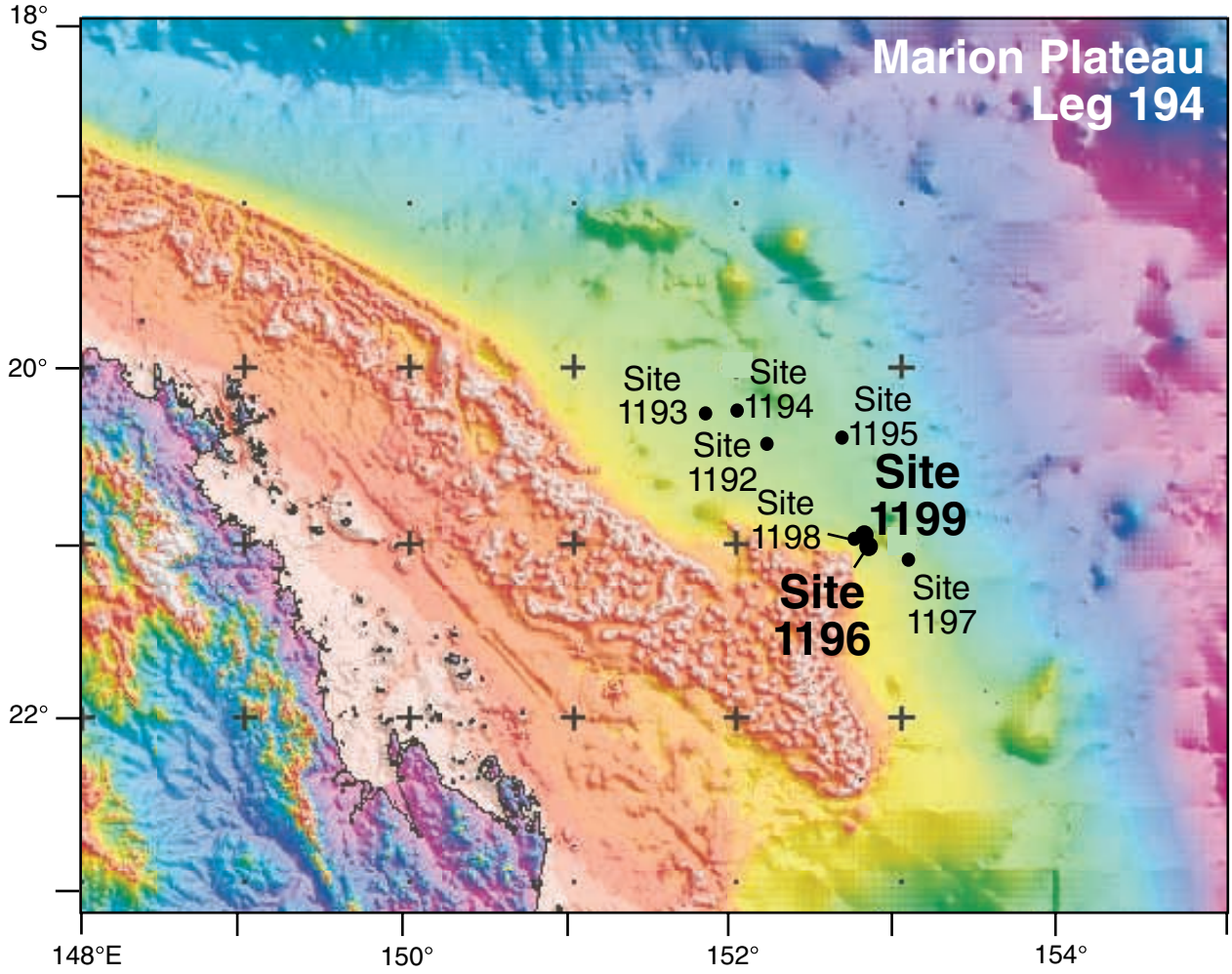

Figure F2. Seismic line MAR07 with locations of Sites 1196, 1197, 1198, and 1199. Sites 1196 and 1199 are positioned on top of the southern carbonate platform (SMP). * = projected into the seismic section parallel to the northwestern Southern Marion Platform (SMP) margin. MS = Mega-sequence.

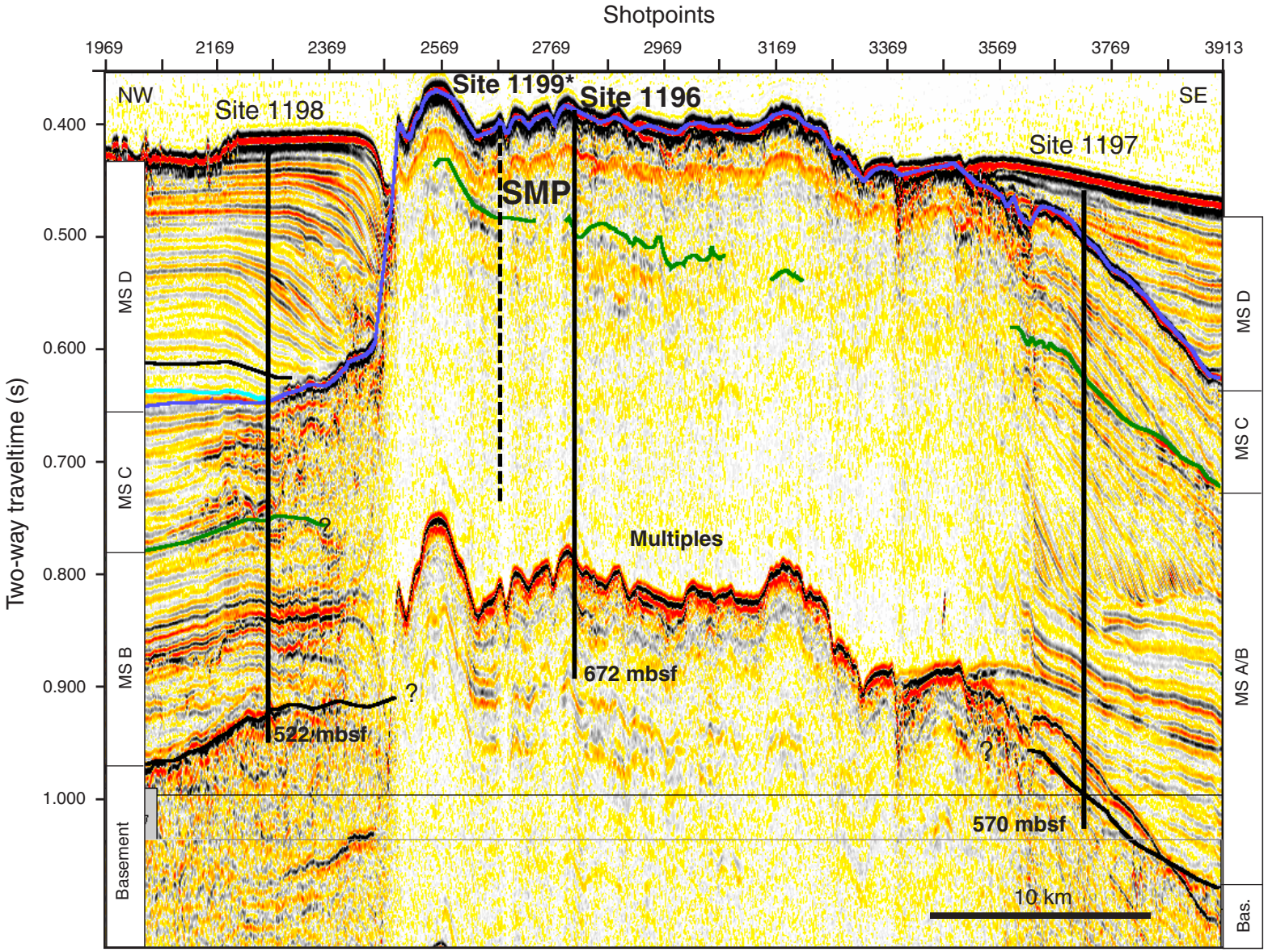

Figure F3. Video sequence of bare-rock reentry of Hole 1196B with an ADCB bit without the aid of a free-fall funnel. The small dial with the arrow attached to the drill string indicates north. The diameter of the hole is ~25 cm; the outer diameter of the ADCB bit is 18.5 cm (7.25 in). (QuickTime software is available for the Macintosh and Windows platforms only. Please see **"QuickTime Movies"** in 194IR.PDF for further information. Click the image to play the movie.)

Figure F4. Lithologic summary for Site 1196. **A.** Core recovery. Black = recovered. White = gaps. **B.** Lithologic units as defined in this section. **C.** Graphic representation of lithology. **D.** Distribution of carbonate and noncarbonate fraction (see "Geochemistry," p. 24). **E.** Dunham (1962) texture classification. **F.** Hard surfaces. **G.** Facies interpretation. **H.** Geological age (see "Biostratigraphy and Paleoenvironments," p. 16, and "Age Model," p. 24).

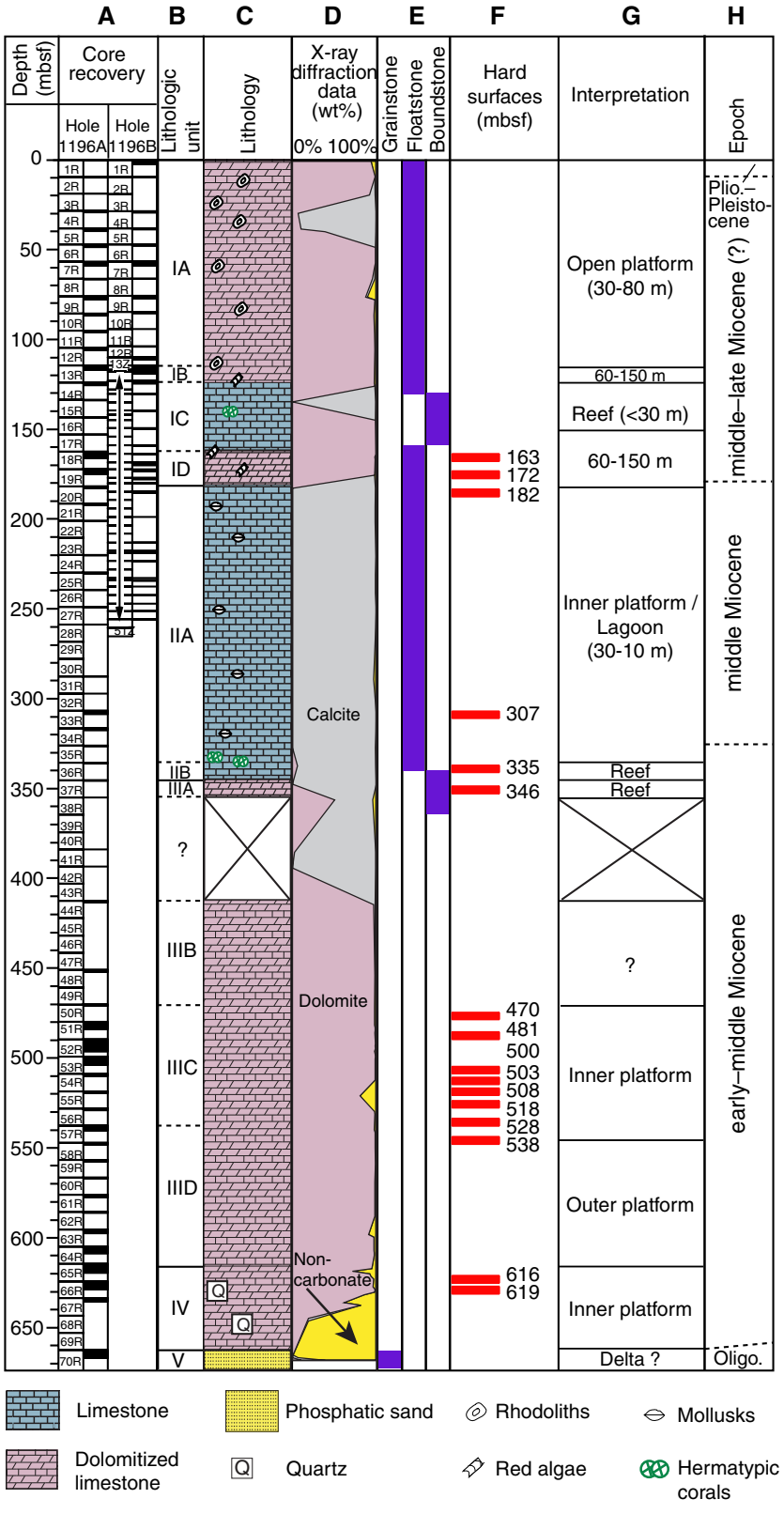

Figure F5. Close-up photograph of the uppermost part of Core 194-1196A-1R. Note the highly corrugated, iron-stained surface forming the top of Unit I (arrows). The pale brown layer above this surface consists of skeletal wakestone with planktonic foraminifers. The pink rock below the surface is a skeletal floatstone with rhodoliths. The floatstone matrix is a grainstone rich in larger benthic foraminifers. The rectangle shows the location of Figure F6, p. 49.

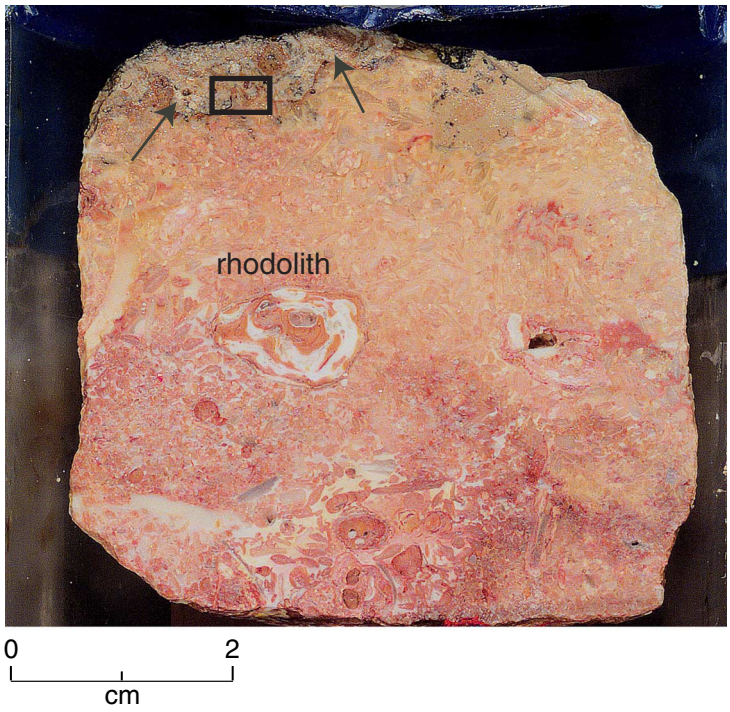

Figure F6. Photomicrograph of the corrugated upper surface (arrows) of the platform carbonates retrieved at this site (cf. Fig. F5, p. 48). The lower facies is a coarse skeletal grainstone with larger benthic foraminifers, red algae and *Halimeda* fragments of Miocene age. The upper facies is a skeletal wackestone with planktonic foraminifers deposited in a deeper depositional environment than the underlying lithology. The circled planktonic foraminifer suggests an age younger than 3.2 Ma (see **"Biostratigraphy and Paleoenvironments,"** p. 16).

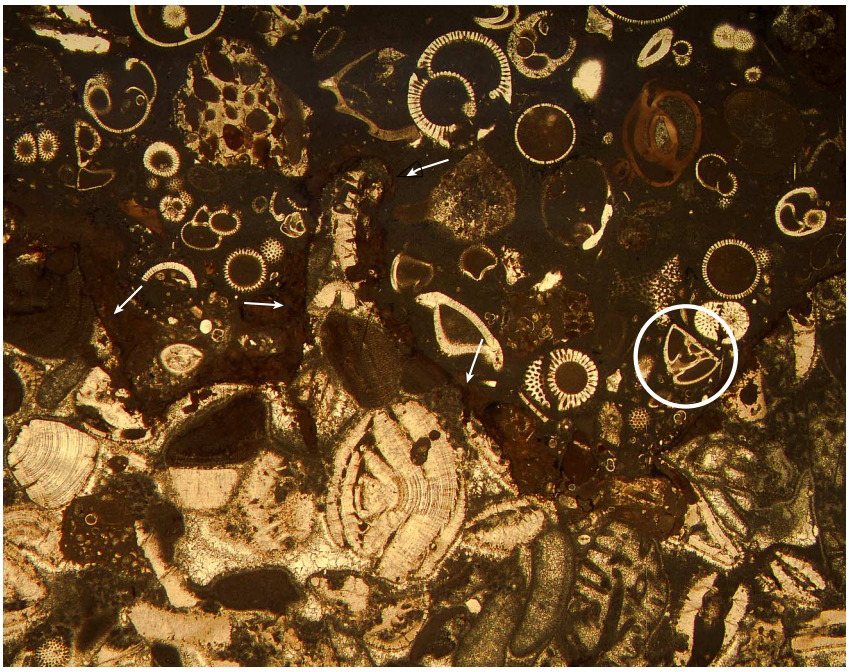

Figure F7. Close-up photograph of stromatolitic crust recovered from the top of Unit I in Hole 1196B (Core 194-1196B-1R). White and black rectangles at the bottom of the photograph are 1 cm long.

Figure F8. Photomicrograph of the stromatolitic crust shown in Figure F7, p. 50. Note planktonic foraminifer trapped within the crust (arrow).

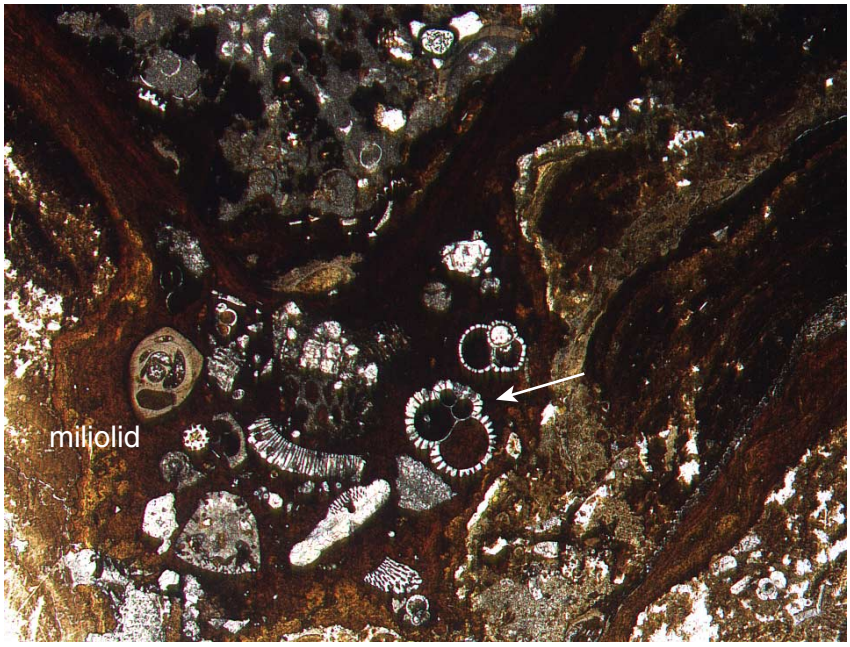

Figure F9. Close-up photograph of macrofacies of the dolomitic floatstone/rudstone with rhodoliths and a grainstone matrix typical of Subunit IA (interval 194-1196B-14Z-1, 33–43 cm).

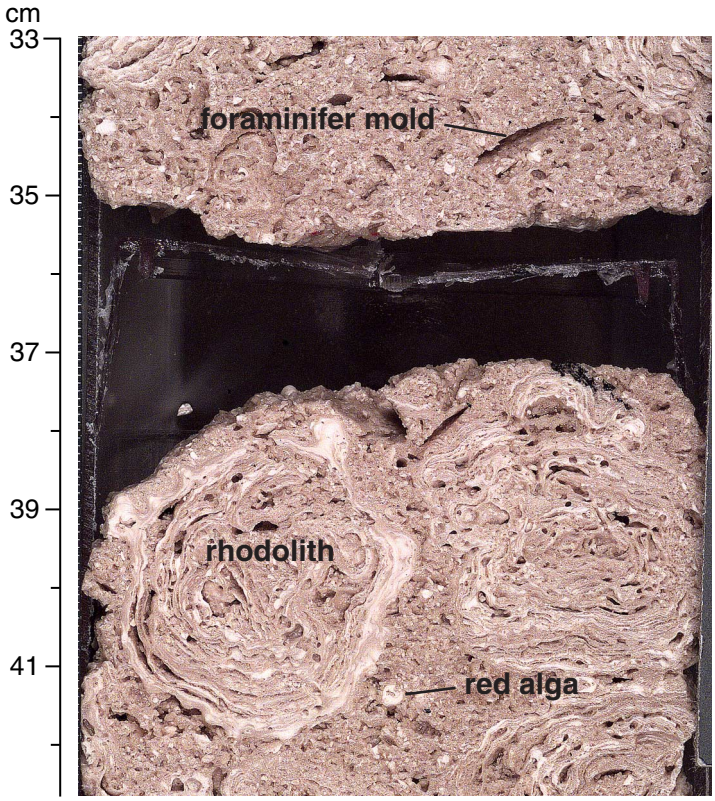

Figure F10. Photomicrograph showing microfacies of the grainstone matrix from Subunit IA (cf. Fig. F9, p. 52). Intergranular pores have been filled by a succession of cements and internal sediment including several generations of isopachous fibrous rims (arrows), vadose silt (V), blocky calcite (B). Vadose silt and unbroken micrite envelopes (me) result from fresh-water action in a near-surface diagenetic environment.

Figure F11. Close-up photograph of macrofacies of dolomitic floatstone with red algae and larger benthic foraminifer molds; Subunit IB (interval 194-1196A-14R-1, 129–139 cm). Note faint cross stratification, which is parallel to foraminifer mold orientation.

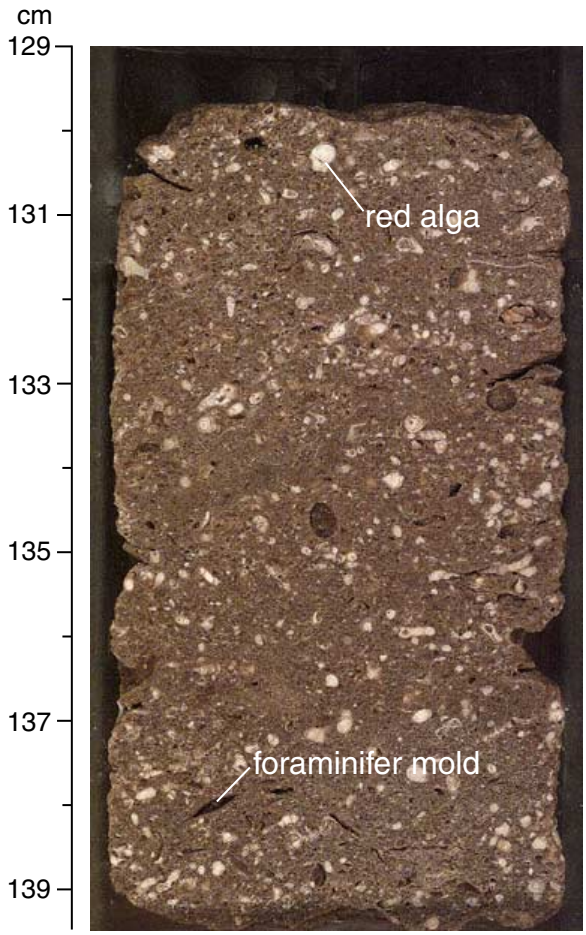

Figure F12. Close-up photograph of coral boundstone/rudstone from Subunit IC (interval 194-1196A-15R-1, 0–10 cm). Unlike the overlying and underlying units, this lithology is not dolomitized.

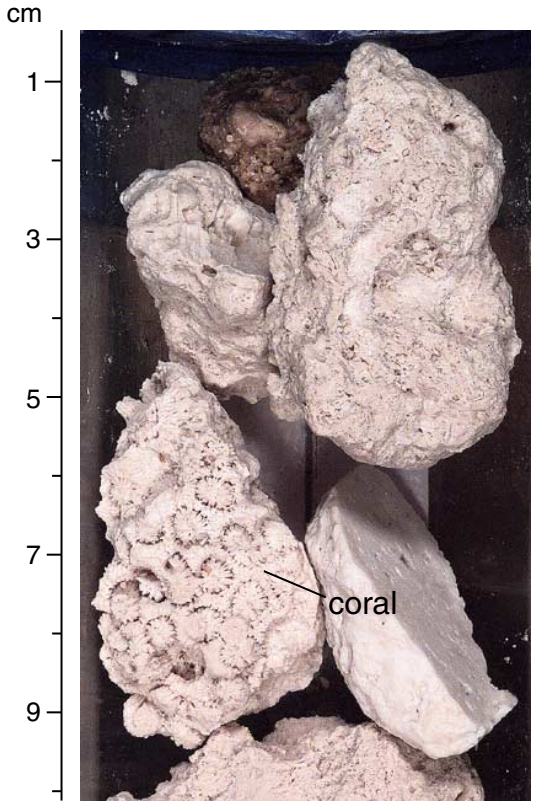

Figure F13. Close-up photograph of dolomitic floatstone with coral and branching red algae fragments from Subunit ID (interval 194-1196A-19R-2, 57–67 cm). Distinct lamination occurs at 65 cm. Note similarity with Subunit IB lithofacies.

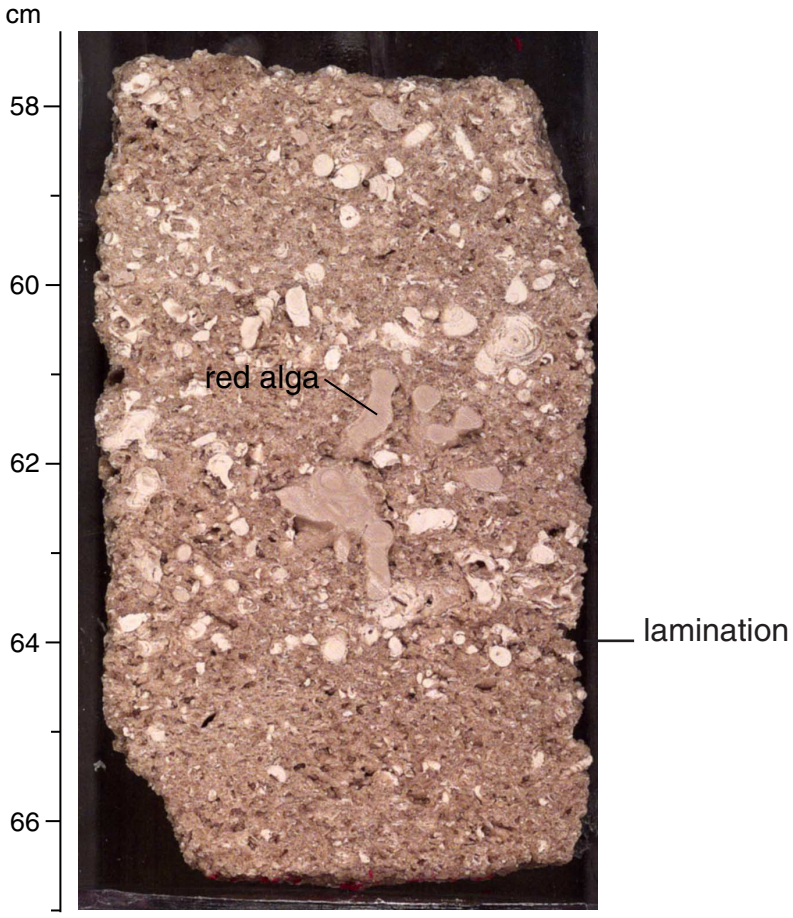

Figure F14. Close-up photograph of boundary between Units I and II (interval 194-1196A-20R-1, 22–31 cm).

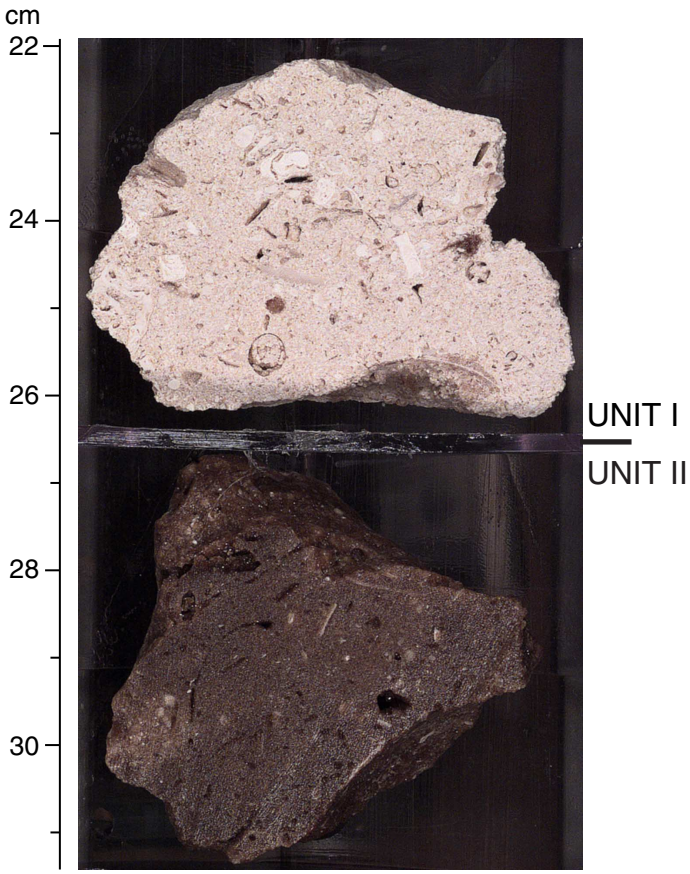

Figure F15. Close-up photograph of skeletal floatstone with mollusk fragments and larger benthic foraminifers, typical of Subunit IIA (interval 194-1196A-33R-1, 18–23 cm).

Figure F16. Photomicrograph of the skeletal floatstone shown on Figure F15, p. 58. Note that interparticle voids are filled with blocky calcite cement (b).

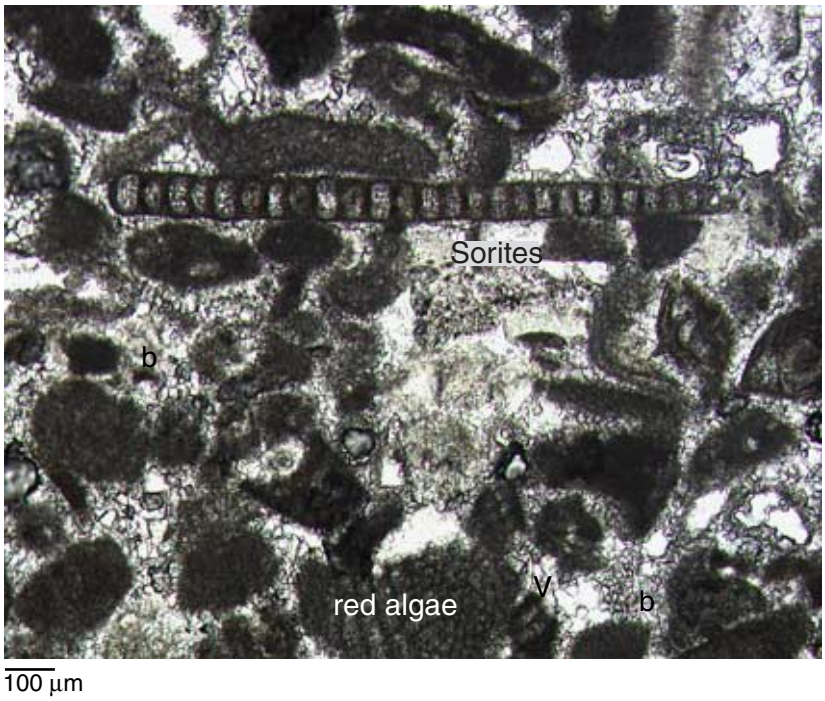

Figure F17. Close-up photograph of the boundary between Unit II and Unit III (interval 194-1196A-37R-1, 22–38 cm). Both units consist of coral rudstone/boundstone facies. The Unit II reef is composed of calcite, whereas the Unit III reef has been pervasively dolomitized.

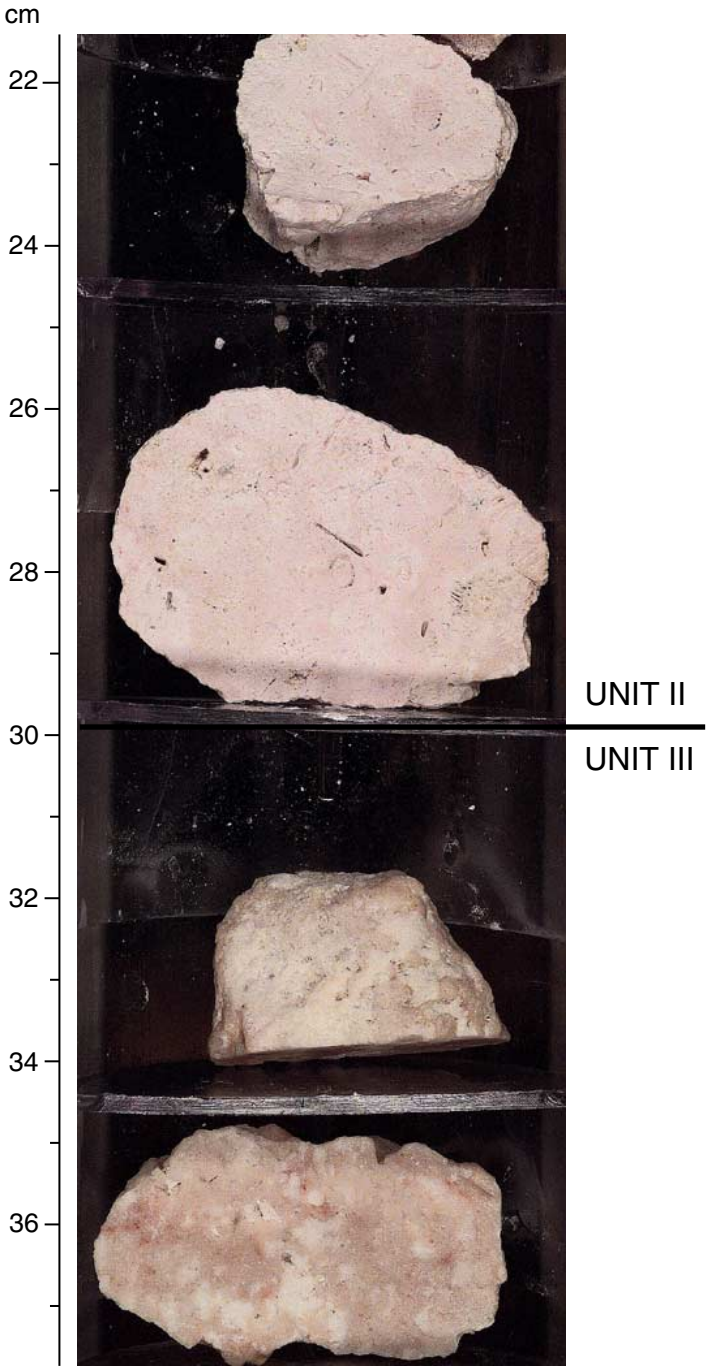

Figure F18. Close-up photograph of macrofacies of the sucrosic dolostone ("snowstone") typical of Subunit IIIB (interval 194-1196A-44R-1, 85–91 cm). Homogenous lithology and the presence of rare fenestrae suggest that this rock could be derived from tidal flat muds.

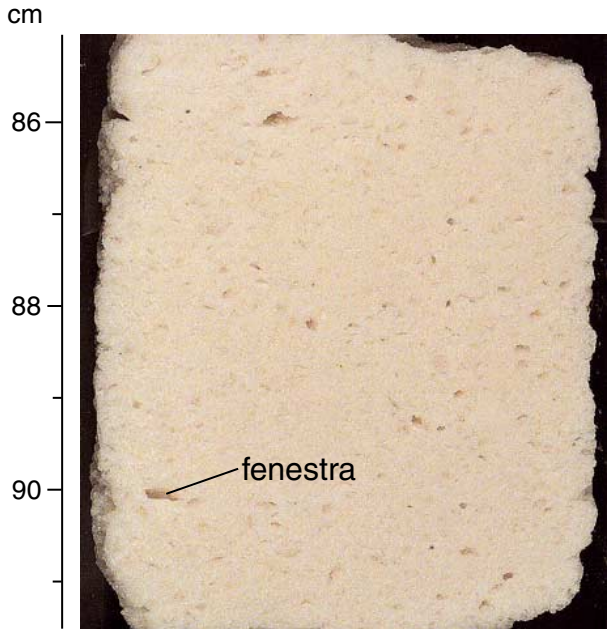

Figure F19. Photomicrograph showing microfacies of the variegated dolostone from Subunit IIIC (Sample 194-1196A-51R-1, 69–71 cm). Note the ghosts of coralline algae fragments and large dolomite crystals.

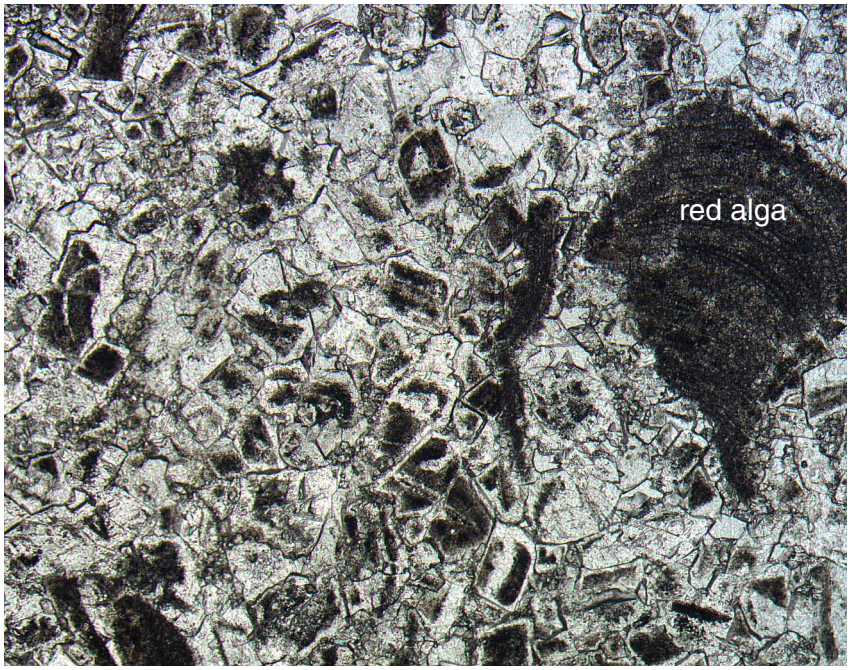

Figure F20. Close-up photograph of possible exposure surface in variegated dolostone, Subunit IIIC (interval 194-1196A-51R-1, 60–66 cm). The fenestrae in the upper piece also suggest subaerial exposure.

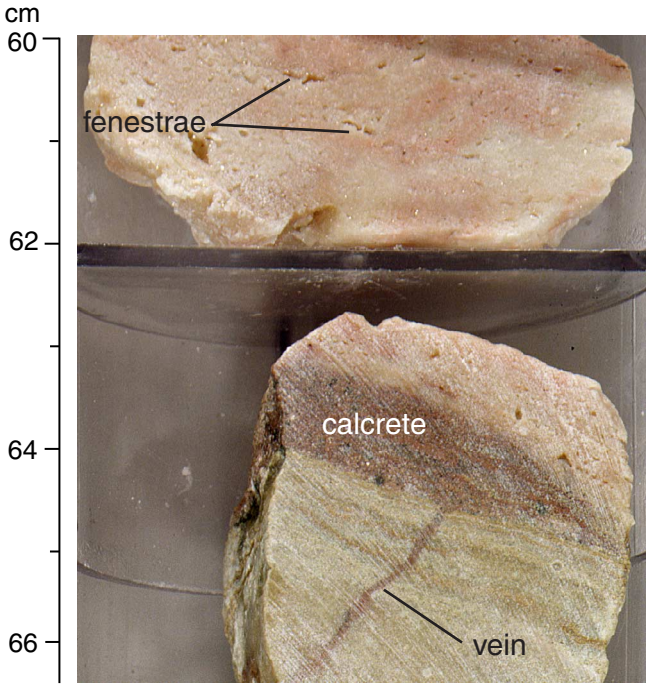

Figure F21. Close-up photograph of macrofacies from Subunit IIID (interval 194-1196A-58R-1, 24–28 cm). Note the ghosts of red algae and foraminifer molds in the dolostone.

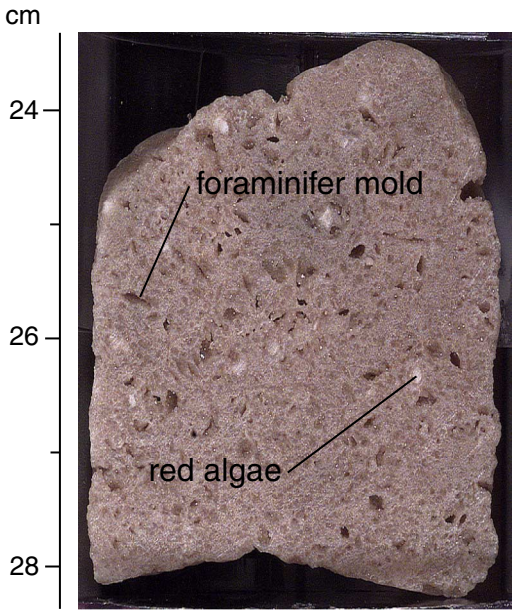

Figure F22. Close-up photograph of facies variability in Unit IV (interval 194-1196A-66R-4, 20–34 cm). This interval is an example of a reddish dolostone and a dolostone with glauconite.

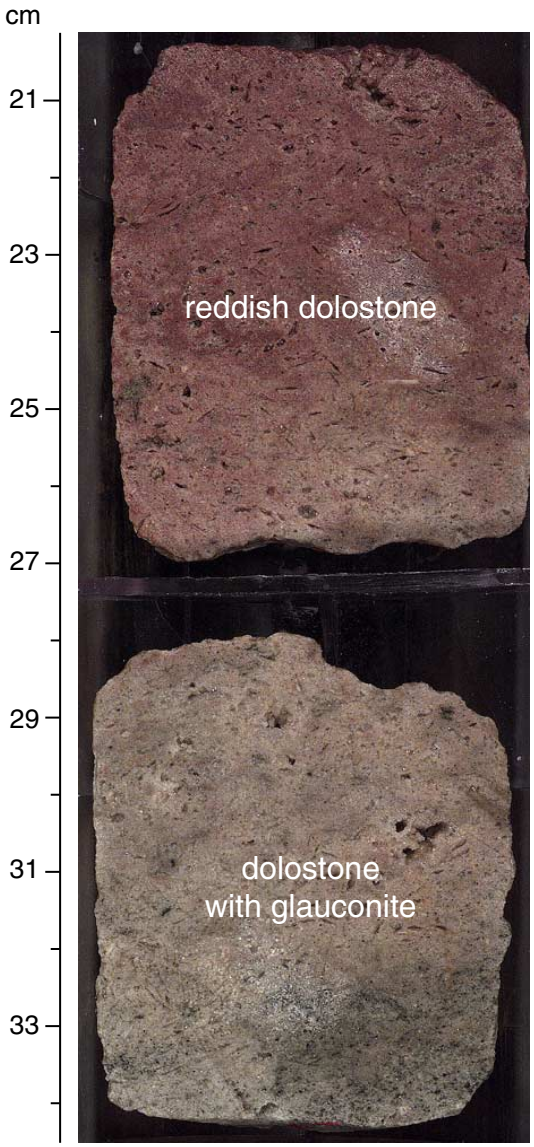

Figure F23. Close-up photograph of macrofacies of the Oligocene rocks recovered from the base of Hole 1196A (interval 194-1196A-70R-1, 1–10 cm).

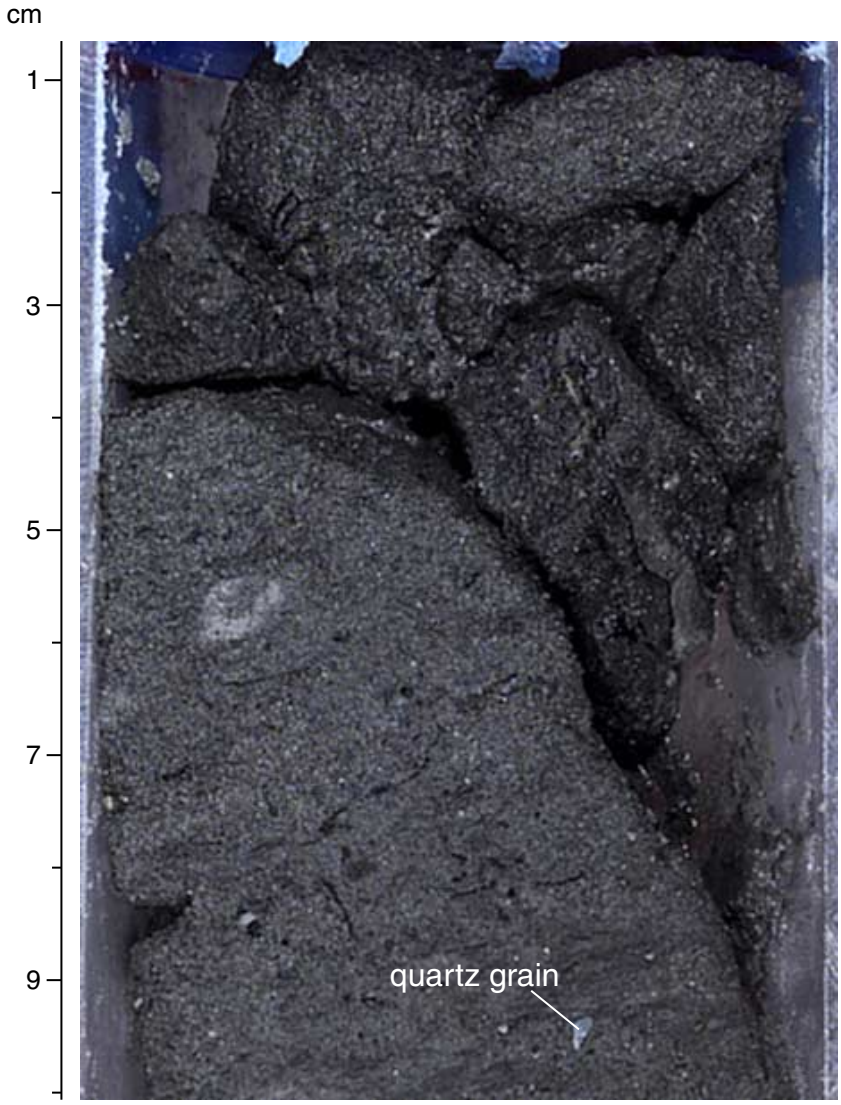

Figure F24. Lithologic summary for Site 1199. **A.** Core recovery. Black = recovery, white = coring gaps. **B.** Lithologic units as defined in this section. **C.** Graphic representation of lithology. **D.** Distribution of carbonate and noncarbonate fraction (see "Geochemistry," p. 24). **E.** Dunham (1962) texture classification. **F.** Hard surfaces. **G.** Facies interpretation. **H.** Epochs (see "Biostratigraphy and Paleoenvironments," p. 16, and "Age Model," p. 24).

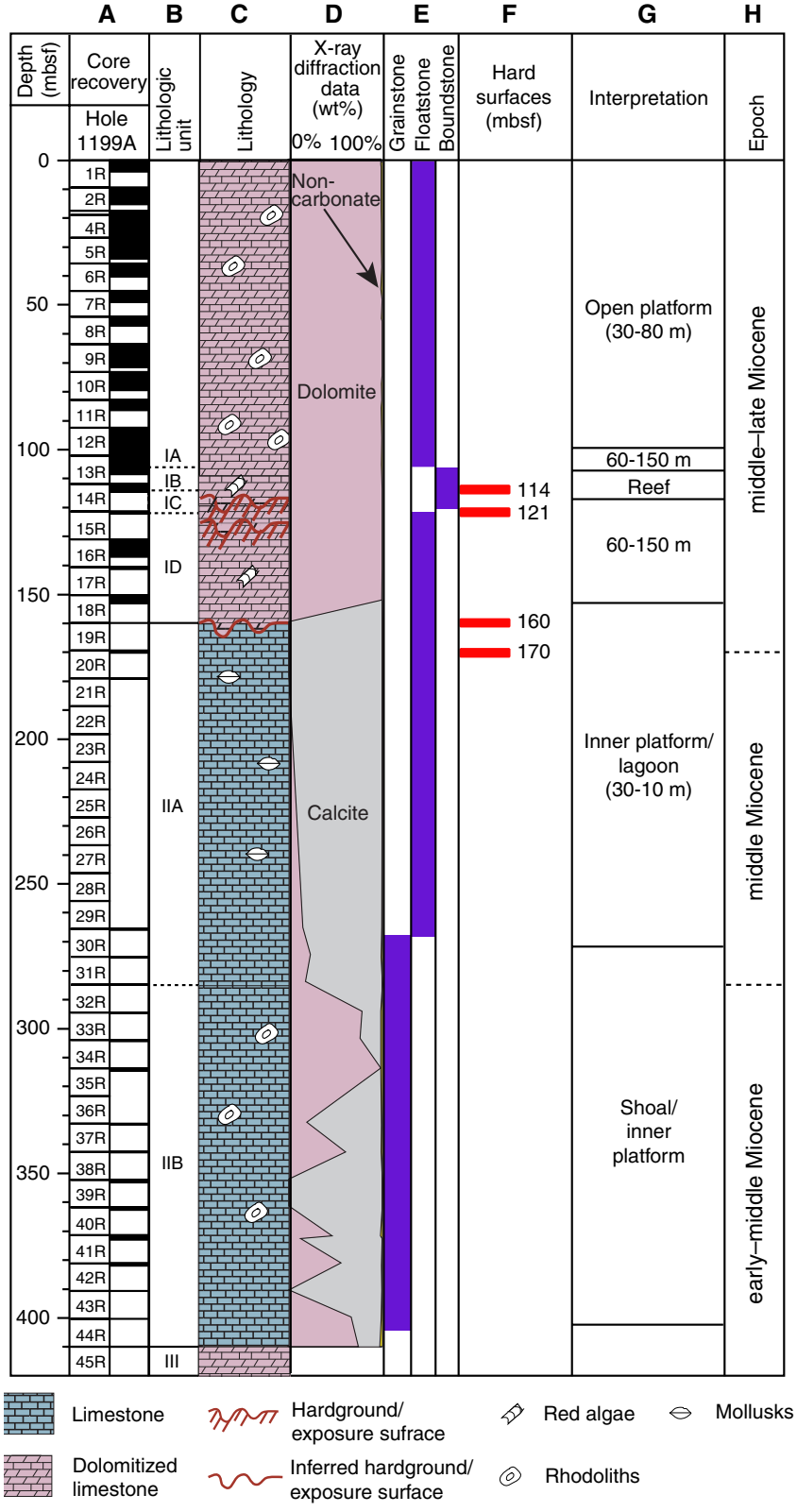

Figure F25. Close-up photograph of geopetal structure (interval 194-1199A-2R-3, 28–32 cm). The large void within a rhodolith has been partly filled with foraminiferal wackestone. The infill surface indicates the ancient horizontal plane, which makes an angle with respect to the core edges because of oblique drilling.

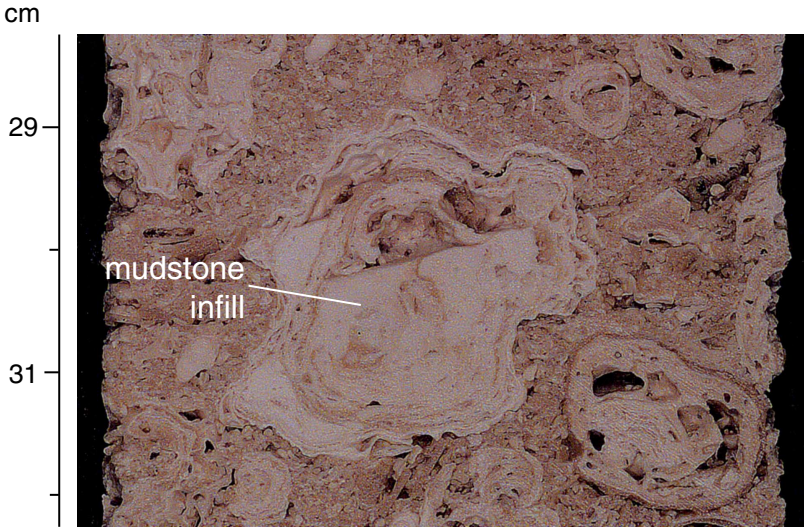

Figure F26. Close-up photograph of interval of crude coarse-tail grading of rhodoliths (arrow) within Subunit IA (interval 194-1199A-5R-3, 112–124 cm), possibly indicating that the latter was deposited at a depth less than storm-wave base.

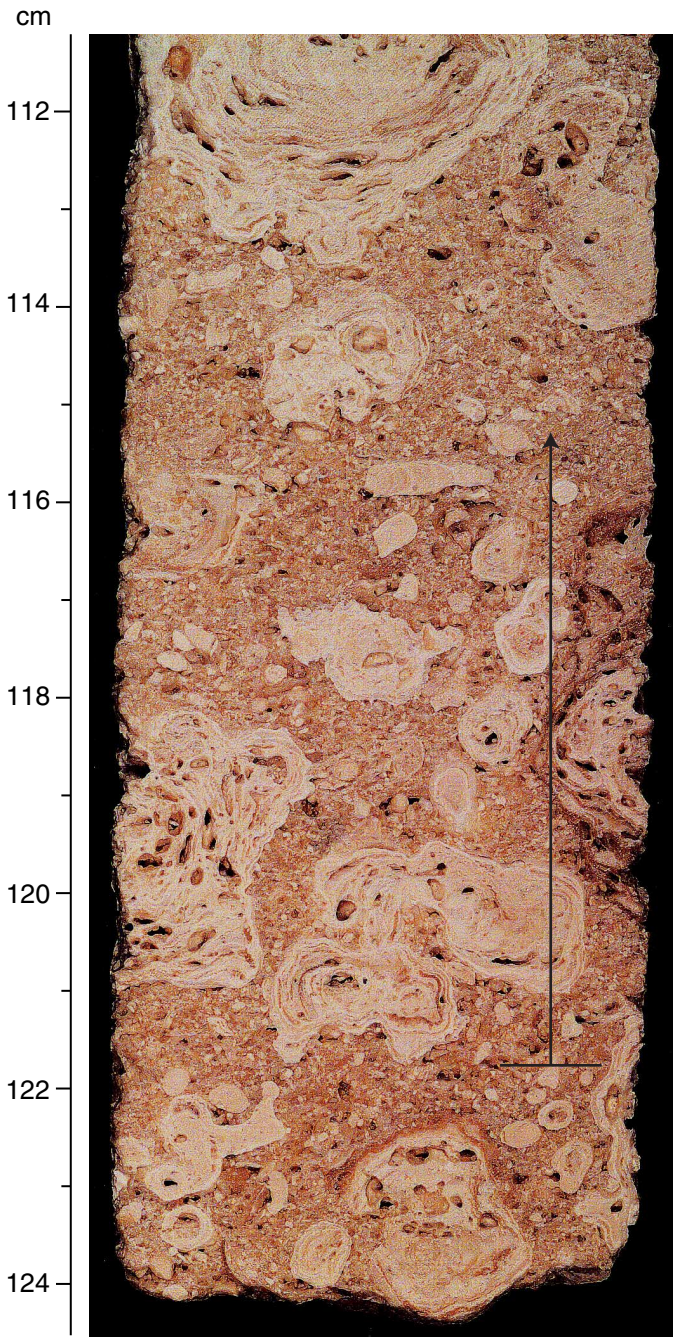

Figure F27. Close-up photograph of boundary between Subunit IB (dolomitic floatstone with red algae fragments) and Subunit IC (dolomitic coral boundstone/rudstone) (interval 194-1199A-14R-2, 82–96 cm). This boundary occurs at 114.1 mbsf and is interpreted as an exposure surface.

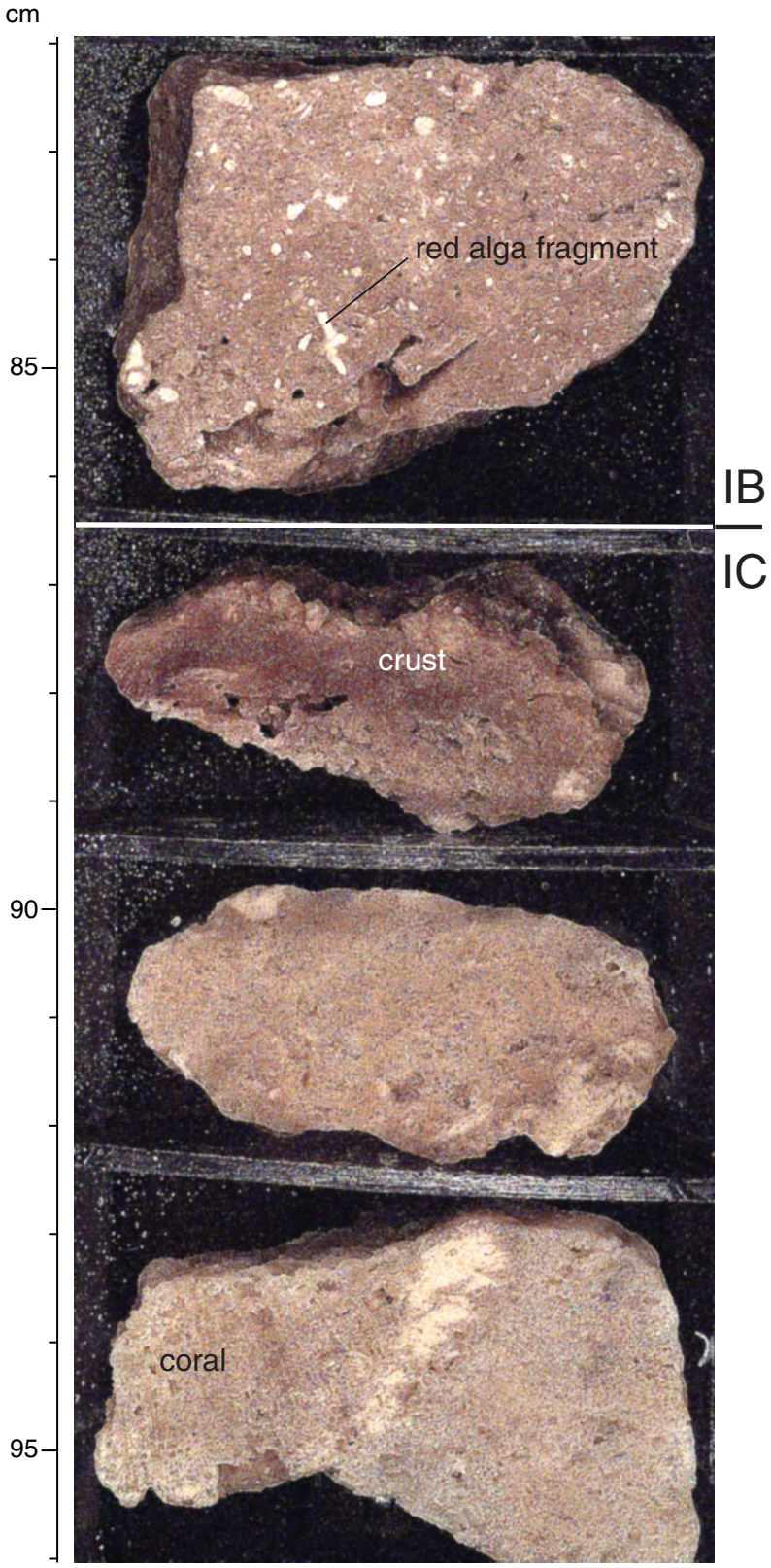

Figure F28. Close-up photograph of vuggy porosity and infiltrated reddish silt within dolomitic skeletal rudstone typical of Subunit IC (interval 194-1199A-15R-1, 5–20 cm). These features indicate pervasive karstification of this unit.

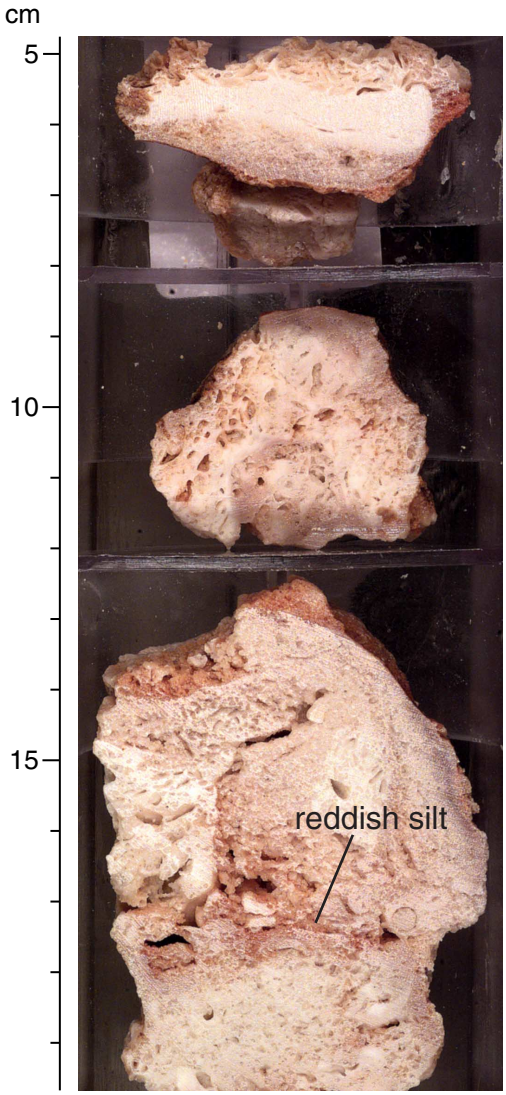

Figure F29. Close-up photograph of boundary between Subunit IC (dolomitic coral boundstone/rudstone) and Subunit ID (dolomitic floatstone with red algae fragments; interval 194-1199A-15R-1, 47–61 cm). This boundary, which occurs at 121.9 mbsf, is characterized by thin red crust containing silt-sized quartz grains. This boundary may correspond to the middle/late Miocene boundary.

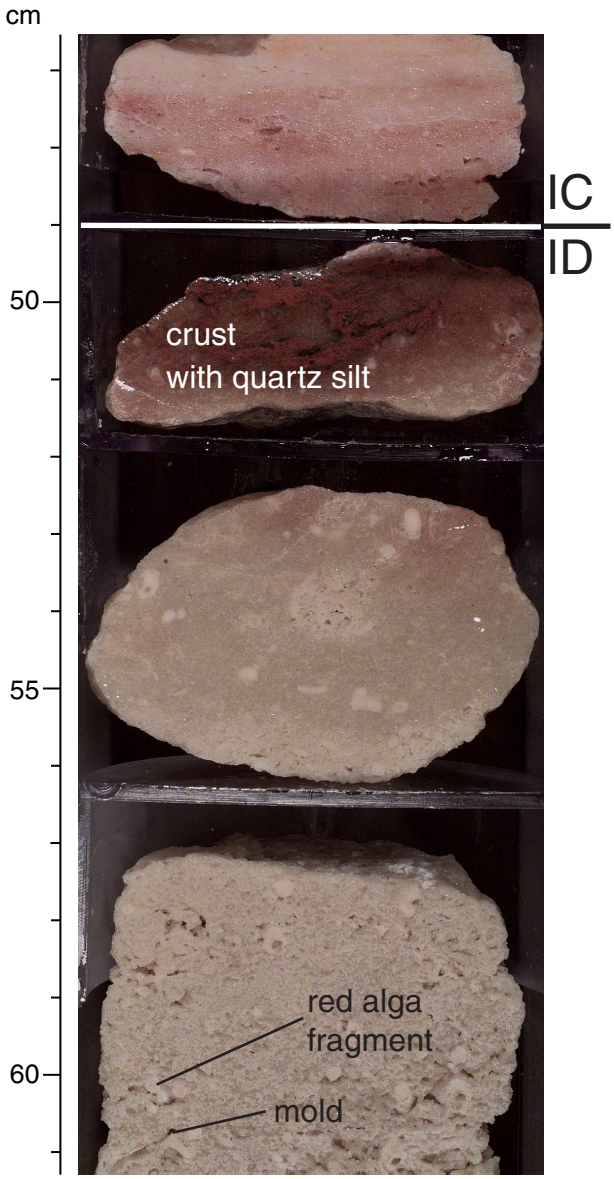

Figure F30. Close-up photograph of skeletal floatstone with mollusk shells, coral fragments (preserved as molds), and porcellaneous benthic foraminifers (within the circle) (interval 194-1199A-20R-1, 22–28 cm; Subunit IIA).

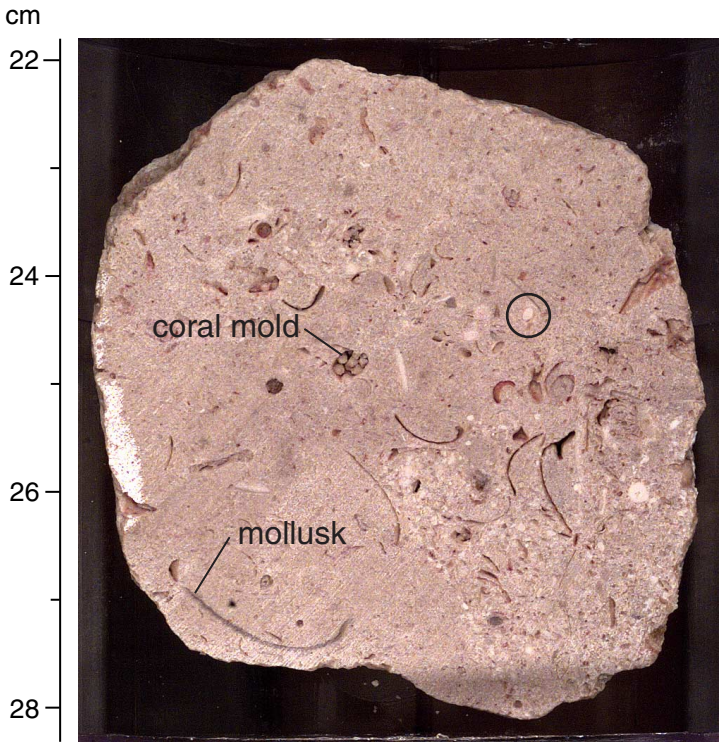

Figure F31. Close-up photograph of friable skeletal grainstone, including benthic foraminifers, echinoderm fragments, *Halimeda,* and coralline algae debris (interval 194-1199A-41R-1, 47–53 cm; Subunit IIB).

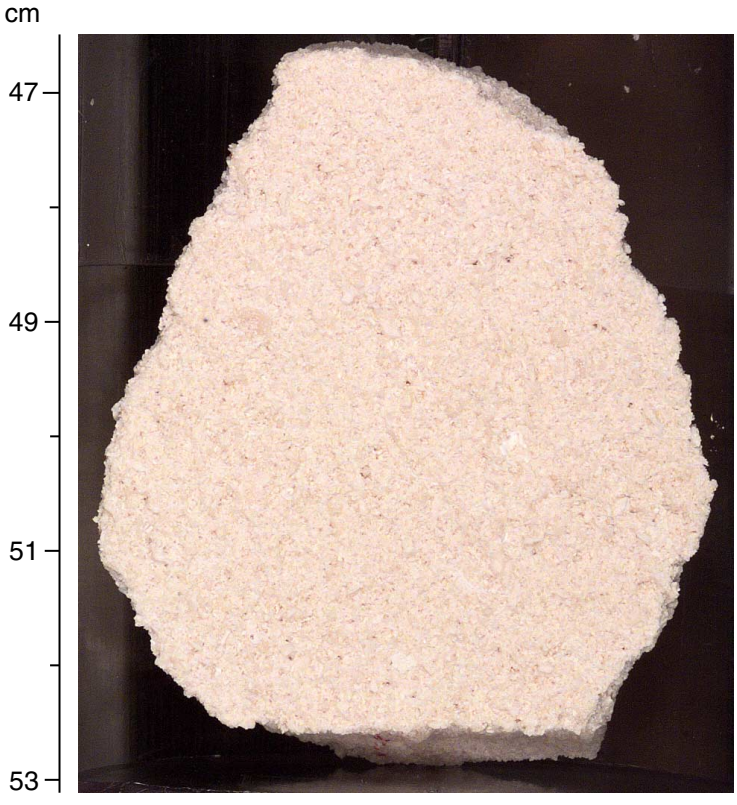

Figure F32. Photomicrograph of transverse section of *Flosculinella botangensis* (Fb) specimen from Sample 194-1196A-33R-1, 19–23 cm. A red algal fragment (RA) is also noted.

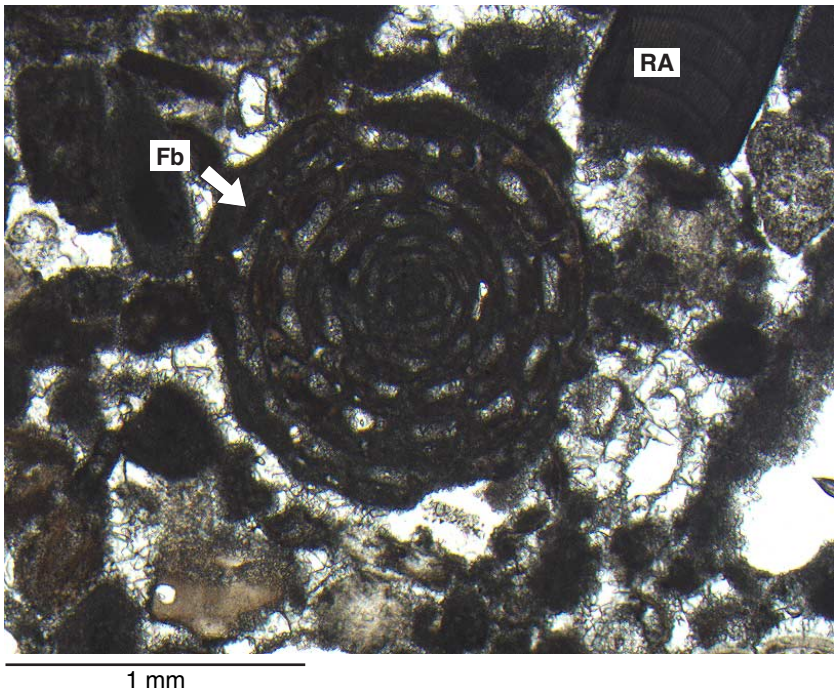

Figure F33. Photomicrograph of vertical section of a specimen of an unidentified Soritidae (Co), possibly belonging to the genus *Cyclorbiculina,* from Sample **194-1196A-33R-1, 19–23 cm.**

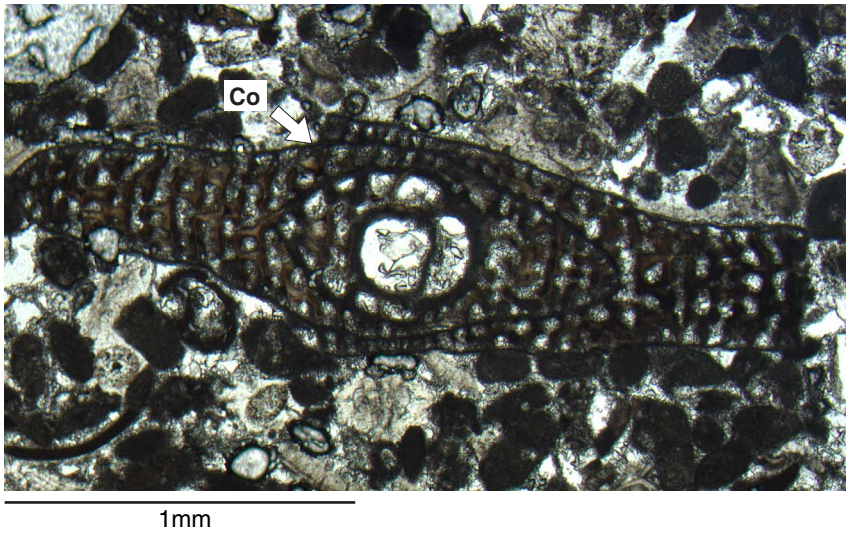

Figure F34. Zijderveld plot for long-core interval measured as continuous sample. Note that although the rock is only partially cleaned at 30-mT demagnetization (demag), the component plots are approaching linear convergence to the origin.

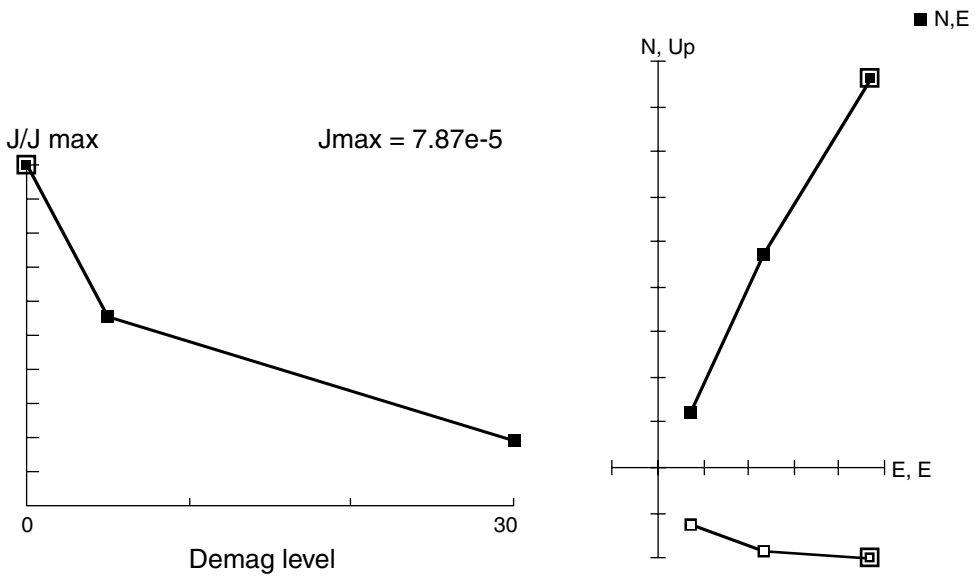

Demag	Declination	Inclination	Intensity
0.0	28.6	11.4	7.87e-5
5.0	25.9	19.1	4.39e-5
30.0	30.2	40.7	1.49e-5

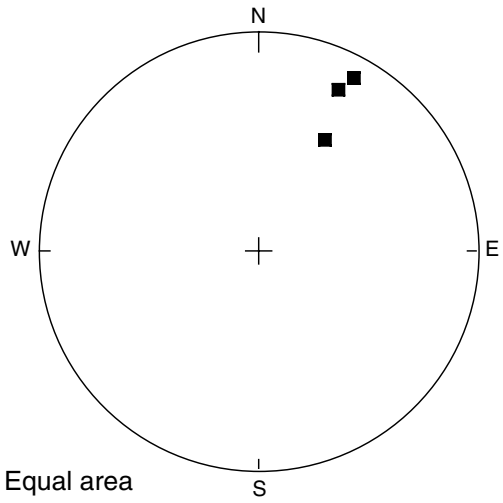

Continuous measurement
Interval 194-1196A-7R-2, 2.5–12.5 cm

Figure F35. Long-core measurements of intensity and inclinations for Hole 1196A.

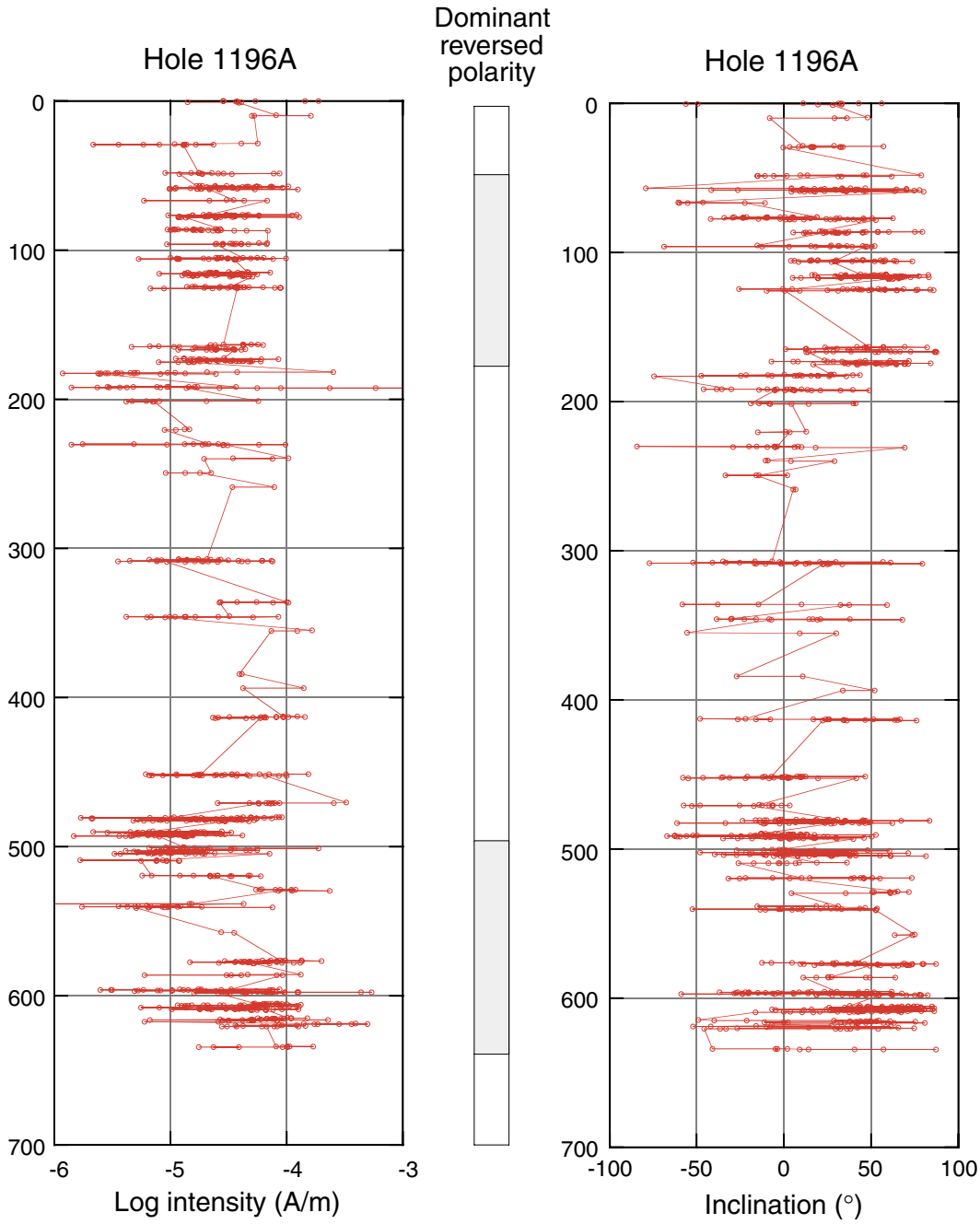

Figure F36. Long-core measurements for Holes 1196A and 1196B for the uppermost 200 mbsf. Note that whereas inclination is given for the RCB cores, the y-component is given for the ADCB cores because of the coordinate transformation. For these cores, a positive value corresponds to a reverse polarity.

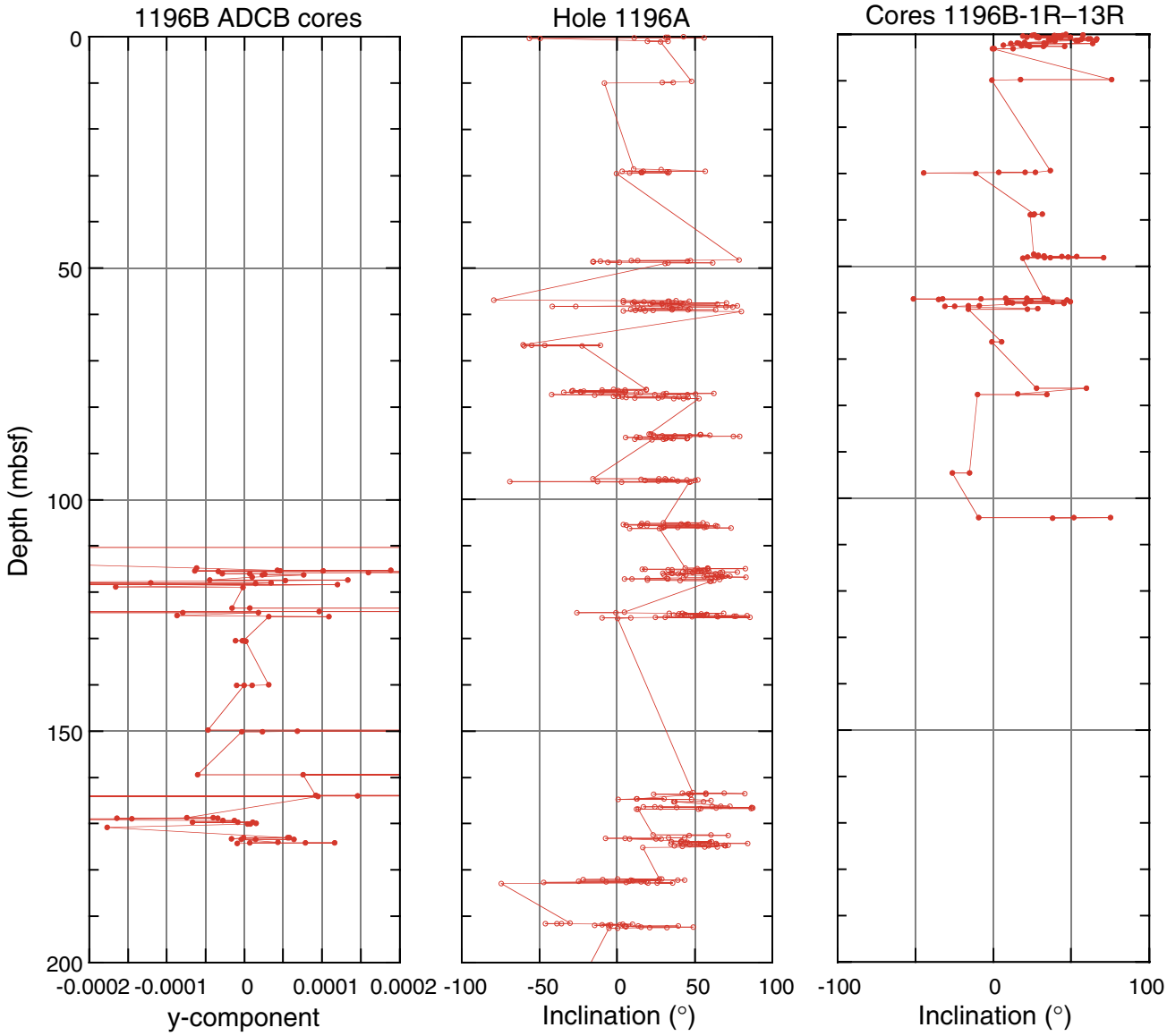

Figure F37. Zijderveld plot for Sample 1196A-65R-3, 94–96 cm. Note that the demagnetization (demag) of NRM has produced no significant change in direction but a small increase in intensity of magnetization.

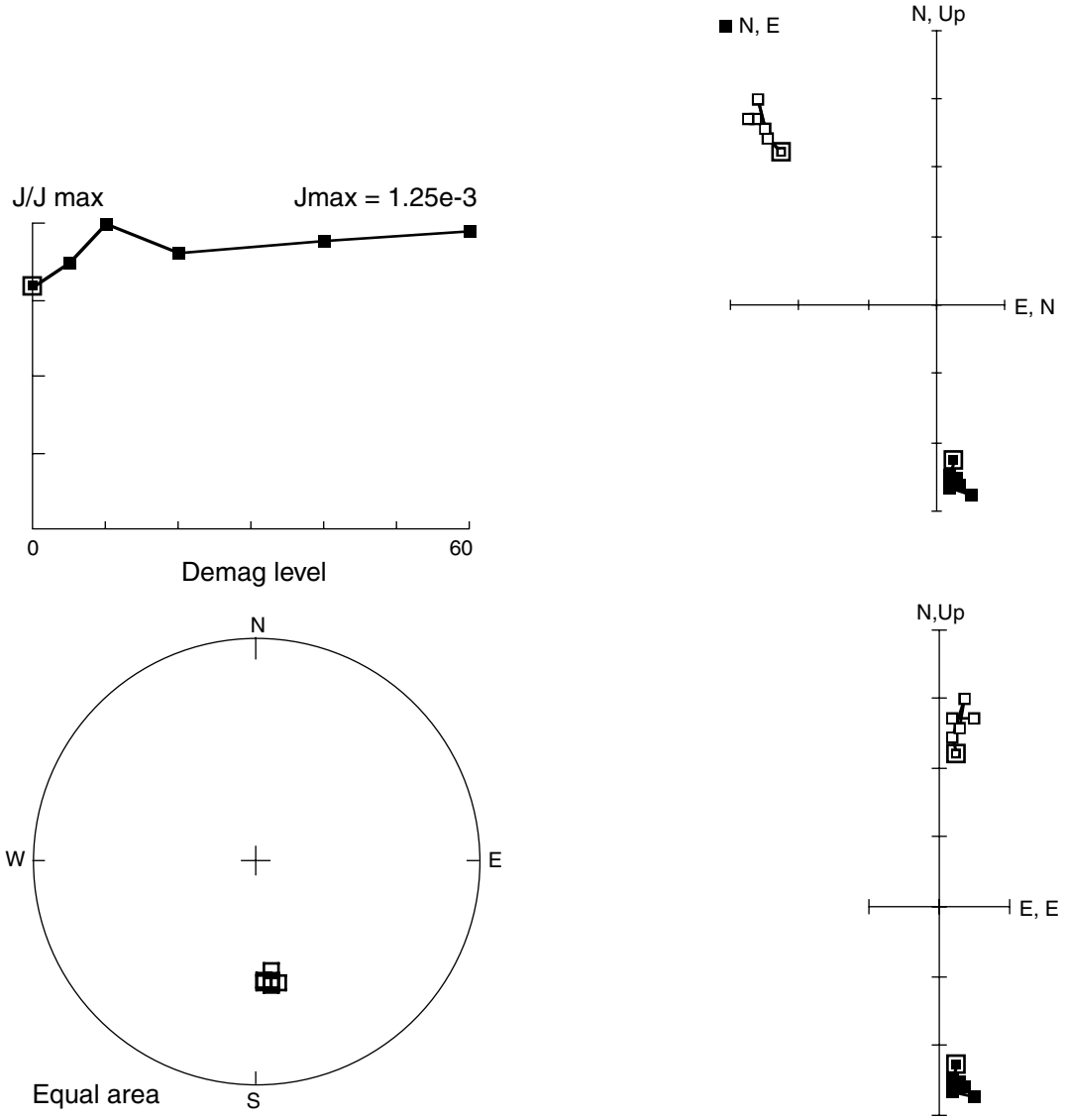

Demag	Declination	Inclination	Intensity
0.0	173.5	-43.9	9.96e-4
5.0	176.1	-44.7	1.09e-3
10.0	172.7	-48.9	1.25e-3
20.0	173.4	-45.7	1.14e-3
40.0	176.6	-45.7	1.19e-3
60.0	169.9	-44.5	1.22e-3

Figure F38. Variation of intensity of natural remanent magnetization (NRM), anhysteretic remanent magetization (ARM), and isothermal remanent magetization (IRM) downcore. Note that the sensitivity of the instrument limits reliable measurement of discrete samples to intensities >~10^{-4} A/m.

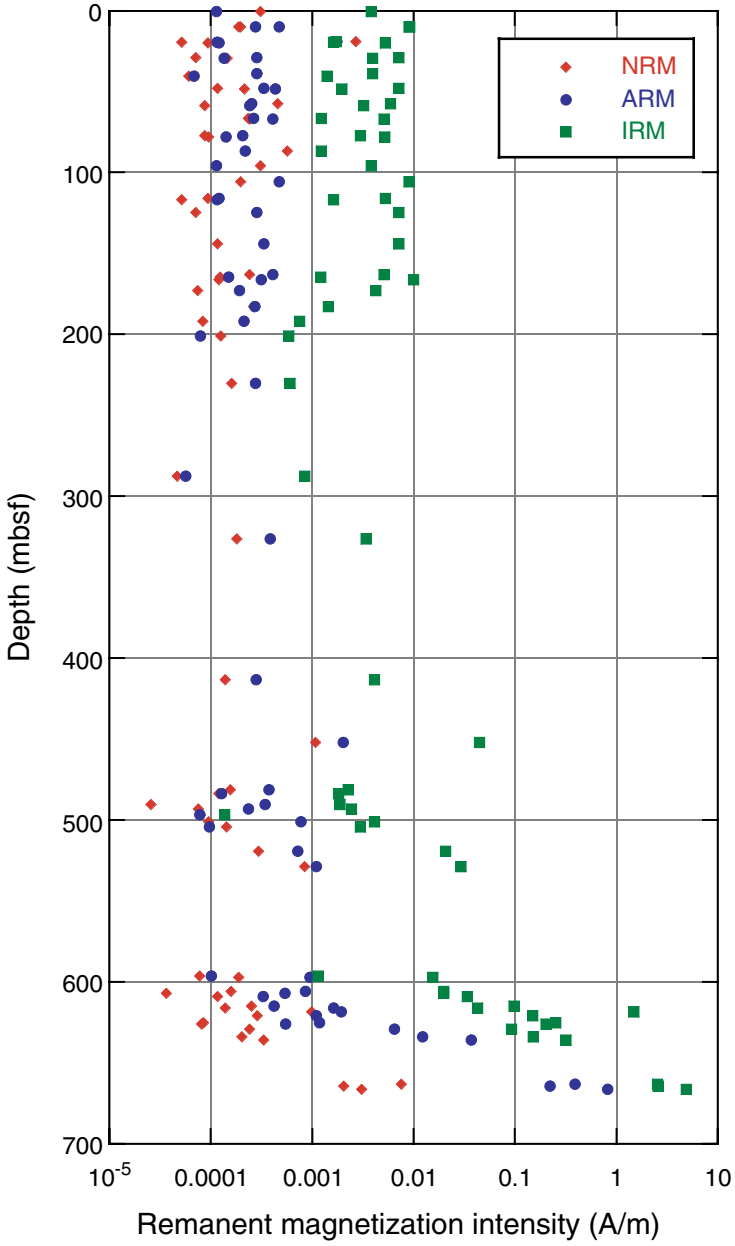

Figure F39. Variation of rock magnetism parameters downcore. Isothermal remanent magetization (IRM) acquisition (acq.) at 100 mT/IRM, IRM demagnetized (demag) to 40 mT/IRM, and anhysteretic remanent magetization (ARM)/IRM.

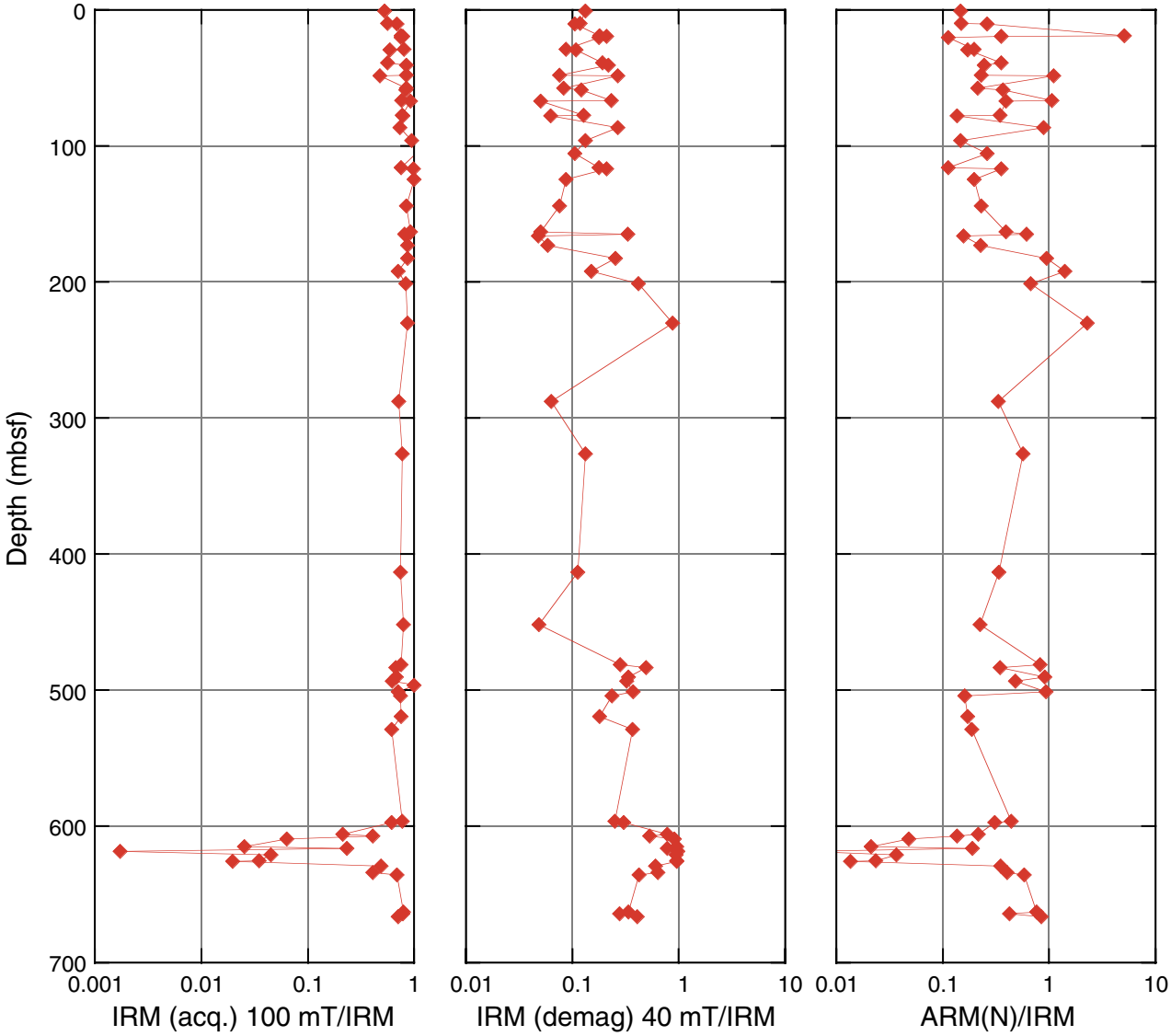

Figure F40. Long-core measurements from for Site 1199 showing intensity and inclination as a function of depth. **A.** 0–100 mbsf. (Continued on next page.)

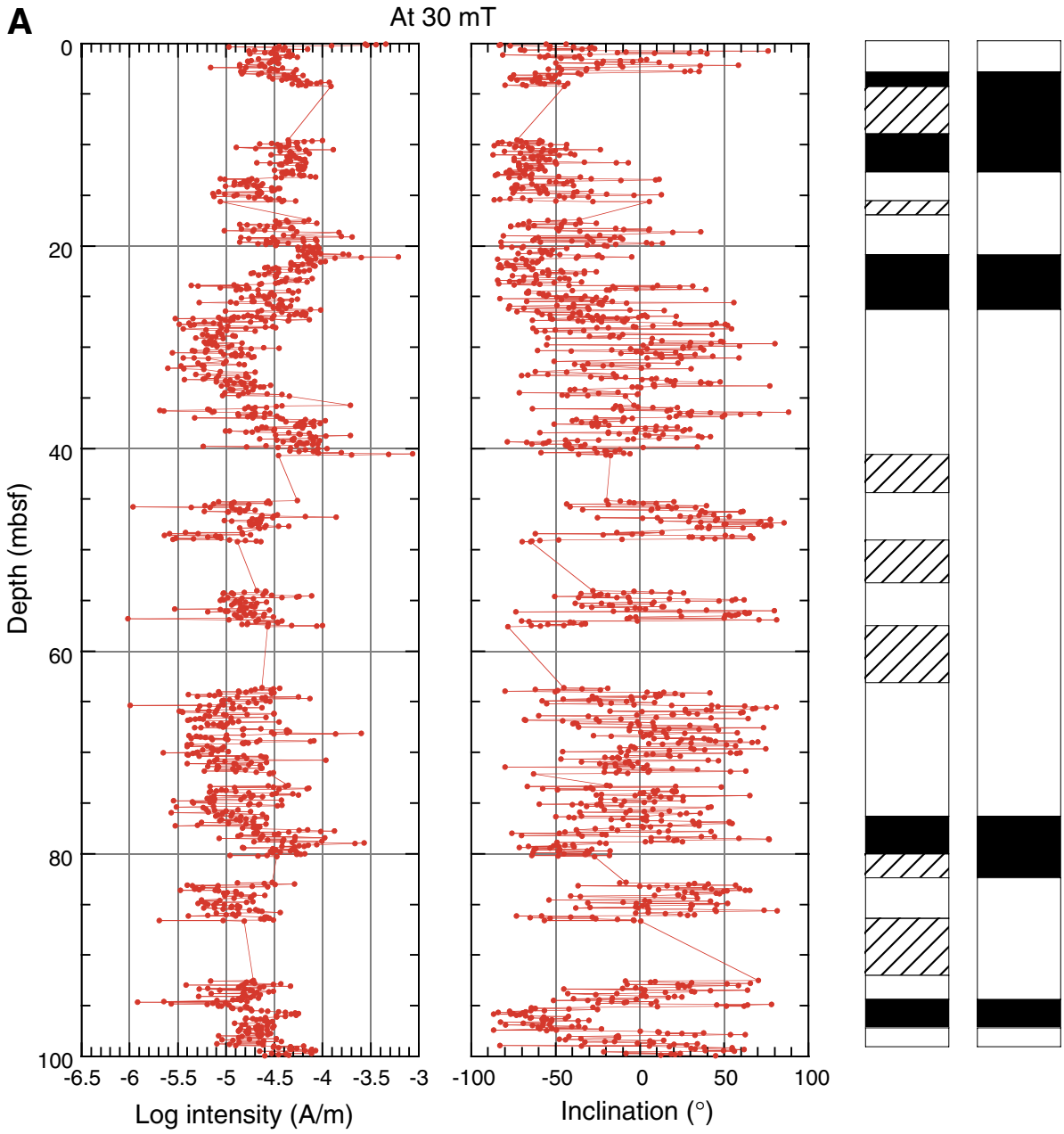

Figure F40 (continued). B. 100–150 mbsf.

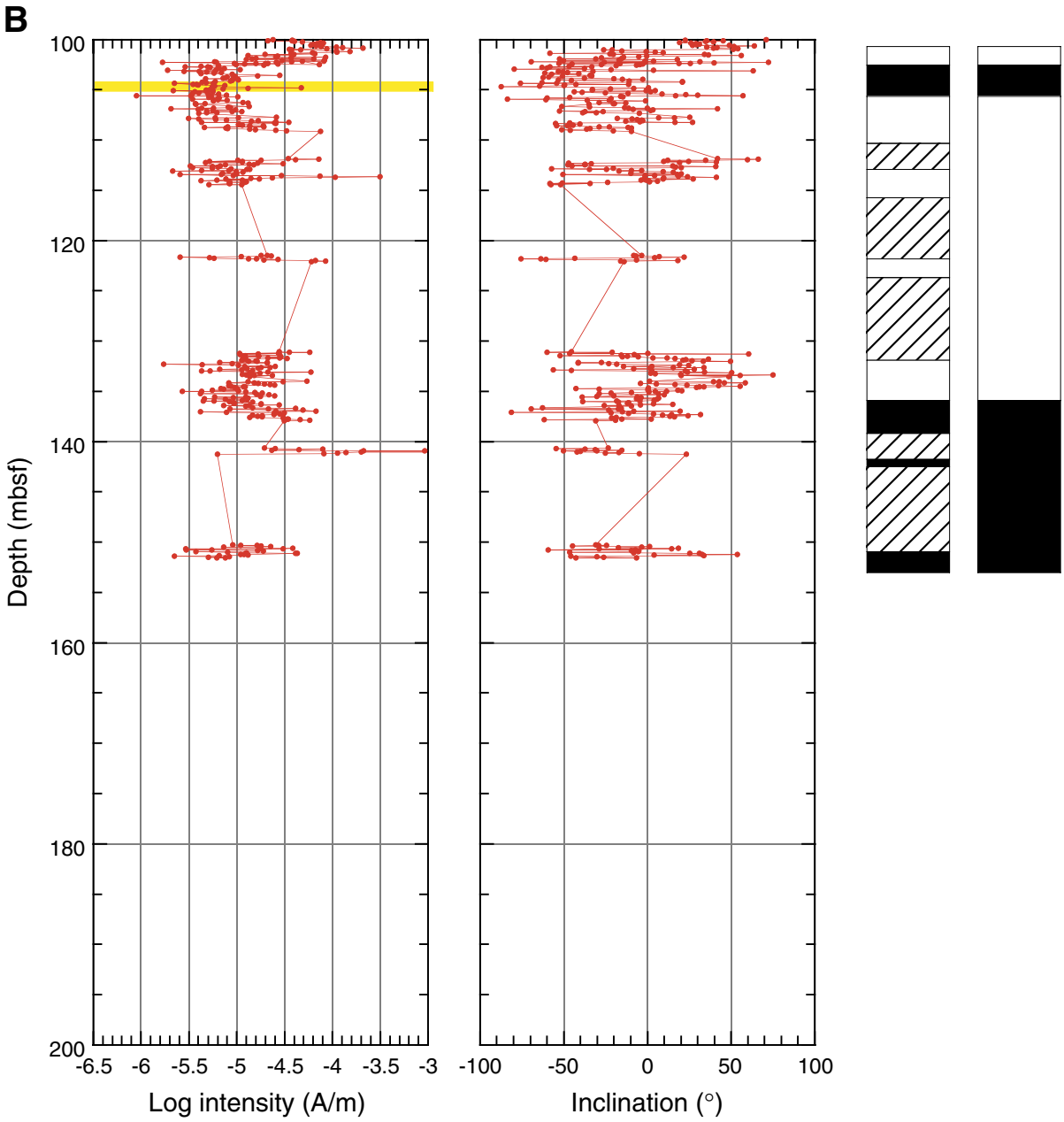

Figure F41. Example of an orthogonal vector component diagram showing straight-forward paleomagnetic directions going to the origin in two different projection axes. Also shown is the normalized decay curve of magnetization. Demag = demagnetization.

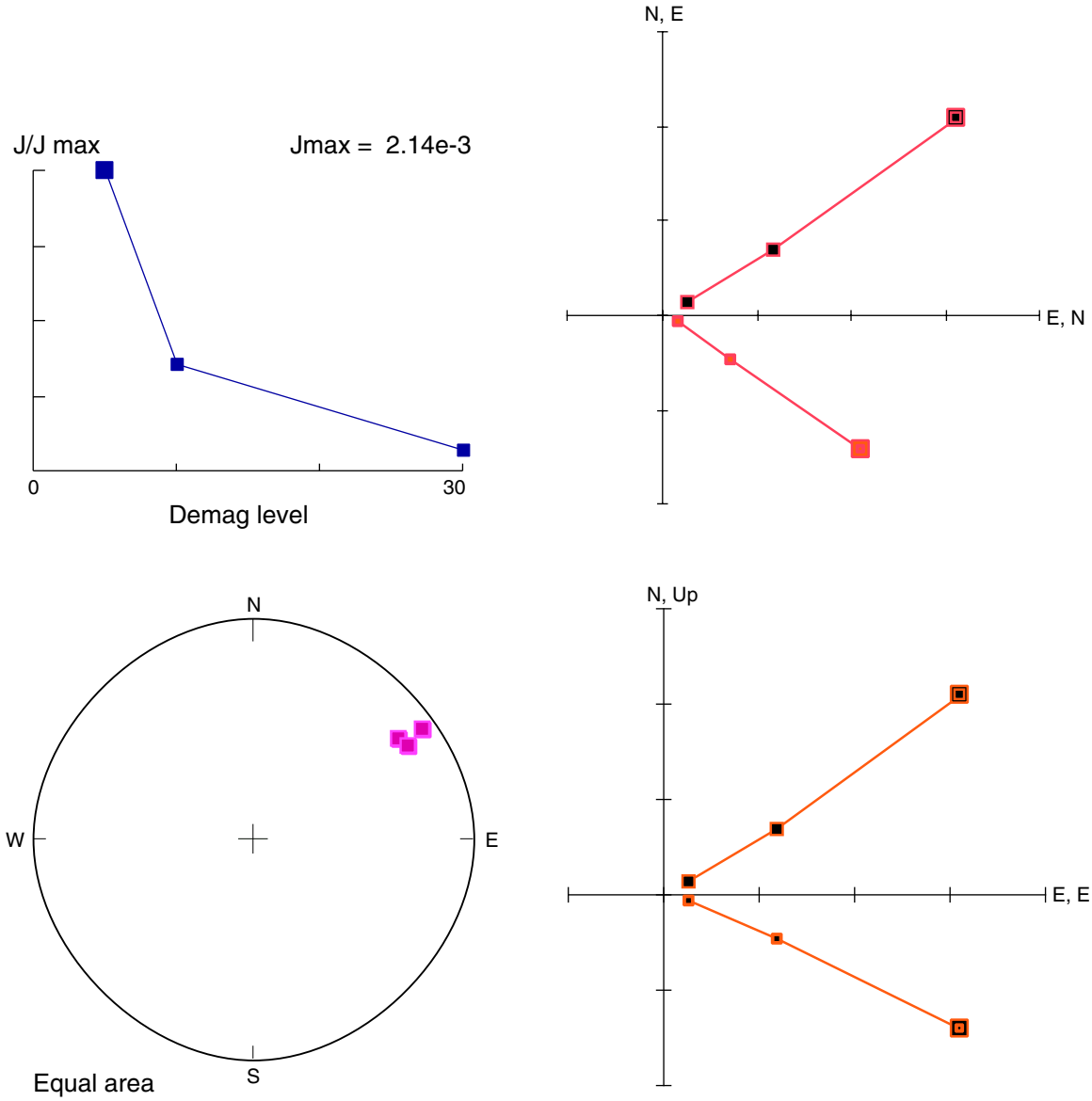

Figure F42. Age-depth model and sedimentation rates at Sites 1196 and 1199. Horizontal lines spanning from the left figure margin to the age-depth curve are lithologic unit (solid) and subunit (dashed) boundaries. The horizontal line spanning from the right margin of the figure to the age-depth curve is a seismic reflection that might correspond to the seismic Megasequence B/C boundary. Vertical lines are epoch boundaries as labeled at the top of the diagram. MS = Megasequence.

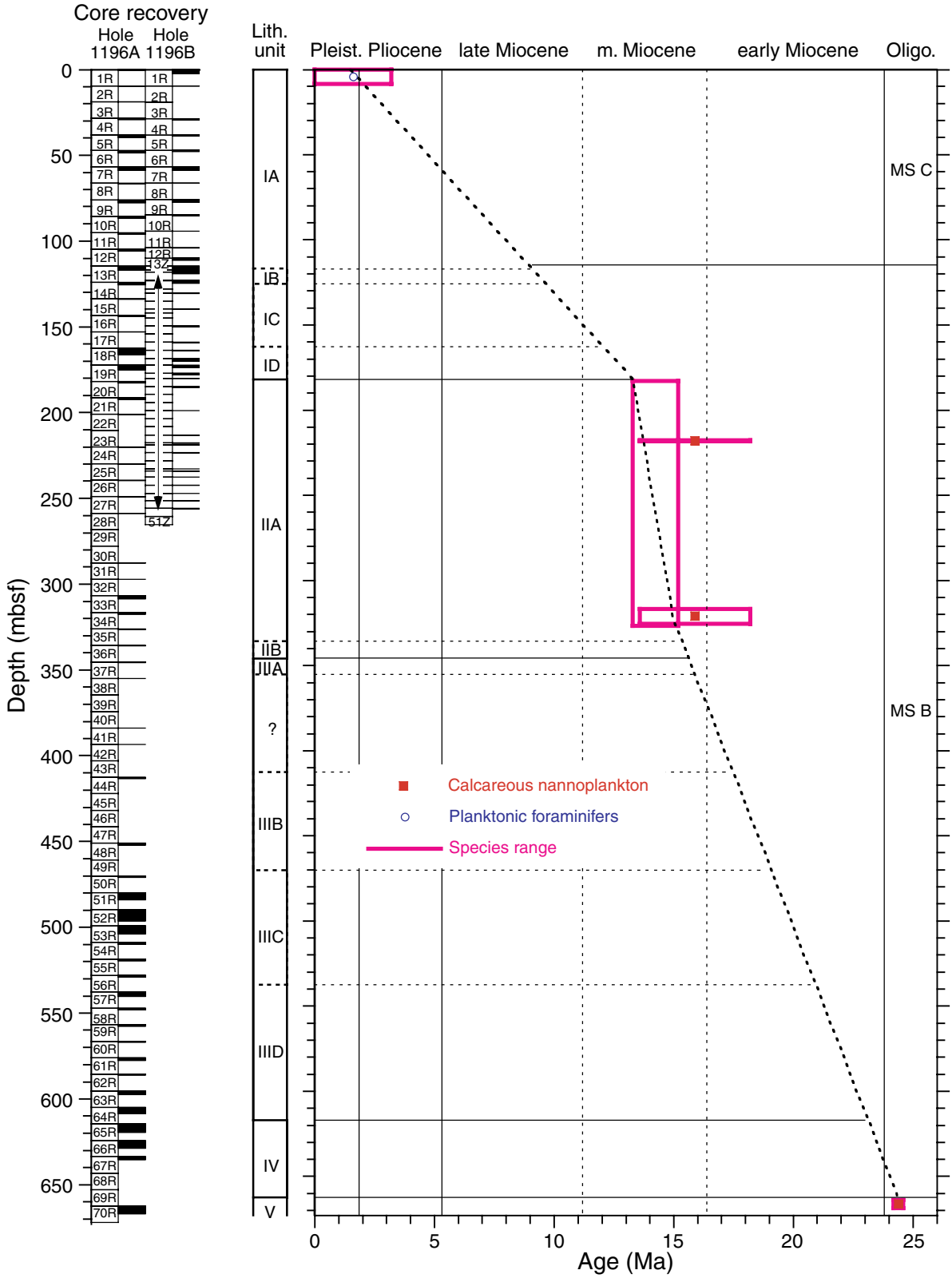

Figure F43. Percentages of carbonate minerals and noncarbonate fraction for Site 1196.

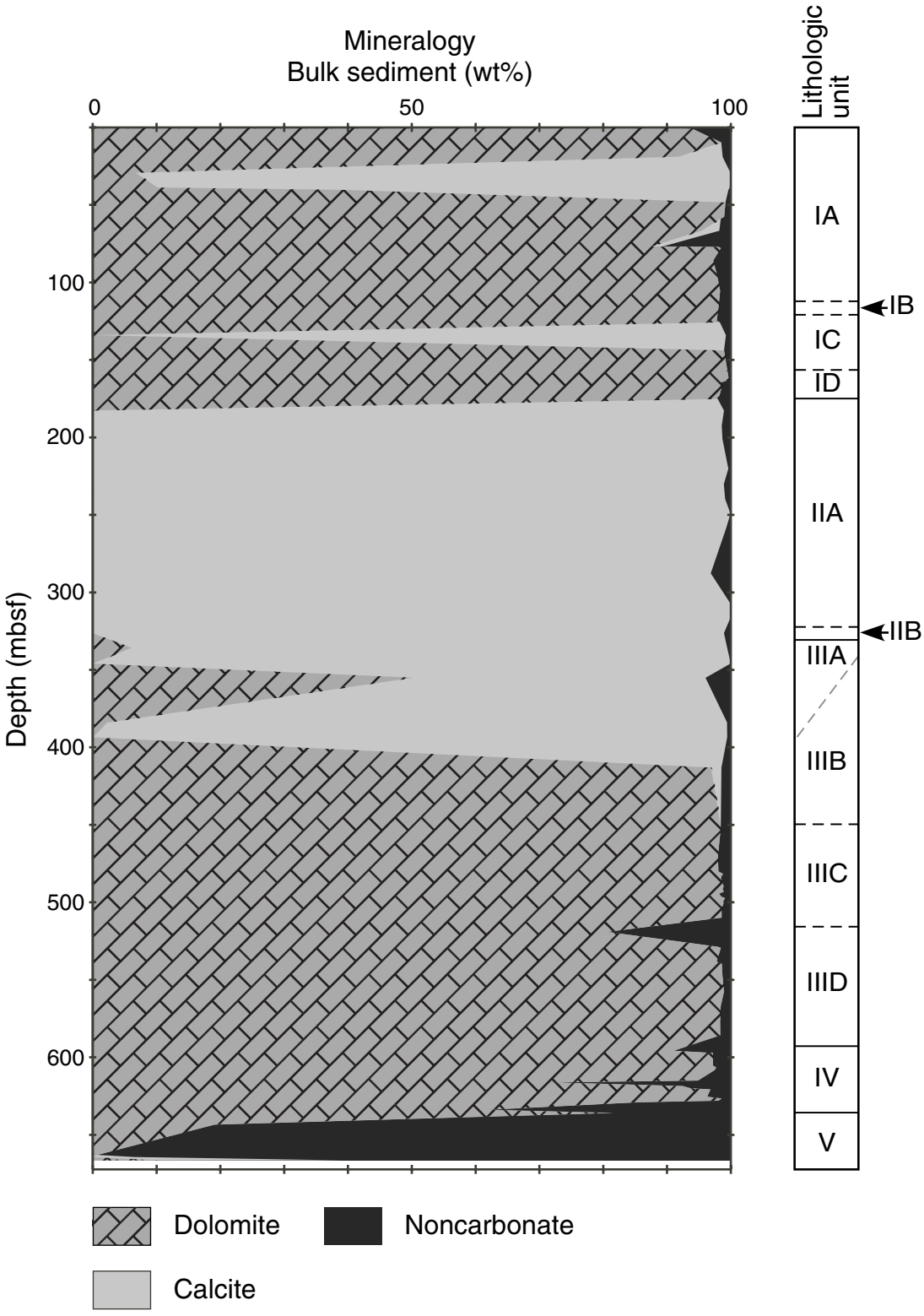

Figure F44. Carbonate and total organic carbon content, hydrogen index (HI) values, total sulfur content, and C/N and C/S ratios, Site 1196. The solid vertical lines at HI = 150 and C/S = 2 mark the approximate boundary between terrigenous (<150) and marine organic matter and the transition between marine and brackish environments of formation, respectively.

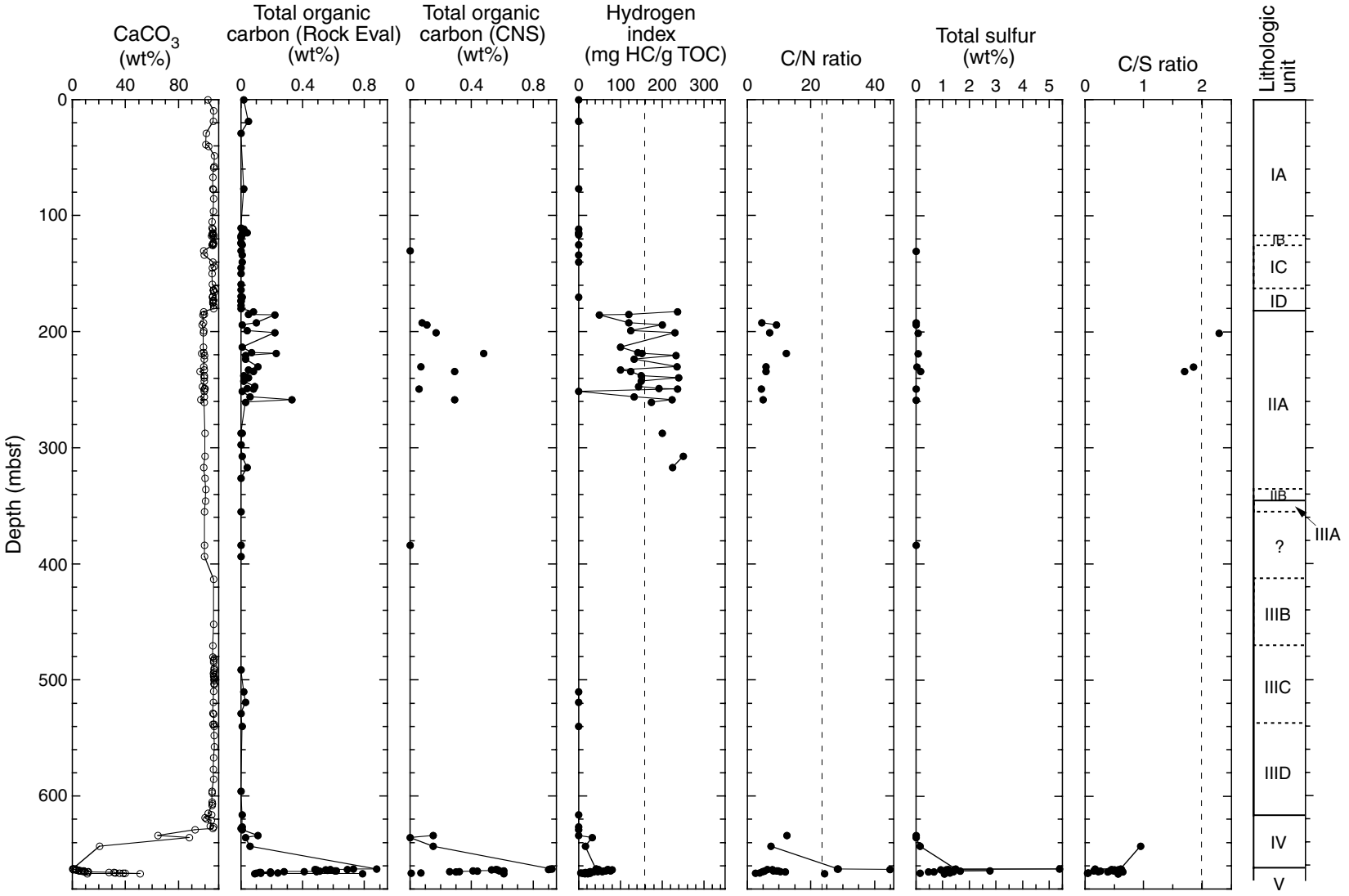

Figure F45. Percentages of carbonate minerals and noncarbonate fraction, as determined by X-ray diffraction.

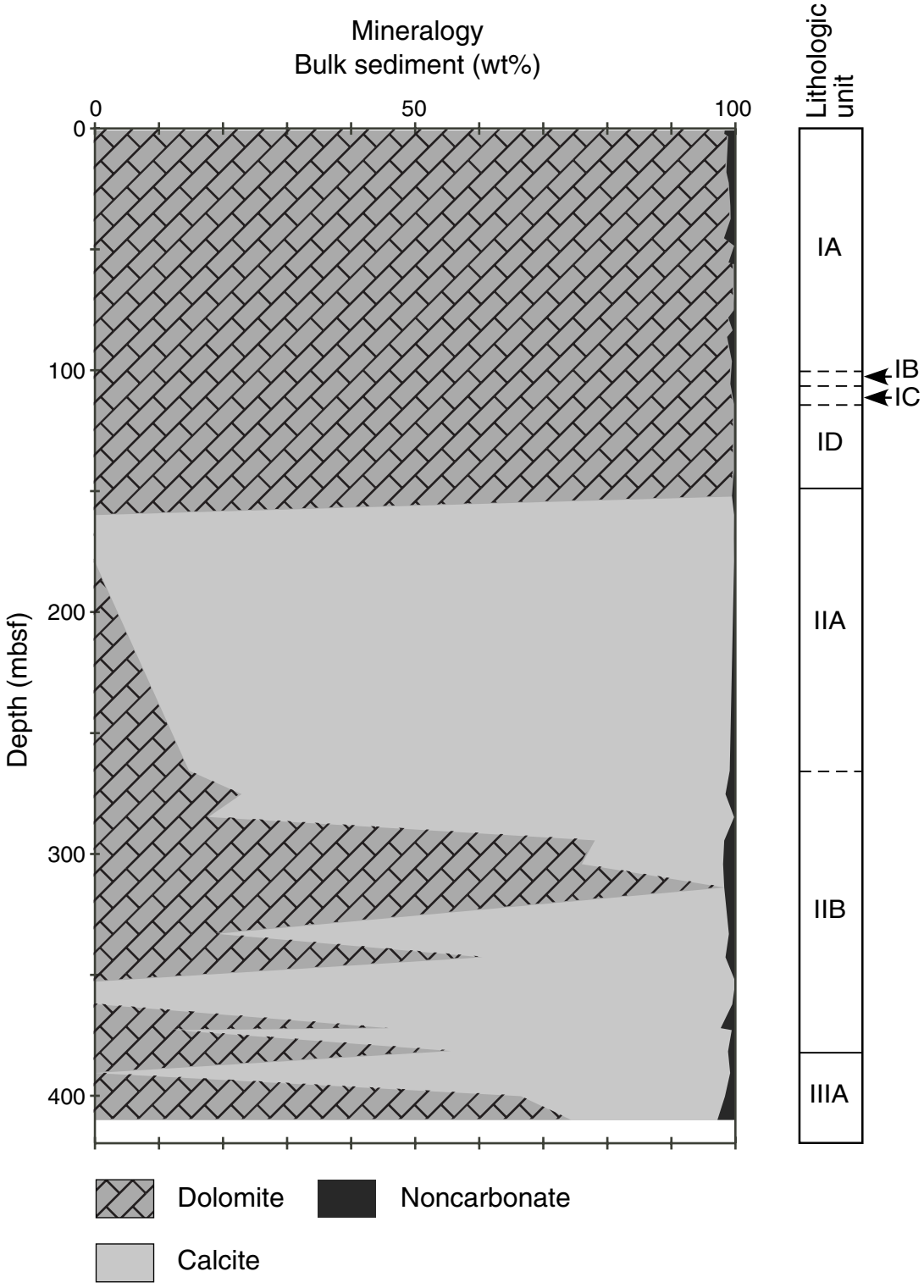

Figure F46. Carbonate content for Site 1199.

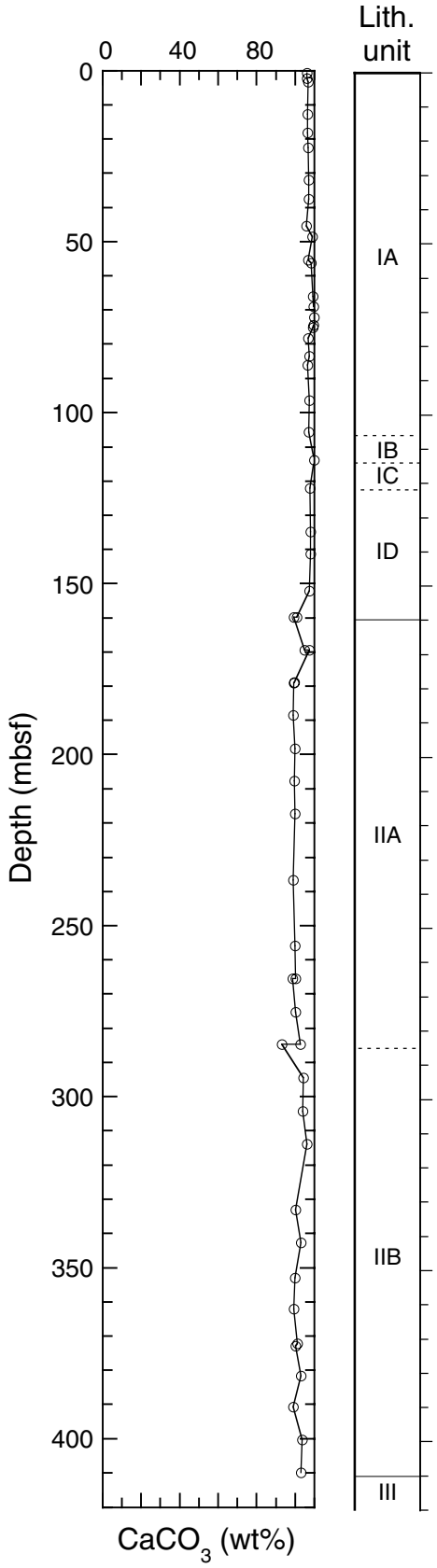

Figure F47. Site 1196 (A) bulk density, (B) grain density, and (C) porosity as a function of depth.

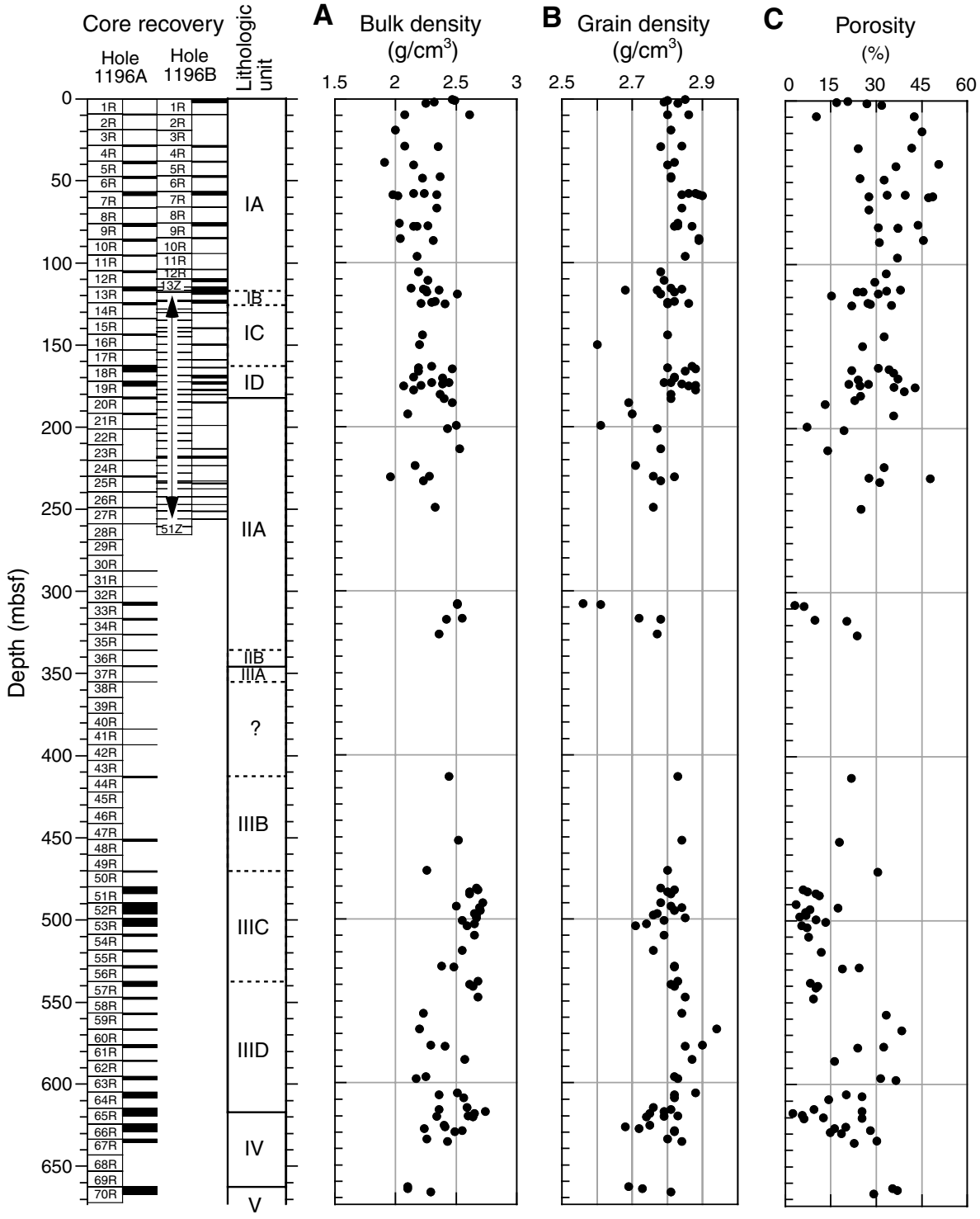

Figure F48. Site 1196 (**A**) grain density and (**B**) dolomite content as a function of depth. Shaded rectangles indicate grain density values >2.80 g/cm³ that correspond to dolomite-rich intervals.

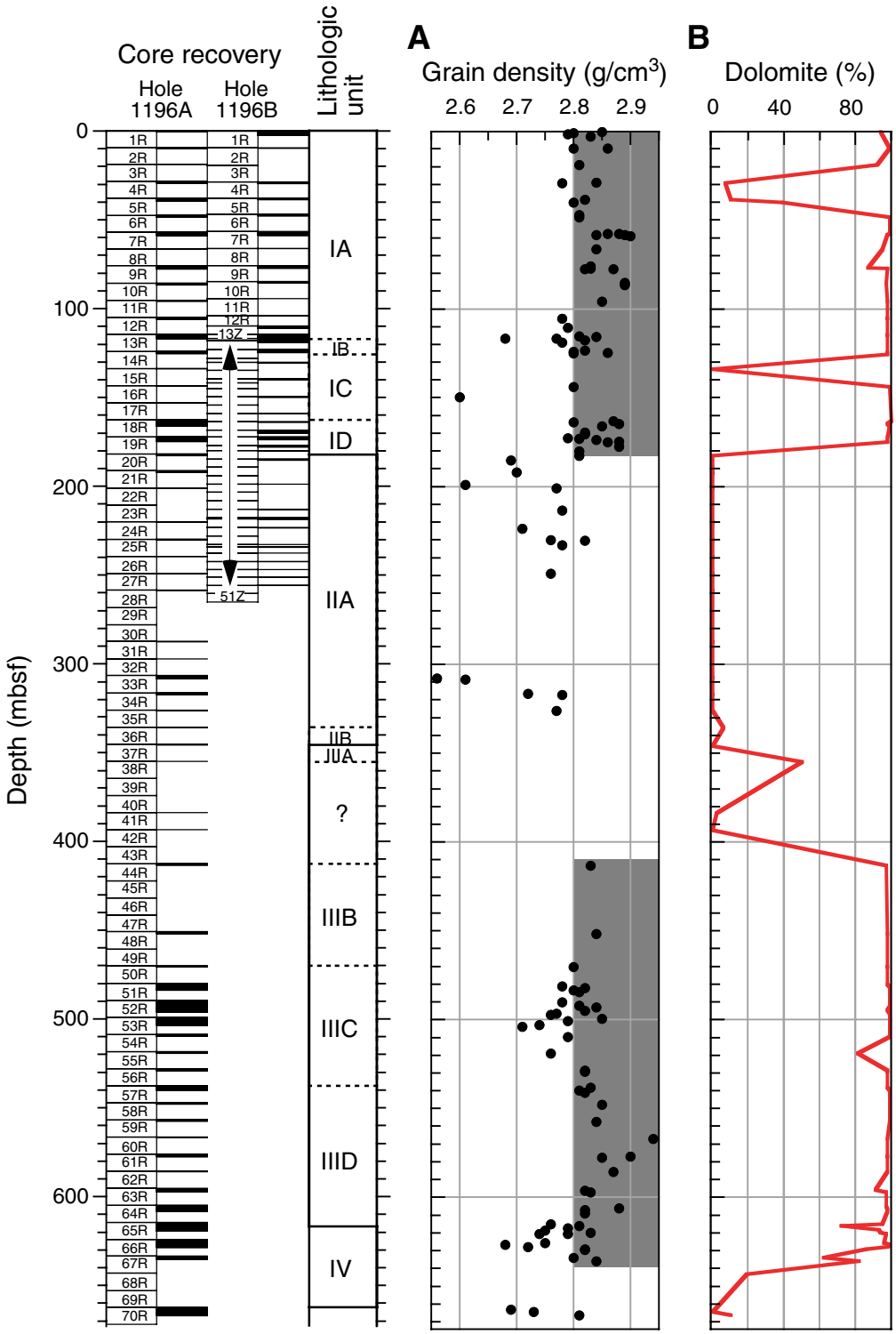

Figure F49. Site 1196 (**A**) *P*-wave velocity and (**B**) anisotropy of *P*-wave velocity as a function of depth.

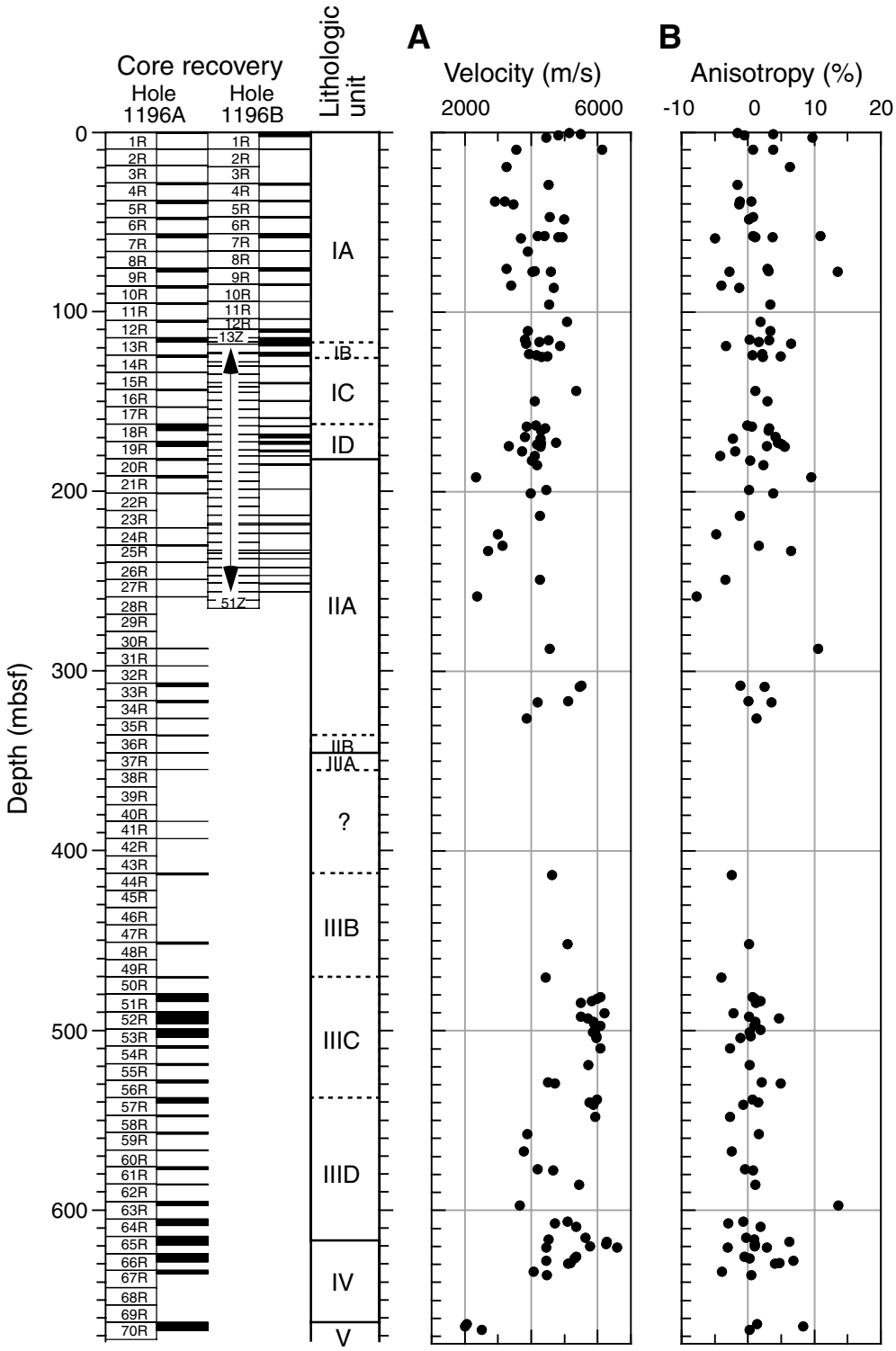

Figure F50. Crossplot of velocity vs. porosity for Site 1196. Solid and dashed lines represent the time-average equations for calcite and dolomite (Wyllie et al., 1956). Solid circles = platform carbonates, open circles = quartz-rich lithologies in lithologic Unit V.

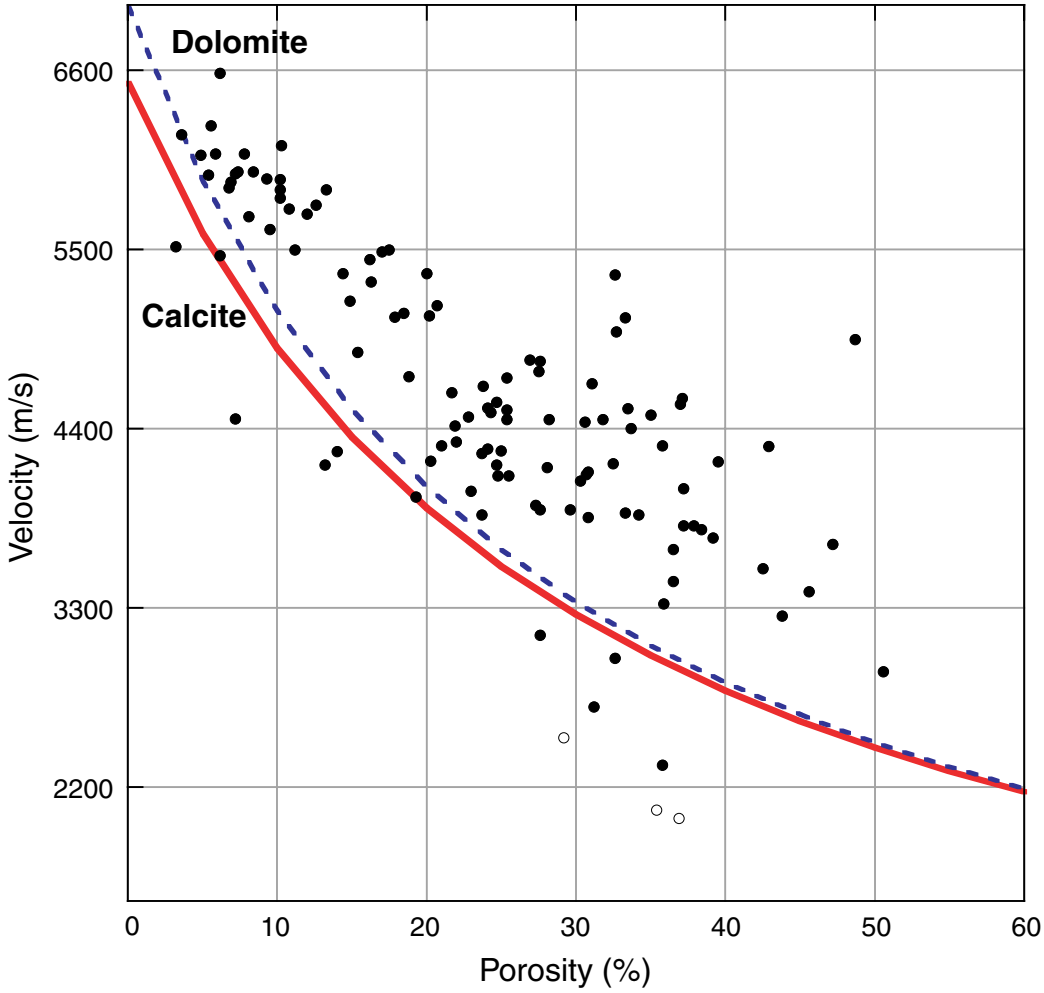

Figure F51. Thermal conductivity for Site 1196 as a function of depth.

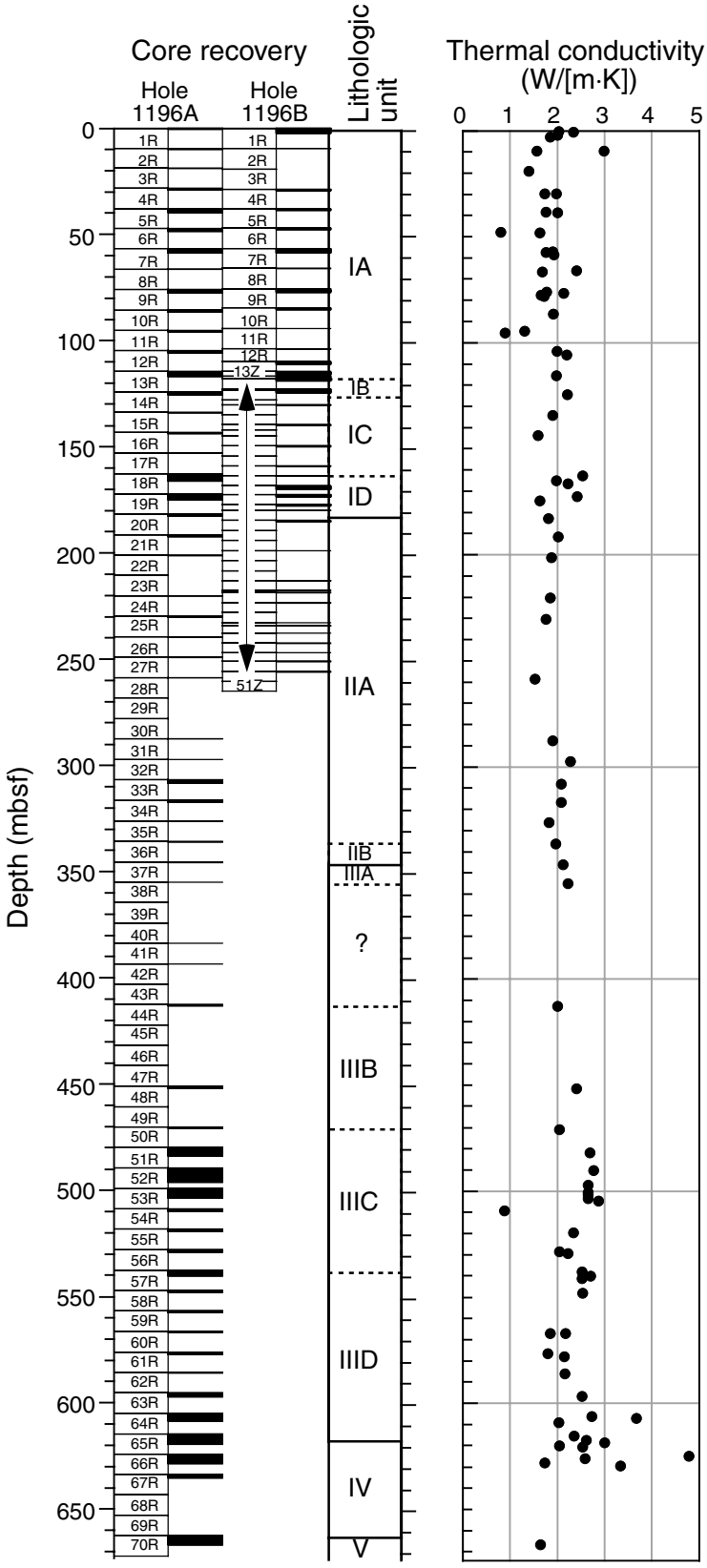

Figure F52. Crossplot of thermal conductivity vs. porosity for Site 1196. Lines = theoretical curves for pure unilithology systems, solid circles = values for carbonate samples, open circles = quartz-rich dolostones.

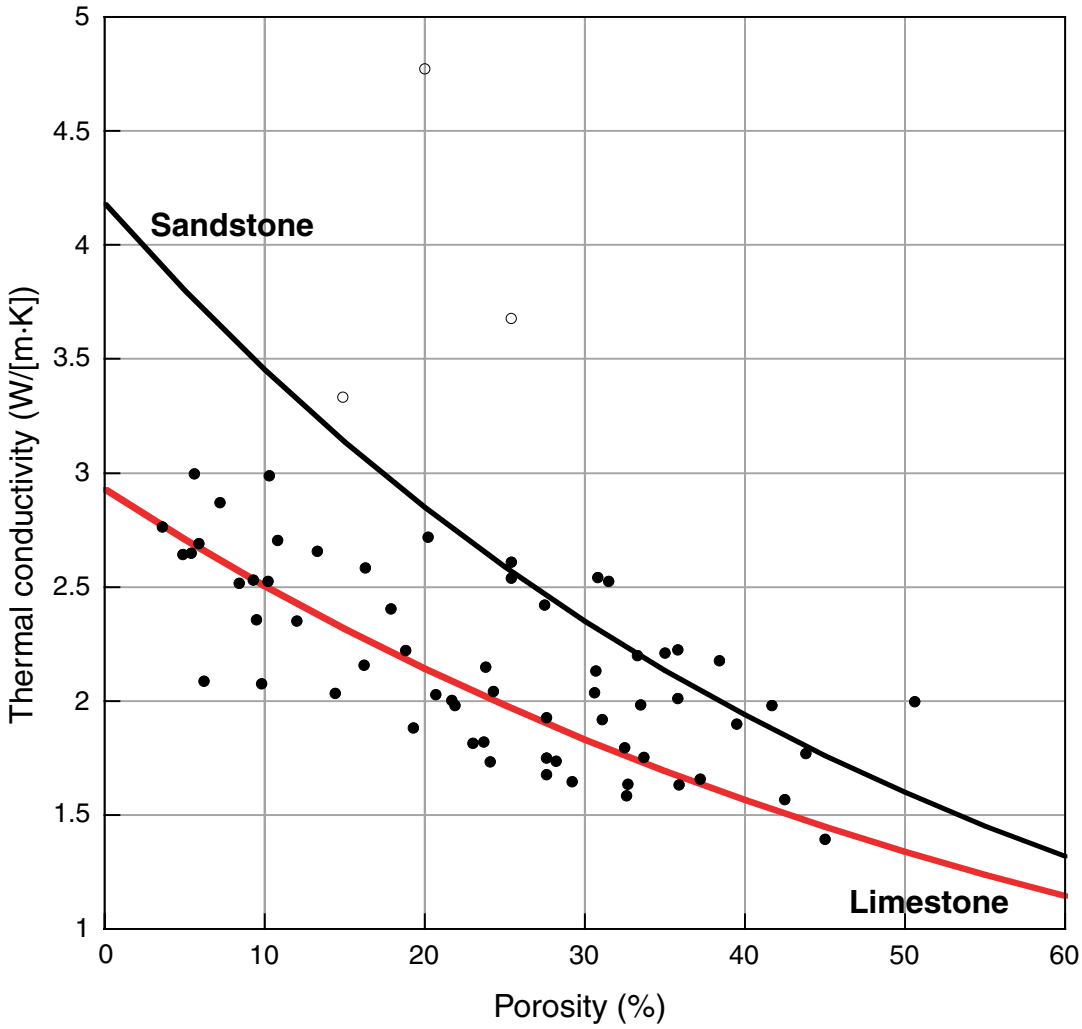

Figure F53. **A.** Magnetic susceptibility (MS) as a function of depth. **B.** Natural gamma radiation (NGR) from MST (dots) and hostile environment gamma ray sonde (HNGS) (line) as a function of depth. **C.** Natural gamma radiation (NGR) from MST (dots) and HNGS (line) as a function of depth with corrected HNGS values for logging through the drill pipe (0–70 mbsf). Note that MS is measured from half cores and thus is not in SI units, which necessarily assume a full core volume.

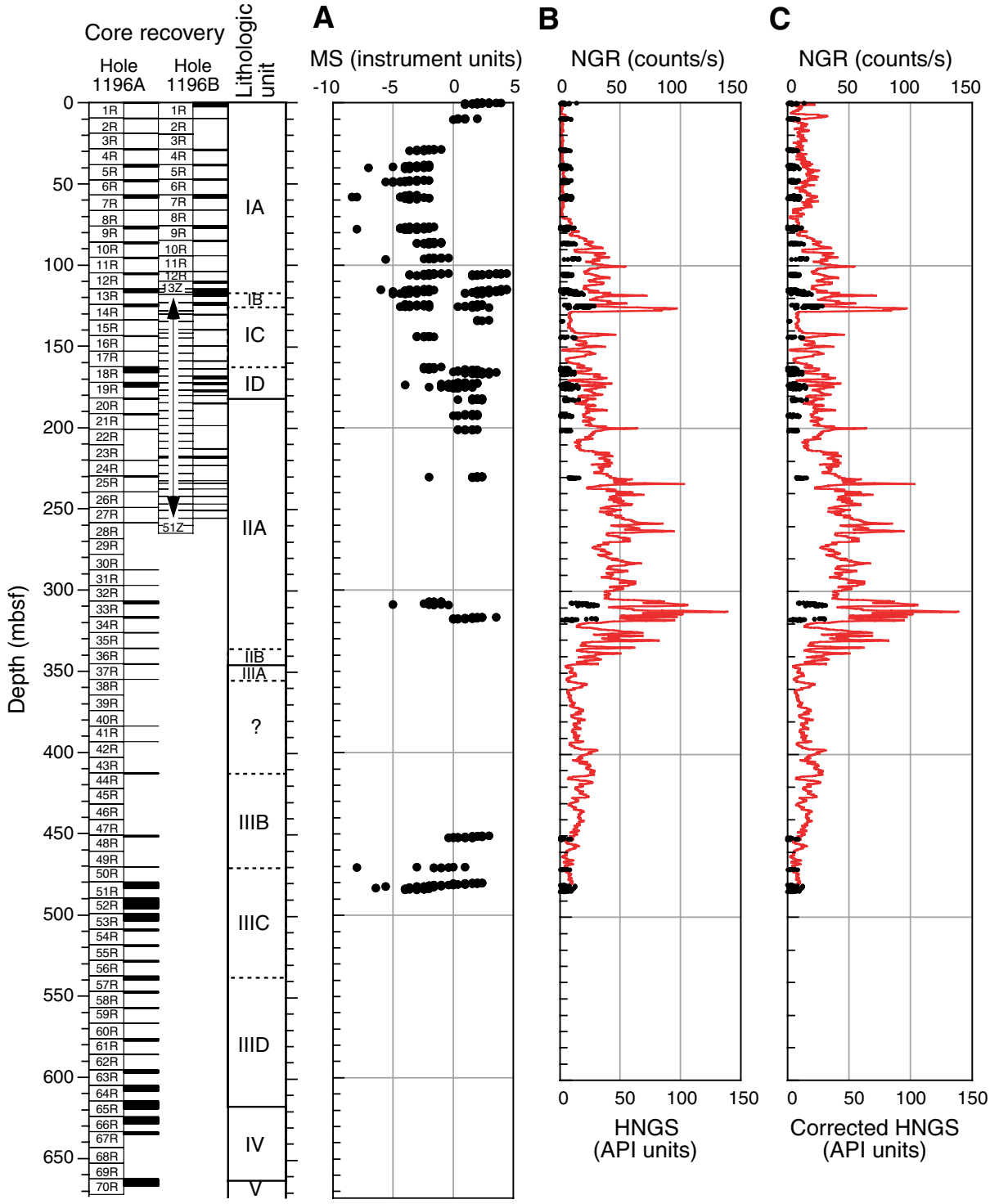

Figure F54. Comparison of natural gamma radiation (NGR) and magnetic susceptibility (MS) measurements on whole-round cores (solid triangles) and split cores (open triangles). Note the good match for NGR values and the offset in MS values.

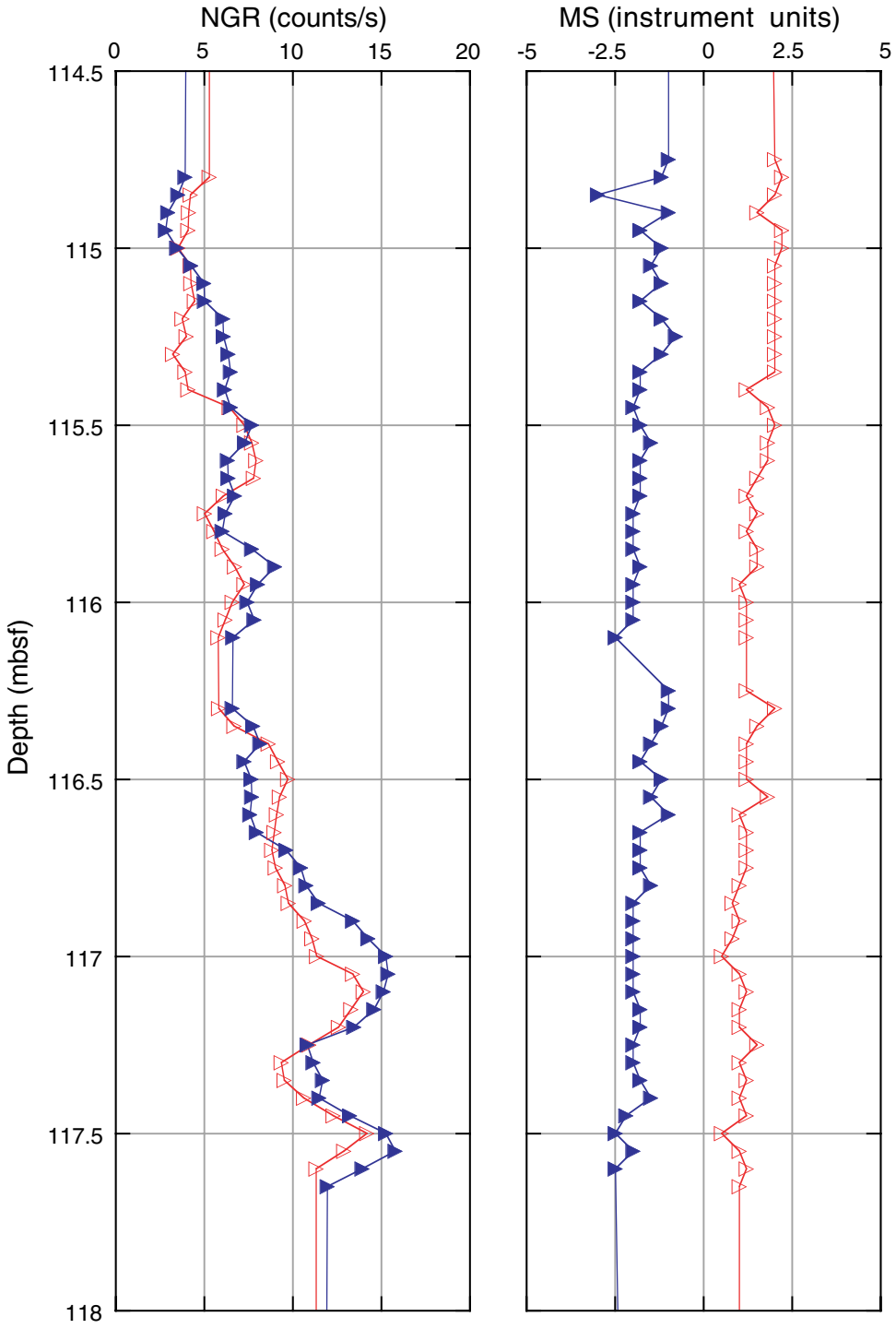

Figure F55. Site 1199 (**A**) GRA (solid circles) and MAD bulk density (open circles), (**B**) grain density, and (**C**) porosity as a function of depth.

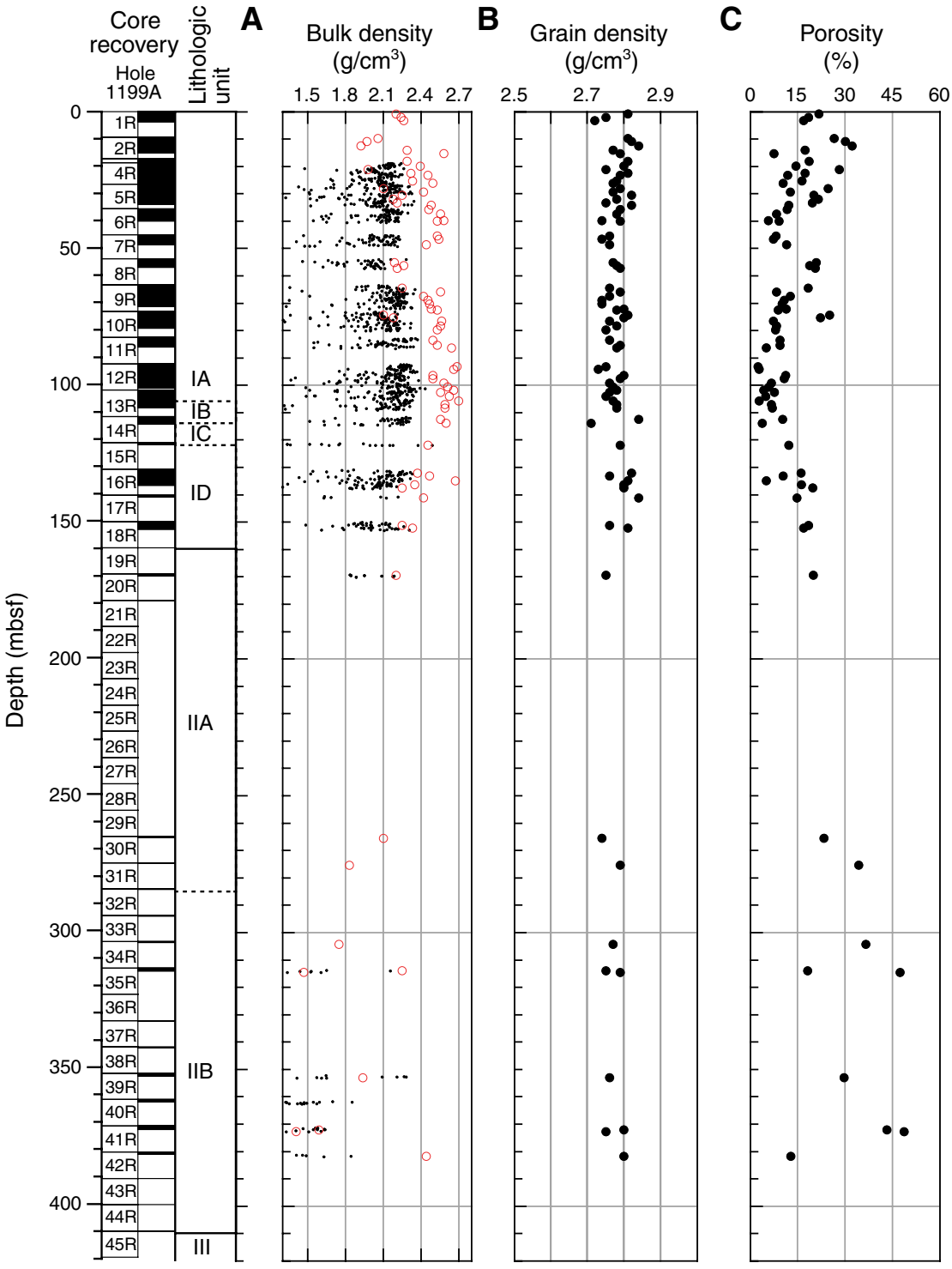

Figure F56. Site 1199 (**A**) *P*-wave velocity and (**B**) anisotropy of *P*-wave velocity as a function of depth.

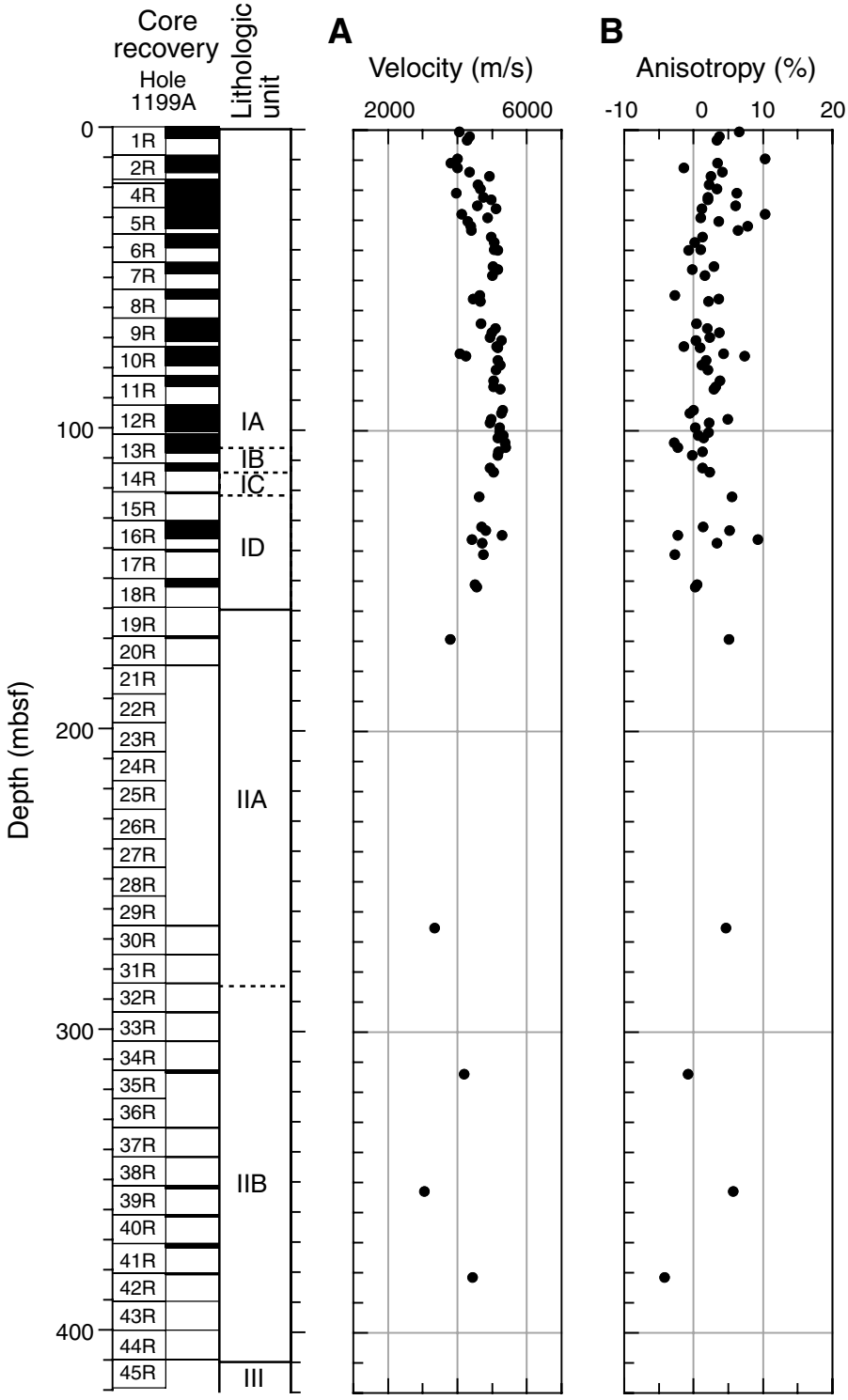

Figure F57. Crossplot of velocity vs. porosity for Site 1199. Solid and dashed lines = the time-average equations for calcite and dolomite (Wyllie et al., 1956). Circles = velocity-porosity pairs from the bottom of lithologic Subunit IA and its boundary with lithologic Subunit IB (90–110 mbsf).

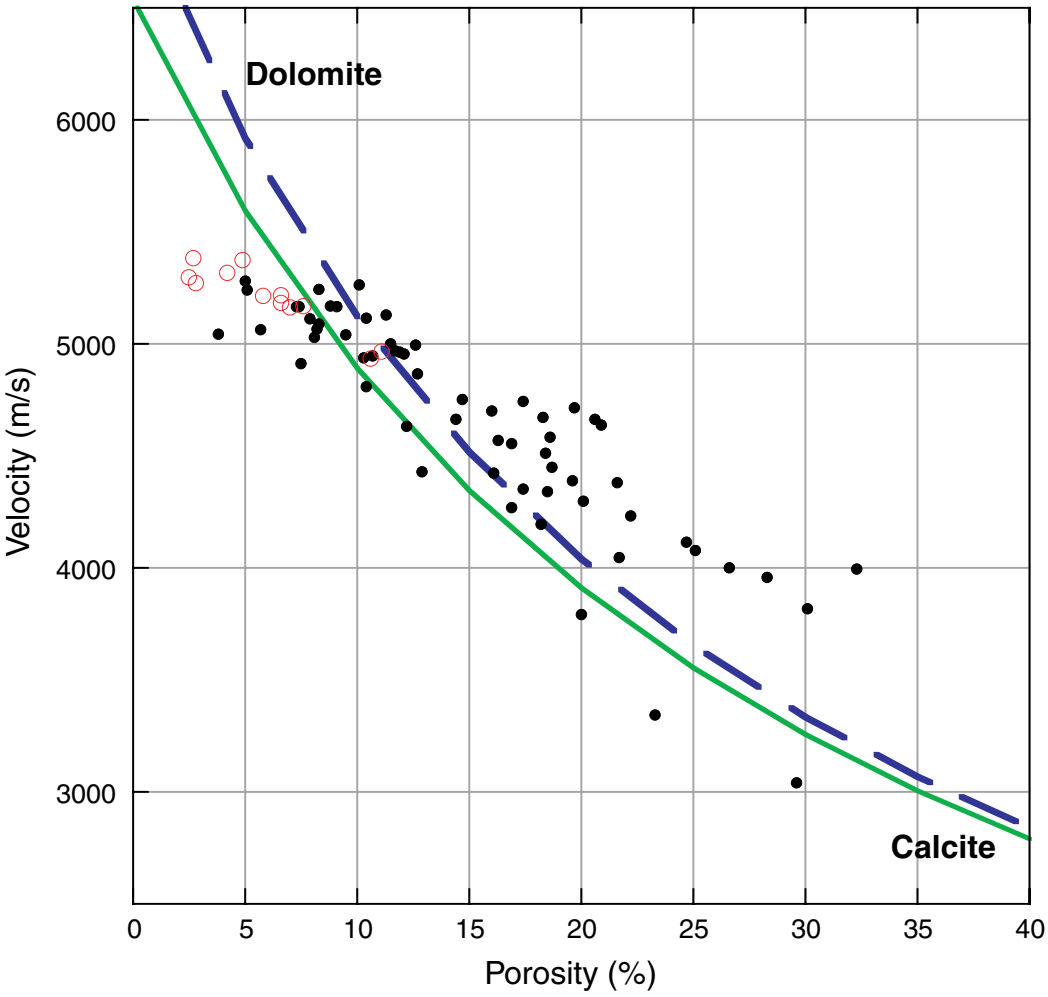

Figure F58. Thermal conductivity for Site 1199 as a function of depth.

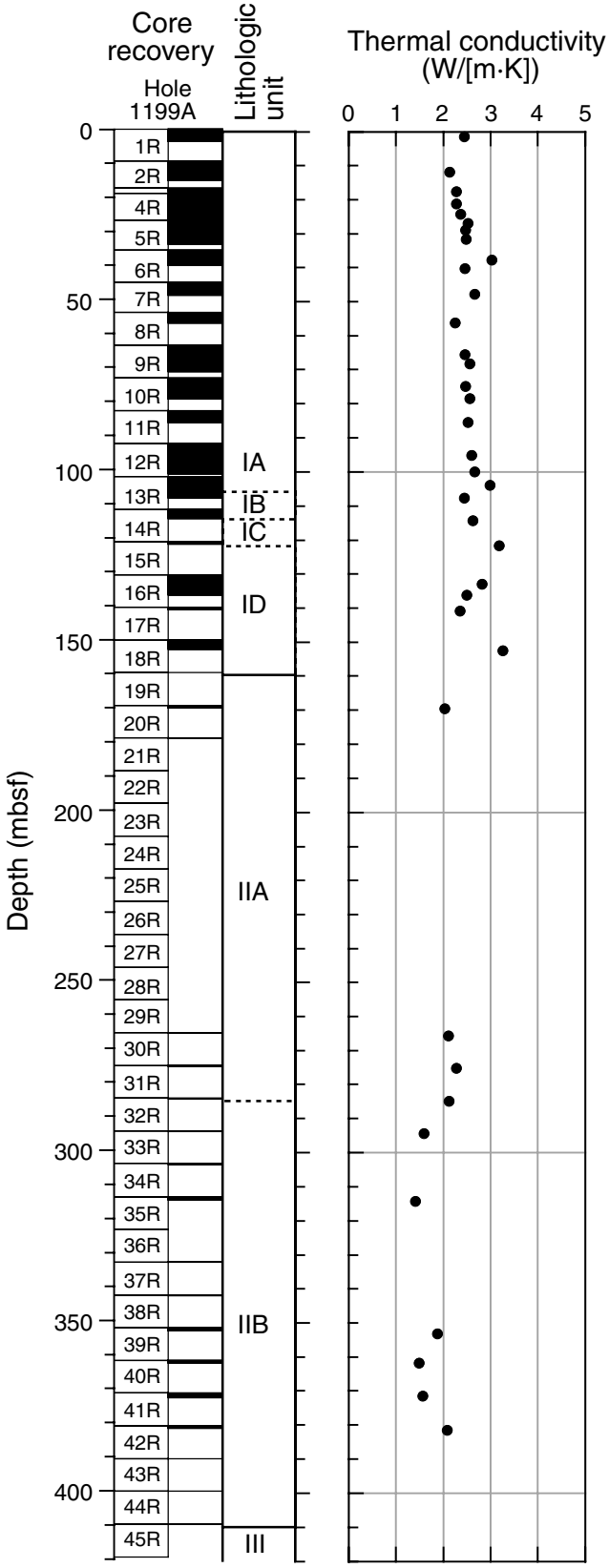

Figure F59. Crossplot of thermal conductivity vs. porosity for Site 1199. Lines = theoretical curves for pure unilithology systems.

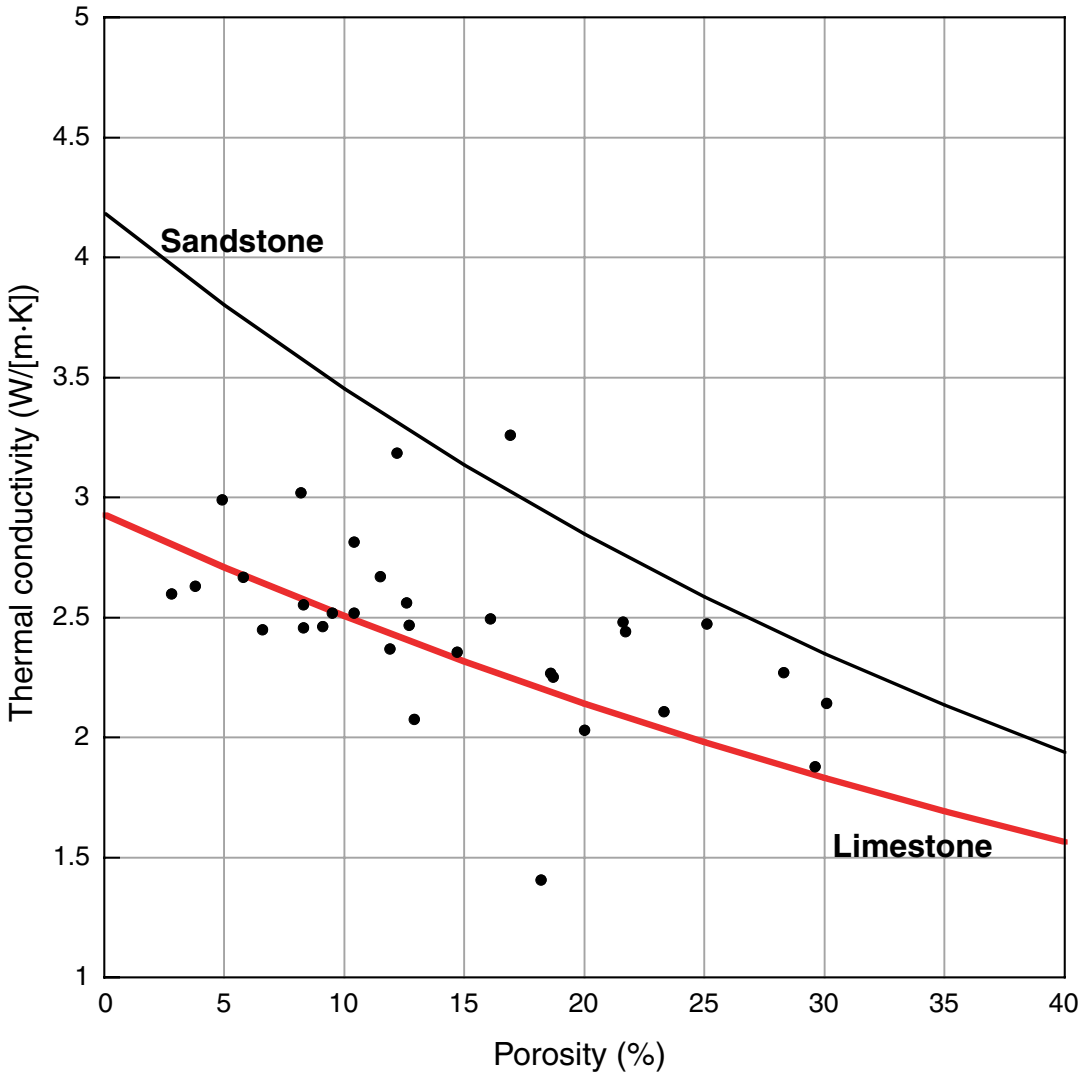

Figure F60. Site 1199 (**A**) magnetic susceptibility (MS) and (**B**) natural gamma radiation (NGR) from MST (dots) and hostile environment gamma ray sonde (HNGS) (line) as a function of depth. HNGS values are corrected for logging through the drill pipe (0–70 mbsf).

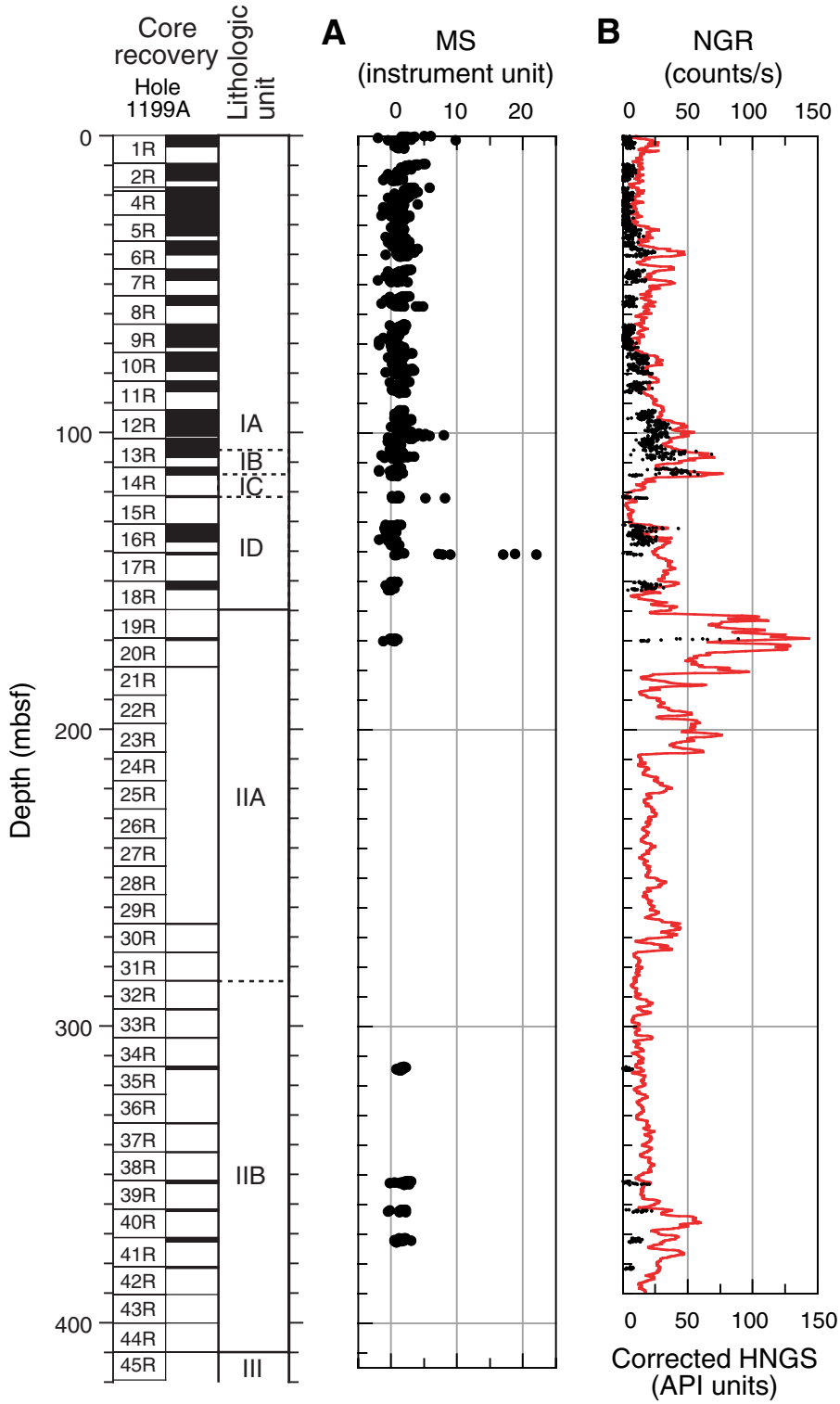

Figure F61. Summary of geophysical logs acquired during the first and second logging runs in Hole 1196A. Note the generally large borehole diameter, which affects the quality of porosity, density, and resistivity data sets. HNGS = hostile environment gamma ray sonde, NGT = natural gamma spectrometry tool.

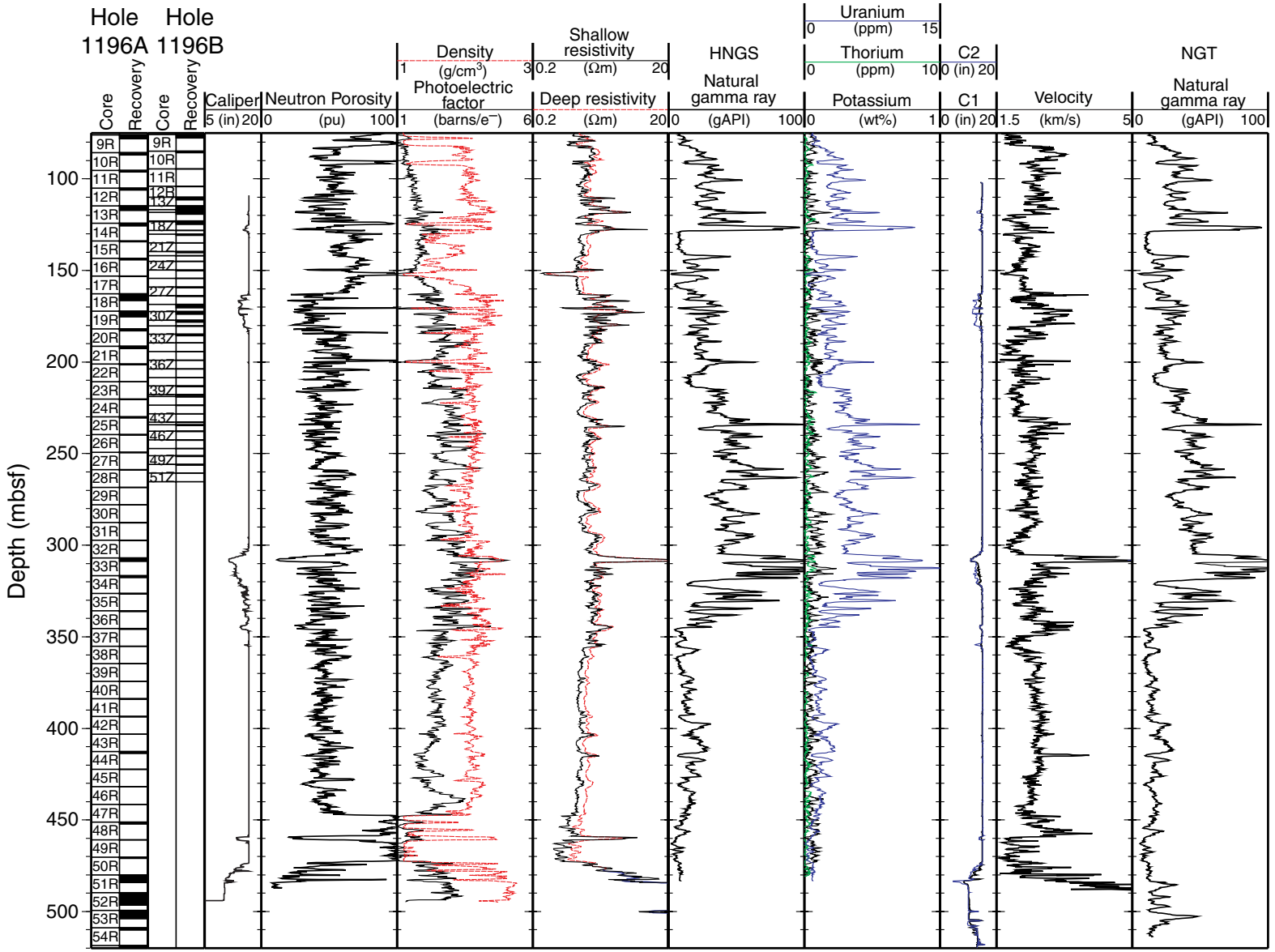

Figure F62. Time-depth curves calculated with three data sets. The check shot traveltimes provide the correct conversion. The integrated sonic log indicates a shallower depth, whereas the *P*-wave velocity (PWS) data largely overestimates the depth.

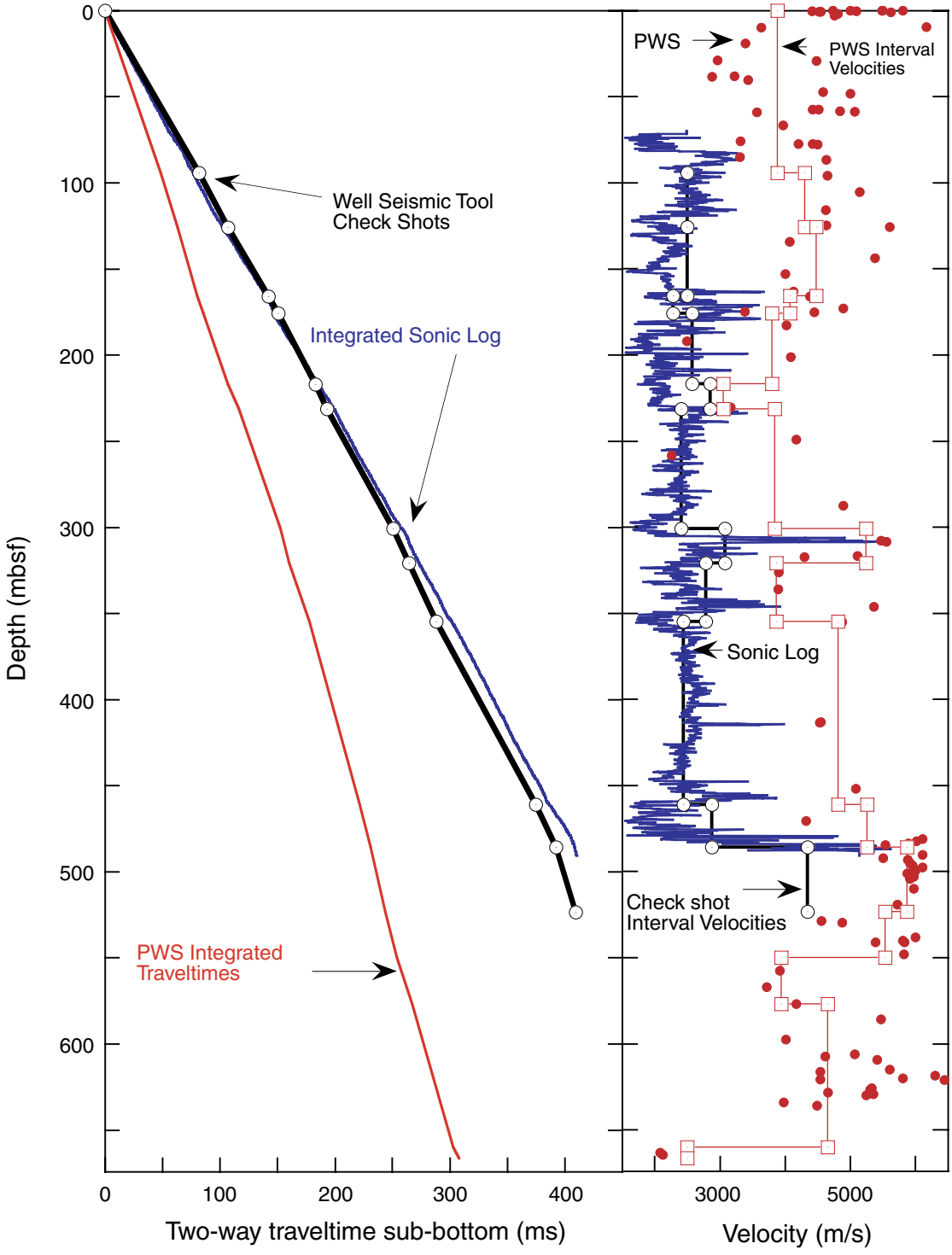

Figure F63. Interpretation of geophysical logging data and correlation to the lithologic units, facies, and mineralogy. Both log unit boundaries coincide with lithologic unit and subunit boundaries.

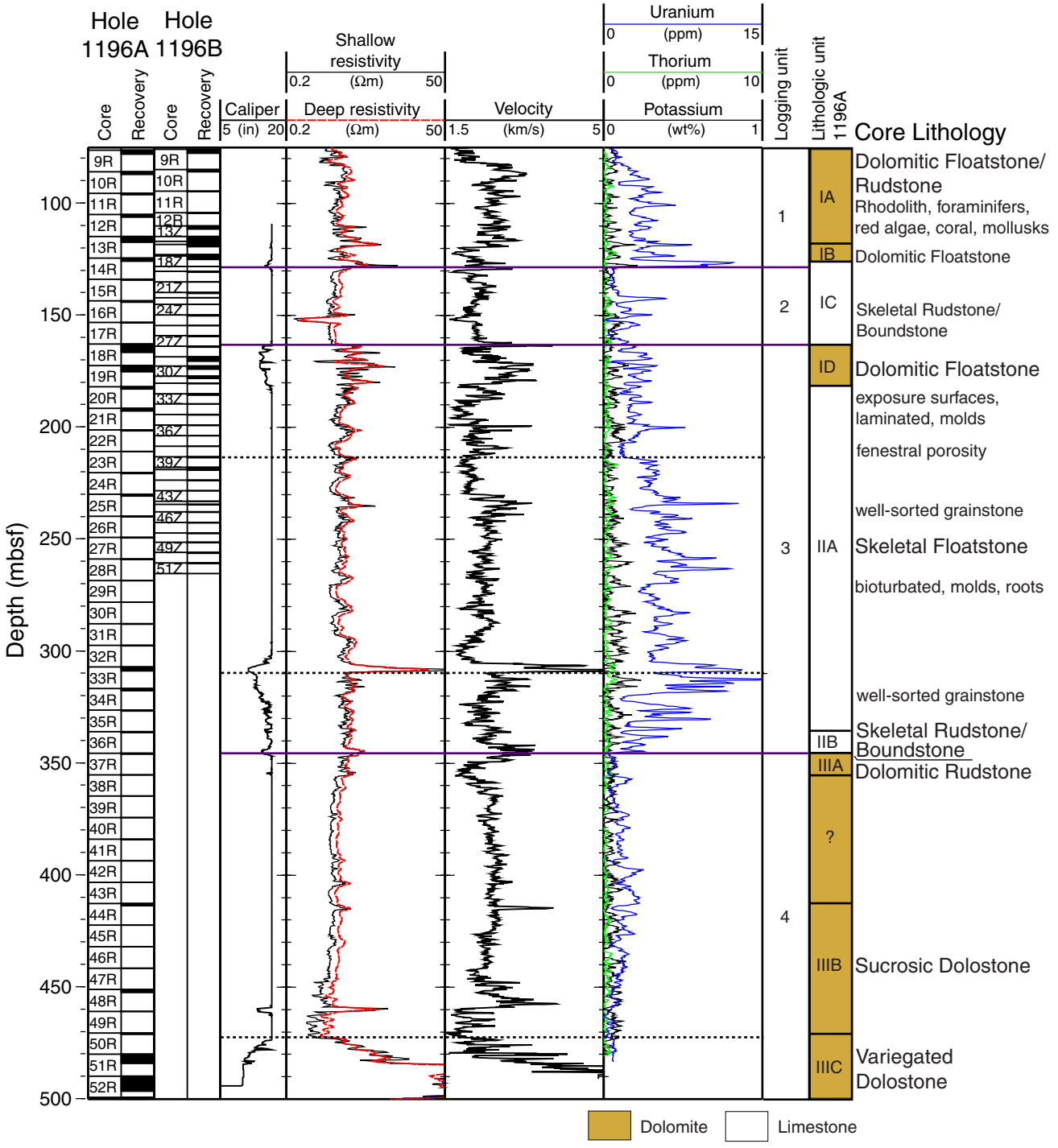

Figure F64. A. Formation MicroScanner (FMS) image of the interval at 121–130.2 mbsf. The arrow points to the log signature change at 128.4 mbsf that corresponds to the lithologic boundary between Subunits IB and IC. The strata above shows increased uranium concentration (red line). **B.** FMS image of the interval at 160–166.2 mbsf. Arrow points to a slightly irregular surface above a high resistivity bed at the top of logging Unit 3 that potentially corresponds to the top of the middle Miocene platform growth phase.

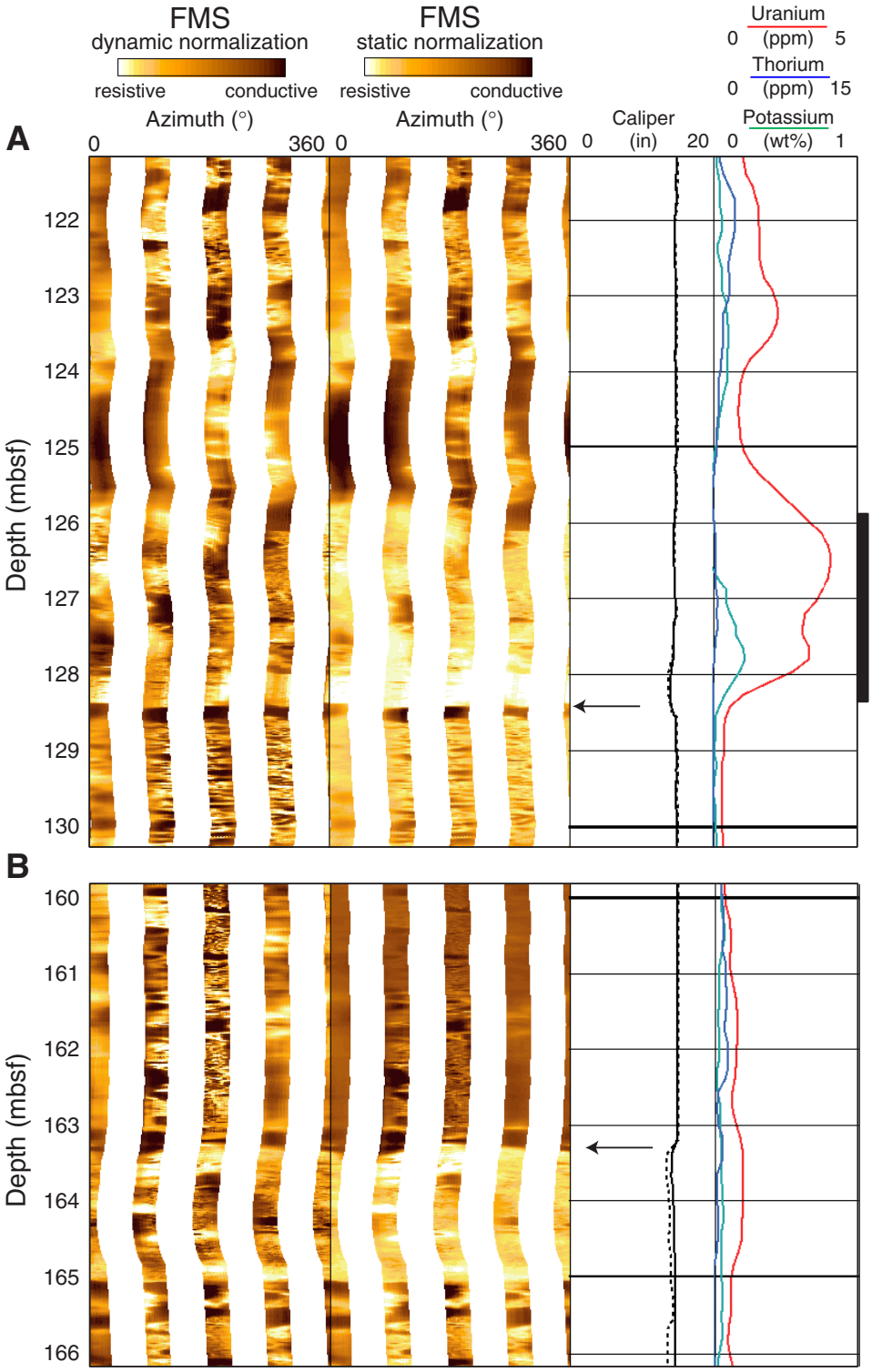

Figure F65. Formation MicroScanner (FMS) image of the interval at 303.5–311 mbsf. Two beds of high resistivity and high uranium content mark the beginning of a log change in the lower part of logging Unit 3 above a slightly irregular surface at 309.1 mbsf (arrow).

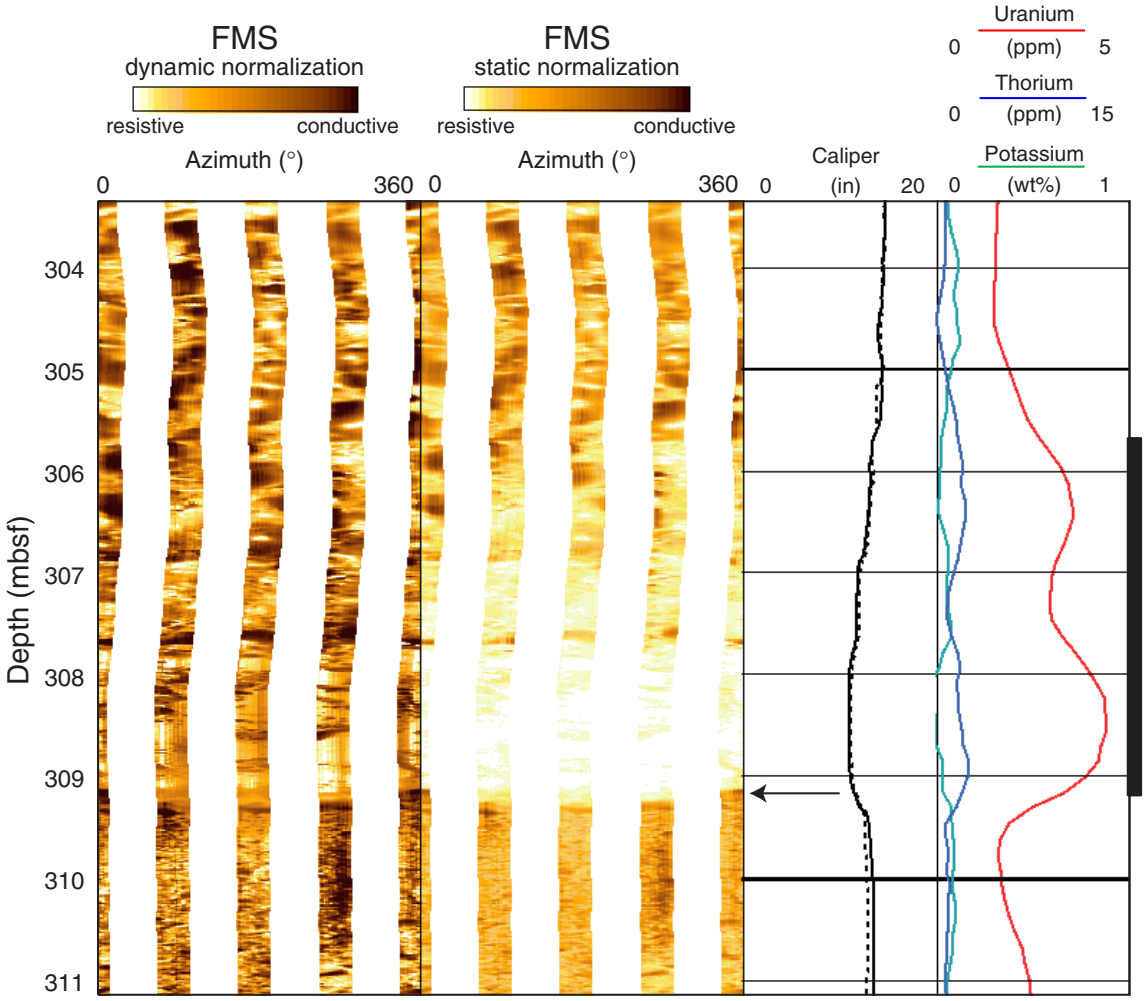

Figure F66. Formation MicroScanner (FMS) image of a fractured interval (490–498.5 mbsf) at the base of logging Unit 3. The inset displays the dip of the fractures that average 160°/60°.

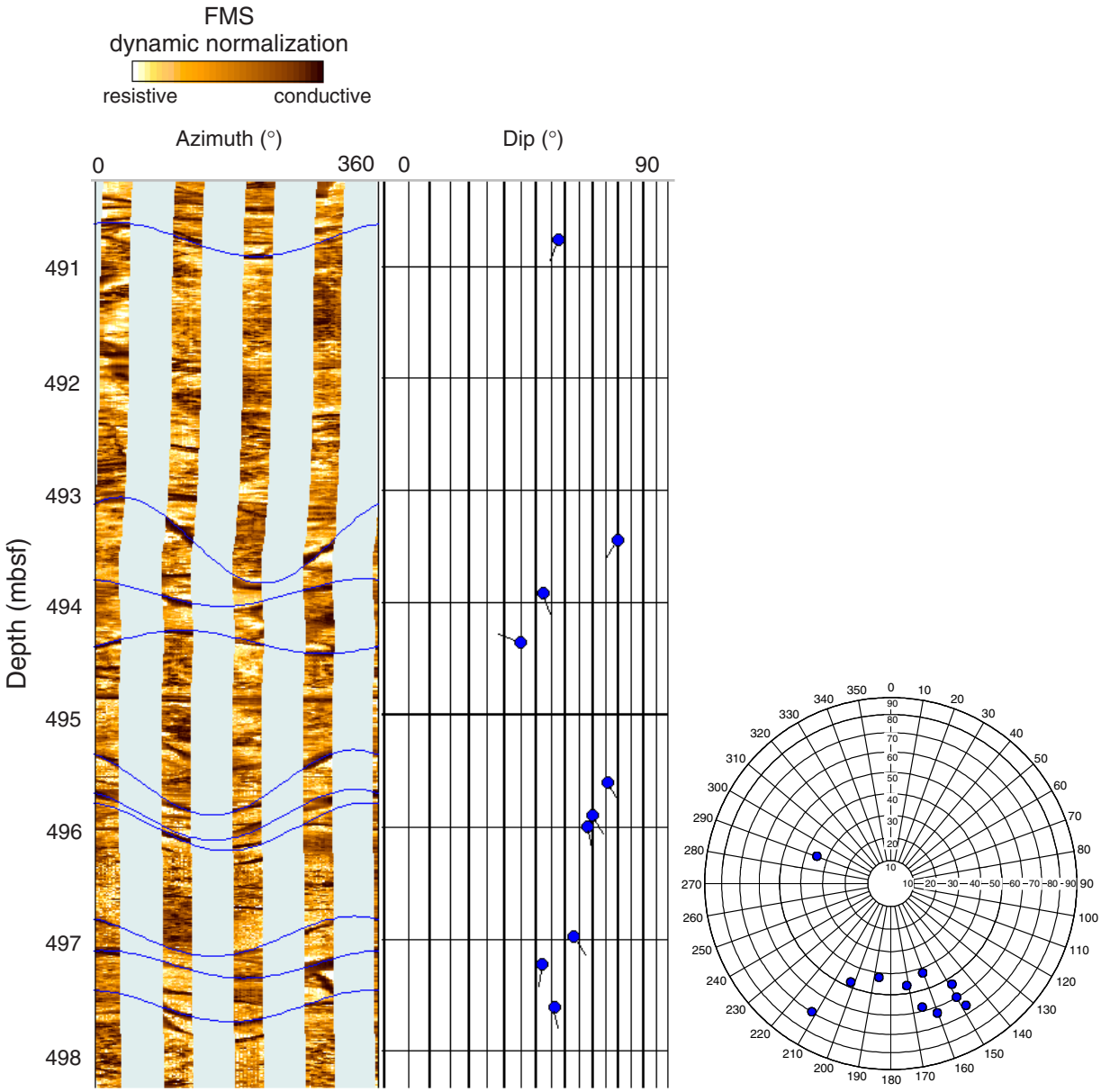

Figure F67. Composite logs of Hole 1199A.

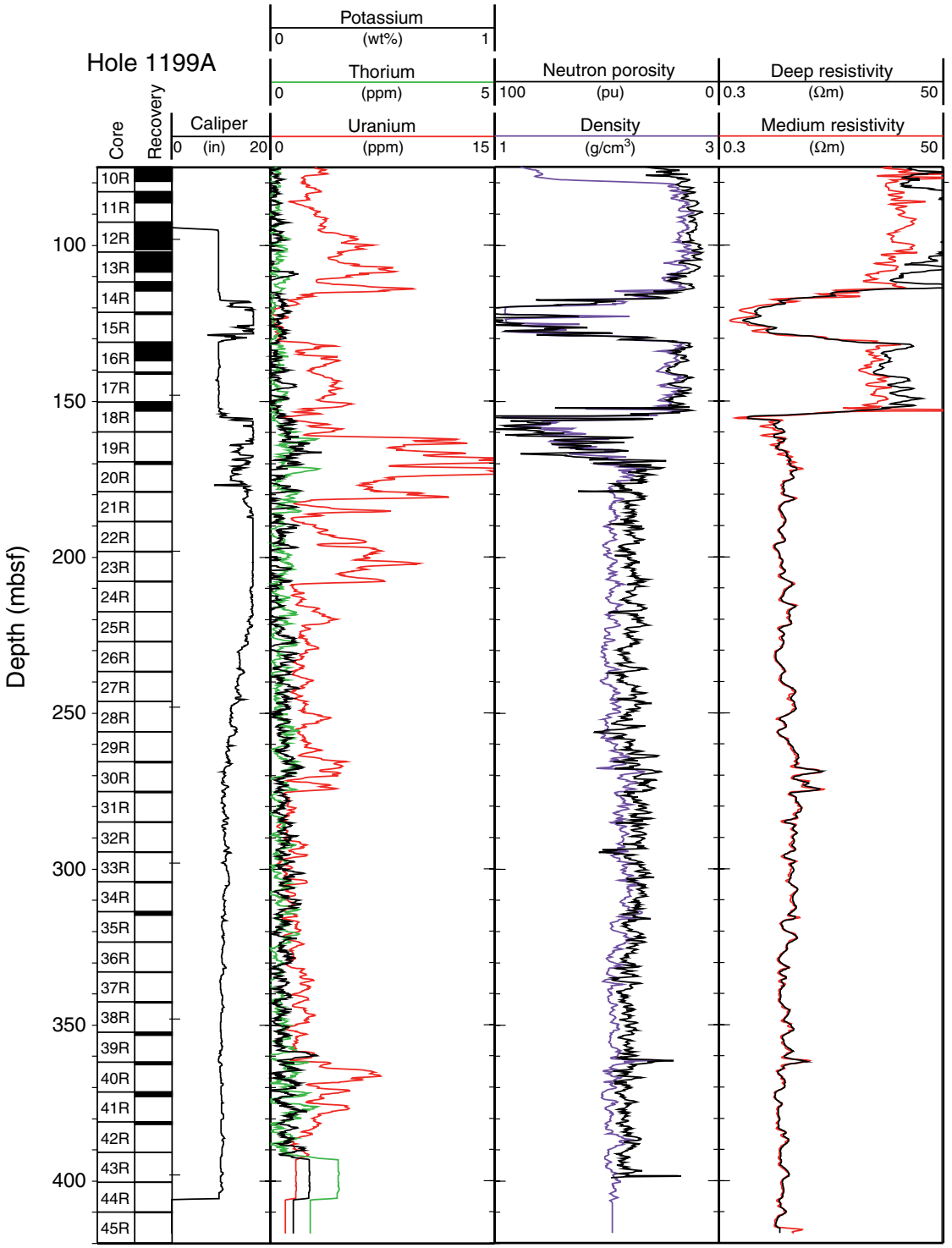

Figure F68. Interpretation of geophysical logging data and correlation to the lithologic units in Hole 1199A.

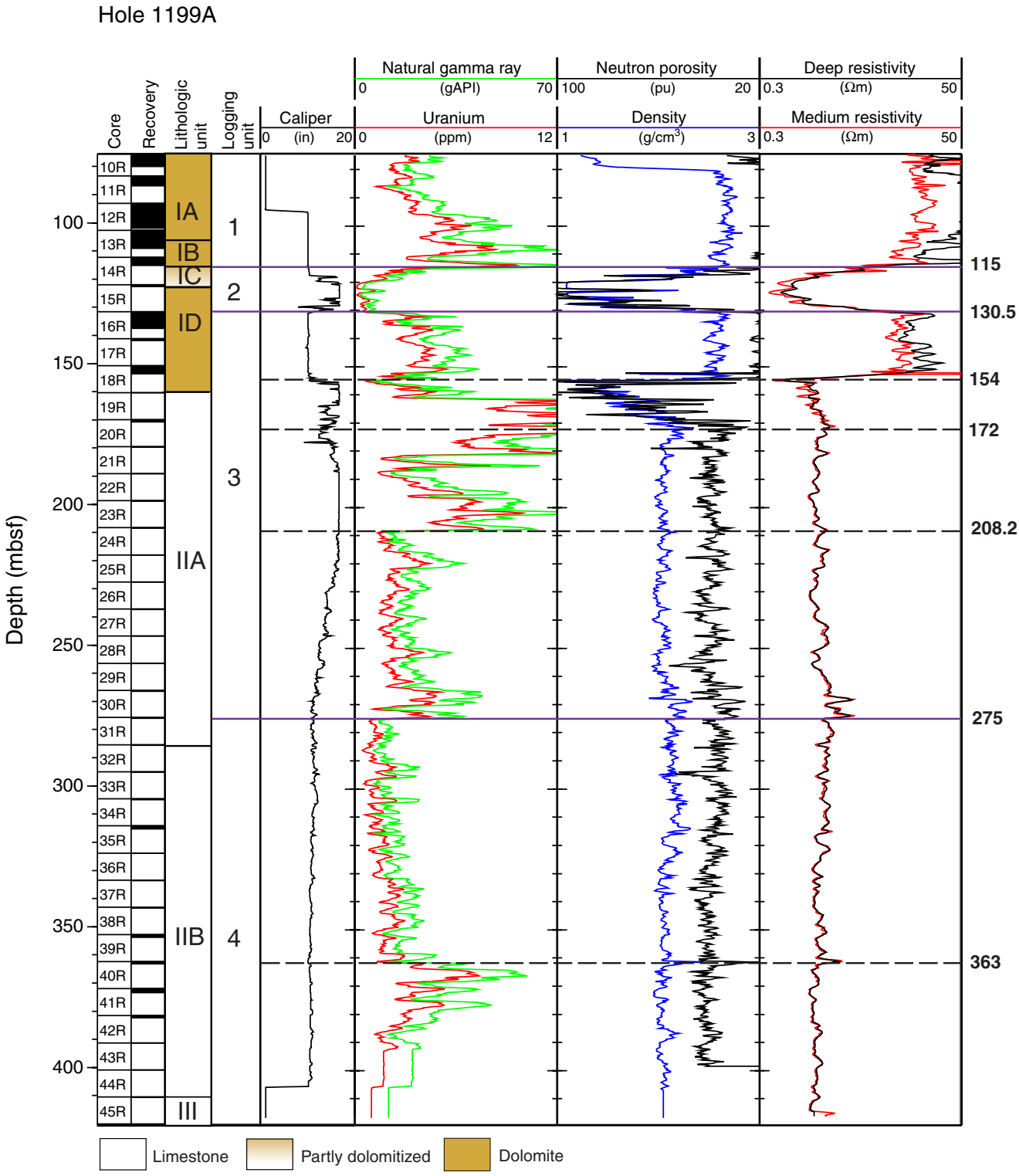

Figure F69. Formation MicroScanner (FMS) image of 103.5–120 mbsf. A high-resistivity bed (arrow) characterizes the lower boundary of logging Unit 1 or lithologic Subunit IB, respectively. This bed and a higher resistive section between 106.5 and 109.5 mbsf show high uranium concentrations (black rectangles).

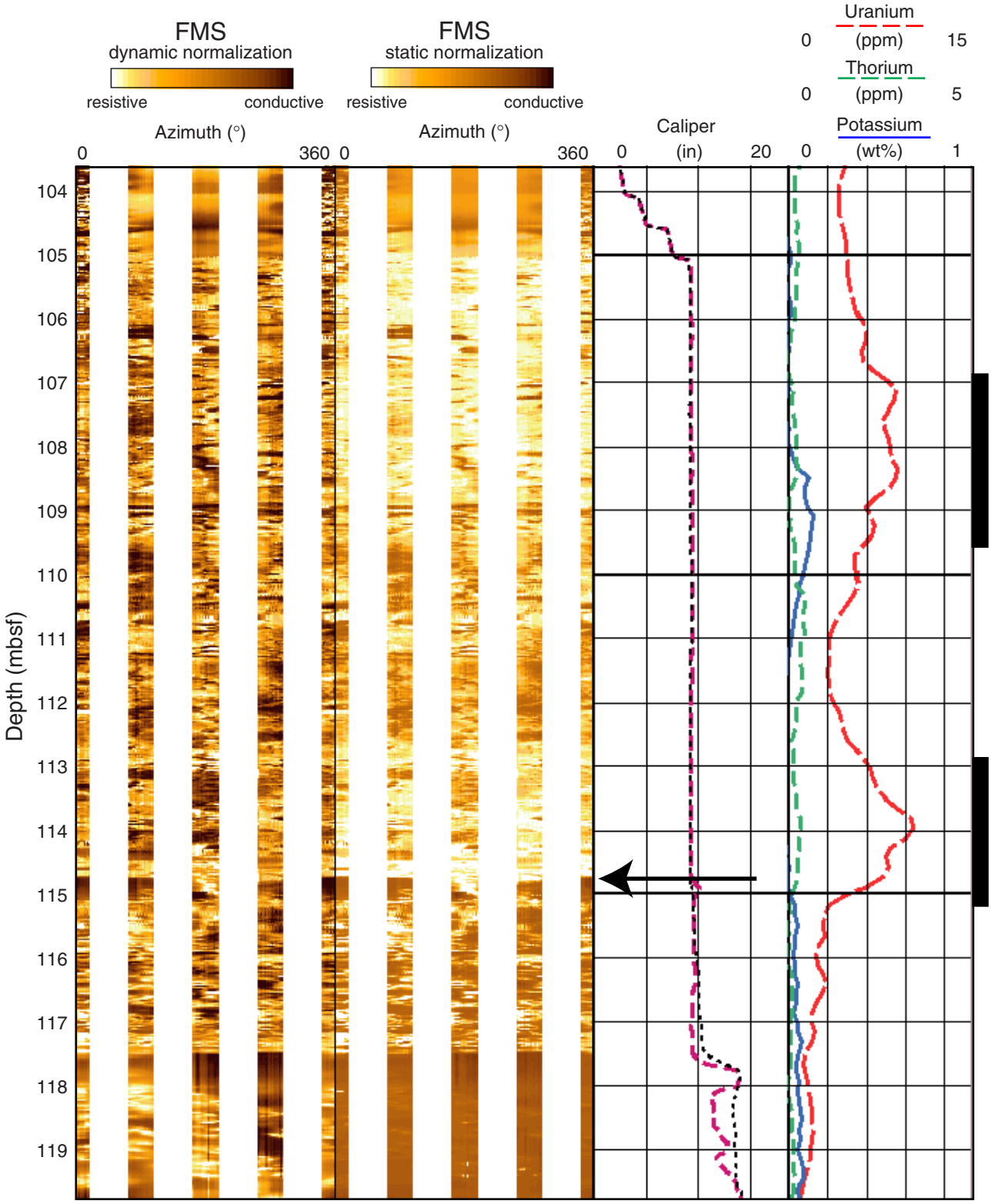

Figure F70. Cross-correlation of log responses in Holes 1196A and 1199A. Datum level is the modern sea level. Seafloor depth at Site 1199 is 11.8 m further below modern sea level than that of Site 1196.

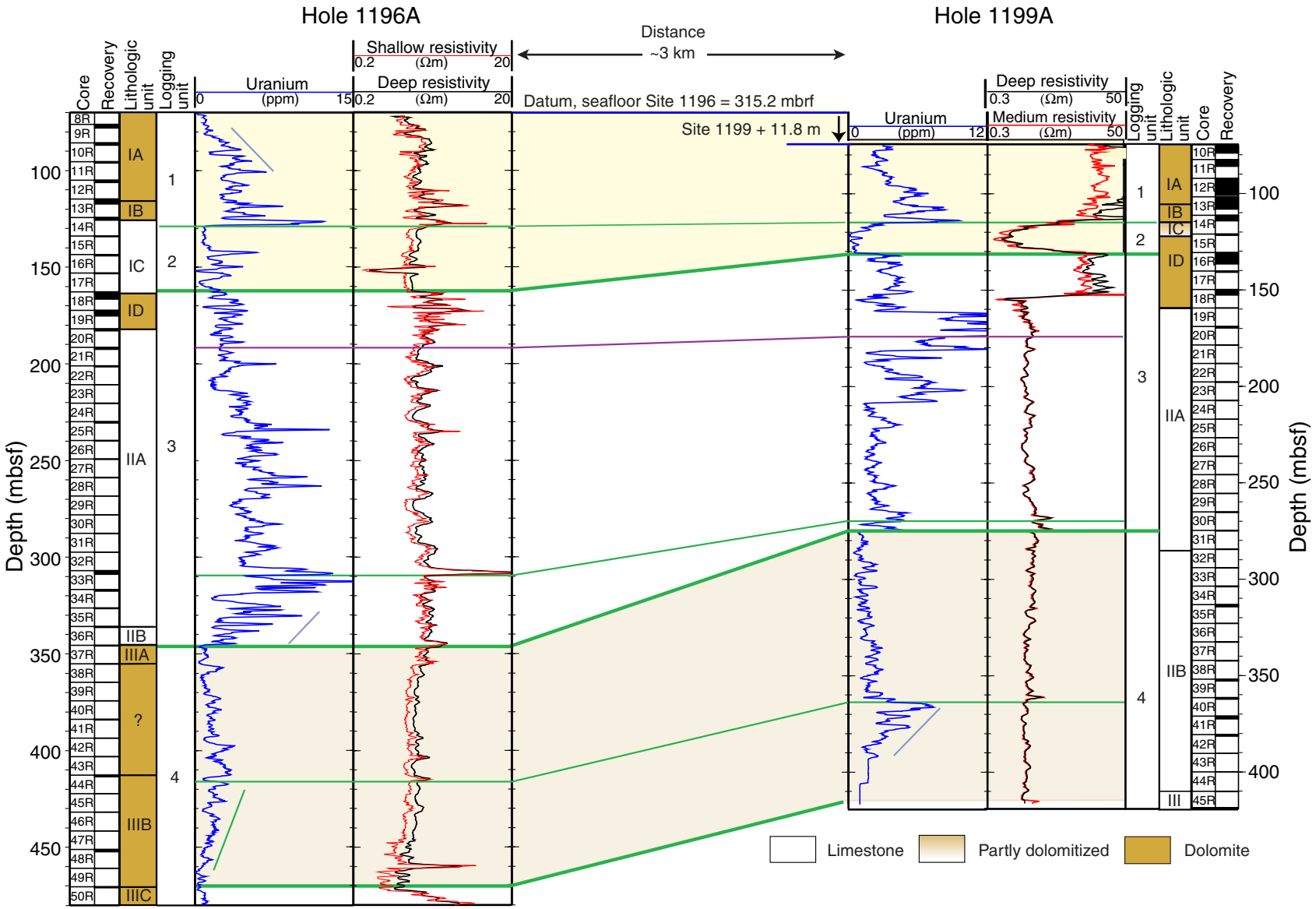

Figure F71. Alternative correlation to Figure F70, p. 114, of log responses in Holes 1196A and 1199A. For discussion, see "Downhole Measurements," p. 32.

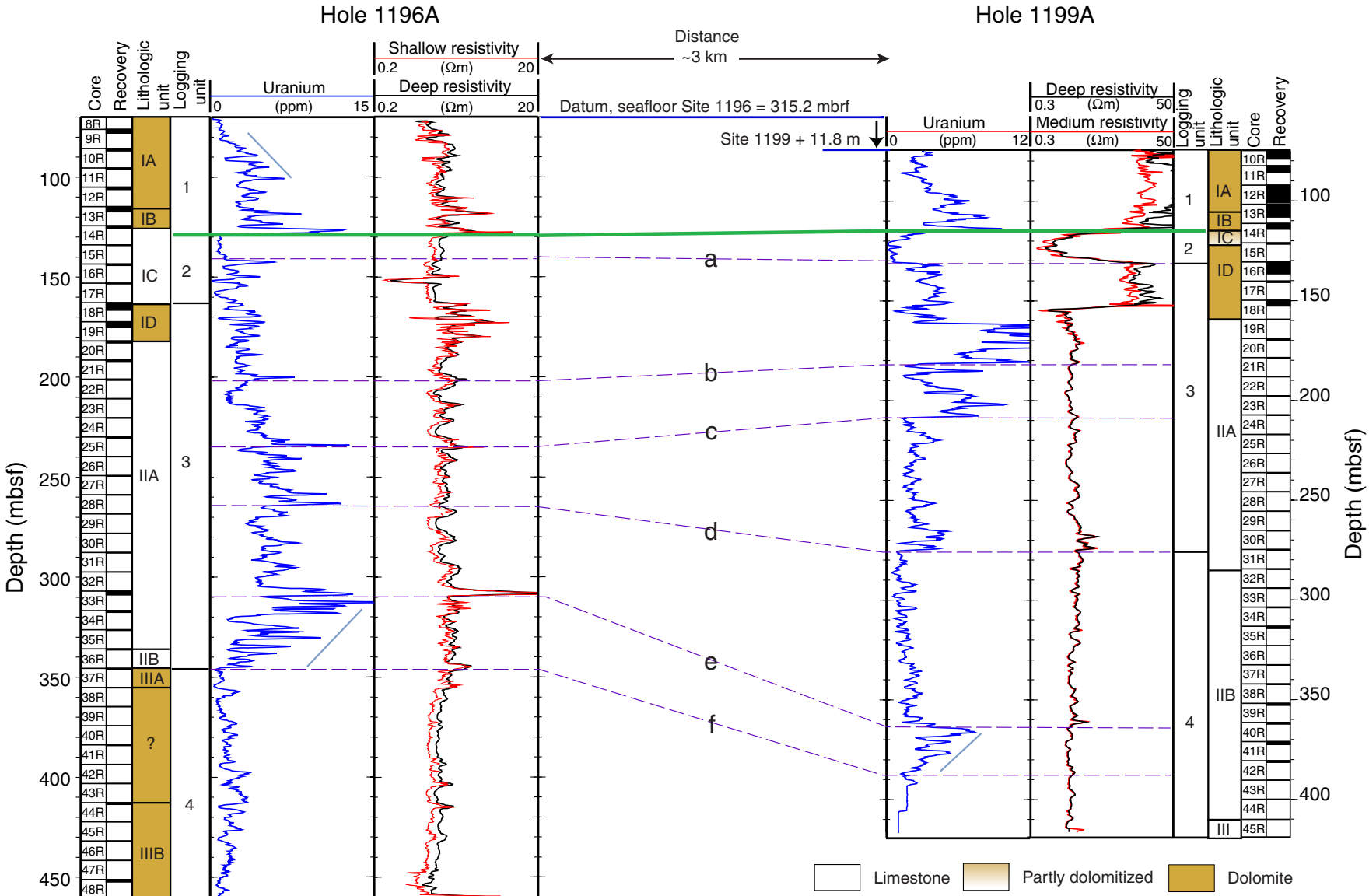

Figure F72. Multichannel line MAR07 with location and penetration depth of Site 1196. The position of Site 1199 was projected into the seismic section parallel to the northwestern SMP margin. Note the irregular, broad low-amplitude reflection ~100 ms below platform top, which is presumed to represent the top of Megasequence B. * = projected margin parallel, MS = Megasequence.

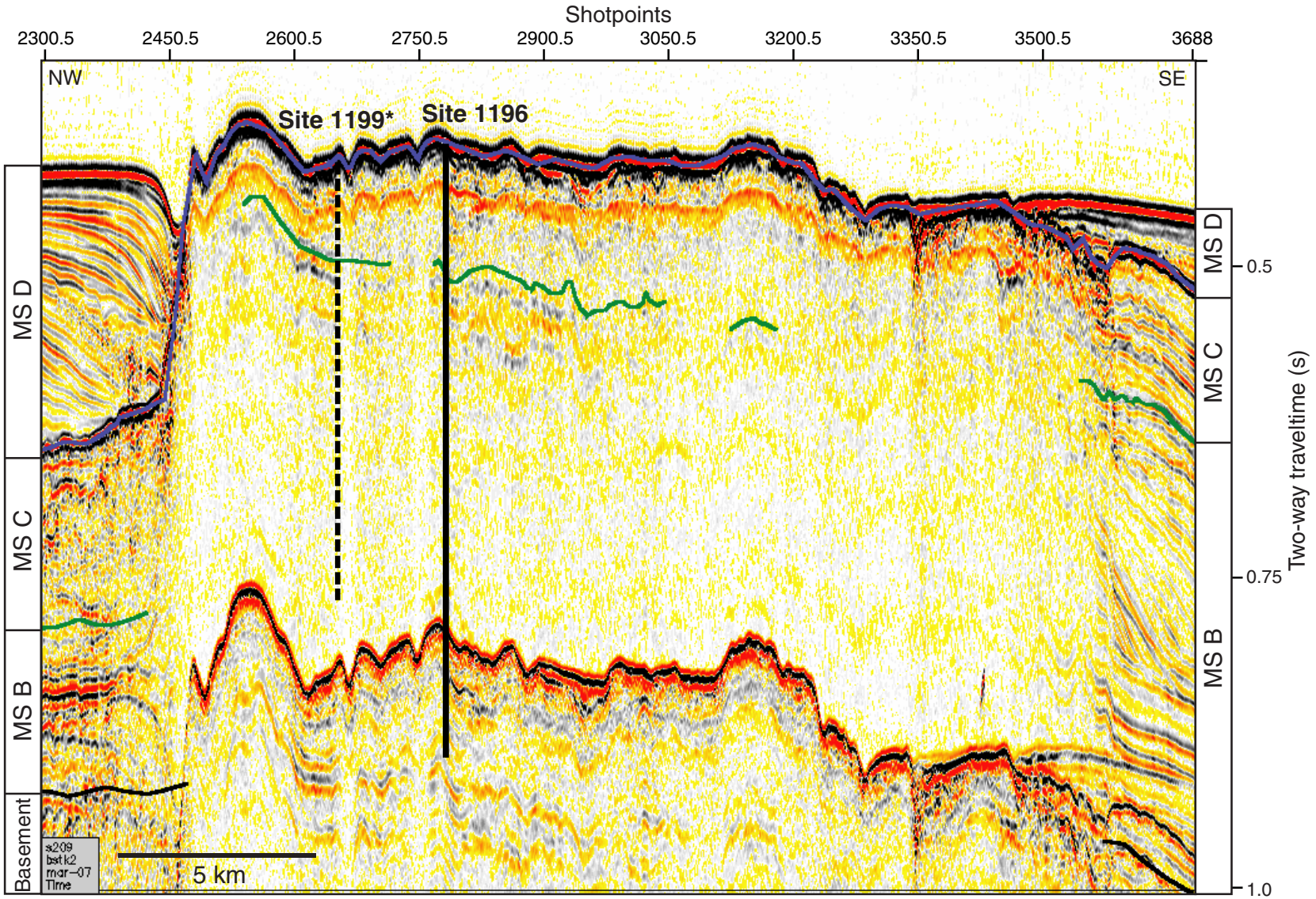

Figure F73. Multichannel line MAR70 with location and penetration depth of Site 1196 connected with seismic line MAR20 showing the location and penetration of Site 1199. The position of Site 1199 was projected into the seismic section parallel to the northwestern SMP margin. The insert shows the orientation of displayed seismic sections. The irregular low-amplitude reflection ~100 ms below the platform top is presumed to represent the top of Megasequence B.

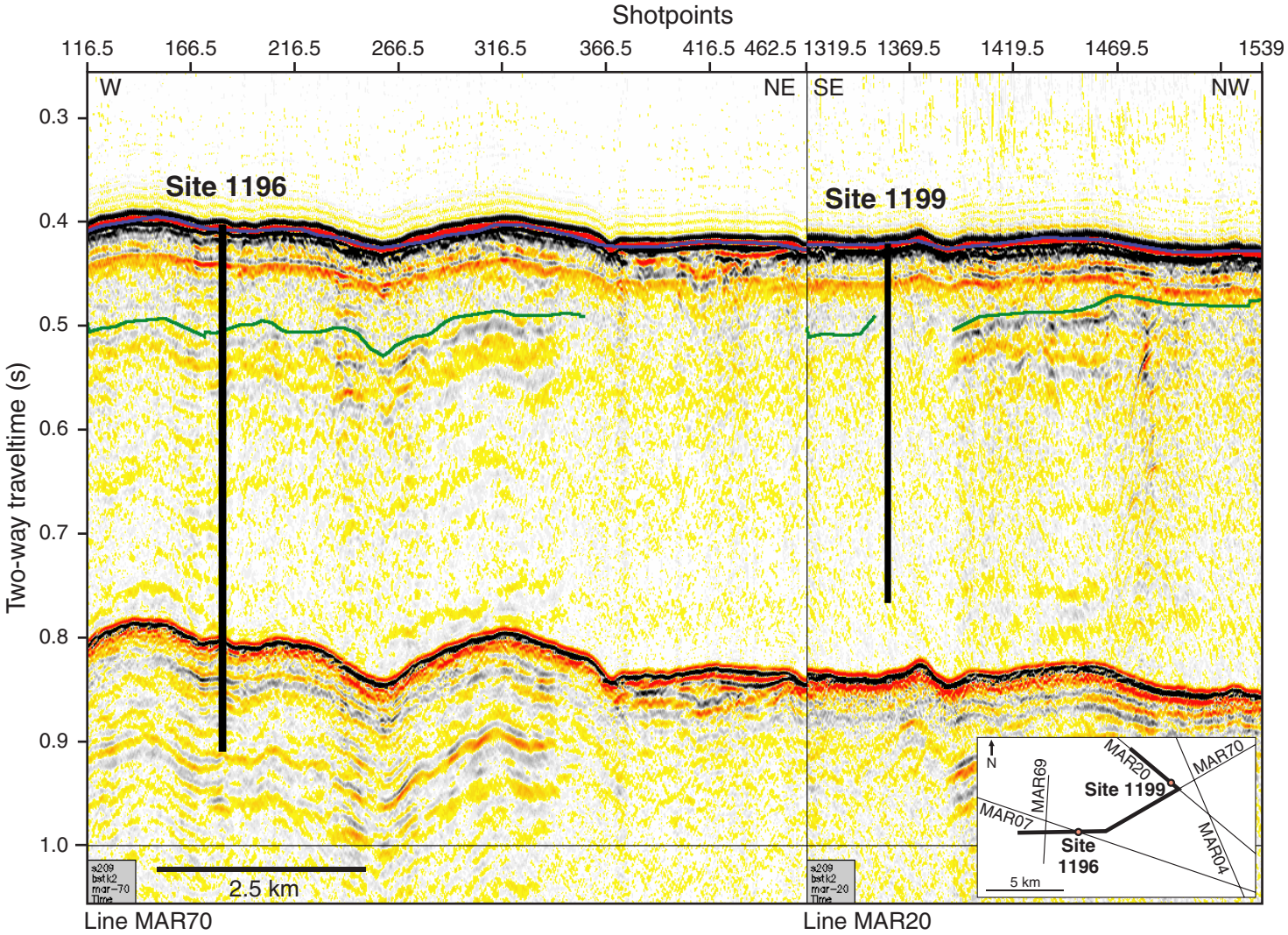

Figure F74. Synthetic seismogram plotted on line MAR07 with two-way traveltime-to-depth velocity data (m/s), *P*-wave velocity with superimposed bulk density, time-depth scales, spike section (reflectivity), extracted wavelet, synthetic seismogram, and lithologic units.

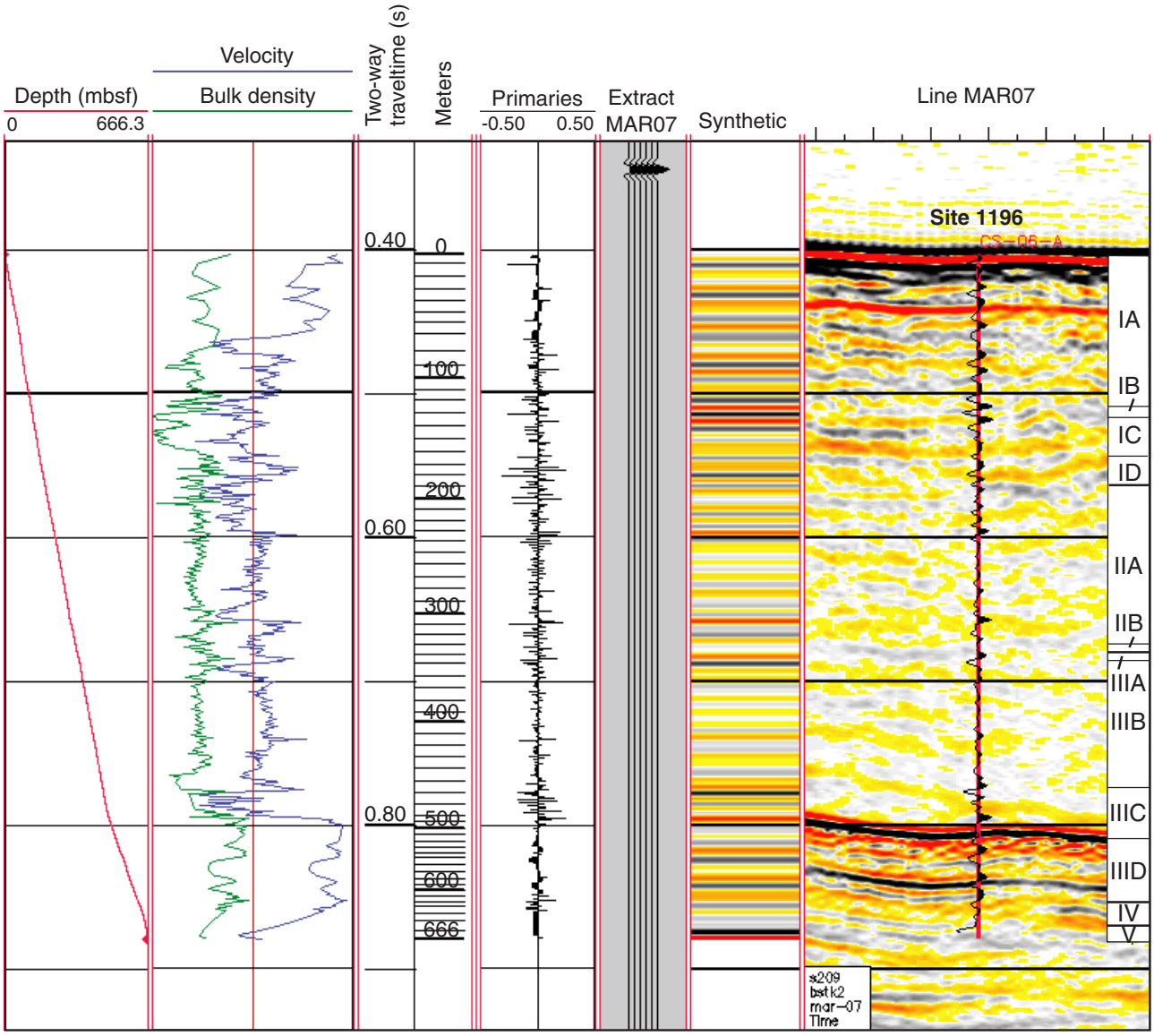

Table T1. Coring summaries, Sites 1196 and 1199. (Continued on next page.)

Core	Date (2001)	Time (local)	Depth (mbsf) Top	Depth (mbsf) Bottom	Length (m) Cored	Length (m) Recovered	Recovery (%)
194-1196A-							
1R	30 Jan	0820	0.0	9.6	9.6	0.88	9.2
2R	30 Jan	0910	9.6	18.9	9.3	0.63	6.8
3R	30 Jan	1005	18.9	28.5	9.6	0.29	3.0
4R	30 Jan	1125	28.5	38.2	9.7	0.97	10.0
5R	30 Jan	1250	38.2	47.5	9.3	1.80	19.4
6R	30 Jan	1355	47.5	56.9	9.4	1.40	14.9
7R	30 Jan	1455	56.9	66.5	9.6	2.23	23.2
8R	30 Jan	1525	66.5	76.1	9.6	0.30	3.1
9R	30 Jan	1615	76.1	85.8	9.7	1.90	19.6
10R	31 Jan	0200	85.8	95.4	9.6	1.18	12.3
11R	31 Jan	0250	95.4	105.0	9.6	0.75	7.8
12R	31 Jan	0350	105.0	114.7	9.7	1.15	11.9
13R	31 Jan	0450	114.7	124.3	9.6	2.57	26.8
14R	31 Jan	0540	124.3	133.9	9.6	1.42	14.8
15R	31 Jan	0625	133.9	143.5	9.6	0.34	3.5
16R	31 Jan	0700	143.5	153.1	9.6	0.63	6.6
17R	31 Jan	0740	153.1	162.7	9.6	0.27	2.8
18R	31 Jan	0900	162.7	172.3	9.6	3.74	39.0
19R	31 Jan	1025	172.3	181.9	9.6	2.94	30.6
20R	31 Jan	1345	181.9	191.5	9.6	1.00	10.4
21R	31 Jan	1440	191.5	201.1	9.6	1.07	11.1
22R	31 Jan	1525	201.1	210.7	9.6	0.39	4.1
23R	31 Jan	1625	210.7	220.3	9.6	0.05	0.5
24R	31 Jan	1710	220.3	229.9	9.6	0.22	2.3
25R	31 Jan	1825	229.9	239.6	9.7	0.65	6.7
26R	31 Jan	1930	239.6	249.2	9.6	0.20	2.1
27R	31 Jan	2030	249.2	258.8	9.6	0.20	2.1
28R	31 Jan	2125	258.8	268.4	9.6	0.22	2.3
29R	31 Jan	2215	268.4	278.0	9.6	0.00	0.0
30R	31 Jan	2300	278.0	287.6	9.6	0.03	0.3
31R	31 Jan	2350	287.6	297.3	9.7	0.27	2.8
32R	1 Feb	0415	297.3	306.9	9.6	0.16	1.7
33R	1 Feb	0530	306.9	316.6	9.7	1.89	19.5
34R	1 Feb	0650	316.6	326.3	9.7	1.01	10.4
35R	1 Feb	0745	326.3	335.9	9.6	0.32	3.3
36R	1 Feb	0905	335.9	345.5	9.6	0.36	3.8
37R	1 Feb	0955	345.5	355.1	9.6	0.46	4.8
38R	1 Feb	1025	355.1	364.7	9.6	0.17	1.8
39R	1 Feb	1115	364.7	374.3	9.6	0.02	0.2
40R	1 Feb	1155	374.3	383.9	9.6	0.00	0.0
41R	1 Feb	1250	383.9	393.5	9.6	0.18	1.9
42R	1 Feb	1325	393.5	403.1	9.6	0.14	1.5
43R	1 Feb	1415	403.1	412.7	9.6	0.05	0.5
44R	1 Feb	1500	412.7	422.3	9.6	0.90	9.4
45R	1 Feb	1545	422.3	431.9	9.6	0.00	0.0
46R	1 Feb	1640	431.9	441.5	9.6	0.00	0.0
47R	1 Feb	1925	441.5	451.1	9.6	0.00	0.0
48R	1 Feb	2020	451.1	460.8	9.7	1.22	12.6
49R	1 Feb	2100	460.8	470.4	9.6	0.00	0.0
50R	1 Feb	2150	470.4	480.0	9.6	0.60	6.3
51R	1 Feb	2355	480.0	489.7	9.7	4.13	42.6
52R	2 Feb	0220	489.7	499.3	9.6	6.74	70.2
53R	2 Feb	0535	499.3	508.9	9.6	4.69	48.9
54R	2 Feb	0645	508.9	518.5	9.6	1.20	12.5
55R	2 Feb	0810	518.5	528.1	9.6	1.16	12.1
56R	2 Feb	1000	528.1	537.7	9.6	1.37	14.3
57R	2 Feb	1235	537.7	547.3	9.6	2.85	29.7
58R	2 Feb	1355	547.3	556.9	9.6	1.07	11.1
59R	2 Feb	1455	556.9	566.6	9.7	0.95	9.8
60R	2 Feb	1555	566.6	576.2	9.6	0.69	7.2
61R	2 Feb	1710	576.2	585.8	9.6	1.63	17.0
62R	2 Feb	1830	585.8	595.5	9.7	0.45	4.6
63R	2 Feb	1950	595.5	605.1	9.6	2.12	22.1
64R	2 Feb	2125	605.1	614.7	9.6	3.77	39.3
65R	2 Feb	2330	614.7	624.4	9.7	5.15	53.1
66R	3 Feb	050	624.4	633.7	9.3	4.65	50.0
67R	3 Feb	0200	633.7	643.4	9.7	1.92	19.8
68R	3 Feb	0300	643.4	653.0	9.6	0.04	0.4
69R	3 Feb	0350	653.0	662.6	9.6	0.00	0.0
70R	3 Feb	0515	662.6	672.2	9.6	4.62	48.1
				Cored total:	672.2	86.37	12.8
				Drilled total:	0.0		
				Total:	672.2		
194-1196B-							
1R	4 Feb	1635	0.0	9.7	9.7	2.72	28.0
2R	4 Feb	1855	9.7	19.4	9.7	0.29	3.0
3R	4 Feb	2030	19.4	28.8	9.4	0.03	0.3
4R	4 Feb	2155	28.8	38.2	9.4	0.96	10.2
5R	4 Feb	2350	38.2	47.2	9.0	0.89	9.9
6R	5 Feb	0130	47.2	56.8	9.6	0.90	9.4
7R	5 Feb	1510	56.8	66.2	9.4	2.25	23.9
8R	5 Feb	1630	66.2	75.8	9.6	0.24	2.5
9R	5 Feb	1730	75.8	84.8	9.0	1.85	20.6
10R	5 Feb	2010	84.8	94.5	9.7	0.93	9.6
11R	5 Feb	2145	94.5	104.1	9.6	0.17	1.8
12R	5 Feb	2245	104.1	110.0	5.9	0.22	3.7
13Z	12 Feb	0045	110.0	114.7	4.7	1.43	30.4
14Z	12 Feb	0140	114.7	116.9	2.2	1.74	79.1
15Z	12 Feb	0230	116.9	118.2	1.3	1.08	83.1
16Z	12 Feb	0345	118.2	122.9	4.7	1.16	24.7
17Z	12 Feb	0430	122.9	123.4	0.5	0.57	114.0
18Z	12 Feb	0540	123.4	128.1	4.7	1.52	32.3
19Z	12 Feb	0615	128.1	130.3	2.2	0.00	0.0
20Z	12 Feb	0655	130.3	135.0	4.7	0.47	10.0
21Z	12 Feb	0740	135.0	139.7	4.7	0.00	0.0
22Z	12 Feb	0820	139.7	142.0	2.3	0.51	22.2
23Z	12 Feb	0855	142.0	145.0	3.0	0.00	0.0
24Z	12 Feb	0945	145.0	149.7	4.7	0.06	1.3
25Z	12 Feb	1040	149.7	154.4	4.7	0.50	10.6
26Z	12 Feb	1120	154.4	159.1	4.7	0.00	0.0
27Z	12 Feb	1215	159.1	163.8	4.7	0.36	7.7
28Z	12 Feb	1320	163.8	168.5	4.7	0.37	7.9
29Z	12 Feb	1420	168.5	172.5	4.0	1.86	46.5
30Z	12 Feb	1520	172.5	177.2	4.7	1.49	31.7
31Z	12 Feb	1625	177.2	180.2	3.0	0.96	32.0
32Z	12 Feb	1715	180.2	184.9	4.7	0.23	4.9
33Z	12 Feb	1820	184.9	189.6	4.7	0.72	15.3
34Z	12 Feb	1920	189.6	194.3	4.7	0.00	0.0
35Z	12 Feb	2025	194.3	199.0	4.7	0.06	1.3
36Z	12 Feb	2125	199.0	203.7	4.7	0.11	2.3
37Z	12 Feb	2240	203.7	208.4	4.7	0.00	0.0
38Z	12 Feb	2325	208.4	213.1	4.7	0.00	0.0
39Z	13 Feb	0040	213.1	217.8	4.7	0.38	8.1
40Z	13 Feb	0130	217.8	218.8	1.0	0.28	28.0
41Z	13 Feb	0230	218.8	223.5	4.7	0.24	5.1
42Z	13 Feb	0315	223.5	228.2	4.7	0.27	5.7
43Z	13 Feb	0405	228.2	232.9	4.7	0.00	0.0
44Z	13 Feb	0455	232.9	234.3	1.4	0.12	8.6
45Z	13 Feb	0555	234.3	237.8	3.5	0.30	8.6
46Z	13 Feb	0640	237.8	242.5	4.7	0.15	3.2
47Z	13 Feb	0720	242.5	247.2	4.7	0.23	4.9
48Z	13 Feb	0810	247.2	251.2	4.0	0.10	2.5
49Z	13 Feb	0855	251.2	255.9	4.7	0.30	6.4
50Z	13 Feb	0950	255.9	260.6	4.7	0.30	6.4
51Z	13 Feb	1045	260.6	265.3	4.7	0.05	1.1
				Cored total:	265.3	29.37	11.1
				Drilled total:	0.0		
				Total:	265.3		
194-1199A-							
1R	18 Feb	1535	0.0	9.5	9.5	3.88	40.8
2R	18 Feb	1830	9.5	17.4	7.9	5.78	73.2
3R	18 Feb	2235	17.4	18.9	1.5	1.16	77.3
4R	19 Feb	0300	18.9	26.8	7.9	7.79	98.6
5R	19 Feb	0610	26.8	35.7	8.9	7.20	80.9
6R	19 Feb	0955	35.7	45.1	9.4	4.60	48.9
7R	19 Feb	1310	45.1	54.0	8.9	3.82	42.9

Table T1 (continued).

Core	Date (2001)	Time (local)	Depth (mbsf) Top	Depth (mbsf) Bottom	Length (m) Cored	Length (m) Recovered	Recovery (%)
8R	19 Feb	1620	54.0	63.6	9.6	3.20	33.3
9R	19 Feb	1825	63.6	73.2	9.6	7.85	81.8
10R	19 Feb	1955	73.2	82.8	9.6	6.33	65.9
11R	19 Feb	2210	82.8	92.5	9.7	3.60	37.1
12R	20 Feb	0020	92.5	102.1	9.6	8.93	93.0
13R	20 Feb	0220	102.1	111.8	9.7	6.42	66.2
14R	20 Feb	0330	111.8	121.4	9.6	2.78	29.0
15R	20 Feb	0415	121.4	131.0	9.6	0.73	7.6
16R	20 Feb	0615	131.0	140.6	9.6	6.01	62.6
17R	20 Feb	0810	140.6	150.2	9.6	0.68	7.1
18R	20 Feb	0920	150.2	159.8	9.6	2.84	29.6
19R	20 Feb	1005	159.8	169.4	9.6	0.07	0.7
20R	20 Feb	1100	169.4	179.0	9.6	0.82	8.5
21R	20 Feb	1150	179.0	188.6	9.6	0.17	1.8
22R	20 Feb	1230	188.6	198.2	9.6	0.01	0.1
23R	20 Feb	1535	198.2	207.8	9.6	0.04	0.4
24R	20 Feb	1625	207.8	217.4	9.6	0.04	0.4
25R	20 Feb	1710	217.4	227.0	9.6	0.02	0.2
26R	20 Feb	1755	227.0	236.7	9.7	0.00	0.0
27R	20 Feb	1850	236.7	246.3	9.6	0.02	0.2
28R	20 Feb	1940	246.3	255.9	9.6	0.00	0.0
29R	20 Feb	2025	255.9	265.5	9.6	0.04	0.4
30R	20 Feb	2125	265.5	275.2	9.7	0.36	3.7
31R	20 Feb	2215	275.2	284.8	9.6	0.30	3.1
32R	20 Feb	2255	284.8	294.4	9.6	0.18	1.9
33R	20 Feb	2340	294.4	304.0	9.6	0.25	2.6
34R	21 Feb	0020	304.0	313.7	9.7	0.32	3.3
35R	21 Feb	0100	313.7	323.3	9.6	1.07	11.1
36R	21 Feb	0145	323.3	332.9	9.6	0.03	0.3
37R	21 Feb	0225	332.9	342.6	9.7	0.23	2.4
38R	21 Feb	0310	342.6	352.2	9.6	0.20	2.1
39R	21 Feb	0400	352.2	361.8	9.6	1.03	10.7
40R	21 Feb	0445	361.8	371.4	9.6	0.86	9.0
41R	21 Feb	0530	371.4	381.1	9.7	1.45	14.9
42R	21 Feb	0615	381.1	390.7	9.6	0.76	7.9
43R	21 Feb	0655	390.7	400.3	9.6	0.09	0.9
44R	21 Feb	0740	400.3	409.9	9.6	0.07	0.7
45R	21 Feb	0840	409.9	419.5	9.6	0.13	1.4
				Cored total:	419.5	92.16	22.0
				Drilled total:	0.0		
				Total:	419.5		

Table T2. Expanded coring summaries, Sites 1196 and 1199. (See table notes. Continued on next eight pages.)

Core	Date (2001)	Time (local)	Core depth (mbsf) Top	Core depth (mbsf) Bottom	Length (m) Cored	Length (m) Recovered	Recovery (%)	Section	Length (m) Liner	Length (m) Curated	Section depth (mbsf) Top	Section depth (mbsf) Bottom	Catwalk samples	Comment
194-1196A-														
1R	30 Jan	0820	0.0	9.6	9.6	0.88	9.2							
								1	0.88	1.14	0.00	1.14	PAL	
								Totals:	0.88	1.14				
2R	30 Jan	0910	9.6	18.9	9.3	0.63	6.8							
								1	0.63	0.8	9.60	10.40	PAL	
								Totals:	0.63	0.8				
3R	30 Jan	1005	18.9	28.5	9.6	0.29	3.0							
								1	0.29	0.36	18.90	19.26	PAL	
								Totals:	0.29	0.36				
4R	30 Jan	1125	28.5	38.2	9.7	0.97	10.0							
								1	0.97	1.18	28.50	29.68	PAL	
								Totals:	0.97	1.18				
5R	30 Jan	1250	38.2	47.5	9.3	1.80	19.4							
								1	1.50	1.50	38.20	39.70	EHWR	
								2	0.30	0.89	39.70	40.59	PAL	
								Totals:	1.80	2.39				
6R	30 Jan	1355	47.5	56.9	9.4	1.40	14.9							
								1	1.40	1.50	47.50	49.00	PAL	
								Totals:	1.40	1.50				
7R	30 Jan	1455	56.9	66.5	9.6	2.23	23.2							
								1	1.50	1.41	56.90	58.31		
								2	0.73	1.12	58.31	59.43	PAL, EHWR	
								Totals:	2.23	2.53				
8R	30 Jan	1525	66.5	76.1	9.6	0.30	3.1							
								1	0.30	0.42	66.50	66.92	PAL	
								Totals:	0.30	0.42				
9R	30 Jan	1615	76.1	85.8	9.7	1.90	19.6							
								1	1.47	1.42	76.10	77.52		
								2	0.43	0.75	77.52	78.27	PAL, EHWR	
								Totals:	1.90	2.17				
10R	31 Jan	0200	85.8	95.4	9.6	1.18	12.3							
								1	1.18	1.34	85.80	87.14	PAL	
								Totals:	1.18	1.34				
11R	31 Jan	0250	95.4	105.0	9.6	0.75	7.8							
								1	0.75	0.90	95.40	96.30	PAL	
								Totals:	0.75	0.90				
12R	31 Jan	0350	105.0	114.7	9.7	1.15	11.9							
								1	1.15	1.32	105.00	106.32	PAL	
								Totals:	1.15	1.32				
13R	31 Jan	0450	114.7	124.3	9.6	2.57	26.8							
								1	1.17	1.50	114.70	116.20		
								2	1.40	1.50	116.20	117.70	PAL, EHWR	
								Totals:	2.57	3.00				
14R	31 Jan	0540	124.3	133.9	9.6	1.42	14.8							
								1	1.42	1.40	124.30	125.70		
								2	0.00	0.27	125.70	125.97	PAL	
								Totals:	1.42	1.67				
15R	31 Jan	0625	133.9	143.5	9.6	0.34	3.5							
								1	0.34	0.38	133.90	134.28	PAL	
								Totals:	0.34	0.38				
16R	31 Jan	0700	143.5	153.1	9.6	0.63	6.6							
								1	0.63	0.76	143.50	144.26	PAL	
								Totals:	0.63	0.76				
17R	31 Jan	0740	153.1	162.7	9.6	0.27	2.8							
								1	0.27	0.28	153.10	153.38	PAL	
								Totals:	0.27	0.28				
18R	31 Jan	0900	162.7	172.3	9.6	3.74	39.0							
								1	0.74	1.46	162.70	164.16		
								2	1.50	1.50	164.16	165.66	EHWR	
								3	1.50	1.39	165.66	167.05	PAL	
								Totals:	3.74	4.35				
19R	31 Jan	1025	172.3	181.9	9.6	2.94	30.6							
								1	0.00	1.43	172.30	173.73		
								2	1.44	1.47	173.73	175.20		
								3	1.50	0.62	175.20	175.82	PAL, EHWR	
								Totals:	2.94	3.52				

Table T2 (continued).

Core	Date (2001)	Time (local)	Core depth (mbsf) Top	Core depth (mbsf) Bottom	Length (m) Cored	Length (m) Recovered	Recovery (%)	Section	Length (m) Liner	Length (m) Curated	Section depth (mbsf) Top	Section depth (mbsf) Bottom	Catwalk samples	Comment
20R	31 Jan	1345	181.9	191.5	9.6	1.00	10.4							
								1	1.00	1.13	181.90	183.03	PAL	
								Totals:	1.00	1.13				
21R	31 Jan	1440	191.5	201.1	9.6	1.07	11.1							
								1	1.07	1.23	191.50	192.73	PAL	
								Totals:	1.07	1.23				
22R	31 Jan	1525	201.1	210.7	9.6	0.39	4.1							
								1	0.39	0.46	201.10	201.56	PAL	
								Totals:	0.39	0.46				
23R	31 Jan	1625	210.7	220.3	9.6	0.05	0.5							
								1	0.05	0.05	210.70	210.75	PAL	All to PAL
								Totals:	0.05	0.05				
24R	31 Jan	1710	220.3	229.9	9.6	0.22	2.3							
								1	0.22	0.28	220.30	220.58	PAL	
								Totals:	0.22	0.28				
25R	31 Jan	1825	229.9	239.6	9.7	0.65	6.7							
								1	0.65	0.80	229.90	230.70	PAL	
								Totals:	0.65	0.80				
26R	31 Jan	1930	239.6	249.2	9.6	0.20	2.1							
								1	0.20	0.26	239.60	239.86	PAL	
								Totals:	0.20	0.26				
27R	31 Jan	2030	249.2	258.8	9.6	0.20	2.1							
								1	0.2	0.25	249.20	249.45	PAL	
								Totals:	0.2	0.25				
28R	31 Jan	2125	258.8	268.4	9.6	0.22	2.3							
								1	0.22	0.22	258.80	259.02	PAL	
								Totals:	0.22	0.22				
29R	31 Jan	2215	268.4	278.0	9.6	0.00	0.0							
30R	31 Jan	2300	278.0	287.6	9.6	0.03	0.3							
								1	0.03	0.03	278.00	278.03	PAL	All to PAL
								Totals:	0.03	0.03				
31R	31 Jan	2350	287.6	297.3	9.7	0.27	2.8							
								1	0.27	0.22	287.60	287.82	PAL	
								Totals:	0.27	0.22				
32R	1 Feb	0415	297.3	306.9	9.6	0.16	1.7							
								1	0.16	0.20	297.30	297.50	PAL	
								Totals:	0.16	0.20				
33R	1 Feb	0530	306.9	316.6	9.7	1.89	19.5							
								1	0.48	1.46	306.90	308.36		
								2	1.41	0.74	308.36	309.10	PAL	
								Totals:	1.89	2.20				
34R	1 Feb	0650	316.6	326.3	9.7	1.01	10.4							
								1	1.01	1.32	316.60	317.92	PAL	
								Totals:	1.01	1.32				
35R	1 Feb	0745	326.3	335.9	9.6	0.32	3.3							
								1	0.32	0.40	326.30	326.70	PAL	
								Totals:	0.32	0.40				
36R	1 Feb	0905	335.9	345.5	9.6	0.36	3.8							
								1	0.36	0.43	335.90	336.33	PAL	
								Totals:	0.36	0.43				
37R	1 Feb	0955	345.5	355.1	9.6	0.46	4.8							
								1	0.46	0.72	345.50	346.22	PAL	
								Totals:	0.46	0.72				
38R	1 Feb	1025	355.1	364.7	9.6	0.17	1.8							
								1	0.17	0.24	355.10	355.34	PAL	
								Totals:	0.17	0.24				
39R	1 Feb	1115	364.7	374.3	9.6	0.02	0.2							
								1	0.02	0.02	364.70	364.72	PAL	All to PAL
								Totals:	0.02	0.02				
40R	1 Feb	1155	374.3	383.9	9.6	0.00	0.0							
41R	1 Feb	1250	383.9	393.5	9.6	0.18	1.9							
								1	0.18	0.18	383.90	384.08	PAL	
								Totals:	0.18	0.18				
42R	1 Feb	1325	393.5	403.1	9.6	0.14	1.5							
								1	0.14	0.16	393.50	393.66	PAL	
								Totals:	0.14	0.16				
43R	1 Feb	1415	403.1	412.7	9.6	0.05	0.5							
								1	0.05	0.05	403.10	403.15	PAL	All to PAL
								Totals:	0.05	0.05				

Table T2 (continued).

Core	Date (2001)	Time (local)	Core depth (mbsf) Top	Core depth (mbsf) Bottom	Length (m) Cored	Length (m) Recovered	Recovery (%)	Section	Length (m) Liner	Length (m) Curated	Section depth (mbsf) Top	Section depth (mbsf) Bottom	Catwalk samples	Comment
44R	1 Feb	1500	412.7	422.3	9.6	0.90	9.4							
								1	0.90	1.07	412.70	413.77	EHWR	
								Totals:	0.90	1.07				
45R	1 Feb	1545	422.3	431.9	9.6	0.00	0.0							
46R	1 Feb	1640	431.9	441.5	9.6	0.00	0.0							
47R	1 Feb	1925	441.5	451.1	9.6	0.00	0.0							
48R	1 Feb	2020	451.1	460.8	9.7	1.22	12.6							
								1	1.22	1.50	451.10	452.60	PAL	
								Totals:	1.22	1.50				
49R	1 Feb	2100	460.8	470.4	9.6	0.00	0.0							
50R	1 Feb	2150	470.4	480.0	9.6	0.60	6.3							
								1	0.60	0.66	470.40	471.06	PAL	
								Totals:	0.60	0.66				
51R	1 Feb	2355	480.0	489.7	9.7	4.13	42.6							
								1	0.00	1.48	480.00	481.48		
								2	1.10	1.48	481.48	482.96	EHWR	
								3	1.53	1.41	482.96	484.37		
								4	1.50	0.58	484.37	484.95	PAL	
								Totals:	4.13	4.95				
52R	2 Feb	0220	489.7	499.3	9.6	6.74	70.2							
								1	0.63	1.47	489.70	491.17		
								2	1.47	1.50	491.17	492.67		
								3	1.50	1.47	492.67	494.14		
								4	1.45	1.50	494.14	495.64		
								5	1.51	1.50	495.64	497.14		
								6	0.18	0.48	497.14	497.62	PAL	
								Totals:	6.74	7.92				
53R	2 Feb	0535	499.3	508.9	9.6	4.69	48.9							
								1	1.50	1.50	499.30	500.80		
								2	1.50	1.50	500.80	502.30		
								3	1.48	1.40	502.30	503.70	EHWR	
								4	0.21	1.24	503.70	504.94	PAL	
								Totals:	4.69	5.64				
54R	2 Feb	0645	508.9	518.5	9.6	1.20	12.5							
								1	1.20	1.46	508.90	510.36	PAL	
								Totals:	1.20	1.46				
55R	2 Feb	0810	518.5	528.1	9.6	1.16	12.1							
								1	1.16	1.43	518.50	519.93	PAL	
								Totals:	1.16	1.43				
56R	2 Feb	1000	528.1	537.7	9.6	1.37	14.3							
								1	1.37	1.18	528.10	529.28	EHWR	
								2	0.00	0.49	529.28	529.77	PAL	
								Totals:	1.37	1.67				
57R	2 Feb	1235	537.7	547.3	9.6	2.85	29.7							
								1	1.42	1.50	537.70	539.20		
								2	1.43	1.43	539.20	540.63	EHWR	
								3	0.00	0.59	540.63	541.22	PAL	
								Totals:	2.85	3.52				
58R	2 Feb	1355	547.3	556.9	9.6	1.07	11.1							
								1	1.07	1.32	547.30	548.62	PAL	
								Totals:	1.07	1.32				
59R	2 Feb	1455	556.9	566.6	9.7	0.95	9.8							
								1	0.95	1.15	556.90	558.05	PAL	
								Totals:	0.95	1.15				
60R	2 Feb	1555	566.6	576.2	9.6	0.69	7.2							
								1	0.69	0.80	566.60	567.40	PAL	
								Totals:	0.69	0.80				
61R	2 Feb	1710	576.2	585.8	9.6	1.63	17.0							
								1	1.45	1.47	576.20	577.67		
								2	0.18	0.48	577.67	578.15	PAL	
								Totals:	1.63	1.95				
62R	2 Feb	1830	585.8	595.5	9.7	0.45	4.6							
								1	0.45	0.47	585.80	586.27	PAL	
								Totals:	0.45	0.47				
63R	2 Feb	1950	595.5	605.1	9.6	2.12	22.1							
								1	0.62	1.49	595.50	596.99		
								2	1.50	1.34	596.99	598.33	PAL	
								Totals:	2.12	2.83				

Table T2 (continued).

Core	Date (2001)	Time (local)	Core depth (mbsf) Top	Core depth (mbsf) Bottom	Length (m) Cored	Length (m) Recovered	Recovery (%)	Section	Length (m) Liner	Length (m) Curated	Section depth (mbsf) Top	Section depth (mbsf) Bottom	Catwalk samples	Comment
64R	2 Feb	2125	605.1	614.7	9.6	3.77	39.3							
								1	0.85	1.50	605.10	606.60		
								2	1.50	1.45	606.60	608.05		
								3	1.42	1.50	608.05	609.55	PAL	
								Totals:	3.77	4.45				
65R	2 Feb	2330	614.7	624.4	9.7	5.15	53.1							
								1	0.45	1.49	614.70	616.19	EHWR	
								2	1.50	1.48	616.19	617.67		
								3	1.50	1.48	617.67	619.15		
								4	1.50	1.50	619.15	620.65		
								5	0.20	0.33	620.65	620.98	PAL	
								Totals:	5.15	6.28				
66R	3 Feb	0050	624.4	633.7	9.3	4.65	50.0							
								1	0.52	1.35	624.40	625.75	EHWR	
								2	1.28	1.48	625.75	627.23		
								3	1.43	1.49	627.23	628.72		
								4	1.42	1.08	628.72	629.80	PAL	
								Totals:	4.65	5.40				
67R	3 Feb	0200	633.7	643.4	9.7	1.92	19.8							
								1	0.54	1.38	633.70	635.08		
								2	1.38	0.93	635.08	636.01	PAL	
								Totals:	1.92	2.31				
68R	3 Feb	0300	643.4	653.0	9.6	0.04	0.4							
								1	0.04	0.05	643.40	643.45	PAL	
								Totals:	0.04	0.05				
69R	3 Feb	0350	653.0	662.6	9.6	0.00	0.0							
70R	3 Feb	0515	662.6	672.2	9.6	4.62	48.1							
								1	1.50	1.50	662.60	664.10		
								2	1.50	1.50	664.10	665.60		
								3	1.46	1.46	665.60	667.06		
								CC (w/ CC)	0.16	0.16	667.06	667.22	PAL	
								Totals:	4.62	4.62				
				Totals:	672.2	86.37	12.8							
194-1196B-														
1R	4 Feb	1635	0.0	9.7	9.7	2.72	28.0							
								1	1.26	1.45	0.00	1.45		
								2	1.46	1.47	1.45	2.92		
								3	0.00	0.40	2.92	3.32	PAL	
								Totals:	2.72	3.32				
2R	4 Feb	1855	9.7	19.4	9.7	0.29	3.0							
								1	0.29	0.39	9.70	10.09	PAL	
								Totals:	0.29	0.39				
3R	4 Feb	2030	19.4	28.8	9.4	0.03	0.3							
								1	0.03	0.03	19.40	19.43	PAL	All to PAL
								Totals:	0.03	0.03				
4R	4 Feb	2155	28.8	38.2	9.4	0.96	10.2							
								1	0.96	1.22	28.80	30.02	PAL	
								Totals:	0.96	1.22				
5R	4 Feb	2350	38.2	47.2	9.0	0.89	9.9							
								1	0.89	1.02	38.20	39.22	PAL	
								Totals:	0.89	1.02				
6R	5 Feb	130	47.2	56.8	9.6	0.90	9.4							
								1	0.90	1.10	47.20	48.30	PAL	
								Totals:	0.90	1.10				
7R	5 Feb	1510	56.8	66.2	9.4	2.25	23.9							
								1	0.75	1.50	56.80	58.30		
								2	1.50	1.12	58.30	59.42	PAL	
								Totals:	2.25	2.62				
8R	5 Feb	1630	66.2	75.8	9.6	0.24	2.5							
								1	0.24	0.27	66.20	66.47	PAL	
								Totals:	0.24	0.27				
9R	5 Feb	1730	75.8	84.8	9.0	1.85	20.6							
								1	0.35	1.50	75.80	77.30		
								2	1.50	0.80	77.30	78.10	PAL	
								Totals:	1.85	2.30				
10R	5 Feb	2010	84.8	94.5	9.7	0.93	9.6							
								1	0.93	1.13	84.80	85.93	PAL	
								Totals:	0.93	1.13				

Table T2 (continued).

Core	Date (2001)	Time (local)	Core depth (mbsf) Top	Core depth (mbsf) Bottom	Length (m) Cored	Length (m) Recovered	Recovery (%)	Section	Length (m) Liner	Length (m) Curated	Section depth (mbsf) Top	Section depth (mbsf) Bottom	Catwalk samples	Comment
11R	5 Feb	2145	94.5	104.1	9.6	0.17	1.8							
								1	0.17	0.19	94.50	94.69	PAL	
								Totals:	0.17	0.19				
12R	5 Feb	2245	104.1	110.0	5.9	0.22	3.7							
								1	0.22	0.27	104.10	104.37	PAL	
								Totals:	0.22	0.27				
13Z	12 Feb	45	110.0	114.7	4.7	1.43	30.4							
								1	1.43	1.39	110.00	111.39	EHWR	
								2	0.00	0.46	111.39	111.85	PAL	
								Totals:	1.43	1.85				
14Z	12 Feb	140	114.7	116.9	2.2	1.74	79.1							
								1	1.50	1.45	114.70	116.15		
								2	0.24	0.69	116.15	116.84	PAL	
								Totals:	1.74	2.14				
15Z	12 Feb	230	116.9	118.2	1.3	1.08	83.1							
								1	1.08	1.23	116.90	118.13	PAL, PAL	
								Totals:	1.08	1.23				
16Z	12 Feb	345	118.2	122.9	4.7	1.16	24.7							
								1	1.16	1.38	118.20	119.58	PAL	
								Totals:	1.16	1.38				
17Z	12 Feb	430	122.9	123.4	0.5	0.57	114.0							
								1	0.57	0.60	122.90	123.50	PAL	
								Totals:	0.57	0.60				
18Z	12 Feb	540	123.4	128.1	4.7	1.52	32.3							
								1	1.52	1.46	123.40	124.86		
								2	0.00	0.51	124.86	125.37	PAL	
								Totals:	1.52	1.97				
19Z	12 Feb	615	128.1	130.3	2.2	0.00	0.0							
20Z	12 Feb	655	130.3	135.0	4.7	0.47	10.0							
								1	0.47	0.64	130.30	130.94	PAL	
								Totals:	0.47	0.64				
21Z	12 Feb	740	135.0	139.7	4.7	0.00	0.0							
22Z	12 Feb	820	139.7	142.0	2.3	0.51	22.2							
								1	0.51	0.57	139.70	140.27	PAL	
								Totals:	0.51	0.57				
23Z	12 Feb	855	142.0	145.0	3.0	0.00	0.0							
24Z	12 Feb	945	145.0	149.7	4.7	0.06	1.3							
								1	0.06	0.10	145.00	145.10	PAL	
								Totals:	0.06	0.10				
25Z	12 Feb	1040	149.7	154.4	4.7	0.50	10.6							
								1	0.50	0.54	149.70	150.24	PAL	
								Totals:	0.50	0.54				
26Z	12 Feb	1120	154.4	159.1	4.7	0.00	0.0							
27Z	12 Feb	1215	159.1	163.8	4.7	0.36	7.7							
								1	0.36	0.49	159.10	159.59	PAL	
								Totals:	0.36	0.49				
28Z	12 Feb	1320	163.8	168.5	4.7	0.37	7.9							
								1	0.37	0.41	163.80	164.21	PAL	
								Totals:	0.37	0.41				
29Z	12 Feb	1420	168.5	172.5	4.0	1.86	46.5							
								1	0.98	1.43	168.50	169.93	EHWR	
								2	0.88	0.99	169.93	170.92	PAL	
								Totals:	1.86	2.42				
30Z	12 Feb	1520	172.5	177.2	4.7	1.49	31.7							
								1	1.49	1.44	172.50	173.94		
								2	0.00	0.55	173.94	174.49	PAL	
								Totals:	1.49	1.99				
31Z	12 Feb	1625	177.2	180.2	3.0	0.96	32.0							
								1	0.96	1.33	177.20	178.53	PAL, EHWR	
								Totals:	0.96	1.33				
32Z	12 Feb	1715	180.2	184.9	4.7	0.23	4.9							
								1	0.23	0.29	180.20	180.49	PAL	
								Totals:	0.23	0.29				
33Z	12 Feb	1820	184.9	189.6	4.7	0.72	15.3							
								1	0.72	0.81	184.90	185.71	PAL	
								Totals:	0.72	0.81				
34Z	12 Feb	1920	189.6	194.3	4.7	0.00	0.0							
35Z	12 Feb	2025	194.3	199.0	4.7	0.06	1.3							
								1	0.06	0.06	194.30	194.36	PAL	
								Totals:	0.06	0.06				

Table T2 (continued).

Core	Date (2001)	Time (local)	Core depth (mbsf) Top	Core depth (mbsf) Bottom	Length (m) Cored	Length (m) Recovered	Recovery (%)	Section	Length (m) Liner	Length (m) Curated	Section depth (mbsf) Top	Section depth (mbsf) Bottom	Catwalk samples	Comment
36Z	12 Feb	2125	199.0	203.7	4.7	0.11	2.3							
								1	0.11	0.11	199.00	199.11	PAL	
								Totals:	0.11	0.11				
37Z	12 Feb	2240	203.7	208.4	4.7	0.00	0.0							
38Z	12 Feb	2325	208.4	213.1	4.7	0.00	0.0							
39Z	13 Feb	40	213.1	217.8	4.7	0.38	8.1							
								1	0.38	0.53	213.10	213.63	PAL	
								Totals:	0.38	0.53				
40Z	13 Feb	130	217.8	218.8	1.0	0.28	28.0							
								1	0.28	0.24	217.80	218.04	PAL	
								Totals:	0.28	0.24				
41Z	13 Feb	230	218.8	223.5	4.7	0.24	5.1							
								1	0.24	0.21	218.80	219.01	PAL	
								Totals:	0.24	0.21				
42Z	13 Feb	315	223.5	228.2	4.7	0.27	5.7							
								1	0.27	0.33	223.50	223.83	PAL	
								Totals:	0.27	0.33				
43Z	13 Feb	405	228.2	232.9	4.7	0.00	0.0							
44Z	13 Feb	455	232.9	234.3	1.4	0.12	8.6							
								1	0.12	0.12	232.90	233.02	PAL	
								Totals:	0.12	0.12				
45Z	13 Feb	555	234.3	237.8	3.5	0.30	8.6							
								1	0.30	0.38	234.30	234.68	PAL	
								Totals:	0.30	0.38				
46Z	13 Feb	640	237.8	242.5	4.7	0.15	3.2							
								1	0.15	0.24	237.80	238.04	PAL	
								Totals:	0.15	0.24				
47Z	13 Feb	720	242.5	247.2	4.7	0.23	4.9							
								1	0.23	0.32	242.50	242.82	PAL	
								Totals:	0.23	0.32				
48Z	13 Feb	810	247.2	251.2	4.0	0.10	2.5							
								1	0.10	0.30	247.20	247.50	PAL	
								Totals:	0.10	0.30				
49Z	13 Feb	855	251.2	255.9	4.7	0.30	6.4							
								1	0.30	0.37	251.20	251.57	PAL	
								Totals:	0.30	0.37				
50Z	13 Feb	950	255.9	260.6	4.7	0.30	6.4							
								1	0.30	0.45	255.90	256.35	PAL	
								Totals:	0.30	0.45				
51Z	13 Feb	1045	260.6	265.3	4.7	0.05	1.1							
								1	0.05	0.05	260.60	260.65	PAL	
								Totals:	0.05	0.05				
				Totals:	265.3	29.37	11.10							
194-1199A-														
1R	18 Feb	1535	0.0	9.5	9.5	3.88	40.8							
								1	0.93	1.46	0.00	1.46		
								2	1.45	1.42	1.46	2.88		
								3	1.50	1.43	2.88	4.31		
								4	0.00	0.23	4.31	4.54	PAL	
								Totals:	3.88	4.54				
2R	18 Feb	1830	9.5	17.4	7.9	5.78	73.2							
								1	0.00	1.37	9.50	10.87		
								2	1.48	1.47	10.87	12.34	EHWR	
								3	1.47	1.47	12.34	13.81		
								4	1.39	1.50	13.81	15.31		
								5	1.44	0.44	15.31	15.75	PAL	
								Totals:	5.78	6.25				
3R	18 Feb	2235	17.4	18.9	1.5	1.16	77.3							
								1	1.16	1.34	17.40	18.74	PAL	
								Totals:	1.16	1.34				
4R	19 Feb	0300	18.9	26.8	7.9	7.79	98.6							
								1	0.29	1.44	18.90	20.34		
								2	1.50	1.35	20.34	21.69		
								3	1.50	1.44	21.69	23.13		
								4	1.50	1.43	23.13	24.56		
								5	1.50	1.42	24.56	25.98		
								6	1.50	1.48	25.98	27.46		
								7	0.00	0.13	27.46	27.59	PAL	
								Totals:	7.79	8.69				

Table T2 (continued).

Core	Date (2001)	Time (local)	Core depth (mbsf) Top	Core depth (mbsf) Bottom	Length (m) Cored	Length (m) Recovered	Recovery (%)	Section	Length (m) Liner	Length (m) Curated	Section depth (mbsf) Top	Section depth (mbsf) Bottom	Catwalk samples	Comment
5R	19 Feb	0610	26.8	35.7	8.9	7.20	80.9							
								1	0.15	1.48	26.80	28.28		
								2	1.44	1.46	28.28	29.74	EHWR	
								3	1.36	1.49	29.74	31.23		
								4	1.32	1.38	31.23	32.61		
								5	1.48	1.49	32.61	34.10		
								6	1.45	0.82	34.10	34.92	PAL	
								Totals:	7.20	8.12				
6R	19 Feb	0955	35.7	45.1	9.4	4.60	48.9							
								1	1.43	1.50	35.70	37.20		
								2	1.47	1.50	37.20	38.70		
								3	1.48	1.48	38.70	40.18		
								4	0.22	0.56	40.18	40.74	PAL	
								Totals:	4.60	5.04				
7R	19 Feb	1310	45.1	54.0	8.9	3.82	42.9							
								1	0.90	1.41	45.10	46.51	EHWR	
								2	1.45	1.47	46.51	47.98		
								3	1.47	1.45	47.98	49.43	PAL	
								Totals:	3.82	4.33				
8R	19 Feb	1620	54.0	63.6	9.6	3.20	33.3							
								1	0.20	1.40	54.00	55.40		
								2	1.50	1.45	55.40	56.85		
								3	1.50	0.84	56.85	57.69	PAL	
								Totals:	3.20	3.69				
9R	19 Feb	1825	63.6	73.2	9.6	7.85	81.8							
								1	0.35	1.45	63.60	65.05		
								2	1.50	1.45	65.05	66.50		
								3	1.50	1.42	66.50	67.92		
								4	1.50	1.40	67.92	69.32		
								5	1.50	1.42	69.32	70.74		
								6	1.50	1.48	70.74	72.22		
								7	0.00	0.48	72.22	72.70	PAL, EHWR	
								Totals:	7.85	9.10				
10R	19 Feb	1955	73.2	82.8	9.6	6.33	65.9							
								1	0.43	1.50	73.20	74.70		
								2	1.42	1.47	74.70	76.17		
								3	1.48	1.44	76.17	77.61		
								4	1.50	1.45	77.61	79.06		
								5	1.50	1.30	79.06	80.36	PAL	
								Totals:	6.33	7.16				
11R	19 Feb	2210	82.8	92.5	9.7	3.60	37.1							
								1	0.92	1.50	82.80	84.30		
								2	1.50	1.49	84.30	85.79		
								3	1.18	0.96	85.79	86.75	PAL	
								Totals:	3.60	3.95				
12R	20 Feb	0020	92.5	102.1	9.6	8.93	93.0							
								1	1.48	1.48	92.50	93.98		
								2	1.48	1.40	93.98	95.38		
								3	1.43	1.42	95.38	96.80		
								4	1.43	1.43	96.80	98.23		
								5	1.50	1.43	98.23	99.66		
								6	1.48	1.50	99.66	101.16		
								7	0.13	1.43	101.16	102.59	PAL	
								Totals:	8.93	10.09				
13R	20 Feb	0220	102.1	111.8	9.7	6.42	66.2							
								1	1.18	1.44	102.10	103.54		
								2	1.31	1.23	103.54	104.77		
								3	1.39	1.44	104.77	106.21		
								4	1.17	1.46	106.21	107.67	EHWR	
								5	1.37	1.50	107.67	109.17	PAL	
								Totals:	6.42	7.07				
14R	20 Feb	0330	111.8	121.4	9.6	2.78	29.0							
								1	1.37	1.46	111.80	113.26		
								2	1.41	1.49	113.26	114.75		
								3	0.00	0.24	114.75	114.99	PAL	
								Totals:	2.78	3.19				
15R	20 Feb	0415	121.4	131.0	9.6	0.73	7.6							
								1	0.73	0.76	121.40	122.16	PAL	
								Totals:	0.73	0.76				

Table T2 (continued).

Core	Date (2001)	Time (local)	Core depth (mbsf) Top	Core depth (mbsf) Bottom	Length (m) Cored	Length (m) Recovered	Recovery (%)	Section	Length (m) Liner	Length (m) Curated	Section depth (mbsf) Top	Section depth (mbsf) Bottom	Catwalk samples	Comment
16R	20 Feb	0615	131.0	140.6	9.6	6.01	62.6							
								1	0.23	1.46	131.00	132.46		
								2	1.48	1.47	132.46	133.93		
								3	1.48	1.46	133.93	135.39		
								4	1.30	1.45	135.39	136.84	EHWR	
								5	1.52	1.15	136.84	137.99	PAL	
								Totals:	6.01	6.99				
17R	20 Feb	0810	140.6	150.2	9.6	0.68	7.1							
								1	0.68	0.71	140.60	141.31	PAL	
								Totals:	0.68	0.71				
18R	20 Feb	0920	150.2	159.8	9.6	2.84	29.6							
								1	0.05	1.48	150.20	151.68	EHWR	
								2	1.41	1.49	151.68	153.17		
								3	1.38	0.35	153.17	153.52	PAL	
								Totals:	2.84	3.32				
19R	20 Feb	1005	159.8	169.4	9.6	0.07	0.7							
								1	0.07	0.11	159.80	159.91	PAL	
								Totals:	0.07	0.11				
20R	20 Feb	1100	169.4	179.0	9.6	0.82	8.5							
								1	0.82	0.95	169.40	170.35	PAL	
								Totals:	0.82	0.95				
21R	20 Feb	1150	179.0	188.6	9.6	0.17	1.8							
								1	0.17	0.20	179.00	179.20	PAL	
								Totals:	0.17	0.20				
22R	20 Feb	1230	188.6	198.2	9.6	0.01	0.1							
								1	0.01	0.01	188.60	188.61	PAL	
								Totals:	0.01	0.01				
23R	20 Feb	1535	198.2	207.8	9.6	0.04	0.4							
								1	0.04	0.04	198.20	198.24	PAL	All to PAL
								Totals:	0.04	0.04				
24R	20 Feb	1625	207.8	217.4	9.6	0.04	0.4							
								1	0.04	0.04	207.80	207.84	PAL	All to PAL
								Totals:	0.04	0.04				
25R	20 Feb	1710	217.4	227.0	9.6	0.02	0.2							
								1	0.02	0.02	217.40	217.42	PAL	
								Totals:	0.02	0.02				
26R	20 Feb	1755	227.0	236.7	9.7	0.00	0.0							
27R	20 Feb	1850	236.7	246.3	9.6	0.02	0.2							
								1	0.02	0.02	236.70	236.72	PAL	All to PAL
								Totals:	0.02	0.02				
28R	20 Feb	1940	246.3	255.9	9.6	0.00	0.0							
29R	20 Feb	2025	255.9	265.5	9.6	0.04	0.4							
								1	0.04	0.04	255.90	255.94	PAL	All to PAL
								Totals:	0.04	0.04				
30R	20 Feb	2125	265.5	275.2	9.7	0.36	3.7							
								1	0.36	0.41	265.50	265.91	PAL	
								Totals:	0.36	0.41				
31R	20 Feb	2215	275.2	284.8	9.6	0.30	3.1							
								1	0.30	0.32	275.20	275.52	PAL	
								Totals:	0.30	0.32				
32R	20 Feb	2255	284.8	294.4	9.6	0.18	1.9							
								1	0.18	0.20	284.80	285.00	PAL, PAL	
								Totals:	0.18	0.20				
33R	20 Feb	2340	294.4	304.0	9.6	0.25	2.6							
								1	0.25	0.32	294.40	294.72	PAL	
								Totals:	0.25	0.32				
34R	21 Feb	0020	304.0	313.7	9.7	0.32	3.3							
								1	0.32	0.39	304.00	304.39	PAL	
								Totals:	0.32	0.39				
35R	21 Feb	0100	313.7	323.3	9.6	1.07	11.1							
								1	1.07	1.32	313.7	315.02	PAL	
								Totals:	1.07	1.32				
36R	21 Feb	0145	323.3	332.9	9.6	0.03	0.3							
								1	0.03	0.03	323.30	323.33	PAL	
								Totals:	0.03	0.03				
37R	21 Feb	0225	332.9	342.6	9.7	0.23	2.4							
								1	0.23	0.28	332.90	333.18	PAL	
								Totals:	0.23	0.28				

Table T2 (continued).

Core	Date (2001)	Time (local)	Core depth (mbsf) Top	Core depth (mbsf) Bottom	Length (m) Cored	Length (m) Recovered	Recovery (%)	Section	Length (m) Liner	Length (m) Curated	Section depth (mbsf) Top	Section depth (mbsf) Bottom	Catwalk samples	Comment
38R	21 Feb	0310	342.6	352.2	9.6	0.20	2.1							
								1	0.20	0.24	342.60	342.84	PAL	
								Totals:	0.20	0.24				
39R	21 Feb	0400	352.2	361.8	9.6	1.03	10.7							
								1	1.03	1.26	352.20	353.46	PAL	
								Totals:	1.03	1.26				
40R	21 Feb	0445	361.8	371.4	9.6	0.86	9.0							
								1	0.86	0.99	361.80	362.79	PAL	
								Totals:	0.86	0.99				
41R	21 Feb	0530	371.4	381.1	9.7	1.45	14.9							
								1	1.45	1.46	371.40	372.86		
								2	0.00	0.30	372.86	373.16	PAL	
								Totals:	1.45	1.76				
42R	21 Feb	0615	381.1	390.7	9.6	0.76	7.9							
								1	0.76	0.89	381.10	381.99	PAL	
								Totals:	0.76	0.89				
43R	21 Feb	0655	390.7	400.3	9.6	0.09	0.9							
								1	0.09	0.14	390.70	390.84	PAL	
								Totals:	0.09	0.14				
44R	21 Feb	0740	400.3	409.9	9.6	0.07	0.7							
								1	0.07	0.13	400.30	400.43	PAL	
								Totals:	0.07	0.13				
45R	21 Feb	0840	409.9	419.5	9.6	0.13	1.4							
								1	0.13	0.25	409.90	410.15	PAL	
								Totals:	0.13	0.25				
				Totals:	419.5	92.16	22.0							

Notes: CC = core catcher (number in parentheses indicates which section the core catcher is stored with). Catwalk samples: PAL = paleontology sample, EHWR = sample request code.

Table T3. Lithologic units and subunits, Site 1196.

		Hole 1196A				Hole 1196B				
		Core		Depth (mbsf)		Core		Depth (mbsf)		
Unit	Subunit	Top	Base	Top	Base	Top	Base	Top	Base	Description
I	IA	1R-1, 0	13R-2, 100	000.0	117.2	1R-1, 0	17Z-1, 0	000.0	122.9	Dolomitic floatstone/rudstone. Grainstone matrix. Distinctive constituents are centimeter-sized rhodoliths. Dolomitization is not pervasive.
	IB	13R-2, 100	14R-2, 20	117.2	125.9	17Z-1, 0	20Z-1, 20	122.9	130.5	Dolomitic floatstone. Constituents include larger benthic foraminifers (seen as molds) and branching red algal debris.
	IC	14R-2, 20	18R-1, 0	125.9	162.8	20Z-1, 20	24Z-1, 0	130.5	145.0	Skeletal rudstone/boundstone with colonial corals alternating with dolomitic floatstone with molds of benthic foraminifers.
	ID	18R-1, 0	20R-1, 27	162.8	182.2	24Z-1, 0	33Z-1, 0	145.0	184.9	Dolomitic floatstone. Predominant constituents include larger benthic foraminifers, which are commonly dissolved, and branching red algal fragments. Rare coral present.
II	IIA	20R-1, 27	35R-1, 40	182.2	335.9	33Z-1, 0	?	184.9		Skeletal floatstone. Predominant constituents are porcellaneous benthic foraminifers and centimeter-sized mollusk fragments. Thin, well-sorted grainstone intervals occur at 232 and 317 mbsf. Nannofossil age: 13.6–18.2 Ma at 218 and at 316 mbsf. Foraminifer age: 13.3–15.2 Ma throughout the unit.
	IIB	36R-1, 0	37R-1, 30	335.9	345.8					Skeletal rudstone/boundstone. Reefal facies containing hermatypic corals, red algae, and mollusk fragments.
III	IIIA	37R-1, 30	38R-1, 20	345.8	355.3					Dolomitic rudstone. Reefal facies showing ghosts of rhodoids, corals, and mollusk fragments.
		39R	42R	355.3	412.7					Insignificant recovery.
	IIIB	44R-1, 0	50R-1, 0	412.7	470.4					Sucrosic dolostone. Rare relicts of centimeter-sized rhodoids are preserved. Coarsely crystalline.
	IIIC	50R-1, 0	57R-1, 0	470.4	537.7					Variegated dolostone. Ghosts of rhodoliths visible locally. Moldic porosity after benthic foraminifers. Contains several brownish layers interpreted as exposure surfaces. Evidence for fracturing. Coarsely crystalline.
	IIID	57R-1, 0	65R-2, 85	537.7	617.1					Dolostone with molds. Molds after benthic foraminifers are typical. Rare rhodoliths, red algae, and mollusk fragments. Two thin intervals of dolomitic skeletal grainstone with abundant benthic foraminifers occur in Core 63R.
IV		65R-2, 85	70R-1, 0	617.1	662.6					Mixed dolomitic rocks. Various facies containing noncarbonate grains (quartz, glauconite) and forming meter-scale sequences separated by exposure surfaces.
V		70R-1, 0	?	662.6	?					Siliciclastic substrate. Dark sandstone, claystone, and phosphatic sands of latest Oligocene age (24.2–24.6 Ma).

Notes: Hole 1196B end of core at 265.3 mbsf. ? = not defined.

Table T4. Lithologic units and subunits, Site 1199, and tentative correlation with units defined at Site 1196.

		Hole 1196A				Hole 1196B				Hole 1199A				
		Core		Depth (mbsf)		Core		Depth (mbsf)		Core		Depth (mbsf)		
Unit	Subunit	Top	Base	Top	Base	Top	Base	Top	Base	Top	Base	Top	Base	Description
I	IA	1R-1, 0	13R-2, 100	0.0	117.2	1R-1, 0	17Z-1, 0	0.0	122.9	1R-1, 0	13R-3, 0	0.0	106.2	Dolomitic floatstone/rudstone. Grainstone matrix. Distinctive constituents are centimeter-sized rhodoliths. Dolomitization is not pervasive.
	IB	13R-2, 100	14R-2, 20	117.2	125.9	17Z-1, 0	20Z-1, 20	122.9	130.5	13R-3, 0	14R-1, 87	106.2	112.7	Dolomitic floatstone. Constituents include larger benthic foraminifers (seen as molds) and branching red algal debris. Natural gamma ray peak at base.
	IC	14R-2, 20	18R-1, 0	125.9	162.8	20Z-1, 20	24Z-1, 0	130.5	145.0	14R-1, 87	15R-1, 49	112.7	121.9	Skeletal rudstone/boundstone with colonial corals. At Site 1199, this facies has been dolomitized and has likely been subaerially exposed.
	ID	18R-1, 0	20R-1, 27	162.8	182.2	24Z-1, 0	33Z-1, 0	145.0	184.9	15R-1, 49	19R-1, 0	121.9	159.8	Dolomitic floatstone. Predominant constituents include larger benthic foraminifers, which are commonly dissolved, and branching red algal fragments. Rare coral is present.
II	IIA	20R-1, 27	35R-1, 40	182.2	335.9	33Z-1, 0	?	184.9		19R-1, 0	32R-1, 6	159.8	285.0	Skeletal floatstone/grainstone. Predominant constituents are porcellaneous benthic foraminifers and centimeter-sized mollusk fragments. Nannofossil age is 13.6–18.2 Ma at 218 mbsf and at 316 mbsf at Site 1196. Foraminifer age is 13.3–15.2 Ma throughout the unit. Friable at Site 1196, harder and slightly dolomitized at Site 1199.
	IIB	36R-1, 0	37R-1, 30	335.9	345.8					32R-1, 10	45R-1, 10	285.0	410.0	Skeletal grainstone/floatstone. Well sorted. Contains benthic foraminifers, echinoids, red algae, and possibly Halimeda. Floatstone intervals include centimeter-sized rhodoliths. Only poorly recovered at Site 1196 where the upper part shows a partly dolomitized reefal facies.
III	IIIA	37R-1, 30	38R-1, 20	345.8	412.7					45R-1, 6	?	409.9	?	Sucrosic dolostone. Rare relicts of centimeter-sized rhodoliths are preserved. Coarsely crystalline.

Notes: Hole 1196A end of core at 672.2 mbsf, Hole 1196B end of core at 265.3 mbsf, Hole 1199A end of core at 419.5 mbsf. ? = not defined.

Table T5. Summary of biostratigraphic and paleoenvironmental interpretations, Site 1196. (**See table notes.** Continued on next two pages.)

Core, section, interval (cm)	Depth (mbsf)	Age (Ma)	Foraminferal assemblages			Comments	Paleowater depth (m)				Depositional setting	Lithologic unit
			RLBF	MLBF	Sm mil		<10	<30	<60	<100		
194-												
1196A-1R-1, 1–4	0.01	3.2–0	A		C	PF date of top; robust *Amphistegina/Operculina*	X				Shallow platform	IA
1196A-1R-1, 112–114	1.12		A			Rhodoliths/coral in *Amphistegina,* red algal and bryozoan fragments		X			Open platform	
1196A-2R-1, 78–80	10.38		A			Rhodoliths/coral in *Amphistegina* and red algal fragments		X			Open platform	
1196A-3R-1, 34–36	19.24		A			Rhodoliths/coral in *Amphistegina* and red algal fragments		X			Open platform	
1196A-4R-1, 102–105	29.52		A			Rhodoliths/coral in *Amphistegina* and red algal fragments		X			Open platform	
1196A-5R-2, 84–89	40.54		A	R		Rhodoliths/coral in *Amphistegina* and red algal fragments		X			Open platform	
1196A-6R-1, 140–142	48.90		A			Rhodoliths/coral in *Amphistegina* and red algal fragments		X			Open platform	
1196A-7R-2, 105–108	59.36		A			Rhodoliths/coral in *Amphistegina* and red algal fragments		X			Open platform	
1196A-8R-1, 24–27	66.74		A			Rhodoliths/coral in *Amphistegina* and red algal fragments		X			Open platform	
1196A-9R-2, 73–75	78.25		A			Rhodoliths/coral in *Amphistegina* and red algal fragments, LBF molds		X			Open platform	
1196A-10R-1, 132–134	87.12		c			Rhodoliths/coral in *Amphistegina* and red algal fragments, LBF molds		?			Open platform	
1196A-11R-1, 88–90	96.28		c			Rhodoliths with abundant red algal fragments					Open platform	
1196A-12R-1, 130–132	106.30		c			Rhodoliths with abundant red algal fragments, flat LBF molds				?	Open platform	
1196A-13R-2, 148–150	117.68		c			Abundant red algal fragments, flat LBF molds				?	Uncertain	IB
1196A-14R-2, 25–27	125.95		c			Abundant red algal fragments, mixed LBF molds		?	?		Uncertain	
1196A-15R-1, 36–38	134.26		a			Coral skeletal boundstone with flat LBF molds		X			Reef?	IC
1196A-16R-1, 74–76	144.24		a			Abundant red algal fragments, flat LBF molds		X			Reef?	
1196A-17R-1, 26–28	153.36		A			Enigmatic fossils, possibly large *Miogypsina;* common *Lepidocyclina*		X			Reef?	
1196A-18R-3, 119–121	166.85		a			Rhodoliths with abundant red algal fragments, intermediate LBF molds		?	?		Uncertain	ID
1196A-19R-3, 60–62	175.80		a			Abundant red algal fragments, exposure surfaces		?	?		Uncertain	
1196A-20R-1, 111–113	183.01	15.2–13.3		A	A	Fine grainstone, miliolid, *Flosculinella* abundant, soritids and organic common	X				Shallow platform	IIA
1196A-21R-1, 104–107	192.54	15.2–13.3		A	A	Fine grainstone, miliolid, *Flosculinella* abundant, soritids and organic common	X				Shallow platform	
1196A-22R-1, 44–46	201.54	15.2–13.3				Fine grainstone, difficult to tell fine components; coral, bivalves present					Shallow platform	
1196A-23R-1, 0–5	210.70	15.2–13.3	C	A	A	Fine grainstone, miliolid, *Flosculinella* abundant, soritids and organic common	X				Shallow platform	
1196A-24R-1, 25–28	220.55	15.2–13.3		A	A	Fine grainstone, miliolid, *Flosculinella* abundant, soritids and organic common	X				Shallow platform	
1196A-25R-1, 78–80	230.68	15.2–13.3		C	A	Fine grainstone, miliolid, soritid, gastropod and bivalve	X				Shallow platform	
1196A-26R-1, 24–26	239.84	15.2–13.3		A	A	Fine grainstone, miliolid, *Flosculinella* abundant, soritids and organic common	X				Shallow platform	
1196A-27R-1, 23–25	249.43	15.2–13.3		A	A	Fine grainstone, miliolid, *Flosculinella* abundant, soritids and organic common	X				Shallow platform	
1196A-28R-1, 11–13	258.91	15.2–13.3		A	A	Fine grainstone, miliolid, *Flosculinella* abundant, soritids and organic common	X				Shallow platform	
1196A-30R-1, 0–3	278.00	15.2–13.3		A	A	Fine grainstone, miliolid, *Flosculinella* abundant, soritids and organic common	X				Shallow platform	
1196A-31R-1, 20–22	287.80	15.2–13.3		A	A	Fine grainstone, miliolid, *Flosculinella* abundant, soritids and organic common	X				Shallow platform	
1196A-32R-1, 18–20	297.48	15.2–13.3		A	A	Fine grainstone, miliolid, *Flosculinella* abundant, soritids and organic common	X				Shallow platform	
1196A-33R-2, 72–74	309.08	15.2–13.3		A	A	Medium grainstone, miliolid, *Flosculinella* abundant, soritids and organic common	X				Shallow platform	
1196A-34R-1, 40–44	317.00	18.2–13.6				Nannofossil sample and date						
1196A-34R-1, 115–117	317.75	15.2–13.3		A	A	Medium grainstone, miliolid, *Flosculinella* abundant, soritids and organic common	X				Shallow platform	
1196A-35R-1, 38–40	326.68	15.2–13.3		A	A	Medium grainstone, miliolid, *Flosculinella* abundant, soritids and organic common	X				Shallow platform	
1196A-36R-1, 41–43	336.31				A	Strange diagenesis; rhodolith, coral, bryozoan, miliolids		X			Uncertain	IIB
1196A-37R-1, 70–72	346.20					Very sucrosic dolomite, little to be seen in hand specimen					Uncertain	
1196A-38R-1, 22–24	355.32					Dolomitized: red algae and bryozoans recognizable					Open platform	
1196A-39R-1, 0–2	364.70		A			Small rhodoliths in a robust *Lepidocyclina* grainstone		X			Open platform	
1196A-41R-1, 0–3	383.90		A			Small rhodoliths in a robust *Lepidocyclina* grainstone		X			Open platform	
1196A-42R-1, 14–16	393.64		A			Rhodolith/red algal with mixed LBF			X		Open platform	
1196A-43R-1, 0–5	403.10					Sucrosic; only red algal fabric still evident					Open platform	

Table T5 (continued).

Core, section, interval (cm)	Depth (mbsf)	Age (Ma)	Foraminferal assemblages			Comments	Paleowater depth (m)				Depositional setting	Lithologic unit
			RLBF	MLBF	Sm mil		<10	<30	<60	<100		
1196A-44R-1, 107–109	413.75		a			Sucrosic; flat *Lepidocyclina/Operculina*-type molds			?		Open platform	IIIA
1196A-48R-1, 147–150	452.57		a			Sucrosic; very large, very flat *Lepidocyclina/Operculina*-type molds				?	Open platform	
1196A-50R-1, 64–66	471.04		a			Sucrosic; very large, very flat *Lepidocyclina/Operculina*-type molds				?	Open platform	IIIB
1196A-51R-4, 56–58	484.93		a			Sucrosic; flat *Lepidocyclina/Operculina*-type molds			?		Open platform	
1196A-52R-6, 46–48	497.60			c	c	Sucrosic with fine grainstone fabric; red algal and alveolinid debris	?				Shallow platform	
1196A-53R-4, 122–124	504.92		a			Sucrosic with fine grainstone fabric; red algal and alveolinid debris	?				Shallow platform	
1196A-54R-1, 127–129	510.17			c	c	Sucrosic with fine grainstone fabric; red algal and soritid debris; few molds	?				Shallow platform	
1196A-55R-1, 141–143	519.91			c	c	Sucrosic with fine grainstone fabric; red algal and soritid debris; few molds	?				Shallow platform	
1196A-56R-2, 47–49	529.75					Sucrosic with fine grainstone fabric; red algal and soritid debris; few molds	?				Shallow platform	
1196A-57R-3, 30–32	540.93		a			Red algal crusts/fragments; coral and robust LBF molds		?			Open platform	IIIC
1196A-58R-1, 127–132	548.57		a			Red algal crusts/fragments; coral and robust LBF molds		?			Open platform	
1196A-59R-1, 112–115	558.02		a			Red algal crusts/fragments; coral and robust LBF molds		?			Open platform	
1196A-60R-1, 78–80	567.38		a			Red algal crusts/fragments; coral and robust LBF molds		?			Open platform	
1196A-61R-2, 46–48	578.13		a			Red algal crusts/fragments; coral and robust LBF molds		?			Open platform	
1196A-62R-1, 42–47	586.22		a			Red algal crusts/fragments; flat *Lepidocyclina/Operculina*-type molds			?		Open platform	
1196A-63R-2, 132–134	598.31		a			Red algal crusts/fragments; coral and flat *Lepidocyclina*-type molds			?		Open platform	
1196A-64R-3, 145–150	609.50		a			Red algal crusts/fragments; *Amphistegina*-type molds		?			Open platform	
1196A-65R-5, 30–33	620.95		a			Red algal crusts/fragments; *Amphistegina*-type molds		?			Open platform	
1196A-66R-4, 106–108	629.78		A			Bryozoan, red algae, *Operculina* grainstone, dispersed pyrite grains		?			Open platform	IV
1196A-67R-2, 90–93	635.98		A			Bryozoan, red algae, *Operculina* grainstone, dispersed pyrite grains		?			Open platform	
1196A-68R-1, 4–5	643.44					Dark sandstone					Deltaic?	V
1196A-70R–1	663.93	24.6–24.2				Muddy interval; nannofossils sample and date					Deltaic?	
1196A-70R-CC, 14–16	667.20					Dark sandstone					Deltaic?	
1196B-1R-3, 37–40	3.29		A			Rhodoliths/coral in red algal/*Amphistegina* grainstone	X				Shallow platform	
1196B-2R-1, 37–39	10.07		C			Rhodoliths in red algal/*Amphistegina* grainstone		X			Shallow platform	
1196B-3R-1, 0–3	19.40					Rhodolith/red algae, highly recrystallized					Shallow platform	
1196B-4R-1, 120–122	30.00		A			Rhodoliths/coral in a red algal/LBF grainstone		X			Shallow platform	
1196B-5R-1, 100–102	39.20		A	C		Rhodoliths/coral in a red algal/LBF grainstone		X			Shallow platform	
1196B-6R-1, 107–110	48.27		A			Rhodoliths/coral in *Amphistegina* and red algal fragments		X			Shallow platform	
1196B-7R-2, 110–112	59.40		C			Rhodolith/red algal, highly recrystallized; *Amphistegina*		X			Shallow platform	
1196B-8R-1, 25–27	66.45					Rhodolith/red algae/coral, highly recrystallized					Open platform?	
1196B-9R-2, 77–80	78.07					Rhodolith/red algae/coral, highly recrystallized					Open platform?	
1196B-10R-1, 110–113	85.90		c			Rhodolith/red algal highly recrystallized; intermediate LBF molds		X			Shallow platform	
1196B-11R-1, 16–19	94.66		a			Rhodoliths in a red algal matrix, intermediate LBF molds		X			Open platform?	
1196B-12R-1, 24–27	104.34		c			Rhodoliths/coral in a red algae, flat LBF molds			X		Open platform?	
1196B-13Z-2, 40–43	111.79		C			Large rhodoliths, branching reds, red algal grainstone, intermediate LBF		X			Open platform?	
1196B-14Z-2, 51–54	116.66		C			Rhodoliths in red algal grainstone; borings, intermediate LBF		X			Open platform?	
1196B-15Z-1, 120–123	118.10		C			Rhodoliths in red algal grainstone; borings, intermediate LBF		X			Open platform?	
1196B-16Z-1, 135–138	119.55		r			Branching red algae in red algal grainstone, small/intermediate LBF molds	?	X			Uncertain	
1196B-17Z-1, 54–60	123.44		r			Branching red algae in red algal grainstone, few LBF molds	?	X			Uncertain	IB
1196B-18Z-2, 48–51	125.34		c			Branching red algae in red algal grainstone, intermediate LBF molds	?	X			Uncertain	
1196B-20Z-1, 61–64	130.91		C			Very few identifiable fragments, a few LBF and echinoid fragments					Reef?	IC
1196B-22Z-1, 54–57	140.24		A			Coral and intermediate rhodoliths in red algal/*Amphistegina* grainstone		X			Reef?	
1196B-24Z-1, 7–10	145.07		a			Very vuggy, very abundant foraminifer molds, intermediate		X			Reef?	

Table T5 (continued).

Core, section, interval (cm)	Depth (mbsf)	Age (Ma)	Foraminferal assemblages			Comments	Paleowater depth (m)				Depositional setting	Lithologic unit
			RLBF	MLBF	Sm mil		<10	<30	<60	<100		
1196B-25Z-1, 52–54	150.22		A	R		Coral, large rhodoliths in robust LBF/red algal grainstone	X				Uncertain	ID
1196B-27Z-1, 46–49	159.56		a			Highly recrystallized, abundant flat LBF molds			X		Uncertain	
1196B-28Z-1, 39–41	164.19		a			Branching red algae, flat/intermediate LBF molds			X		Uncertain	
1196B-29Z-2, 88–93	170.81		a			Highly recrystallized, abundant flat LBF molds			X		Uncertain	
1196B-30Z-2, 52–55	174.46		a			Highly recrystallized, abundant mixed LBF molds		X			Uncertain	
1196B-31Z-1, 120–123	178.40		c			Branching red algae, flat/intermediate LBF molds		X			Uncertain	
1196B-32Z-1, 27–29	180.47		c			Branching red algae, flat/intermediate LBF molds		X			Uncertain	
1196B-33Z-1, 79–81	185.69	15.2–13.3		A	A	Fine grainstone, miliolid, *Flosculinella* abundant, soritids and organic common	X				Shallow platform	IIA
1196B-35Z-1, 3–6	194.33	15.2–13.3	R	A	A	No obvious organics; *Marginopora, Cyclorbiculina, Miogypsina,* bivalve molds	X				Shallow platform	
1196B-36Z-1, 9–11	199.09	15.2–13.3				Gastropods, miliolids, soritids, organic abundant	X				Shallow platform	
1196B-39Z-1, 50–53	213.60	15.2–13.3		A	A	Coral with miliolid/red algal grainstone infill	X				Shallow platform	
1196B-40Z-1, 2–3	217.80	18.2–13.6				Nannofossil sample	X				Shallow platform	
1196B-40Z-1, 22–24	218.02	15.2–13.3	A	A	A	Coral in miliolid/red algal grainstone; also *Amphistegina hauerina*	X				Shallow platform	
1196B-41Z-1, 19–21	218.99	15.2–13.3			A	Coral, *Cyclorbiculina* and bivalves in fine matrix	X				Shallow platform	
1196B-42Z-1, 11–13	223.61	15.2–13.3		A	A	Bivalve-rich in fine algal/miliolid grainstone	X				Shallow platform	
1196B-44Z-1, 10–12	233.00	15.2–13.3		A	A	Fine grainstone, miliolid, *Flosculinella* abundant, soritids and bivalves common	X				Shallow platform	
1196B-45Z-1, 35–38	234.65	15.2–13.3		A	A	Poorly lithified foraminifers and algal grainstone	X				Shallow platform	
1196B-46Z-1, 21–24	238.01	15.2–13.3		A	A	Fine grainstone, miliolid, very large *Marginopora* and bivalves	X				Shallow platform	
1196B-47Z-1, 29–32	242.79	15.2–13.3	A	A	A	Fine grainstone, miliolid, *Flosculinella* abundant, soritids and bivalves	X				Shallow platform	
1196B-48Z-1, 27–30	247.47	15.2–13.3		A	A	Fine grainstone, miliolid, *Flosculinella* abundant, soritids and bivalves	X				Shallow platform	
1196B-49Z-1, 30–37	251.50	15.2–13.3		A	A	Bivalves, red algae in fine foraminifer grainstone; *Austrotillina* and *Miogypsina*	X				Shallow platform	
1196B-50Z-1, 23–25	256.13	15.2–13.3		A	A	Fine red algal/miliolid matrix, molluscan molds and soritids	X				Shallow platform	
1196B-51Z-1, 0–5	260.60	15.2–13.3		A	A	Fine red algal/miliolid matrix, molluscan molds and soritids	X				Shallow platform	

Notes: Based primarily on analysis of larger benthic foraminifers from core catcher samples. Foraminifer assemblages: RLBF = rotalline larger benthic foraminifers, MLBF = milioline larger benthic foraminifers, Sm mil = smaller miliolids; A = abundant, C = common, R = rare; lower case symbols = abundance of molds of larger foraminiferal shells. Comments: PF = planktonic foraminifers. Paleowater depth: shaded zone = the lower limit of precision for the paleowater depth estimate, ? = uncertain. Age range based on planktonic foraminifers for part of Sample 1196-1R-1, 1–4 cm ; ages based on nannofossils for Samples 194-1196A-34R-1, 40–44 cm, and 70R-1, 133 cm, and 194-1196B-40Z-1, 2 cm.

Table T6. Summary of biostratigraphic and paleoenvironmental interpretations, Hole 1199A. (**See table notes.** Continued on next page.)

Hole, core, section (cm)	Depth (mbsf)	Age (Ma)	Foraminiferal assemblages					Comments	Paleowater depth (m)			Depositional setting	Lithologic unit
			PF	ONBF	Sm Mil	RLBF	MLBF		<30	<60	<100		
194-													
1199A-1R-4, 21–23	4.52					A		Rhodoliths/coral in red algal fragments and *Amphistegina* matrix		?	X	Open platform	IA
1199A-2R-5, 42–44	15.73				C	A		Rhodoliths and red algal fragments with LBF		?	X	Open platform	
1199A-3R-1, 132–134	18.72				C	A		Rhodoliths and red algal fragments with LBF		?	X	Open platform	
1199A-4R-7, 11–13	27.57				C	A		Rhodoliths and red algal fragments with small, relatively flat *Amphistegina, Cycloclypeus*?		?	X	Open platform	
1199A-5R-6, 64–67	34.74					A		Rhodoliths and red algal fragments with small, relatively flat *Amphistegina, Operculina*?		?	X	Open platform	
1199A-6R-4, 54–56	40.72					A		Rhodoliths and red algal fragments with small, intermediate *Amphistegina, Operculina*?		?	X	Open platform	
1199A-7R-3, 143–145	49.41					A		Rhodoliths and red algal fragments with small, intermediate *Amphistegina, Operculina*?		?	X	Open platform	
1199A-8R-3, 82-–84	57.67					A		Rhodoliths and red algal fragments with small, intermediate *Amphistegina, Operculina*?		?	X	Open platform	
1199A-9R-7, 46–48	72.68					A		Rhodoliths and red algal fragments with small, intermediate *Amphistegina, Operculina*?		?	X	Open platform	
1199A-10R-5, 128–130	80.34					A		Rhodoliths and red algal fragments with small, intermediate *Amphistegina, Operculina*?		?	X	Open platform	
1199A-11R-3, 94–96	86.73					A		Rhodoliths and red algal fragments with small, intermediate *Lepidocyclina, Operculina*?		?	X	Open platform	
1199A-12R-7, 141–143	102.57					A		Smaller rhodoliths (<2 mm) and red algal fragments in recrystallized matrix		?	X	Open platform	
1199A-13R-5, 148–150	109.15							Heavily dolomitized, can barely even see red algae		?	X	Open platform	IB
1199A-14R-3, 22–24	114.97							Heavily dolomitized, can barely even see red algae, large coral? vugs		?	X	Open platform	IC
1199A-15R-1, 74–76	122.14							Heavily dolomitized; ~2-cm rhodoliths, red algal fragments		?	X	Open platform	
1199A-16R-5, 113–115	137.97					a		Heavily dolomitized; mostly red algal fragments, abundant intermediate LBF molds		?	X	Open platform	ID
1199A-17R-1, 69–71	141.29					a		Dolomitzed; ~2-cm rhodoliths, red algal fragments, coral (?), large flat *Lepidocyclina* molds		?	X	Open platform	
1199A-18R-3, 33–35	153.50					a		Heavily dolomitized, red algae fragments, large coral? Vugs, relatively flat *Amphistegina*-type molds		?	X	Open platform	
1199A-19R-1, 7–11	159.87				A			Very fine grainstone, miliolids, red algae				Open platform	IIA
1199A-20R-1, 93–95	170.33	15.2–13.3			A	C	C	Fine grainstone, algal fragments, miliolids, molluscan molds, *Flosculinella*, soritids	X			Open platform	
1199A-21R-1, 18–20	179.18	15.2–13.3			A	C	C	Fine grainstone, algal fragments, miliolids, molluscan molds, *Flosculinella*, soritids	X			Open platform	
1199A-22R-1, 0–1	188.60				a	A		LBF, miliolids, alcyonarian spicules, red algal fragments, gastropod molds	X			Open platform	
1199A-23R-1, 0–4	198.20				C	R		LBF, miliolids, alcyonarian spicules, red algal fragments, gastropod molds	X			Open platform	
1199A-24R-1, 0–4	207.80				C	R		LBF, miliolids, red algal fragments, gastropod molds	X			Open platform	
1199A-25R-1, 0–2	217.40				C	R		LBF, miliolids, alcyonarian spicules, red algal and bryozoan fragments	X			Open platform	
1199A-27R-1, 0–2	236.70				C	R		Red algal fragments, LBF, miliolids, gastropod molds	X			Open platform	
1199A-29R-1, 0–4	255.90	15.2–13.3			A	R	R	Tiny flat bivalve?, large snail vugs, miliolids, *Flosculinella* and *Miogypsina*	X			Open platform	
1199A-30R-1, 39–41	265.89	15.2–13.3			A	R	R	Mollusk vugs, miliolid/red algae grainstone, soritids and *Flosculinella*	X			Open platform	
1199A-31R-1, 28–32	275.48				C			Large gastropod and bivalve vugs, miliolids, and red algae grainstone	X			Open platform	
1199A-32R-1, 18–20	284.98					C		Recrystallized/dolomitized; red algae, bryozoans, *Lepidocyclina*	?	X		Open platform	
1199A-33R-1, 30–32	294.70							Dolomitized; ~2-cm rhodoliths, red algal fragments, little recognizable	?	X		Open platform	IIB
1199A-34R-1, 37–39	304.37							Dolomitized; ~2-cm rhodoliths, red algal fragments, possible coral, little recognizable	?	X		Open platform	
1199A-35R-1, 130–132	315.00					A		Red alga/*Lepidocyclina* grainstone, small rhodoliths	?	X		Open platform	
1199A-36R-1, 0–3	323.30					A		Dolomitized; sizeable rhodoliths, with intermediate *Lepidocyclina*	?	X		Open platform	
1199A-37R-1, 26–28	333.16					A		Rhodoliths (~5 cm), bioeroded, coral?, *Lepidocyclina* in matrix	?	X		Open platform	
1199A-38R-1, 22–24	342.82					A		Rhodoliths (~5 cm), bioeroded, bryozoan, *Lepidocyclina* in matrix	?	X		Open platform	
1199A-39R-1, 124–126	353.44					A		Very coarse red algal fragments with *Lepidocyclina*	?	X		Open platform	
1199A-40R-1, 97–99	362.77					A		*Lepidocyclina*/red algal coarse grainstone	?	X		Open platform	
1199A-41R-2, 28–30	373.14					A		*Lepidocyclina*/red algal coarse grainstone	?	X		Open platform	
1199A-42R-1, 87–89	381.97					A		*Lepidocyclina*/red algal coarse grainstone/rudstone	?	X		Open platform	
1199A-43R-1, 12–14	390.82					A		*Lepidocyclina*/red algal coarse grainstone/rudstone	?	X		Open platform	

Table T6 (continued).

Hole, core, section (cm)	Depth (mbsf)	Age (Ma)	Foraminiferal assemblages					Comments	Paleowater depth (m)			Depositional setting	Lithologic unit
			PF	ONBF	Sm Mil	RLBF	MLBF		<30	<60	<100		
1199A-44R-1, 11–13	400.41					A		*Lepidocyclina*/red algal coarse grainstone/rudstone	?	X		Open platform	
1199A-45R-1, 16–18	410.06					A		*Lepidocyclina*/red algal coarse grainstone/rudstone, partly dolomitized	?	X		Open platform	

Notes: Based primarily on analysis of larger benthic foraminifers from core catcher samples. Foraminiferal assemblages: PF = planktonic foraminifers, ONBF = outer neritic/upper bathyal foraminifers, Sm Mil = smaller miliolids, LBF = rotalline larger benthic foraminifers, LBF = milioline larger benthic foraminifers, A = abundant; C = common; R = rare, lower case symbols indicate abundance of molds of larger foraminiferal shells. Paleowater depth: ? = uncertain.

Table T7. Age-depth control points, Sites 1196 and 1199.

Source	Datum	Age (Ma)	Top: FO presence or LO absence		Bottom: LO presence or FO absence		Average depth (mbsf)	Uncertainty (m)	
			Core, section, interval (cm)	Depth (mbsf)	Core, section, interval (cm)	Depth (mbsf)		Up-section	Down-section
			194-		194-				
PF	Range of *Globorotalia tosaensis-truncatulinoides*	0–3.2	1196A-1R-1, 2	0.02	1196A-1R-BCI	8.48	4.25	4.23	4.23
BF	Range of *Flosculinella botangensis*	13.3–15.2	1196A-20R-1, 112	183.02	1196A-35R-BCI	335.90			
CN	Range of *Sphenolithus heteromorphus*	13.6–18.2	1196B-40Z-1, 2	217.82	1196B-40Z-BCI	218.58	218.20	0.38	0.38
CN	Range of *Sphenolithus heteromorphus*	13.6–18.2	1196A-34R-1, 42	317.02	1196A-34R-BCI	325.40	321.21	4.19	4.19
CN	Range of assemblage	24.2–24.6	1196A-70R-1, 133	663.93	1196A-70R-BCI	668.91	666.42	2.49	2.49
BF	Range of *Flosculinella botangensis*	13.3–15.2	1199A-20R-1, 94	170.34	1199A-30R-1, 40	275.20			

Notes: Source: PF = planktonic foraminifers, BF = Benthic foraminifers, CN = calcareous nannoplankton. Core, section, interval: BCI = Bottom of cored interval.

Table T8. Interpolated ages of lithologic unit boundaries and seismic reflectors, Sites 1196 and 1199.

	Site 1196; top of unit		Site 1199; top of unit		
	Depth (mbsf)	Age (Ma)	Depth (mbsf)	Age (Ma)	Comments
Lithologic unit:					
I	0		0		
II	182.2	13.2	159.8	12.8	Large uncertainty
III	345.8	15.5	410.0	18.2	Large uncertainty
IV	617.1	23.0	Not drilled		Large uncertainty
V	662.6	24.4	Not drilled		Large uncertainty
Seismic sequences and reflectors:					
Megasequence D	Not present				
D-black	Not present				
D-turquoise	Not present				
Megasequence C	Not defined				
Megasequence B	115	9.1	90	7.8	Large uncertainty
Megasequence A	Not defined				
Basement	Not defined				

Table T9. Percentages of aragonite, calcite, dolomite, and noncarbonate minerals, Site 1196.

Core, section, interval (cm)	Depth (mbsf)	Aragonite (wt%)	Calcite (wt%)	Dolomite (wt%)	Non-carbonate (wt%)
194-1196A-					
1R-1, 54–55	0.54	0	0	94	6
2R-1, 31–32	9.91	0	0	99	1
3R-1, 15–16	19.05	0	7	92	1
4R-1, 91–92	29.41	0	94	7	0
5R-1, 60–61	38.80	0	90	10	0
5R-2, 70–71	40.40	0	61	39	0
6R-1, 99–100	48.49	0	0	99	1
7R-1, 81–82	57.71	0	0	99	1
7R-2, 40–41	58.71	0	0	98	2
8R-1, 33–34	66.83	0	3	95	2
9R-1, 83–84	76.93	0	2	87	11
9R-1, 137–138	77.47	0	0	98	2
9R-2, 32–33	77.84	0	0	98	2
9R-2, 34–35	77.86	0	0	98	2
10R-1, 0–1	85.80	0	0	97	3
11R-1, 67–68	96.07	0	0	98	2
12R-1, 68–69	105.68	0	0	98	2
13R-1, 9–10	114.79	0	0	98	2
14R-1, 50–51	124.80	0	0	98	2
14R-2, 16–17	125.86	0	0	98	2
15R-1, 17–18	134.07	0	99	0	1
16R-1, 54–55	144.04	0	0	99	1
18R-1, 55–56	163.25	0	0	100	0
18R-2, 55–56	164.71	0	0	98	2
18R-3, 44–45	166.10	0	0	99	1
19R-1, 65–66	172.95	0	0	98	2
19R-2, 105–106	174.78	0	0	98	2
19R-3, 2–3	175.22	0	0	98	2
20R-1, 87–89	182.77	0	99	0	1
21R-1, 94–96	192.44	0	99	0	1
22R-1, 7–9	201.17	0	99	0	1
24R-1, 9–11	220.39	0	100	0	0
25R-1, 40–42	230.30	0	99	0	1
26R-1, 16–18	239.76	0	99	0	1
27R-1, 2–4	249.22	0	100	0	0
28R-1, 8–10	258.88	0	99	0	1
31R-1, 12–13	287.72	0	97	0	3
33R-1, 64–65	307.54	0	100	0	0
34R-1, 64–65	317.24	0	100	0	0
35R-1, 8–9	326.38	0	99	0	1
36R-1, 2–3	335.92	0	93	6	1
37R-1, 55–56	346.05	0	101	0	0
38R-1, 8–9	355.18	0	46	50	4
41R-1, 14–15	384.04	0	97	2	1
42R-1, 11–12	393.61	0	99	0	1
44R-1, 55–56	413.25	0	2	97	1
48R-1, 90–91	452.00	0	0	98	2
50R-1, 14–15	470.54	0	0	98	2
51R-1, 24–26	480.24	0	0	98	2
51R-2, 20–22	481.68	0	0	99	1
51R-3, 61–63	483.57	0	0	99	1
51R-4, 27–29	484.64	0	0	99	2
52R-1, 21–23	489.91	0	0	99	1
52R-2, 10–12	491.27	0	0	99	1
52R-3, 35–37	493.02	0	0	99	1
52R-4, 49–51	494.63	0	0	98	2
52R-5, 96–98	496.60	0	0	99	1
52R-6, 42–44	497.56	0	0	99	1
53R-1, 20–21	499.50	0	0	99	1
53R-2, 15–16	500.95	0	0	99	1
53R-3, 72–73	503.02	0	0	99	1
53R-4, 47–48	504.17	0	0	99	1
54R-1, 97–98	509.87	0	0	99	1
55R-1, 74–75	519.24	0	0	81	19
56R-1, 61–62	528.71	0	0	98	2
56R-2, 26–27	529.54	0	0	98	2
57R-1, 52–53	538.22	0	0	98	2
57R-2, 66–67	539.86	0	0	99	1
58R-1, 62–64	547.92	0	0	99	1
59R-1, 71–72	557.61	0	0	99	1
60R-1, 60–61	567.20	0	0	98	2
61R-1, 81–82	577.01	0	0	98	2
62R-1, 2–3	585.82	0	0	98	2
63R-1, 32–34	595.82	0	0	91	9
63R-2, 36–38	597.35	0	0	97	3
64R-1, 18–20	605.28	0	0	97	3
64R-2, 16–18	606.76	0	0	98	2
64R-3, 15–17	608.20	0	0	98	2
65R-1, 31–33	615.01	0	0	95	5
65R-2, 6–8	616.25	0	0	72	28
65R-3, 94–96	618.61	0	0	93	8
65R-4, 82–84	619.97	0	0	94	6
65R-5, 20–22	620.85	0	0	97	3
66R-1, 130–132	625.70	0	0	96	4
66R-2, 97–99	626.72	0	0	99	1
66R-3, 91–93	628.14	0	0	98	2
66R-4, 47–49	629.19	0	0	86	14
67R-1, 36–38	634.06	0	0	62	38
67R-2, 84-86	635.92	0	0	82	18
68R-1, 2–3	643.42	0	0	19	81
70R-1, 53–55	663.13	0	0	1	99
70R-2, 34–36	664.44	0	7	0	93
70R-3, 93–95	666.53	0	29	10	61

Table T10. Carbon, nitrogen, sulfur, and hydrogen values and C/N and C/S ratios in sediments, Site 1196. (See table notes. Continued on next two pages.)

Core, section	Depth (mbsf)	IC (wt%)	$CaCO_3$ (wt%)	TC (wt%)	TOC (wt%)	Total N (wt%)	Total S (wt%)	Total H (wt%)	C/N ratio	C/S ratio
194-1196A-										
1R-1	0.55	12.23	101.9	—	—	—	—	—	—	—
2R-1	9.92	12.78	106.5	—	—	—	—	—	—	—
3R-1	19.06	12.74	106.1	—	—	—	—	—	—	—
4R-1	29.42	12.11	100.9	—	—	—	—	—	—	—
5R-1	38.81	12.08	100.7	—	—	—	—	—	—	—
5R-2	40.41	12.34	102.8	—	—	—	—	—	—	—
6R-1	48.50	12.86	107.1	—	—	—	—	—	—	—
7R-1	57.71	12.83	106.9	—	—	—	—	—	—	—
7R-2	58.71	12.77	106.4	—	—	—	—	—	—	—
8R-1	66.83	12.71	105.9	—	—	—	—	—	—	—
9R-1	76.93	12.70	105.8	—	—	—	—	—	—	—
9R-2	77.84	12.73	106.0	—	—	—	—	—	—	—
10R-1	85.80	12.76	106.3	—	—	—	—	—	—	—
11R-1	96.08	12.75	106.2	—	—	—	—	—	—	—
12R-1	105.69	12.62	105.1	—	—	—	—	—	—	—
13R-1	114.80	12.69	105.8	—	—	—	—	—	—	—
13R-2	116.76	12.76	106.3	—	—	—	—	—	—	—
14R-1	124.81	12.72	106.0	—	—	—	—	—	—	—
14R-2	125.86	12.68	105.6	—	—	—	—	—	—	—
15R-1	134.07	11.91	99.2	—	—	—	—	—	—	—
16R-1	144.05	12.83	106.9	—	—	—	—	—	—	—
18R-1	163.26	12.93	107.7	—	—	—	—	—	—	—
18R-2	164.72	12.75	106.2	—	—	—	—	—	—	—
18R-3	166.11	12.80	106.6	—	—	—	—	—	—	—
19R-1	172.96	12.74	106.1	—	—	—	—	—	—	—
19R-2	174.79	12.68	105.7	—	—	—	—	—	—	—
19R-3	175.23	12.71	105.9	—	—	—	—	—	—	—
20R-1	182.77	11.88	99.0	—	—	—	—	—	—	—
21R-1	192.44	11.84	98.6	11.92	0.08	0.02	0.00	0.07	4.63	—
22R-1	201.17	11.85	98.7	12.02	0.17	0.02	0.07	0.10	7.07	2.29
24R-1	220.39	11.96	99.6	—	—	—	—	—	—	—
25R-1	230.30	11.88	99.0	11.95	0.07	0.01	0.04	0.07	5.88	1.86
26R-1	239.76	11.90	99.1	—	—	—	—	—	—	—
27R-1	249.22	12.00	100.0	—	—	—	—	—	—	—
27R-1	249.43	11.92	99.3	11.98	0.06	0.01	0.00	0.06	4.46	—
28R-1	258.88	11.63	96.9	11.92	0.29	0.06	0.00	0.16	5.01	—
31R-1	287.72	12.01	100.0	—	—	—	—	—	—	—
33R-1	307.54	11.99	99.9	—	—	—	—	—	—	—
34R-1	317.24	11.88	99.0	—	—	—	—	—	—	—
35R-1	326.38	12.00	99.9	—	—	—	—	—	—	—
36R-1	335.92	12.08	100.6	—	—	—	—	—	—	—
37R-1	346.05	12.01	100.1	—	—	—	—	—	—	—
38R-1	355.18	11.96	99.6	—	—	—	—	—	—	—
41R-1	384.04	11.94	99.5	11.89	0.00	0.01	0.00	0.02	—	—
42R-1	393.61	11.97	99.7	—	—	—	—	—	—	—
44R-1	413.25	12.76	106.3	—	—	—	—	—	—	—
48R-1	452.00	12.77	106.4	—	—	—	—	—	—	—
50R-1	470.54	12.70	105.8	—	—	—	—	—	—	—
51R-1	480.24	12.72	106.0	—	—	—	—	—	—	—
51R-2	481.68	12.81	106.7	—	—	—	—	—	—	—
51R-3	483.57	12.78	106.4	—	—	—	—	—	—	—
51R-4	484.64	12.77	106.4	—	—	—	—	—	—	—
52R-1	489.91	12.83	106.8	—	—	—	—	—	—	—
52R-2	491.27	12.80	106.6	—	—	—	—	—	—	—
52R-3	493.02	12.83	106.9	—	—	—	—	—	—	—
52R-4	494.63	12.73	106.0	—	—	—	—	—	—	—
52R-5	496.60	12.78	106.5	—	—	—	—	—	—	—
52R-6	497.56	12.85	107.1	—	—	—	—	—	—	—
53R-1	499.50	12.82	106.8	—	—	—	—	—	—	—
53R-2	500.95	12.82	106.8	—	—	—	—	—	—	—
53R-3	503.02	12.79	106.6	—	—	—	—	—	—	—
53R-4	504.17	12.79	106.5	—	—	—	—	—	—	—
54R-1	509.87	12.78	106.5	—	—	—	—	—	—	—
55R-1	519.25	12.75	106.2	—	—	—	—	—	—	—
56R-1	528.72	12.71	105.9	—	—	—	—	—	—	—

Table T10 (continued).

Core, section	Depth (mbsf)	IC (wt%)	$CaCO_3$ (wt%)	TC (wt%)	TOC (wt%)	Total N (wt%)	Total S (wt%)	Total H (wt%)	C/N ratio	C/S ratio
56R-2	529.55	12.77	106.3	—	—	—	—	—	—	—
57R-1	538.23	12.79	106.6	—	—	—	—	—	—	—
57R-1	538.27	12.68	105.7	—	—	—	—	—	—	—
57R-2	539.87	12.79	106.5	—	—	—	—	—	—	—
58R-1	547.92	12.80	106.6	—	—	—	—	—	—	—
59R-1	557.62	12.83	106.9	—	—	—	—	—	—	—
60R-1	567.21	12.77	106.4	—	—	—	—	—	—	—
61R-1	577.02	12.75	106.2	—	—	—	—	—	—	—
62R-1	585.83	12.76	106.3	—	—	—	—	—	—	—
63R-1	595.82	12.64	105.3	—	—	—	—	—	—	—
63R-2	597.35	12.60	105.0	—	—	—	—	—	—	—
64R-1	605.28	12.61	105.1	—	—	—	—	—	—	—
64R-2	606.76	12.68	105.6	—	—	—	—	—	—	—
64R-3	608.20	12.64	105.3	—	—	—	—	—	—	—
65R-1	615.01	12.30	102.4	—	—	—	—	—	—	—
65R-2	616.25	12.60	104.9	—	—	—	—	—	—	—
65R-3	618.61	11.99	99.9	—	—	—	—	—	—	—
65R-4	619.97	12.15	101.2	—	—	—	—	—	—	—
65R-5	620.85	12.55	104.6	—	—	—	—	—	—	—
66R-1	625.70	12.49	104.0	—	—	—	—	—	—	—
66R-2	626.72	12.78	106.5	—	—	—	—	—	—	—
66R-3	628.14	12.71	105.9	—	—	—	—	—	—	—
66R-4	629.19	11.09	92.4	—	—	—	—	—	—	—
67R-1	634.06	7.72	64.3	7.87	0.15	0.01	0.00	0.07	12.50	—
67R-2	635.92	10.58	88.2	9.97	0.00	0.01	0.00	0.08	—	—
68R-1	643.42	2.48	20.7	2.63	0.15	0.02	0.16	0.10	7.48	0.95
70R-1	662.80	0.06	0.5	0.98	0.92	0.03	1.49	0.49	28.61	0.61
70R-1	663.00	0.08	0.7	0.99	0.91	0.03	5.38	0.43	28.33	0.17
70R-1	663.13	0.10	0.8	1.00	0.90	0.02	1.45	0.45	44.95	0.62
70R-1	663.20	0.11	0.9	—	—	—	—	—	—	—
70R-1	663.36	0.26	2.2	0.82	0.56	0.09	1.22	0.94	6.33	0.46
70R-1	663.57	0.37	3.1	0.90	0.53	0.07	0.93	0.94	7.86	0.57
70R-1	663.78	0.45	3.8	1.02	0.57	0.07	1.13	0.92	8.03	0.50
70R-1	663.99	0.62	5.2	—	—	—	—	—	—	—
70R-2	664.28	0.60	5.0	1.21	0.61	0.07	1.25	0.97	8.26	0.49
70R-2	664.44	0.79	6.6	1.37	0.58	0.06	1.36	0.87	9.72	0.43
70R-2	664.47	1.03	8.6	1.44	0.41	0.05	2.78	0.94	9.18	0.15
70R-2	664.70	0.85	7.1	1.29	0.44	0.08	1.66	0.97	5.44	0.27
70R-2	664.91	1.20	10.0	1.52	0.32	0.07	1.42	0.92	4.84	0.23
70R-2	665.09	1.08	9.0	—	—	—	—	—	—	—
70R-2	665.30	1.49	12.4	1.75	0.26	0.03	0.67	0.84	10.40	0.39
70R-2	665.49	1.39	11.6	1.69	0.30	0.03	0.47	0.90	12.04	0.65
70R-2	665.78	3.34	27.9	—	—	—	—	—	—	—
70R-3	666.00	3.80	31.7	—	—	—	—	—	—	—
70R-3	666.21	3.89	32.4	3.96	0.07	0.02	1.28	0.54	3.93	0.06
70R-3	666.42	4.62	38.5	—	—	—	—	—	—	—
70R-3	666.53	4.47	39.9	4.48	0.01	0.00	0.16	0.56	2.67	0.05
70R-3	666.61	4.26	35.5	—	—	—	—	—	—	—
70R-3	666.78	6.14	51.2	—	—	—	—	—	—	—
70R-3	666.99	1.37	11.4	1.98	0.61	0.03	1.07	0.71	24.38	0.57
194-1196B-										
13Z-1	110.80	12.62	105.1	—	—	—	—	—	—	—
13Z-2	111.64	12.68	105.7	—	—	—	—	—	—	—
14Z-1	115.49	12.67	105.6	—	—	—	—	—	—	—
14Z-2	116.63	12.66	105.5	—	—	—	—	—	—	—
15Z-1	117.64	12.58	104.8	—	—	—	—	—	—	—
16Z-1	119.18	12.73	106.1	—	—	—	—	—	—	—
17Z-1	123.41	12.73	106.1	—	—	—	—	—	—	—
18Z-1	124.25	12.70	105.8	—	—	—	—	—	—	—
18Z-2	125.04	12.63	105.2	—	—	—	—	—	—	—
20Z-1	130.55	11.89	99.0	11.85	0.00	0.01	0.00	0.03	—	—
22Z-1	139.88	12.71	105.9	—	—	—	—	—	—	—
24Z-1	145.01	12.66	105.5	—	—	—	—	—	—	—
25Z-1	149.98	12.65	105.3	—	—	—	—	—	—	—
27Z-1	159.32	12.66	105.4	—	—	—	—	—	—	—
28Z-1	163.84	12.73	106.1	—	—	—	—	—	—	—
29Z-1	169.63	12.69	105.7	—	—	—	—	—	—	—
29Z-2	170.57	12.67	105.5	—	—	—	—	—	—	—
30Z-1	173.09	12.74	106.1	—	—	—	—	—	—	—

Table T10 (continued).

Core, section	Depth (mbsf)	IC (wt%)	$CaCO_3$ (wt%)	TC (wt%)	TOC (wt%)	Total N (wt%)	Total S (wt%)	Total H (wt%)	C/N ratio	C/S ratio
30Z-2	173.99	12.71	105.9	—	—	—	—	—	—	—
31Z-1	177.63	12.78	106.4	—	—	—	—	—	—	—
32Z-1	180.22	12.77	106.3	—	—	—	—	—	—	—
33Z-1	185.41	11.92	99.3	—	—	—	—	—	—	—
33Z-1	185.69	11.79	98.2	—	—	—	—	—	—	—
35Z-1	194.30	11.73	97.7	11.84	0.11	0.01	0.00	0.06	9.17	—
36Z-1	199.03	11.88	99.0	—	—	—	—	—	—	—
39Z-1	213.59	11.85	98.7	—	—	—	—	—	—	—
40Z-1	217.96	11.87	98.8	—	—	—	—	—	—	—
41Z-1	218.86	11.67	97.2	12.15	0.48	0.04	0.09	0.14	12.31	5.39
42Z-1	223.74	11.90	99.2	—	—	—	—	—	—	—
44Z-1	232.93	11.92	99.3	—	—	—	—	—	—	—
45Z-1	234.38	11.56	96.3	11.85	0.29	0.05	0.17	0.17	5.92	1.71
46Z-1	237.91	11.92	99.3	—	—	—	—	—	—	—
47Z-1	242.61	11.92	99.3	—	—	—	—	—	—	—
48Z-1	247.29	11.77	98.0	—	—	—	—	—	—	—
49Z-1	251.52	11.91	99.2	—	—	—	—	—	—	—
50Z-1	256.12	11.93	99.4	—	—	—	—	—	—	—
51Z-1	260.60	11.91	99.2	—	—	—	—	—	—	—

Notes: IC = inorganic carbon, TC = total carbon, TOC = total organic carbon, C/N = carbon/nitrogen, C/S = carbon/sulfur. — = not analyzed.

Table T11. Results of Rock-Eval analyses on sediments, Site 1196. (See table notes. Continued on next page.)

Core, section, interval (cm)	Depth (mbsf)	T_{max}	S_1	S_2	S_3	HI	OI	TOC (wt%)
194-1196A-								
1R-1, 55	0.55	—	0.00	0.00	5.71	0	28,550	0.02
3R-1, 16	19.06	—	0.00	0.00	3.41	0	6,820	0.05
4R-1, 92	29.42	—	0.00	0.00	2.42	—	—	0.00
9R-1, 83	76.93	—	0.00	0.00	2.00	0	10,000	0.02
13R-1, 10	114.80	—	0.00	0.00	1.01	0	2,525	0.04
15R-1, 17	134.07	—	0.00	0.00	0.00	0	0	0.01
20R-1, 87	182.77	429	0.03	0.19	2.92	237	3,650	0.08
21R-1, 94	192.44	429	0.02	0.12	1.79	120	1,790	0.10
22R-1, 7	201.17	429	0.09	0.51	1.81	231	822	0.22
24R-1, 9	220.39	433	0.00	0.07	0.12	233	400	0.03
25R-1, 40	230.30	433	0.04	0.26	0.83	236	754	0.11
26R-1, 16	239.76	439	0.01	0.12	10.73	240	21,460	0.05
27R-1, 2	249.22	418	0.01	0.06	5.58	192	12,162	0.04
27R-1, 23	249.43	437	0.03	0.19	0.52	237	650	0.08
28R-1, 8	258.88	428	0.12	0.73	13.84	224	3,870	0.33
31R-1, 12	287.72	443	0.00	0.02	0.06	200	600	0.01
31R-CC	287.50	337	0.00	0.01	2.65	—	—	0.00
32R-CC	297.53	366	0.00	0.02	2.62	—	—	0.00
33R-1, 64	307.54	436	0.01	0.05	0.39	250	0	0.01
34R-1, 64	317.24	440	0.05	0.09	9.37	225	23,425	0.04
35R-1, 8	326.38	—	0.00	0.00	1.69	—	—	0.00
38R-1, 8	355.18	314	0.00	0.01	1.39	—	—	0.00
41R-1, 14	384.04	—	0.00	0.00	8.15	—	—	0.00
42R-1, 11	393.61	326	0.01	0.01	2.27	—	—	0.00
52R-2, 10	491.27	—	0.00	0.00	0.68	—	—	0.00
54R-1, 97	510.22	—	0.00	0.00	1.27	0	6,350	0.02
55R-1, 75	519.25	—	0.00	0.00	0.23	0	562	0.03
56R-1, 62	529.08	—	0.00	0.00	0.46	—	—	0.00
57R-2, 67	539.87	—	0.00	0.00	1.74	0	17,400	0.01
63R-1, 32	595.82	—	0.01	0.00	1.00	—	—	0.00
65R-2, 6	616.25	—	0.02	0.00	1.22	0	1,050	0.01
66R-2, 97	626.72	—	0.00	0.00	3.16	0	31,600	0.01
66R-3, 91	628.14	—	0.01	0.00	4.01	—	—	0.00
66R-4, 47	629.19	—	0.11	0.00	6.52	0	65,200	0.01
67R-1, 36	634.06	—	0.07	0.00	4.45	0	4,434	0.11
67R-2, 84	635.92	—	0.19	0.01	8.65	33	28,833	0.03
68R-1, 2	643.42	414	0.05	0.01	4.09	16	6,816	0.06
70R-1, 20	662.80	418	0.03	0.37	1.35	42	150	0.88
70R-1, 40	663.00	421	0.02	0.32	1.56	43	213	0.73
70R-1, 53	663.13	409	0.29	0.33	16.58	48	2,450	0.69
70R-1, 60	663.20	419	0.02	0.24	0.79	45	111	0.58
70R-1, 76	663.36	409	0.06	0.34	3.03	70	631	0.48
70R-1, 97	663.57	412	0.02	0.34	5.31	69	1,083	0.49
70R-1, 118	663.78	412	0.03	0.45	4.60	81	836	0.55
70R-1, 139	663.99	411	0.03	0.42	6.70	75	1,196	0.56
70R-2, 18	664.28	408	0.04	0.41	4.46	66	719	0.62
70R-2, 34	664.44	407	0.24	0.47	24.55	77	4,059	0.61
70R-2, 37	664.47	408	0.03	0.29	19.20	48	3,232	0.61
70R-2, 60	664.70	402	0.04	0.31	6.81	60	1,335	0.51
70R-2, 81	664.91	401	0.04	0.28	2.66	57	542	0.49
70R-2, 99	665.09	399	0.02	0.19	3.28	46	800	0.41
70R-2, 120	665.30	404	0.01	0.08	10.98	28	4,140	0.28
70R-2, 139	665.49	406	0.03	0.07	4.46	36	2,347	0.19
70R-3, 18	665.78	385	0.00	0.03	0.95	23	730	0.13
70R-3, 40	666.00	323	0.01	2.00	3.32	16	2,766	0.12
70R-3, 61	666.21	333	0.01	0.02	11.07	5	4,632	0.24
70R-3, 82	666.42	407	0.01	0.02	16.13	20	16,150	0.10
70R-3, 93	666.53	382	0.28	0.06	22.15	28	11,822	0.19
70R-3, 101	666.61	356	0.01	0.03	15.30	10	8,985	0.13
70R-3, 118	666.78	401	0.01	0.02	8.94	22	8,750	0.09
70R-3, 139	666.99	414	0.01	0.12	20.05	15	2,700	0.79
194-1196B-								
13Z-1, 80	110.80	—	0.00	0.00	0.23	—	—	0.00
13Z-2, 25	111.64	—	0.00	0.00	11.18	0	31,850	0.02
14Z-1, 79	115.49	—	0.00	0.00	8.76	0	—	0.01
14Z-2, 48	116.63	—	0.00	0.00	2.23	0	22,300	0.01

Table T11 (continued).

Core, section, interval (cm)	Depth (mbsf)	T_{max}	S_1	S_2	S_3	HI	OI	TOC (wt%)
15Z-1, 74	117.64	—	0.00	0.00	11.18	—	—	0.00
16Z-1, 98	119.18	—	0.00	0.00	3.07	—	—	0.00
17Z-1, 51	123.41	—	0.00	0.00	0.65	—	—	0.00
18Z-1, 85	124.25	—	0.00	0.00	6.30	—	—	0.00
18Z-2, 18	125.04	—	0.00	0.00	9.34	0	—	0.01
20Z-1, 25	130.55	—	0.00	0.00	2.03	—	—	0.00
22Z-1, 18	139.88	—	0.00	0.00	7.08	0	—	0.01
24Z-1, 1	145.01	—	0.00	0.00	3.55	—	—	0.00
25Z-1, 28	149.98	—	0.00	0.00	2.37	—	—	0.00
27Z-1, 22	159.32	—	0.00	0.00	1.50	—	—	0.00
28Z-1, 4	163.84	—	0.04	0.01	5.02	—	—	0.00
29Z-1, 113	169.63	—	0.00	0.00	0.29	—	—	0.00
29Z-2, 64	170.57	—	0.00	0.00	8.20	0	—	0.01
30Z-1, 59	173.09	—	0.00	0.00	4.30	—	—	0.00
30Z-2, 5	173.99	—	0.00	0.00	1.85	—	—	0.00
31Z-1, 43	177.63	—	0.00	0.00	5.16	—	—	0.00
32Z-1, 2	180.22	—	0.00	0.00	3.69	—	—	0.00
33Z-1, 51	185.41	419	0.00	0.02	2.98	120	5,960	0.05
33Z-1, 79	185.69	421	0.01	0.11	15.84	50	7,200	0.22
35Z-1, 0	194.30	420	0.00	0.02	5.98	200	59,800	0.01
36Z-1, 3	199.03	423	0.01	0.05	7.06	125	17,650	0.04
39Z-1, 49	213.59	419	0.00	0.01	8.36	100	—	0.01
40Z-1, 16	217.96	416	0.01	0.10	8.60	142	12,285	0.07
41Z-1, 6	218.86	414	0.02	0.35	4.74	152	2,060	0.23
42Z-1, 24	223.74	418	0.01	0.04	7.72	133	25,733	0.03
44Z-1, 3	232.93	418	0.01	0.05	9.19	100	18,380	0.05
45Z-1, 8	234.38	422	0.04	0.10	5.05	125	6,312	0.08
46Z-1, 11	237.91	418	0.00	0.03	6.39	150	31,950	0.02
47Z-1, 11	242.61	422	0.01	0.03	6.72	150	33,600	0.02
48Z-1, 9	247.29	417	0.03	0.13	13.23	144	14,700	0.09
49Z-1, 32	251.52	—	0.00	0.01	6.97	0	—	0.01
50Z-1, 22	256.12	417	0.01	0.08	6.13	133	10,216	0.06
51Z-1, 0	260.60	417	0.01	0.06	8.03	175	24,666	0.03

Notes: T_{max} = temperature of maximum hydrocarbon generation during pyrolysis in °C, S_1 = milligrams of free hydrocarbons per gram of rock, S_2 = milligrams of pyrolyzed hydrocarbons per gram of rock, S_3 = milligrams of carbon dioxide per gram of rock, HI = hydrogen index in milligrams of hydrocarbon per gram of TOC, OI = milligrams of carbon dioxide per gram of TOC, TOC = total organic carbon. — = not available.

Table T12. Inorganic carbon and calcium carbonate content in sediments, Hole 1199A.

Core, section, interval (cm)	Depth (mbsf)	IC (wt%)	$CaCO_3$ (wt%)
194-1199A-			
1R-1, 81–82	0.81	12.75	106.23
1R-2, 82–83	2.28	12.74	106.12
1R-3, 54–55	3.42	12.82	106.80
2R-3, 39–40	12.73	12.79	106.61
3R-1, 85–86	18.25	12.78	106.48
4R-3, 85–86	22.54	12.83	106.87
5R-4, 85–86	32.08	12.86	107.17
6R-2, 33–34	37.53	12.87	107.21
7R-1, 35–36	45.45	12.73	106.11
7R-3, 64–65	48.62	13.08	108.96
8R-2, 4–5	55.44	12.82	106.85
8R-2, 88–89	56.28	13.04	108.64
9R-2, 104–105	66.09	13.13	109.39
9R-4, 111–113	69.03	13.15	109.55
9R-6, 142–144	72.16	13.22	110.13
10R-1, 125–127	74.45	13.17	109.76
10R-2, 56–58	75.26	13.13	109.40
10R-4, 64–66	78.25	12.82	106.84
11R-1, 76–77	83.56	12.90	107.52
11R-3, 48–50	86.27	12.80	106.66
12R-3, 101–102	96.39	12.89	107.41
13R-3, 89–90	105.66	12.86	107.17
14R-2, 71–72	113.97	13.21	110.09
15R-1, 70–71	122.10	12.96	107.98
16R-3, 102–103	134.95	12.97	108.10
17R-1, 66–68	141.26	12.97	108.07
18R-2, 55–56	152.23	12.90	107.45
19R-1, 0–1	159.80	12.13	101.05
19R-1, 0–5	159.80	11.93	99.40
20R-1, 0–5	169.40	12.61	105.03
20R-1, 12–13	169.52	12.89	107.44
21R-1, 0–5	179.00	11.96	99.68
21R-1, 5–7	179.05	11.94	99.49
22R-1, 0–1	188.60	11.89	99.12
23R-1, 0–2	198.20	12.00	100.00
24R-1, 0–2	207.80	11.97	99.74
25R-1, 0–2	217.40	12.00	99.98
27R-1, 0–2	236.70	11.91	99.24
29R-1, 0–2	255.90	12.01	100.06
30R-1, 0–2	265.50	12.04	100.29
30R-1, 10–12	265.60	11.87	98.92
31R-1, 15–17	275.35	12.04	100.34
32R-1, 0–2	284.80	12.33	102.78
32R-1, 1–3	284.81	11.19	93.24
33R-1, 18–20	294.58	12.54	104.48
34R-1, 25–27	304.25	12.50	104.16
35R-1, 30–32	314.00	12.74	106.18
37R-1, 21–23	333.11	12.06	100.52
38R-1, 11–12	342.71	12.40	103.31
39R-1, 81–83	353.01	12.00	100.01
40R-1, 28–30	362.08	11.95	99.54
41R-1, 80–82	372.20	12.17	101.42
41R-2, 2–4	372.88	12.05	100.40
42R-1, 59–61	381.69	12.40	103.33
43R-1, 0–2	390.70	11.90	99.18
44R-1, 0–3	400.30	12.45	103.70
45R-1, 10–12	410.00	12.38	103.20

Note: IC = inorganic carbon.

Table T13. Percentages of aragonite, calcite, dolomite, and noncarbonate minerals, Hole 1199A.

Core, section, interval (cm)	Depth (mbsf)	Aragonite (wt%)	Calcite (wt%)	Dolomite (wt%)	Non-carbonate (wt%)
194-1199A-					
1R-1, 82–83	0.82	0	0	98	2
1R-2, 81–82	2.27	0	0	98	2
1R-3, 55–56	3.43	0	0	99	1
2R-3, 39–40	12.73	0	0	99	1
3R-1, 85–86	18.25	0	0	99	1
4R-3, 85–86	22.54	0	0	99	1
5R-4, 85–86	32.08	0	0	99	1
6R-2, 33–34	37.53	0	0	99	1
7R-1, 35–36	45.45	0	0	98	2
7R-3, 64–65	48.62	0	0	100	0
8R-2, 4–5	55.44	0	0	99	1
8R-2, 88–90	56.28	0	0	100	0
9R-2, 104–105	66.09	0	0	100	0
9R-4, 111–113	69.03	0	0	100	0
9R-6, 142–144	72.16	0	0	100	0
10R-1, 125–127	74.45	0	0	100	0
10R-2, 56–58	75.26	0	0	100	0
10R-4, 64–66	78.25	0	0	99	1
11R-1, 76–77	83.56	0	0	100	0
11R-3, 48–50	86.27	0	0	99	1
12R-3, 101–102	96.39	0	0	99	1
13R-3, 89–90	105.66	0	0	99	1
14R-2, 71–72	113.97	0	0	100	0
15R-1, 70–71	122.10	0	0	100	0
16R-3, 102–103	134.95	0	0	100	0
17R-1, 66–68	141.26	0	0	100	0
18R-2, 55–56	152.23	0	0	99	1
19R-1, 0–1	159.80	0	100	0	0
20R-1, 12–13	169.52	0	100	0	0
21R-1, 5–7	179.05	0	100	0	0
30R-1, 10–12	265.60	0	84	15	1
31R-1, 15–17	275.35	0	76	23	1
32R-1, 1–3	284.81	0	82	18	0
33R-1, 18–20	294.58	0	20	78	2
34R-1, 25–27	304.25	0	22	76	2
35R-1, 30–32	314.00	0	0	98	2
37R-1, 21–23	333.11	0	80	19	1
38R-1, 11–12	342.71	0	38	60	2
39R-1, 81–83	353.01	0	100	0	0
40R-1, 28–30	362.08	0	100	0	0
41R-1, 80–82	372.20	0	52	46	2
41R-2, 2–4	372.88	0	87	12	1
42R-1, 59–61	381.69	0	43	56	1
43R-1, 0–2	390.70	0	99	0	1
44R-1, 0–3	400.30	0	32	67	2
45R-1, 10–12	410.00	0	23	74	3

Table T14. Logging operations, Hole 1196A.

Date (Feb 2001)	Time (local)	Comments
3	1030	Hole preparation complete; rig up wireline.
	1135	RIH with MGT-HNGS-APS-HLDS-DITE (+TAP).
	1140	Tools pulled back. MGT is taken off the combination because of connection problems.
	1215	RIH with HNGS-APS-HLDS-DITE (+TAP).
	1315	Uplog with triple combo at 900 ft/hr from tight spot at 510 mbsf to seafloor.
	1515	Pull tools out of hole and rig down.
	1615	Rig up NGT-LSS-FMS.
	1425	RIH with NGT-LSS-FMS.
	1720	Tool cannot pass obstacle in the pipe. Pull tools back on the rig floor and start clearing pipe.
	2135	RIH with NGT-LSS-FMS.
	2220	Uplog at 900 ft/hr from 523 mbsf to pipe. Going down again for a repeat run.
4	0020	Uplog at 900 ft/hr from 520 to pipe. Pull out of hole.
	0300	Rig up WST.
	0350	Start check shots from 523.5 mbsf with 13 shotpoints.
	0530	Pull out of hole and rig down.
	0645	End of logging operations.

Notes: RIH = run in hole, MGT = Lamont multisensor gamma ray tool, HNGS = hostile environment natural gamma ray sonde, APS = accelerator porosity sonde, HLDS = high-temperature lithodensity sonde, DITE = dual induction tool, TAP = high-temperature/acceleration/pressure tool, NGT = natural gamma-ray tool, LSS = long-spaced sonic tool, FMS =Formation MicroScanner, WST = well seismic tool. Drillers total depth = 672.2 mbsf, water depth = 315.2 mbrf, end of pipe = 71.8 mbsf.

Table T15. Time-depth correlation from check shot survey, Hole 1196A.

Check shot station	Depth (mbsl)	TWT below sea level (ms)	Depth (mbsf)	TWT below seafloor (ms)	Interval velocity (m/s)
1	397.1	484.94	94.4	81.94	2502.98
2	428.7	510.20	126.0	107.20	2502.90
3	468.7	545.24	166.0	142.24	2282.89
4	478.7	554.08	176.0	151.08	2573.76
5	519.7	585.94	217.0	182.94	2859.07
6	534.2	596.08	231.5	193.08	2406.36
7	603.6	653.76	300.9	250.76	3081.65
8	623.6	667.40	320.9	264.40	2784.79
9	657.7	691.22	355.0	288.22	2444.65
10	763.6	777.86	460.9	374.86	2877.16
11	788.7	795.32	486.0	392.32	4350.77
12	826.2	812.56	523.5	409.56	

Note: TWT = two-way traveltime.

Table T16. Summary of logging operations, Hole 1199A.

Date (Feb 2001)	Time (local)	Comments
21	1715	Hole preparation complete. Rig up wireline.
	1830	RIH with HNGS-APS-HLDS-DITE.
	2240	Uplog with triple combo at 900 ft/hr from 417 mbsf to seafloor.
	2200	Pull tools out of hole and rig down.
	2300	RIH with NGT-LSS-FMS.
22	0030	Tool cannot pass tight spot at 129.2 mbsf. Pull tools back on the rig floor.
	0130	Wiper trip to 186 mbsf.
	0600	Hole preparation complete. Rig up wireline.
	0630	RIH with NGT-LSS-FMS.
	0700	Tool cannot pass tight spot at 129.2 mbsf.
	0720	Uplog with NGT-LSS-FMS at 900 ft/hr from 128 mbsf to 87 mbsf.
	0745	Tools on the rig floor. Put two pieces of pipe with bow spring at bottom.
	0900	RIH with NGT-LSS-FMS.
	0915	Tool cannot pass tight spot at 129.2 mbsf.
	1000	Pull tools out of hole and rig down.
	1015	End of logging operations.

Notes: RIH = run in hole, HNGS = hostile environment natural gamma ray sonde, APS = accelerator porosity sonde, HLDS = high-temperature lithodensity sonde, DITE = dual induction tool, NGT = natural gamma ray tool, LSS = long-spaced sonic tool, FMS = Formation MicroScanner. Drillers total depth = 419.5 mbsf; water depth = 326 mbrf; end of pipe = 69 mbsf.